AD_____

AWARD NUMBER: DAMD17-99-1-9571

TITLE: Molecular Mechanisms of Soft Tissue Regeneration and Bone Formation in Mice: Implications in Fracture Repair and Wound Healing in Humans

PRINCIPAL INVESTIGATOR: Subburaman Mohan, Ph.D.

CONTRACTING ORGANIZATION: Loma Linda Veterans Association for
Research and Education
Loma Linda, California 92357

REPORT DATE: April 2007

TYPE OF REPORT: Annual

PREPARED FOR: U.S. Army Medical Research and Materiel Command
Fort Detrick, Maryland 21702-5012

REPORT DOCUMENTATION PAGE

Form Approved
OMB No. 0704-0188

1. REPORT DATE	2. REPORT TYPE	3. DATES COVERED
01-04-2007	Annual	15 Mar 2006 – 14 Mar 2007

4. TITLE AND SUBTITLE

Molecular Mechanisms of Soft Tissue Regeneration and Bone Formation in Mice: Implications in Fracture Repair and Wound Healing in Humans

5a. CONTRACT NUMBER

5b. GRANT NUMBER
DAMD17-99-1-9571

5c. PROGRAM ELEMENT NUMBER

6. AUTHOR(S)

Subburaman Mohan, Ph.D.

E-Mail: subburaman.mohan@va.gov

5d. PROJECT NUMBER

5e. TASK NUMBER

5f. WORK UNIT NUMBER

7. PERFORMING ORGANIZATION NAME(S) AND ADDRESS(ES)

Loma Linda Veterans Association for
Research and Education
Loma Linda, California 92357

8. PERFORMING ORGANIZATION REPORT NUMBER

9. SPONSORING / MONITORING AGENCY NAME(S) AND ADDRESS(ES)
U.S. Army Medical Research and Materiel Command
Fort Detrick, Maryland 21702-5012

10. SPONSOR/MONITOR'S ACRONYM(S)

11. SPONSOR/MONITOR'S REPORT NUMBER(S)

12. DISTRIBUTION / AVAILABILITY STATEMENT
Approved for Public Release; Distribution Unlimited

13. SUPPLEMENTARY NOTES

14. ABSTRACT

The primary goal of the proposed work is to identify genes which play an anabolic role in bone and soft tissue function and to clarify the function of these genes. Three hypotheses have been proposed: 1) The high bone density gene in chromosome 1 in our CAST/B6 congenic mice can be cloned; 2) Genes that regulate soft- and hard-tissue regeneration can be identified by using appropriate mouse strains that exhibit differences in regeneration; and 3) ENU mutagenesis, applied to our mouse model, will lead to the identity of genes that regulate soft and hard tissue function. During the last funding period, we have proposed several specific objectives for each of the above-mentioned hypotheses. As disclosed in the progress report, we have successfully accomplished all of the specific objectives. Our work during the first year of the funding period has resulted in two manuscripts in press, two published manuscripts, and three abstracts. We believe that the successful accomplishment of the proposed studies will provide a better understanding of the molecular mechanisms involved in hard- and soft-tissue regeneration and will provide a framework for future development of therapies for hard and soft tissue injuries.

15. SUBJECT TERMS
Soft- and hard-tissue regeneration; bone density; gene function; cDNA microarray analysis; congenic mice; QTL analysis; mouse genetics; musculoskeletal genes

16. SECURITY CLASSIFICATION OF:			17. LIMITATION OF ABSTRACT	18. NUMBER OF PAGES	19a. NAME OF RESPONSIBLE PERSON
a. REPORT	b. ABSTRACT	c. THIS PAGE			USAMRMC
U	U	U	UU	119	19b. TELEPHONE NUMBER *(include area code)*

Table of Contents

Page

I. General Introduction

The primary goal of the project funded by the U.S. Army is to identify genes which play an anabolic role in bone tissue and soft tissue function, particularly during regeneration, and to clarify the function of these genes. To accomplish this goal, we have proposed 3 technical objectives during the funding period. These 3 Technical Objectives are as follows:

A. Technical Objective 1:

Studies proposed in the first technical objective are designed to employ state-of-the-art molecular biotechniques to identify the gene located in mouse chromosome 1 that is involved in the regulation of peak bone density.

B. Technical Objective 2:

Our second technical objective has been focused on identifying the key genes that are involved in soft tissue repair/regeneration using inbred strains of mice as model systems.

C. Technical Objective 3:

The goal of our third technical objective is to identify and characterize novel genes, using ENU mutagenesis techniques and to elucidate the function of known genes that play a key role in the metabolism of bone and soft tissue.

Our progress for the technical objective1 is described below.

II. Technical Objectives

TECHNICAL OBJECTIVE 1: TO CLONE THE GENE REGULATING PEAK BONE DENSITY ON CHROMOSOME 1 IN THE CAST/B6 CONGENIC MICE.

Introduction

Our long-term goal in this study is to identify the genes involved in the acquisition of peak bone density and evaluate the functions of those genes. Such genes are particularly relevant to determine both one's risk of fractures resulting from battlefield injury and to corresponding gene therapy treatment for such fractures.

In our studies on the identification of candidate genes regulating peak bone density, we focused on a quantitative trait locus (QTL) that contributes significantly to high bone density on mouse chromosome 1 (Chr. 1) from a cross between C57BL/6J (B6) and CAST/EiJ (CAST) mouse strains. We chose the chromosome 1 QTL for our studies based on the following rationale:

1) It contributes to approximately 40% of the total variation of femur volumetric bone mineral density (vBMD) between CAST and B6 mice;

2) It has a LOD (logarithm of the odds) score of 8, which is the statistically strongest QTL identified from B6 X CAST cross; and

3) It is located in a region syntenic with that of human chromosome 1q21-q23, which has been implicated in peak bone density regulation in humans (Koller et al., 2000 and Ralston, 2002)

B6-Cast congenic mouse lines were generated by transferring CAST Chr. 1 alleles (donor) into the B6 strain (recipient) to confirm the contribution of Chr. 1 QTL on vBMD

variation. We found that the bone density of B6-CAST congenic mice containing Chr. 1 QTL from CAST mice was significantly higher than that of B6 mice, confirming that the CAST Chr. 1 QTL contains gene/s that contribute to high bone density in B6 mice (previous report).

In order to further narrow down the size of the Chr. 1 QTL (25cM) to a more manageable size for the screen of candidate genes, we have produced several subcongenic lines containing smaller pieces of the CAST Chr. 1 QTL in B6 mice. Our subcongenic approach not only confirmed the biological activity of the QTL gene in this region, but also further narrowed the size of the QTL within Chr. 1 from 25 cM to approximately 7 cM. If this mouse QTL is homologous to the human QTL on Chr. 1q21-1q25, it follows that the QTL region could be within 2 cM, a size feasible for our proposed studies to identify candidate genes by the various approaches proposed below.

To achieve the goal of identifying the candidate gene in Chr. 1 involved in bone density regulation, we have designed state-of art molecular techniques, which include differences in gene expression, sequence polymorphism, presence of functional motif consistent with bone formation or resorption action in candidate genes, and *in vitro* functional testing of candidate genes.

Our Specific Objectives during the final 4 months **of this continuation grant period are as follows:**

8) To continue the fine mapping and candidate gene testing and sequencing initiated during the first 12 months of the grant period.

9) To determine if this gene is syntenic with the human gene present in the human syntenic region (1q21-1q25).

10) We will further evaluate the conservation of this gene by examining the gene sequence in drosophila, c-elegans and zebrafish.

Body

Our progress during the final 4 months of this continuation grant period are as follows:

8) To continue the fine mapping and candidate gene testing and sequencing initiated during the first 12 months of the grant period.

We have identified two BMD candidate genes; the Duffy antigen receptor for chemokines (*Darc* gene) located at BMD1-2 locus and the growth arrest specific 5 (Gas5) gene which underlies BMD1-1 locus. The data on the identification of Darc as a BMD QTL gene have been reported in previous reports.

Real Time PCR was performed for 11 candidate genes located in the region 160-165 Mb covering the BMD1-1 locus using femur without bone marrow. Only Gas5 gene showed significantly higher expression in both C100-169 and C133-165 subcongenic line of mice compared to B6 control mice. Using Real Time PCR, we have found that Gas5 is also expressed in marrow cells as well as in immature and mature osetoblast cells. Thus Gas5 gene was further analyzed.

Both human and murine Gas5 genes contain in their introns sequences homologous to the small nucleolar RNAs (snoRNAs) that are involved in the methylation of ribosomal RNA. In the last 4 months we had sequenced almost the whole sequence of Gas5 gene for the low BMD B6 strain of mice and for the high BMD CAST mice. In order to identify the polymorphisms that could be

involved in the BMD variation we have compared the two sequences from B6 and CAST mice with C3H and the sequence X67267 X59729 available at NCBI database (Figure 1).

```
B6              GCTTTCTTGCAGAGCCNNCTCCNCTCAGCCTGTACTCNTCAGGGAGGCGNAGGGCCTATC 120
CAST            GCTTTCTTGCAGAGCCNNCTCCCNTCAGCCTGTACTCNTCAGGGAGGCGGAGGNCCTATC 120
NCBI_DNA        GCTTTCTTGCAGAGCCCCCTCCCCTCAGCCTGTACTCCTCAGGGAGGCGGAGGGCCTATC 120
C3H             GCTTTCTTGCAGAGCCNNCTCCCNTCAGCCTGTACTCNNCAGGGAGGCGGAG GCCTATC 120

B6              GTGCCCGCGGCAACTCCCTCCGGGCTCTCGGGGCGTGGCCAGAGGGAAAGTTTTGTGGGC 180
CAST            GTGCCCGCGGCAACTCCCTCCGGGCTCTCGNNGGCGTGGCCAGAGGGAAAGTTTNGTGGGC 180
NCBI_DNA        GTGCCCGCGGCAACTCCCTCCGGGCTCTCGGGGCGTGGCCAGAGGGAAAGTTTTGTGGGC 180
C3H             GTGCCCGCGGCAACTCCCTCCGGGCTCTCGGGNCGTGGCCAGAGGGAAAGTTNTGTGGGC 180

B6              CTGAAGAAGGTGGGGCTTGAGGAGGAGTCTGAGGGCGTGTGAGGGGCNNNGTTTAAGTGG 240
CAST            CTGAAGAAGGTGGGGCTTGAGGAGGAGTCTGAGGGCGTGTGAGGGNNNGGGTTTAAGTGG 240
NCBI_DNA        CTGAAGAAGGTGGGGCTTGAGGAGGAGTCTGAGGGCGTGTGAGGGGCGGGGTTTAAGTGG 240
C3H             CTGAAGAAGGTGGGGCTTGAGGAGGAGTCTGAGGGCGTGTGAGGNNCGGGGTTTAAGTGG 240

B6              ACGCAGCAAGCAGCTTTGCGTCTTGACGTCACGAAGACCTTATATACTCGACTCAGCCGC 300
CAST            ACGCAGCAAGCAGCTTTGCGTCTTGACGTCACGAAGACCTTATATACTCGACTCAGCCGC 300
NCBI_DNA        ACGCAGCAAGCAGCTTTGCGTCTTGACGTCACGAAGACCTTATATACTCGACTCAGCCGC 300
C3H             ACGCAGCAAGCAGCTTTGCGTCTTGACGTCACGAAGACCTTATATACTCGACTCAGCCGC 300

B6              GGTGAGCTTAGTTCAGGGCACAAGCTGGAAACTTTAGGAGGTTGGTTCTGCGTGTATTTG 480
CAST            GGTGAGCTTAGTTCAGGGCACAAGCTGGAAACTTTAGGAGGTTGGTTCTGCGTGTATTTG 480
NCBI_DNA        GGTGAGCTTAGTTCAGGGCACAAGCTGGAAACTTTAGGAGGTTGGTTCTGCGTGTATTTG 480
C3H             GGTGAGCTTAGTTCAGGGCACAAGCTGGAAACTTTAGGAGGTTGGTTCTGCGTGTATTTG 480

B6              TGACATAAAATAGCATTGGGTTTTGGTCTNNNNNNNNCACCATGGGATGAAGGCTTTTGC 540
CAST            TGACATAAAATAGCATTGGGTTTTGGTCTNNNNNNNNCACCATGGGATGAAGGCTTTTGC 540
NCBI_DNA        TGACATAAAATAGCATTGGGTTTTGGTCTNNNNNNNNCACCATGGGATGAAGGCTTTTGC 540
C3H             TGACATAAAATAGCATTGGGTTTTGGTCTNNNNNNNNCACCATGGGATGAAGGCTTTTGC 540

B6              TAGAGA-TGCCAGCAGGCCTTAGTCACTAACAAAGAGGACGATTGCTCTTGGGAAGTACC 600
CAST            TAGAGA-TGCCAGCAGGCCTTAGTCACTAACAANGAGGACNATTGCTCTTGGGAAGTACC 600
NCBI_DNA        TAGAGATTGCCAGCAGGCCTTAGTCACTAACAAAGAGGACGATTGCTCTTGGGAAGTACC 600
C3H             TAGAGA-TGCCAGCAGGCCTTAGTCACTAACAAAGAGGACGATTGCTCTTGGGAAGTACC 600


B6              GGAGTTCTTTGTAAGACAGGTCCATTTTGTGGAAGTAGAACTACTAAAGATTAACATTTT 720
CAST            GGAGTTCTTTGTAAGACAGGTCCATTTTGTGGAAGTAGAACTACTAAAGATTAACATTTT 720
NCBI_DNA        GGAGTTCTTTGTAAGACAGGTCCATTTTGTGGAAGTAGAACTACTAAAGATTAACATTTT 720
C3H             GGAGTTCTTTGTAAGACAGGTCCATTTTGTGGAAGTAGAACTACTAAAGATTAACATTTT 720

B6              TANCTCAGTGGNNGAGNGGCATGACTAGNACATAANGACCACAAAGCCCATGATGGTATG 840
CAST            TAANTCAGTGGNNGAGGGNCATGACTAGAACATANTGACCACAAAGCNNATGATGGTATG 840
NCBI_DNA        TAACTCAGTGGGGGAGGGGCATGACTAGAACATAATGACCACAAAGCCCATGATGGTATG 840
C3H             TNNCTCAGTGGGGGAGGGGCATGACTAGAACATAATGACCACAANGCCCATGATGGTATG 840

B6              AGAGTAGTGGACAGAAGGGATTTCTGAANAACACNTTTCTGAGGCTTTAATTCAGCTACT 900
CAST            AGAGTAGTGGACAGANGGGATTTCTGAAAAACACTTNTCTGAGGCTTTAATTCAGCTACT 900
NCBI_DNA        AGAGTAGTGGACAGAAGGGATTTCTGANAAACACTTTTCTGAGGCTTTAATTCAGCTACT 900
C3H             AGAGTAGTGGACAGAAGGGATTTCTGAAAAACACTTTNCTGAGGCTTTAATTCAGCTACT 900

B6              GGAAAGGGTTTAGTTCCGTGAAGAAGGGGACTCACTGTTCACATCTCTTATTTCCAGTTC 960
CAST            GGAAAGGGTTTAGTTCCGTGAAGAAGGGGACTCACTGTTCACATCTCTTATTTCCAGTTC 960
NCBI_DNA        GGAAAGGGTTTAGTTCCGTGAAGAAGGGGACTCACTGTTCACATCTCTTATTTCCAGTTC 960
C3H             GGAAAGGGTTTAGTTCCGTGAAGAAGGGGACTCACTGTTCACATCTCTTATTTCCAGTTC 960

B6              TGTGGCAAAGGAGGATGAAGGCTTACGAGGTGAGTACTGAATAGTAATGAGAAGTTAGGT 1020
CAST            TGTGGCAAAGGAGGATGAAGGCTTACGAGGTGAGTACTGAATAGTAATGAGAAGTTAGGT 1020
NCBI_DNA        TGTGGCAAAGGAGGATGAAGGCTTACGAGGTGAGTACTGAATAGTAATGAGAAGTTAGGT 1020
C3H             TGTGGCAAAGGAGGATGAAGGCTTACGAGGTGAGTANTGAATAGTAATGAGAAGTTAGGT 1020

B6              TGAAAGGACAGTGCCACAATGATGACATCATATTTGCTACTCTTGACAGCTGGGGTGACG 1080
```

```
CAST            TGAAAGGACAGTGCCACAATGATGACATCATATTTGCTACTCTTGACAGCTGGGGTGACG 1080
NCBI_DNA        TGAAAGGACAGTGCCACAATGATGACATCATATTTGCTACTCTTGACAGCTGGGGTGACG 1080
C3H             TGAAAGGACAGTGCCACAATGATGACATCATATTTGCTACTCTTGACAGCTGGGGTGACG 1080

B6              ATAGCTTTAATTNNGTCTACTTACAGAGTAAGCAGTTTTACATNAAGATTCNNNNCCCCC 1140
CAST            ATAGCTTTAATTGGGTCTACTTACAGAGTAAGCAGTTTTACATNAAGATTCCNNNNNCCC 1140
NCBI_DNA        ATAGCTTTAATTGGGTCTACTTACAGAGTAAGCAGTTTTACATAAAGATTCCCCCCCCCC 1140
C3H             ATAGCTTTAATTGGNTCTACTTACAGAGTAAGCAGTTTTACATAANGATTCCNNNNCCCC 1140

B6              AGGACTCGTCAGGAAGCTGGATAACAGAGCGAGNGCAATGTAAGCAATTTTGTGTGTGCA 1200
CAST            AGGACTCGTCAGGAAGCTGGATAACAGAGCGAGNGCAATGTAAGCAATTTTGTGTGTGCA 1200
NCBI_DNA        AGGACTCGTCAGGAAGCTGGATAACAGAGCGAGCGCAATGTAAGCAATTTTGTGTGTGCA 1200
C3H             AGGACTCGTCAGGAAGCTGGATAACAGAGCGAGNGCAATGTAAGCAATTTTGTGTGTGCA 1200

B6              TGTGGTCCCATTACAAGGAATACCCAATGGCAANTGAGCACTAAAGATCNNTCAACCCAC 1260
CAST            TGTGGTCCCATTACAAGGAATACCCAATGGCAAATGAGCACTAAAGATCCNTCAACCCAC 1260
NCBI_DNA        TGTGGTCCCATTACAAGGAATACCCAATGGCAAATGAGCACTAAAGATCCCTCAACCCAC 1260
C3H             TGTGGTCCCATTACAAGGAATACCCAATGGCAAATGAGCACTAAAGATCNCTCAACCCAC 1260

B6              ACATTGAATGTATTGTTCCCTGAGAGCAATTGTAGATAGAGGAGTGGGTGGGAAGTCTGA 1320
CAST            ACATTGAATGTATTGTTCCCTGAGAGCAATTGTAGATAGAGGAGTGGGTGGGAAGTCTGA 1320
NCBI_DNA        ACATTGAATGTATTGTTCCCTGAGAGCAATTGTAGATAGAGGAGTGGGTGGGAAGTCTGA 1320
C3H             ACATTGAATGTATTGTTCCCTGAGAGCAATTGTAGATAGAGGAGTGGGTGGGAAGTCTGA 1320

B6              AGTCAGGGCATTGTTTCTGCGTATCTGAGGAGGCTGGTTTTTGATATGTGGGAGCTAGTG 1380
CAST            AGTCAGGGCATTGTTTCTGCCTATCTGAGGAGGCTGGTTTTTGATATGTGGGAGCTAGTG 1380
NCBI_DNA        AGTCAGGGCATTGTTTCTGCGTATCTGAGGAGGCTGGTTTTTGATATGTGGGAGCTAGTG 1380
C3H             AGTCAGGGCATTGTTTCTGCTTATCTGAGTAGGCTGGTTTTTGATATGTGGGAGCTAGTG 1380

B6              GTCGTTAACGCATTTACCCCCTATTTGGTGGACTCTGGTTCCCCCATCTTAAGTGCTGAG 1440
CAST            GTCGTTAACGCATTTACCCCCTATTTGGTGGACTCTGGTTCCCCCATCTTAAGTGCTGAG 1440
NCBI_DNA        GTCGTTAACGCATTTACCCCCTATTTGGTGGACTCTGGTTCCCCCATCTTAAGTGCTGAG 1440
C3H             GTCGTTAACGCATTTACCCCCTATTTGGTGGACTCTGGTTCCCCCATCTTAAGTGCTGAG 1440

B6              TCAGGGGCCTAACCGGGCAGCTTTAACTATTTGTTTGTTGTAGGTGCTAGAATAGAAGAC 1500
CAST            TCAGGGGCCTAACCGGGCAGCTTTAACTATTTGTTTGTTGTAGGTGCTAGAATAGAAGAC 1500
NCBI_DNA        TCAGGGGCCTAACCGGGCAGCTTTAACTATTTGTTTGTTGTAGGTGCTAGAATAGAAGAC 1500
C3H             TCAGGGGCCTAACCGGGCAGCTTTAACTATTTGTTTGTTGTAGGTGCTAGAATAGAAGAC 1500

B6              CAGAAAATGAAATGGTAAGTCAAACTAAAGGAATTGTAGATGCTAAACAGGCTTGGCTTT 1560
CAST            CAGAAAATGAAATGGTAAGTCAAACTAAAGGAATTGTAGATGCTAAACAGGCTTGGCTTT 1560
NCBI_DNA        CAGAAAATGAAATGGTAAGTCAAACTAAAGGAATTGTAGATGCTAAACAGGCTTGGCTTT 1560
C3H             CAGAAAATGAAATGGTAAGTGAAACTAAAGGAATTGTAGATGCTAAACAGGCTTGGCTTT 1560

B6              GTTGCACTCTGCCAAATACTGGCCACGTGTTCCATCCTGGTCATAGCTGAACACAGCCTG 1620
CAST            GTTGCACTCTGCCAAATACTGGCCACGTGTTCCATCCTGGTCATAGCTGAACACAGCCTG 1620
NCBI_DNA        GTTGCACTCTGCCAAATACTGGCCACGTGTTCCATCCTGGTCATAGCTGAACACAGCCTG 1620
C3H             GTTGCACTCTGCCAAATACTGGCCACGTGTTCCATCCTGGTCATAGCTGAACACAGCCTG 1620

B6              CATGATGACGAACAAATACTGACTACCTGAAGATCTTATTAGCTCTATCTGATGGTGGGC 1680
CAST            CATGATGACGAACAAATACTGACTACCTGAAGATCTTATTAGCTCTATCTGATGGTGGGC 1680
NCBI_DNA        CATGATGACGAACAAATACTGACTACCTGAAGATCTTATTAGCTCTATCTGATGGTGGGC 1680
C3H             CATGATGACGAACAAATACTGACTACCTGAAGATCTTATTAGCTCTATCTGATGGTGGGC 1680

B6              TTCCTTGACATTTATTGTGGGGCAAACTCAAATCTGTTGACTGCATTGAAAAGCTCTTTA 1740
CAST            TTCCTTGACATTTATTGTGGGGCAAACTCAAATCTGTTGACTGCATTGAAAAGCTCTTTA 1740
NCBI_DNA        TTCCTTGACATTTATTGTGGGGCAAACTCAAATCTGTTGACTGCATTGAAAAGCTCTTTA 1740
C3H             TTCCTTGGCATTTATTGTGGGGCAAACTCAAATCTGTTGACTGCATTGAAAAGCTCTTTA 1740

B6              ATGTTTTTTTTCTAGGTGGAGTNTGAGGCTGGATAGACAGTTTGAAAGGTAAGTATTGAAA 1800
CAST            ATGTTTTTTTTCTAGGTGGAGTNTGAGGCTGGATAGACAGTTTGAAAGTGTAAGTATTGAAA 1800
NCBI_DNA        ATGTTTTTTTTCTAGGTGGAGTTTGAGGCTGGATAGACAGTTTGAAAGGTAAGTATTGAAA 1800
C3H             ATGTTTTTTTTCTAGGTGGAGTNTGAGGCTGGATAGACAGTTTGAAAGNTAAGTATTGAAA 1800

B6              AACACTTGAATTTGGGTCAGTACAAAGGGACNTGCAGAGACTTTGAATCATCAAAACTCC 1860
CAST            AACACTTGAATTTGGGTCAGTACAAAGGGACNTGCAGAGACTTTGAATCATCAAAACTCC 1860
NCBI_DNA        AACACTTGAATTTGGGTCAGTACAAAGGGACATGCAGAGACTTTGAATCATCAAAACTCC 1860
C3H             AACACTTGAATTTGGGTCAGTACAAAGGGNCATGCAGAGACTTTGAATCATCAAAACTCC 1860
```

```
B6              AGCATGCATTGTCTTACGGATGTTTAGATAGGTGTGTTTTGGACAACACTCTGGGTTCTT 1920
CAST            AGCATGCATTGTCTTACGGATGTTTAGATAGGTGTGTTTTGGACAACACTCTGGGTTCTT 1920
NCBI_DNA        AGCATGCATTGTCTTACGGATGTTTAGATAGGTGTGTTTTGGACAACACTCTGGGTTCTT 1920
C3H             AGCATGCATTGTCCTACGGATGTTTAGATAGGTGTGTTTTGGACAACACNCTGGGTTCTT 1920

B6              GTAATGATGTTGATCAAATGTCTGAGCTGNAAATAACTTGTAGACAATTTTTAACACTGA 1980
CAST            GTAATGATGTTGATCAAATGTCTGAGCTGNAAATAACTTGTAGACAATTTTTAACACTGA 1980
NCBI_DNA        GTAATGATGTTGATCAAATGTCTGAGCTGAAAATAACTTGTAGACAATTTTTAACACTGA 1980
C3H             GTAATGATGTTGATCAAATGTCTGAGCTGNAAATAACTTGTAGACAATTTTTAACACTGA 1980

B6              AGAACCTTGTGGCAGGCAACTAAGAATAGTCGAATGATGNTTAGCATATTTGTAAGAGGT 2040
CAST            AGAACCTTGTGGCAGGCAACTAAGAATAGTCGAATGATGNTTAGCATATTTGTAAGAGGT 2040
NCBI_DNA        AGAACCTTGTGGCAGGCAACTAAGAATAGTCGAATGATGTTTAGCATATTTGTAAGAGGT 2040
C3H             AGAACCCTGTGGCAGGCAACTAAGAATAGTCGAATGATGNTTAGCATATTTGTAAGAGGT 2040

B6              ATNNTCTTTTAATTCTAGTTAACTGGTTGCATGCTTGTTCATTTGGCTGGCTTGCTTGGG 2100
CAST            ATNNTCTTTTAATTCTAGTTAACTGGTTGCATGCTTGTTCATTTGGCTGGCTTGCTTGGG 2100
NCBI_DNA        ATTTTCTTTTAATTCTAGTTAACTGGTTGCATGCTTGTTCATTTGGCTGGCTTGCTTGGG 2100
C3H             ATNNTCTTTTAATTCTAGTTAACTGGTTGCATGCTTGTTCATTTGGCTGGCTTGCTTGGG 2100

B6              TAAGAAGCCATTGGGGGCCTTGAATTCNCTCCAGTCATTTGCAGTATTTACTGCATAACA 2160
CAST            TAAGAAGCCATTGGGGGCCTTGAATTCNCTCCAGTCATTTGCAGTATTTACTGCATAACA 2160
NCBI_DNA        TAAGAAGCCATTGGGGGCCTTGAATTCCCTCCAGTCATTTGCAGTATTTACTGCATAACA 2160
C3H             TAAGAAGCCATTGGGGGCCTTGAATTCNCTCCAGTCATTTGCAGTATTTACTGCATAACA 2160

B6              TTTAGCTTTTGAACATGCATGTGCTACCATNAGTACTAAATGGTGCCTTAAATTTTTTTC 2220
CAST            TTTAGCTTTTGAACATGCATGTGCTACCATNAGTACTAAATGGTGCCTTAAATTTTTTTC 2220
NCBI_DNA        TTTAGCTTTTGAACATGCATGTGCTACCATCAGTACTAAATGGTGCCTTAAATTTTTTTC 2220
C3H             TTTAGCTTTTGAACATGCATGTGCTACCATNAGTACTAAATGGTGCCTTAAATTTTTTTC 2220

B6              AGGTACAAATAAATGGTTTGANTAANGAAAGGTAAGCATTGTAAGTTNGGTATTTACTATA 2280
CAST            AGGTACAAATGATGGTTTGAATAANGAAAGGTAAGCATTGTAAGTTNGGTATTTACTATA 2280
NCBI_DNA        AGGTACAAATAATGGTTTGAATAAAGAAAGGTAAGCATTGTAAGTTTGGTATTTACTATA 2280
C3H             AGGTACAAATGATGGTTTGAATAANGAAAGGTAAGCATTGTAAGTTTGGTATTTACTATA 2280

B6              TGAATTAAGGTACTGTTAGTGATGNTCAATAAAGTTAAACAGATGGGAATCTCTCTGAAT 2340
CAST            TGAATTAAGGTACTGTTAGTGATGNTCAATAAAGTTAAACAGATGGGAATCTCTCTGAAT 2340
NCBI_DNA        TGAATTAAGGTACTGTTAGTGATGATCAATAAAGTTAAACAGATGGGAATCTCTCTGAAT 2340
C3H             TGAATTAAGGTACTGTTAGTGATGNCCAATAAAGTTAAACAGATGGGAATCTCTCTGAAT 2340

B6              AAGATTGAAGATTGATTGNNAAGCTGAAACAGTATTTAAGGACATCAGTAAATATACTTT 2400
CAST            AAGATTGAAGATTGATTGNNAAGCTGAAACAGTATTTAAGGACATCAGTAAATATACTTT 2400
NCBI_DNA        AAGATTGAAGATTGATTGTTAAGCTGAAACAGTATTTAAGGACATCAGTAAATATACTTT 2400
C3H             AAGATTGAAGATTGATTGNNAAGCTGAAACAGTATTTAAGGACATCAGTAAATATANTTT 2400

B6              ACAAATACATATTTCTAAACGGAGTGTAATTTCTTACAGGTATTAATGGGTCACCTCAAG 2460
CAST            ACAAATACATATTTCTAAACGGAGTGTAATTTCTTACAGGTATTAATGGGTCACCTCAAG 2460
NCBI_DNA        ACAAATACATATTTCTAAACGGAGTGTAATTTCTTACAGGTATTAATGGGTCACCTCAAG 2460
C3H             ACAAATACATATTTCTAAACGGAGTGTAATTTCTTACAGGTATTAATGGGTCACCTCAAG 2460

B6              TGAAGGCACTGCAAACACAATGGTAAGTCNTTGAAATGTGCATGTATTAGTTACTTTCAA 2520
CAST            TGAAGGCACTGCAAACACAATGGTAAGTCTNNGAAATGTGCATGTATTAGTTACTNTCAA 2520
NCBI_DNA        TGAAGGCACTGCAAACACAATGGTAAGTCTTTGAAATGTGCATGTATTAGTTACTTTCAA 2520
C3H             TGAAGGCACTGCAAACAAAATGGTAAGTCNNTGAAATGTGCATGTATTAGTTACTNNCAA 2520

B6              NNNCCTTCAAACAAGCCGATACCATGATGATAACATAGTTCAGCAGACTTAACTCTGATG 2580
CAST            CCNNNTTCAAACAAGCCGATACCATGATGATAACATAGTTCAGCAGACTTAACTCTGATG 2580
NCBI_DNA        CCCCCTTCAAACAAGCCGATACCATGATGATAACATAGTTCAGCAGACTTAACTCTGATG 2580
C3H             CCNNNTTCAAACAAGCCGATACCATGATGATAACATAGTTCAGCAGACTTAACTCTGATG 2580

B6              AACAATCATGTCTTTCGCTCCTATCTGATGTATCTGGCTGTAATGTNNTAAAGAGTTNTC 2640
CAST            AACAATCATGTCTTTCGCTCCTATCTGATGTATCTGGCTGTAATGTTNNAAAGAGTTNTC 2640
NCBI_DNA        AACAATCATGTCTTTCGCTCCTATCTGATGTATCTGGCTGTAATGTTTTAAAGAGTTTTC 2640
C3H             AACAATCATGTCTTTCGCTCCTATCTGATGTATCTGGCTGTAATGTNNTAAAGAGTNNTC 2640

B6              CTTGAATAGTATTAGGAAATACAAGATAAGAGTCCCAAGTGATGAGGCCAAAGCCTGATG 2700
CAST            CTTGAATAGTATTAGGAAATACAAGATAAGAGTCCCAAGTGATGAGGCCAAAGCCTGATG 2700
NCBI_DNA        CTTGAATAGTATTAGGAAATACAAGATAAGAGTCCCAAGTGATGAGGCCAAAGCCTGATG 2700
C3H             CTTGAATAGTATTAGGAAATACAAGATAAGAGTCCCAAGTGATGAGGCCAAAGCCTGATG 2700

B6              CTAAGGTGGCATGTGCTGTGCCACTGACTTAACCCAGTAGGACAATTTTATTGTGANNAA 2760
CAST            CTAAGGTGGCATGTGCTGTGCCACTGACTTAACCCAGTAGGACAATTTTATTGTGANNNA 2760
```

```
NCBI_DNA        CTAAGGTGGCATGTGCTGTGCCACTGACTTAACCCAGTAGGACAATTTTATTGTGAAAAA 2760
C3H             CTAAGGTGGCATGTGCTGTGCCACTGACTTAACCCAGTAGGACAATTTTATTGTGANNAA 2760

B6              TACATAAGTTCCCTAGGGTATGAGCATTGAAACTATAAATCTCAGGCCTCTTGGCAAGAG 2820
CAST            TACATAAGTTCCCTAGGGTATGAGCATTGAAACTATAAATCTCAGGCCTCTTGGCAAGAG 2820
NCBI_DNA        TACATAAGTTCCCTAGGGTATGAGCATTGAAACTATAAATCTCAGGCCTCTTGGCAAGAG 2820
C3H             TACATAAGTTCCCTAGGGTATGAGCATTGAAACTATAAATCTCAGGCCTCTTGGCAAGAG 2820

B6              AATTGATGTGAGCCCATGGAGACTAGTGAAGACAACTGAACACTGAGAGAATAGTGTGAA 2880
CAST            AATTGATGTGAGCCCATGGAGACTAGTGAAGACAACTGAACACTGAGAGAATAGTGTGAA 2880
NCBI_DNA        AATTGATGTGAGCCCATGGAGACTAGTGAAGACAACTGAACACTGAGAGAATAGTGTGAA 2880
C3H             AATTGATGTGAGCCCATGGAGACTAGTGAAGACAACTGAACACTGAGAGAATAGTGTGAA 2880

B6              ATAAAATGAAGATAAGTAACTGCACTAATTATTTTTAATTTTCAAACAGATTGGTCATTC 2940
CAST            ATAAAATGAAGATAAGTAACTGCACTAATTATTTTTAATTTTCAAACAGATTGGTCATTC 2940
NCBI_DNA        ATAAAATGAAGATAAGTAACTGCACTAATTATTTTTAATTTTCAAACAGATTGGTCATTC 2940
C3H             ATAAAATGAAGATAAATAACTGCACTAATTATTTTTAATTTTCAAACAGATTGGTCATTC 2940

B6              TGAATTTCCGGTCCTTCATTCTGAATTTCAAAGTAAGTCTGTCACTTGTTTTTGTACAGA 3000
CAST            TGAATTTCCGGTCCTTCATTCTGAATTTCAAAGTAAGTCTGTCACTTGTTTNTGTACAGA 3000
NCBI_DNA        TGAATTTCCGGTCCTTCATTCTGAATTTCAAAGTAAGTCTGTCACTTGTTTTTGTACAGA 3000
C3H             TGAATTTCCGGTCCTTCATTCTGAATTTCAAAGTAAGTCTGTCACTTGTNNTTGTACAGA 3000

B6              TTGTAATATAGCTTGTAACCAGTGATGTGATGATTCTGCCAAATGATACAAAGTGATATC 3060
CAST            TTGTAATATAGCTTGTAACCAGTGATGTGATGATTCTGCCAAATGATACAAAGTGATATC 3060
NCBI_DNA        TTGTAATATAGCTTGTAACCAGTGATGTGATGATTCTGCCAAATGATACAAAGTGATATC 3060
C3H             TTGTAATATAGCTTGTAACCAGTGATGTGATGATTCTGCCAAATGATACAAAGTGATATC 3060

B6              ACCTTTAAACCGTTCCATTTTATTTCTGAGGTTACTATACTAACATGTANNATTTAACTA 3120
CAST            ACCTTNAAACCGTTCCATTNTATTTCTGAGGTTACTATACTAACATGTANAATTTAACTA 3120
NCBI_DNA        ACCTTTAAACCGTTCCATTTTATTTCTGAGGTTACTATACTAACATGTAAAATTTAACTA 3120
C3H             ACCTTTAAACCGTTCCATTNNATTTCTGANGTTACTATACTAACATGTNNAATTTAACTA 3120

B6              CTCTAAGCCAGAGAAGTAAGTCAGTCTTTGTTTTCTTAGGGCTCCTGTGACAAGTGGACA 3180
CAST            CTCTAAGCCAGAGAAGTAAGTCAGTCTTTGTTTTCTTAGGGCTCCTGTGACAAGTGGACA 3180
NCBI_DNA        CTCTAAGCCAGAGAAGTAAGTCAGTCTTTGTTTTCTTAGGGCTCCTGTGACAAGTGGACA 3180
C3H             CTCTAAGCCAGAGAAGTAAGTCAGTCTTTGTTNTCTTAGGGCTCCTGTGNCAAGTGGACA 3180

B6              TGCAGTGACTGCACCTTTGTTTCTGAGGTGAGAACTGCAANTGCTTAACCGGGAACCTAC 3240
CAST            TGCAGTGACTGCACCTTTGTTTCTGAGGTGAGAACTGCANATGCTTAACCGGNAACCTAC 3240
NCBI_DNA        TGCAGTGACTGCACCTTTGTTTCTGAGGTGAGAACTGCAAATGCTTAACCGGGAACCTAC 3240
C3H             TGCAGTGACTGCACCTTTGTTNNTGAGGTGAGAACTGCAAATGCTTAACCGGGAACCTAC 3240

B6              TCCAGAATACNTGATGATCTCACACAACTTGAACTCTNTCACTGATTACTTGATGATAGT 3300
CAST            TCCAGAATACATGATGATCTCACACAACTTGAACTCTCTCACTGATTACTTGATGATAGT 3300
NCBI_DNA        TCCAGAATACATGATGATCTCACACAACTTGAACTCTCTCACTGATTACTTGATGATAGT 3300
C3H             TCCAGANTACATGATGATCTCACNCAACTTGAACTCTCTCACTGATTACTTGATGATAGT 3300
```

Figure 1. CLUSTAL W (1.83) multiple sequence alignment. Comparison of Gas5 gene sequences from B6, CAST, C3H and NIH3T3 strain of mice. The polymorphisms are highlighted in purple color, 'N' data not available.

9) To determine if this gene is syntenic with the human gene present in the human syntenic region (1q21-1q25).

We have compared the sequences of the two BMD candidate genes, identified in our previous work, with human genome database (using Blat Search Genome at: http://www.genome.ucsc.edu). The two genes analyzed are: Gas5 gene which underlies BMD1-1 locus and Darc gene which was identified within BMD1-2 locus.

Gas5 gene from mice showed 91.2% with Gas5 gene, located at 1q-23.3 (172.0999 Mb within 1q21-1q25) in human chromosome 1 (Figure 2).

The sequence of mouse Darc gene is syntenic with human 1q21-1q22 at 157.44 Mb (within 1q21-1q25), and showed 60% similarities with human DARC gene from Human (Figure 3). This region in human chromosome 1 was identified as a BMD QTL by previous studies using different human populations (Koller et al., 2000 and Ralston, 2002). In humans, the Duffy blood group system consists of four alleles, five phenotypes, and five antigens (Pogo and Chaudhuri, 2000). Duffy negative individuals are predominantly Africans and American blacks; they lack the Duffy protein on erythrocytes and are resistant to *Plasmodium vivax* and *Plasmodium knowlesi* infections (Miller et al., 1975 and 1976). In addition, it has been well established that African Americans exhibit significantly higher BMD compared to Caucasians (Yanovski et al., 2000 and Cauley et al., 2005). Our finding that total femur vBMD is increased in DARC-KO mice compared to B6 mice raises the interesting possibility that BMD variation between African Americans and Caucasians could be, in part, due to a difference in the function of DARC between the two groups.

```
000000841 agagtagtggacagaagggatttctgaaa 000000869
<<<<<<<<< |||||||||||||||||||||||||||| <<<<<<<<<
172102683 agagtagtggacagaagggatttctgaaa 172102655
```

```
000000877 ttctgaggctttaat 000000891
<<<<<<<<< ||||||||||||||| <<<<<<<<<
172102649 ttctgaggctttaat 172102635
```

```
000000931 ctcactgtt 000000939
<<<<<<<<< ||||||||| <<<<<<<<<
172102591 ctcactgtt 172102583
```

```
000001031 gtgccacaatgatgacatcatatttgctactcttga 000001066
<<<<<<<<< |||||||||||||||||   |||||||||||||||| <<<<<<<<<
172102477 gtgccacaatgatgacagtttatttgctactcttga 172102442
```

```
000001508 tgaaatggtaagtcaaact 000001526
<<<<<<<<< |||||||||||||  ||||| <<<<<<<<<
172101944 tgaaatggtaagtgaaact 172101926
```

```
000001700 gggcaaact 000001708
<<<<<<<<< ||||||||| <<<<<<<<<
172101903 gggcaaact 172101895
```

```
000001748 tttc.taggtggagt 000001761
<<<<<<<<< |||| |||||||||| <<<<<<<<<
172101663 tttcttaggtggagt 172101649
```

```
000001787 ggtaagtatt...gaaaa 000001801
<<<<<<<<< ||||||||||   ||||| <<<<<<<<<
172101618 ggtaagtattaatgaaaa 172101601
```

```
000001920 tgtaatgatgttgatcaaatgtctgagctgaaaataacttgtagacaa 000001967
<<<<<<<<< ||||||||||||||||||||||||| ||||||  | | ||||||||| <<<<<<<<<
172101446 tgtaatgatgttgatcaaatgtctgacctgaaatgagcatgtagacaa 172101399
```

```
000001972 taacactgaagaaccttgtg 000001991
<<<<<<<<< ||||||||||||||| |||| <<<<<<<<<
172101395 taacactgaagaaccctgtg 172101376

000002013 aatgatgtttagcat 000002027
<<<<<<<<< ||||||||||||||| <<<<<<<<<
172101352 aatgatgtttagcat 172101338

000002091 cttgcttgggtaag 000002104
<<<<<<<<< |||||||||||||| <<<<<<<<<
172101279 cttgcttgggtaag 172101266

000002291 tactgttagtgatgat 000002306
<<<<<<<<< |||||||||||||||| <<<<<<<<<
172101193 tactgttagtgatgat 172101178

000002310 taaagttaaa.cagatgggaatctctctga 000002338
<<<<<<<<< |||| ||||| |||||||||||||||||||| <<<<<<<<<
172101175 taaaattaaagcagatgggaatctctctga 172101146

000002453 acctcaagtga 000002463
<<<<<<<<< |||||||||| <<<<<<<<<
172100769 acctcaagtga 172100759

000002533 aagccgataccatgatgataacatagttcagcagacttaactctgatgaa 000002582
<<<<<<<<< |||||||||| ||||||||||||||||||||||||| ||| ||||||| <<<<<<<<<
172100672 aagccgatacaatgatgataacatagttcagcagact.aacgctgatgag 172100624

000002583 caat 000002586
<<<<<<<<< |||| <<<<<<<<<
172100623 caat 172100620

000002590 gtctttcgctcctatctgatgtatctggctgtaa 000002623
<<<<<<<<< |||||||||||||||||||||||||||||| |||| <<<<<<<<<
172100614 gtctttcgctcctatctgatgtatctggcggtaa 172100581

000003014 tgtaaccagtgatgtgatgattctgccaaatgatacaaagtgatatcacc 000003063
<<<<<<<<< |||||||| |||||| |||||||||||||||| | | | |||||||||  <<<<<<<<<
172100209 tgtaaccaatgatgtaatgattctgccaaatgaaatataatgatatcact 172100160

000003064 tttaaaccgttccattttatttctgaggttactatactaaca 000003105
<<<<<<<<<  | ||||||||||||||  |||||||||||| |||||||| <<<<<<<<<
172100159 gtaaaaccgttccattttgattctgaggttactctactaaca 172100118

000003243 cagaatacatgatgatctca 000003262
<<<<<<<<< |||||||||||||||||| <<<<<<<<<
172099983 cagaatacatgatgatctca 172099964

000003265 caacttgaactctctcactgattacttgatga 000003296
<<<<<<<<< |||||||||||||||||||||||||||||||| <<<<<<<<<
172099960 caacttgaactctctcactgattacttgatga 172099929
```

Figure 2. Side by Side Alignment of Gas5 gene from mouse with human genome, (http://www.genome.ucsc.edu). 841-3296 bp represents the murine Gas5 sequence and 172102683-172099929 bp is the GAS5 sequence from Human genome.

```
000000643 cccttcttcatgctcaccagtgtcctggg 000000671
>>>>>>>>> |||||||||||| |||||||||||||||| >>>>>>>>>
157442040 cccttcttcatcctcaccagtgtcctggg 157442068
```

```
000000738 cagctggc 000000745
>>>>>>>>> |||||||| >>>>>>>>>
157442154 cagctggc 157442161
```

```
000000766 gtgggcagtgccctgttcagcattgcagtgcccatcctggcaccaggctt 000000815
>>>>>>>>> |||||||||||||| ||||||||||  |||||| || |||| |||||  | >>>>>>>>>
157442163 gtgggcagtgccctcttcagcattgtggtgcccgtcttggccccagggct 157442212

000000816 acacagcgcccacagcacagccctatgcaacctgggctactg.....ggt 000000860
>>>>>>>>> |   ||| | | |||| | ||||| || | ||||||||||||     ||| >>>>>>>>>
157442213 aggtagcactcgcagctctgccctgtgtagcctgggctactgtgtctggt 157442262

000000861 atgg 000000864
>>>>>>>>> |||| >>>>>>>>>
157442263 atgg 157442266
```

```
000000877 tttgcccaagctctgttgataggatgctatgcttgcctgaaccccagact 000000926
>>>>>>>>> |||||||| ||| || || |||| ||| |||| | ||||  || |||||| >>>>>>>>>
157442274 tttgcccaggctttgctgctagggtgccatgcctccctgggccacagact 157442323

000000927 gaatattggtcaactccgtggcttcaccttgggactcagtgtgggacttt 000000976
>>>>>>>>> |  |   || ||  |||  ||| ||||| |||| |||| ||||||| ||| >>>>>>>>>
157442324 gggtgcaggccaggtcccaggcctcaccctggggctcactgtgggaattt 157442373

000000977 ggggagcagctgccctcttagggctgccagtcgccctggccagtgatgct 000001026
>>>>>>>>> ||||||  ||||||||  |    ||||| ||| |||||||||||| |||| >>>>>>>>>
157442374 ggggagtggctgccctactgacactgcctgtcaccctggccagtggtgct 157442423

000001027 t 000001027
>>>>>>>>> | >>>>>>>>>
157442424 t 157442424
```

```
000001131 tttggcagccaaggggctgaagatagcactgagcaaggggcctggcccct 000001180
>>>>>>>>> ||||| |||||||||||||||  ||| || | | |||||| ||||||| >>>>>>>>>
157442529 tttgg.agccaaggggctgaagaaggcattgggtatggggccaggcccct 157442577

000001181 gggttagtgtcttgtggatctggttcattttctggtggcctcatgggatg 000001230
>>>>>>>>> || | | | || |||||  |||||| |||||||||||||||||||| || >>>>>>>>>
157442578 ggatgaatatcctgtgggcctggtttattttctggtggcctcatggggtg 157442627

000001231 gttctcatatttgatgctttggtgaggtccaaaattgttcttctgtatac 000001280
>>>>>>>>> |||||   | | |||    ||||||||||||  |  | ||  |||  || >>>>>>>>>
157442628 gttctaggactggatttcctggtgaggtccaagctgttgctgttgtcaac 157442677

000001281 atgccaatcccagaagattcttgatgcgatgctgaatgtgacagaagccc 000001330
>>>>>>>>> ||| |   ||||| ||  ||| ||   | |||||||  || ||||||||| >>>>>>>>>
157442678 atgtctggcccagcaggctctggacctgctgctgaacctggcagaagccc 157442727

000001331 tgagtatgctgcactgtgtggctaccccactgctcctggccctgttctgc 000001380
>>>>>>>>> ||   ||  |||||||||||||||| || |||||||| ||||| |||||| >>>>>>>>>
157442728 tggcaattttgcactgtgtggctacgcccctgctcctcgccctattctgc 157442777
```

```
000001381 catcagaccacccg 000001394
>>>>>>>>> || ||| ||||||| >>>>>>>>>
157442778 caccaggccacccg 157442791
```

Figure 3 Side by Side Alignment of Darc gene from B6 mice compared to Human Genome (http://www.genome.ucsc.edu). 643-1394 bp represents mouse Darc sequence and 157442040-157442791 bp is the DARC gene in Human genome.

10) We will further evaluate the conservation of this gene by examining the gene sequence in drosophila, c-elegans and zebrafish.

The sequences of both Darc gene and Gas5 gene were blast searched with the whole genomes of *Drosophila*, *C. elegans*, as well as zebrafish, but no significant similarities were found with the sequence of any gene from these three species.

ADDITIONAL WORK

Gender specificity in chromosome 1

In order to further narrow down the size of the BMD loci in Chr 1 and allow for a successful screening of BMD gender effect candidate gene, in this study, we have generated four congenic sublines of mice by backcrossing the C168-185 subline of mice (previously described by Edderkaoui et al., 2006) with B6 progenitors. The congenic sublines of mice used in this study are described in figure 1. To investigate the sex specificity of the volumetric BMD, we analyzed the skeletal phenotypes of both males and females of the C100-169 subline previously described by Edderkaoui et al., (2006) and the new sublines generated in this study (Fig. 4).

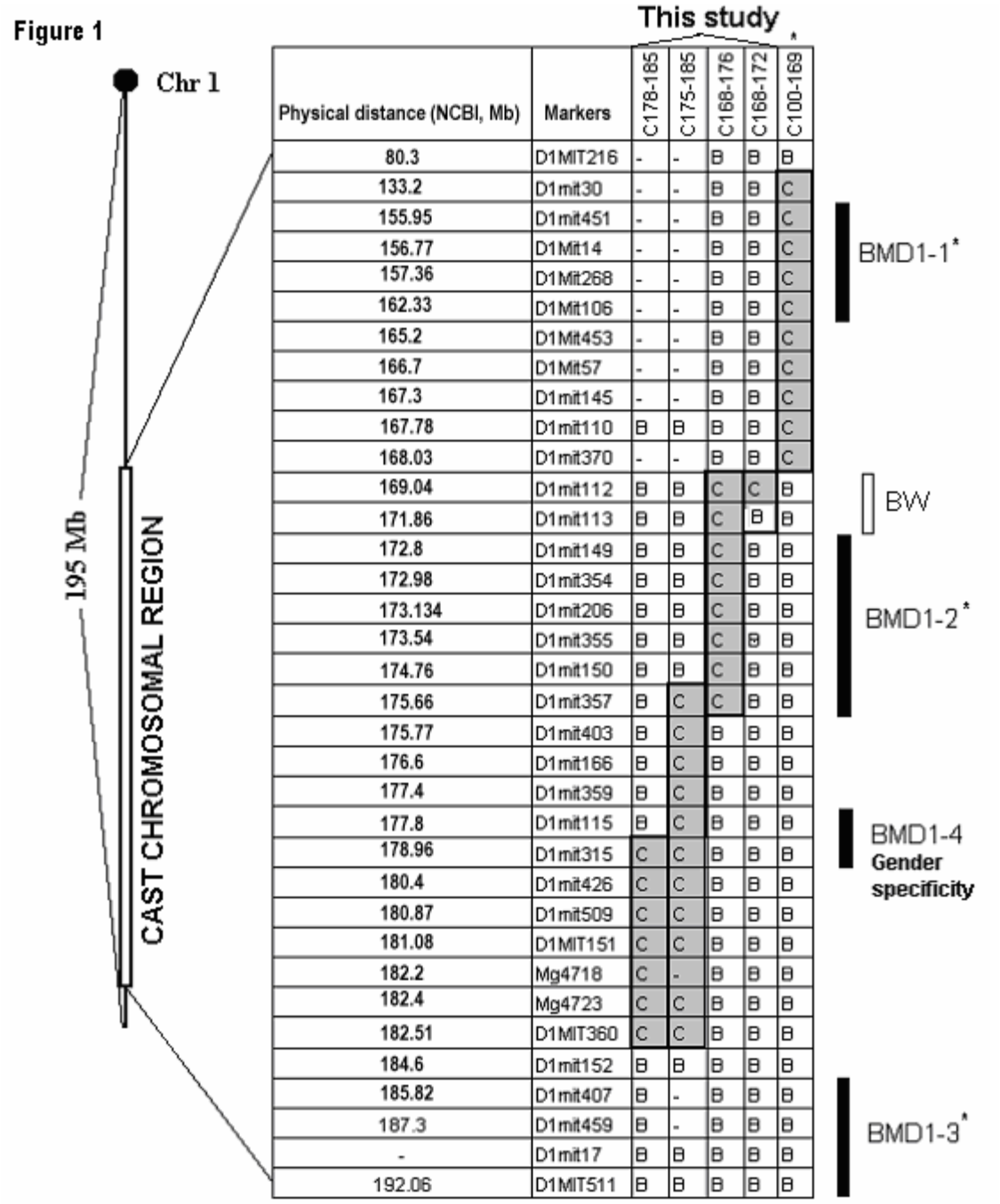

Physical distance (NCBI, Mb)	Markers	C178-185	C175-185	C168-176	C168-172	C100-169*
80.3	D1MIT216	-	-	B	B	B
133.2	D1mit30	-	-	B	B	C
155.95	D1mit451	-	-	B	B	C
156.77	D1Mit14	-	-	B	B	C
157.36	D1Mit268	-	-	B	B	C
162.33	D1Mit106	-	-	B	B	C
165.2	D1Mit453	-	-	B	B	C
166.7	D1Mit57	-	-	B	B	C
167.3	D1mit145	-	-	B	B	C
167.78	D1mit110	B	B	B	B	C
168.03	D1mit370	-	-	B	B	C
169.04	D1mit112	B	B	C	C	B
171.86	D1mit113	B	B	C	B	B
172.8	D1mit149	B	B	C	B	B
172.98	D1mit354	B	B	C	B	B
173.134	D1mit206	B	B	C	B	B
173.54	D1mit355	B	B	C	B	B
174.76	D1mit150	B	B	C	B	B
175.66	D1mit357	B	C	C	B	B
175.77	D1mit403	B	C	B	B	B
176.6	D1mit166	B	C	B	B	B
177.4	D1mit359	B	C	B	B	B
177.8	D1mit115	B	C	B	B	B
178.96	D1mit315	C	C	B	B	B
180.4	D1mit426	C	C	B	B	B
180.87	D1mit509	C	C	B	B	B
181.08	D1MIT151	C	C	B	B	B
182.2	Mg4718	C	-	B	B	B
182.4	Mg4723	C	C	B	B	B
182.51	D1MIT360	C	C	B	B	B
184.6	D1mit152	B	B	B	B	B
185.82	D1mit407	B	-	B	B	B
187.3	D1mit459	B	-	B	B	B
-	D1mit17	B	B	B	B	B
192.06	D1MIT511	B	B	B	B	B

Figure 4. **The regions of CAST Chr 1 transferred from CAST mice onto B6 background for the five congenic sublines.** The genotyping data for every marker are represented with "B" referring to homozygous *b6/b6*, "C" referring to *cast/cast*, or "-" for data not available. The names of the congenic sublines of mice are at the top. We used a letter "C" followed by the proximal and distal limits of *cast* alleles carried by the congenic sublines in megabases. The gray squares denote the CAST chromosomal regions carried by each congenic subline. The solid bars indicate the vBMD QTLs, and the open bar presents the QTL related with body weight (BW) trait. The polymorphic markers used for genotyping, with their physical positions along Chr 1 are presented at the left. vBMD loci are designated as *BMD1-1* for the first locus, *BMD1-2* for the

second locus, *BMD1-3* for the third locus (Edderkaoui et al., 2006), and *BMD1-4* for the fourth locus [13 and this study). * Previously identified/described by Edderkaoui et al., (2006).

Within female mice, the four congenic sublines of mice; C100-169, C168-176, C175-185 and C178-185 exhibited significantly higher femur BMD compared to B6 female mice. However, C168-172 female mice did not show any significant difference in femur vBMD when compared with B6 female mice (Fig.5). The C100-169 subline which carries CAST alleles at the *BMD1-1* locus and C168-176 subline which underlies the *BMD1-2* locus exhibited 4.2% and 8.0% increase of total vBMD (tot-BMD) compared to B6 female mice, respectively ($p<0.02$, Fig. 5A) and for femur mid-BMD; 10.0% and 6.8%, respectively ($p<0.02$, Fig. 5B) . The C175-185 and C178-185 congenic sublines of female mice showed 5% and 4.3% increase of total BMD, respectively (Fig. 5A), and 4.2.% and 4.8% increase of mid-BMD compared to B6 female mice (Fig. 5B).

Femur BMD of male mice showed a different phenotype than femurs of female mice when compared to gender matched B6 control mice, only C100-169 and C168-176 male mice showed significantly higher total BMD (3.5% and 5.2%, respectively) compared to B6 male mice (Fig. 5A), while C175-185 and C178-185 male mice have similar femur BMD as the B6 male mice (Fig. 5A), the gender specificity was confirmed after running 2-way-ANOVA and correction with Bonerroni *Post-hoc* test. The fact that total femur vBMD in congenic sublines of mice C175-185 and C178-185 is gender specific, while the vBMD in femurs isolated from C100-169 was not significantly affected by the gender, provided evidence for the presence of *BMD1-4* locus at 178-185 Mb of chromosome 1. As for femur mid-BMD (Fig. 2B), C100-169 male mice showed 4% increase compared to B6 male mice, while C168-176 male mice did not show any significant difference with B6 male mice. The 2-way ANOVA and *post-hoc* Bonferroni test confirmed the sex-specificity of femur mid-BMD phenotype showed by C168-176, it is likely that the region 168-176 Mb of Chr 1 carries two BMD genes; one gene affects femur total BMD in both male and female mice and another gene which is involved in mid-BMD variation for female mice only.

Figure 5A

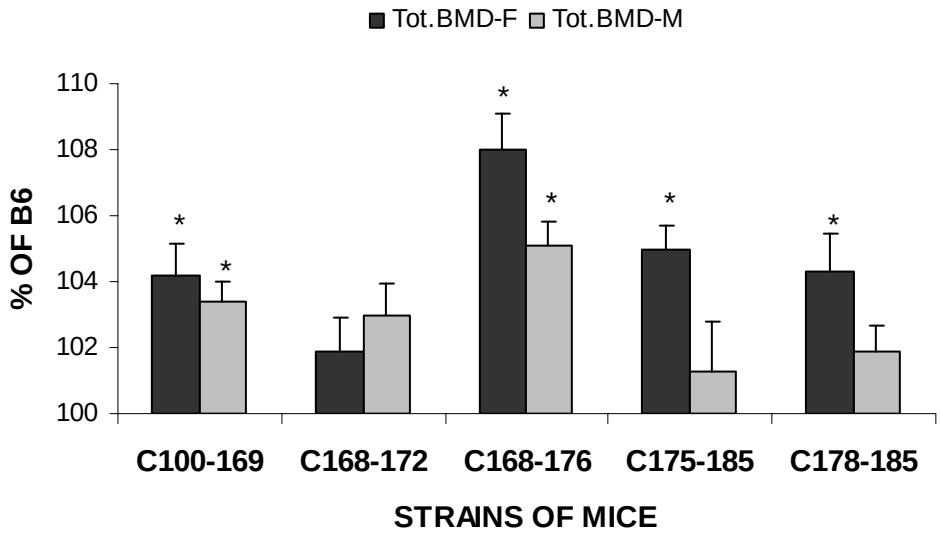

Figure 5B

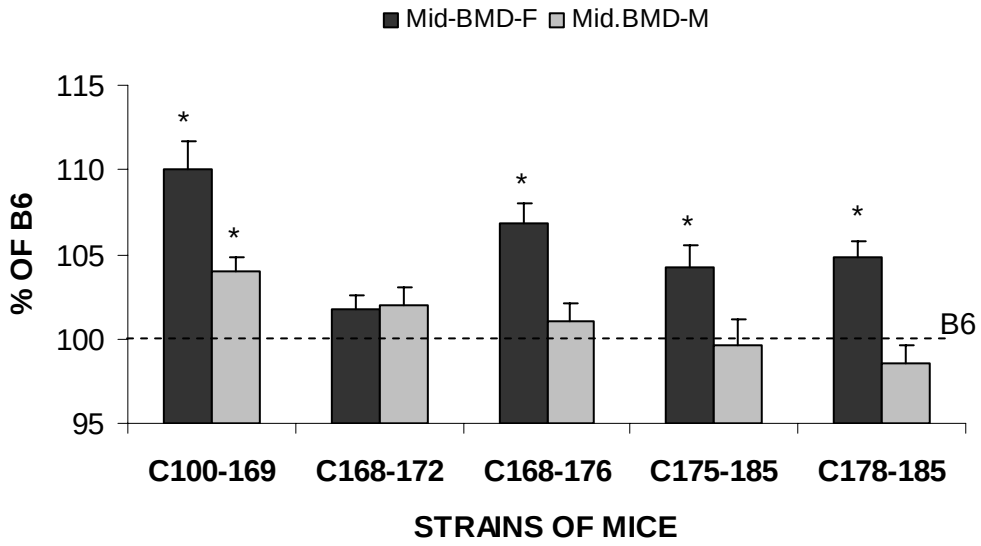

Figure 5. **Femoral vBMD of the five congenic sublines and B6 mice from both male and female mice. A. Total femur vBMD of the five congenic subline of mice compared to gender-matched B6 mice. B. Femur mid-diaphyseal vBMD of the five congenic subline of mice compared to gender-matched B6 control mice.** The data are expressed as a percentage of the gender-matched B6 mice. One-way ANOVA with LSD post-hoc test was ran to determine the significant differences between all congenic sublines and the gender-matched B6 mice. Then two-way ANOVA and bonferroni tests were ran to identify the sex specificity loci. The difference is considered significant when $*p<0.05$ after correction with post-hoc bonferroni test . Tot.BMD-F; refers to total femur vBMD in female mice, Tot. BMD-M; refers to total femur vBMD in male mice, mid.BMD-F; refers to femur mid-diaphysis vBMD in female mice, and mid.BMD-M refers to femur mid-diaphysis vBMD in male mice

We have also evaluated the body weights and femur length of these congenic sublines to determine if these two parameters co-segregate with femur BMD (Fig. 6); among all congenic sublines of female mice only C168-172 subline exhibited a smaller femur (3%) and a 7.5% reduced body weight compared to female B6 control mice ($p<0.03$). Body weight and femur length in the other sublines of female mice were similar to B6 female mice. However, among male mice C100-169, C168-172 and C168-176 sublines showed a significant decrease of body weight compared to age and gender-matched B6 control mice (9%, 6.2% and 6%, respectively, $p<0.01$). Femur length was slightly reduced in C100-169 and C168-172 sublines of mice compared with B6 control male mice. 2-way ANOVA and *post-hoc* bonferroni test confirmed the sex specificity of body weight showed by C100-169 and C168-176 but not C168-172 subline of mice.

Figure 6

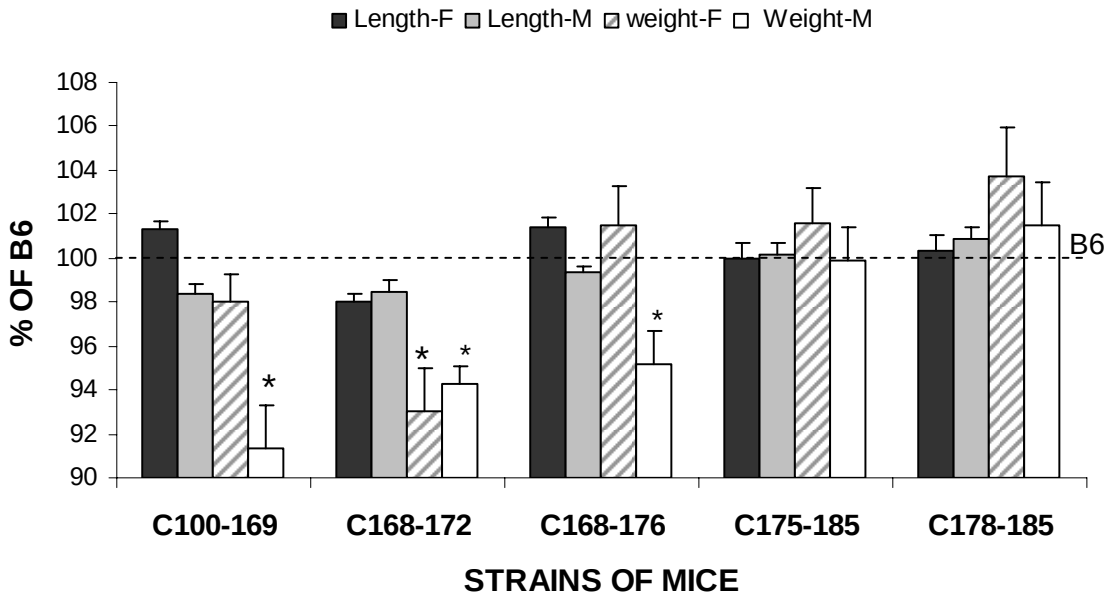

Figure 6. Femur length and body weight from the five congenic sublines and compared to gender-matched B6 mice. Length-F is femur length of female mice and Length-M: refers to femur length of male mice. Weight-F: is body weight of female mice Weight-M: refers to body weight of male mice. Body weight and femur length are expressed as a percentage of gender-matched B6 mice. *$p<0.05$ after correction with post-hoc bonferroni test.

In our previous studies, using B6.CAST congenic sublines of mice we found evidence that Chr 1 QTL is complex and carries at least three vBMD loci (Edderkaoui et al., 2006); *BMD1-1* and BMD1-2 exert a positive effect on femur vBMD while *BMD1-3* affects femur vBMD negatively. Furthermore, linkage analyses using B6-CAST. F2 female mice suggested the presence of another *BMD1-4* genetic locus (2007). In the present study, we have generated additional B6.CAST congenic sublines of mice; C100-169, C168-176 sublines of mice carry CAST

chromosomal segments which do not overlap with the CAST segment carried by C175-185 and C178-185 sublines, the fact that the female mice of these four sublines exhibit significantly greater femur BMD compared to female B6 mice suggests the presence of the *BMD1-4* at 178-185 Mb. Since our previous data (Edderkaoui et al., 2006) provided evidence that the region 180-184 Mb of Chr 1 is not involved in femur BMD variations, and by superimposing the CAST chromosomal regions carried by the C175-185 and C178-185 sublines we have narrowed down the size of the BMD1-4 to 2 Mb at 178-180 Mb in Chr 1.

Studies on B6.C3H-1T congenic mice have revealed evidence for the presence of sex effect (Turner et al., 2003) on Chr 1 vBMD QTL. Furthermore, based in our recent findings (Edderkaoui et al., 2006, and Edderkaoui et al., in press) and the finding of this study that the Chr 1 QTL contains four vBMD loci, we evaluated the skeletal phenotype of male and female mice to determine if one of these vBMD loci in Chr 1 QTL exhibits gender specific effect. Our present study provided evidence that *BMD1-4* locus exerts sex-specific effect on femoral vBMD. In contrast, no clear gender effect on *BMD1-1* locus was identified since the C100-169 congenic subline of mice that covers *BMD1-1* locus showed higher total femur and mid-diaphysis vBMD compared to B6 control mice in both male and females. However, the C168-176 subline of mice which carries the CAST chromosomal region that underlies *BMD1-2* locus exhibited a higher total femur vBMD in both male and female mice compared to age and gender matched B6 control mice, while femur mid-diaphysis vBMD (mid-BMD) was significantly greater in female but not male C168-176 subline of mice compared to gender-matched B6 progenitors. These data suggest that CAST chromosomal region at 168-176 Mb of the centromere carries two genes; one gene affects total femur vBMD in both male and female mice while the second gene affects mid-BMD for only female mice.
Furthermore, a body weight genetic locus determinant was identified at 168-172 Mb of Chr 1. Since both male and female C168-172 mice showed significantly smaller body weight compared to gender-matched B6 mice, while only male mice of C100-169 and C168-176 sublines exhibited smaller body weights compared to B6 male mice, it is possible that other CAST genes carried by C100-169 and C168-176 interact with CAST genes at 168-172 Mb to alter the effect of the body weight gene in female mice only.

Key Research Accomplishments

- We have sequenced Gas5 gene from the low bone mineral density B6 mice and the high bone mineral density CAST mice and identified the polymorphisms that could be responsible for the BMD variation between B6 and CAST mice.
- We have found that mouse Darc gene is syntenic with human 1q21-1q22; where a BMD QTL was identified in different human populations.
- We have identified a gender specificity BMD QTL at 178-180 Mb of chromosome 1

Reportable Outcomes

- **Accepted article in Genome Research Journal.**
Title: Identification of mouse Duffy Antigen Receptor for Chemokines (Darc) as a BMD QTL gene

Authors: Edderkaoui B, Baylink DJ, Beamer WG, Wergedal JE, Porte R, Chaudhuri A, and Mohan S.

Yu H, Mohan S, Edderkaoui B, Masinde G, Davidson H, Wergedal JE, Beamer, Baylink DJ. Detecting Novel Bone Density and Bone Size QTL Using a Cross of MRL/JpJ and CAST/EiJ Inbred Mice. Calcif Tissue Int. 80:103-110, 2007

- Submitted article to Bone Journal

Title: Complexity of sex effect in chromosome 1 revealed by congenic sublines of mice

Authors: Edderkaoui B, Baylink DJ, Beamer WG, Sultz KL, Wergedal JE, and Mohan S.

Conclusions

- We have found that mouse Darc gene is syntenic with human 1q21-1q22 at 157.44 Mb (within 1q21-1q25), mouse Darc shows 60% similarities with human DARC gene. In humans, the Duffy blood group system consists of four alleles, five phenotypes, and five antigens (Pogo and Chaudhuri, 2000). Duffy negative individuals are predominantly Africans and American blacks; they lack the Duffy protein on erythrocytes and are resistant to *Plasmodium vivax* and *Plasmodium knowlesi* infections (Miller et al., 1975 and 1976). In addition, it has been well established that African Americans exhibit significantly higher BMD compared to Caucasians (Yanovski et al., 2000 and Cauley et al., 2005). Our finding that total femur vBMD is increased in *DARC*-KO mice compared to B6 mice raises the interesting possibility that BMD variation between African Americans and Caucasians could be, in part, due to a difference in the function of *DARC* between the two groups.
- We have found that the BMD1-1 candidate gene Gas5 is located at the syntenic region in human chromosome 1.
- We have identified a gender specific BMD QTL at 178-180 Mb of chromosome 1 which will facilitate the screen for genes that affect BMD phenotype in a gender specific manner.

References

- Koller, D.L., Econs, M.J., Morin, P.A., Christian, J.C., Hui, S.L., Parry, P., Curran, M.E., Rodriguez, L.A., Conneally, P.M., Joslyn, G. et al. 2000. Genome screen for QTLs contributing to normal variation in bone mineral density and osteoporosis. *J Clin Endocrinol Metab.* **85**(9):3116-20.

- Ralston, S.H. 2002. Genetic control of susceptibility to osteoporosis. *J Clin Endocrinol Metab*. **87**(6):2460-6.

- Pogo, A.O. and Chaudhuri, A. 2000. The Duffy protein: a malarial and chemokine receptor. *Semin Hematol.* **37**(2):122-9.

- Miller, L.H., Mason, S.J., Dvorak, J.A., McGinniss, M.H., and Rothman, I.K. 1975. Erythrocyte receptors for (Plasmodium knowlesi) malaria: Duffy blood group determinants. *Science* **189**(4202):561-3.

- Miller, L.H., Mason, S.J., Clyde, D.F., and McGinniss, M.H. 1976. The resistance factor to Plasmodium vivax in blacks. The Duffy-blood-group genotype, FyFy. *N Engl J Med.* **295**(6):302-4.

- Yanovski, J.A., Sovik, K.N., Nguyen, T.T., and Sebring, N.G. 2000. Insulin-like growth factors and bone mineral density in African American and White girls. *J Pediatr.* **137**(6):826-32.

- Cauley, J.A., Lui, L.Y., Ensrud, K.E., Zmuda, J.M., Stone, K.L., Hochberg, M.C., and Cummings S.R. 2005. Bone mineral density and the risk of incident nonspinal fractures in black and white women. *JAMA*. **293**(17):2102-8.

- Edderkaoui B, Baylink DJ, Beamer WG, Wergedal JR, Dunn NR, Shultz KL, and Mohan S. 2006. Multiple Genetic Loci From CAST/EiJ Chromosome 1 Affect vBMD Either Positively or Negatively in a C57BL/6J Background. *J Bone Miner Res*. **21**:97-104.

- Turner CH, Sun Q, Schriefer J, Pitner N, Price R, Bouxsein ML, Rosen CJ, Donahue LR, Shultz KL, Beamer WG. 2003. Congenic mice reveal sex-specific genetic regulation of femoral structure and strength. *Calcif Tissue Int.* **73**:297-303.

- Edderkaoui B, Baylink DJ, Beamer WG, Wergedal JE, Porte R, Chaudhuri A, and Mohan S. Identification of mouse Duffy Antigen Receptor for Chemokines (*DARC*) as a BMD QTL gene. Accepted for publication in *Genome Research*.

TECHNICAL OBJECTIVE 2: TO IDENTIFY THE KEY GENES THAT ARE INVOLVED IN THE SOFT-TISSUE REPAIR/REGENERATION IN MRL/MPJ AND SJL/J MICE.

1. INTRODUCTION

Clinical treatments resulting in rapid wound healing without scar formation would lead to a better life for patients with various types of injuries, especially those wounded in the battlefield situations. It would also change the life of ordinary people by improving their cosmetic appearance. However, development of novel clinical treatments such as gene therapy would primarily depend on our understanding of the molecular mechanisms that are operating in wound healing and tissue regeneration.

One way to study the molecular mechanisms is to conduct genetic studies in comparable animals. Laboratory animals such as mice provide an economical and controlled environment to do so. It was found recently that the MRL/MpJ mouse strain could heal ear punch hole completely with no scar formation (Clark et al 1998; Heber-Katz, 1999). Our pioneering work in characterizing ear wound repair/regeneration in 20 representatively sampled inbred strains of mice has found that MRL/MpJ and its progenitor strain LG/J healed four times faster than other strains such as Balb/cByJ and SJL/J (Li et al., 2001). The same study also showed that the mouse ear hole healing rate was highly inheritable, with a heritability of 86%. Our quantitative trait locus (QTL) study has identified 10 QTLs for wound healing/soft tissue regeneration in the F2 of a cross between super healer MRL/MpJ (MRL) and poor healer SJL/J (SJL) (Masinde et al, 2001). The largest QTL was on chromosome (Chr) 9 with a LOD score of 16. It explained 15% of the phenotypic variance in the F2 population of MRL X SJL.

The ultimate goal of the project is to isolate genes that are responsible for the fast-wound healing/soft tissue regeneration phenotype within the identified QTL chromosome regions of the super healer MRL mice, with a priority on Chr 9. This would be the first major step in our understanding of the molecular mechanisms of wound healing/soft tissue regeneration.

To realize our goal, we propose to use a combination of approaches including in vitro functional assays. In the functional assays, the candidate genes identified in the QTL analysis and in the form of siRNA are applied directly in the cultures of cells such as those derived from the injured sites of the ear tissues. The inhibition or stimulation of the cultured cells by these genes will lead to identification of a more likely candidate gene. The specific objectives of the final grant period were to continue fine mapping of the Chr 4 and 9 QTL by using genotyping and congenic techniques. In addition, they also include developing in vitro functional testing methods and implementing them in the testing of the candidate genes identified through the QTL mapping.

Our specific objectives during the **final 4 months** of this grant period are as follows:

4) To continue fine mapping and functional testing and sequencing of candidate genes. This objective includes fine mapping of the QTL chromosomal regions (such as that on Chr 9, congenic analysis of the QTL regions using sub congenic lines, and sequencing of

the candidate genes in the QTL regions. Fine mapping and sequencing of the Chr 9 QTL has been done and covered in previous reports. This report mainly covers the congenic analysis of the Chr 9, 4 and 1 QTL. It also covers fine mapping of the Chr 4 QTL.

5) To continue to evaluate the likely candidate gene by comparing *in vitro* the phenotype produced by the MRL allele compared with the SJL allele.
This objective includes developing the in vitro siRNA assay using the cultured cells derived from the injured sites of the ears, and testing candidate genes using this in vitro assay.

2. BODY

Our progress in the final grant period for each of Specific Objectives 4-5 is summarized below.

Specific Objective 4: To continue fine mapping and functional testing and sequencing of candidate genes.

The Chr 9 QTL: congenic analysis

One way to narrow down the QTL region is to develop congenic strains which contain the desired allele of the QTL. After one or more congenic strains are created, sub-congenic lines can be generated that carry different length fragments of the QTL chromosomal region. Phenotypic analysis of these sub-congenic lines would lead to identification of the exact chromosomal location of the QTL. The objective of our congenic analysis was to develop congenic and sub-congenic lines in the poor healer SJL background that contain the better healing allele of the Chr 9 QTL from super healer MRL, then evaluating the performance of these congenic lines in the healing phenotype.

In order to develop congenic lines, we first crossed F1 female mice of MRL X SJL back to SJL/J males (recurrent parent). We obtained N2 mice. N2 mice were genotyped using markers specific for the QTL region on Chr 9 (**Table 1**). N2 heterozygous females that carried the MRL genotype in the QTL region were crossed back to SJL/J males to produce N3 congenics, which were again genotyped using the same markers. This process was repeated for more than 8 generations (N8). The overall proportion of contribution of genome by the non-recurrent parent can be estimated by the formulae of $(1/2)^{(8-1)}$. Thus, the MRL/MpJ genome present at the N8 congenics was only 0.78%. In other words, the genomic composition of an N8 congenic is almost identical to the recurrent SJL/J parent, with the exception of the MRL/MpJ contribution of the selected QTL region.

For phenotypic evaluation in healing, ear punch was done on the 3 weeks old animals of the congenic mice. Ear punch closure measurement was made at days 3, 7, 15, 21, and 25 after the punch was made. Fifteen male and fifteen female mice from each homozygous congenic line plus the MRL and SJL parental lines were used in the phenotype analysis. The methods of both phenotyping and genotyping were described previously (Li et al., 2001; Masinde et al., 2001; Masinde et al., 2006).

In the previous year, i.e. 2006, we reported that we have obtained a full congenic line named 9-1. Evaluation of this congenic strain has indicated that the male congenic mice showed significant better healing than male SJL mice. Their average ear hole size at 25 days post injury was 12% smaller than that of the male progenitor mice of poor healing SJL. The female congenic also healed better than female SJL mice at day 25 and later, but the difference was not significant.

As we reported last year, the Chr 9 QTL has been confirmed present in both male and female mice of our new MRL X SJL cross. Why did the Chr 9 congenic only exhibit significant phenotypic effect in male mice? Our further analysis indicated that it was due to sexual dimorphism that exists in the ear healing phenotype. Sexual dimorphism refers to the obervation that females heal better than males. Because of sexual dimorphism, any effect on healing would be masked in the better healing female mice, and in contrast, would be more pronounced in the poor healing male mice. We also observed a consistent trend of sexual dimorphism. **Figure 1** shows a typical response of male and female MRL mice to the ear punch injury. Therefore, we believe that void of sexual dimorphism, the congenic mice of the 9-1 line would show a significant healing improvement in both male and female mice compared to the poor healing progenitor mice of SJL.

The 9-1 line contains the entire region of the Chr 9 QTL, which is 38.2 cM (60.7 Mb) long. We have also obtained one sub congenic line at N10 generation, 9-2 (**Table 2**). This sub congenic strain only covers part of the Chr 9 QTL region, i.e. 9.8 cM (15.7 Mb) long on the proximal end of the Chr 9 QTL. We have evaluated this sub congenic line for healing response. There is a significant difference between congenic 9-2 male mice and SJL male mice. No significant difference exists between congenic 9-2 female mice and SJL female mice due to sexual dimorphism. The average ear hole size of the 9-2 line based on 16 mice was 13.70% smaller than the corresponding male SJL mice. These results are similar to what we obtained from the 9-1 full congenic line.

Although the 9-2 line only contains part of the Chr 9 QTL, the phenotypic effect of the congenic mice on healing rates is the same as that of the longer congenic line. There are two possibilities to explain this observation. First, the gene(s) that contributes to the Chr 9 QTL resides within the 9-2 region. In this sense, we have narrowed the whole Chr 9 QTL region from 38.2 cM to 9.8 cM. We can next identify the genes that are located between 38.2 cM (60.7 Mb) and 41.5 cM (76.45 Mb) of Chr 9, where the 9-2 line covers. We can now screen these genes to identify the candidate genes for wound healing and soft tissue regeneration. Secondly, the numbers of mice used in these experiments are not sufficiently large to make the assumption that congenic lines 9-1 and 9-2 have similar amount of phenotypic effect on ear healing. Much large numbers of mice are needed to make this determination. Just to make sure that 9-1 and 9-2 lines have the same amount of phenotypic effect, we will conduct experiments with much large numbers of mice for both the congenic lines and the SJL progenitor.

<u>The Chr 4 QTL: fine mapping and congenic analysis.</u>

The reasons to study the Chr 4 QTLs are multi-folds. First, like the Chr 9, Chr 4 harbors two QTLs for wound healing/soft tissue regeneration: Sth3 at 21.9 cM and Sth4 at 50.3 cM (Masinde et al., 2001). With LOD scores of above 6, they each explained about 6% of the phenotypic

variance in the F2 of MRL X SJL. They can be considered the third largest QTLs in this cross. Secondly, one of the Chr 4 QTLs, Sth4, is present in multiple crosses. We believe that it is the same as heal8, identified in the MRL X B6 cross, associated with markers D4Mit13 at 71 cM (Blankenhorn et al., 2003) and D4Mit148 at 66.7 cM (Heber-Katz et al., 2004). It was also found as Earheal2, associated with D4Mit170 at 66.6 cM in DBA X 129, with a better healing allele contributed by DBA (Masinde et al., 2006). Our recent analysis with the cross of MRL X CAST also showed that two markers at positions 60 and 66.6 cM on Chr 4, D4Mit203 and D4Mit170, were also associated with peaks of significant LOD scores (Yu et al., 2005).

If the Chr 4 QTL contains an important gene that regulates wound healing, then it should contribute to the wound healing phenotype in both male and female mice. Similar to what we have done for the Chr 9 QTL, we used additional 947 F2 mice (474 males and 473 females) in a second MRL X SJL cross to confirm the QTL. The markers used for linkage analyses of Chr 4 QTL are shown in **Table 3**. In these studies, we obtained significant LOD scores from both the female (**Figure 3A**) and male (**Figure 3B**) mice of the new cross. The highest LOD score was 7.42, and occurred between D4Mit31 and D4Mit308 in the females (**Figure 3A**). In the males, the highest LOD score was 5.72 and occurred between D4Mit178 and D4Mit31 (**Figure 3B**). In a separate analysis, we have combined these data with the 633 female mice from the original study (Masinde et al., 2001) to obtain a total of 1,580 mice. The LOD score for the combined F2 population was 20.02 at the highest peak at 115.07 Mb between D4Mit31 and D4Mit308 (**Figure 3C**). The 2-LOD Interval spanned from 107.07 Mb to 123.07 Mb. This region explained 7.3% of the phenotypic variance. In addition, we have also carried a preliminary analysis using the Bayesian Shrinkage method for the combined data (**Figure 4**). The results show that there are two major QTL peaks at 87.9 and 103.8 Mb, corresponding to the major peak region of the MapQTL analysis (**Figure 3C**). There is no peak at 50 Mb, where MapQTL analysis showed a peak. In conclusion, we have confirmed existence of Sth4 in the male mice as well as in a second group of female mice of MRL X SJL. This has provided a strong rationale for further study of Sth4. Furthermore, the Shrinkage analysis has provided a clue to how many genes may be present in the QTL region.

For the Chr 4 congenics, we have advanced the crossing to the N9-10 generations. The congenic fragment from the MRL parent in congenic #1 is from 8.7 cM to 76.5 cM (**Table 4**). This chromosomal fragment covers both QTLs Sth3 at 21.9 cM and Sth4 at 50.3 cM. **Table 4** also shows that we have congenic mice with a shorter chromosomal fragment, congenic #2. We are now crossing N10 heterozygous mice with each other to obtain homozygous congenic lines.

Preliminary analysis of four heterozygous mice of the #2 congenic line at N10 generation, i.e. the line that contains a shorter Chr 9 fragment, showed very promising results. Based on two measurements for each ear hole on both left and right for each mouse, wound healing rates were significantly different between the congenic mice and the poor healing SJL mice 15 days after ear punch (**Figure 5**). The congenic mice showed much smaller hole size than the SJL mice even in the heterozygous state. We anticipate an even larger difference between homozygous congenic mice vs. SJL mice. These data and the QTL data showing the presence of Chr 4 QTL in multiple crosses provide definitive evidence that Chr 4 contains key wound healing gene/s. We have planned experiments to confirm these data using homozygous congenic mice and using the ear punch model as well as the tail wounding model.

The Chr 1 QTL: congenic analysis.

As we have mentioned, there are 10 QTLs that were identified in the cross of MRL X SJL (Masinde et al., 2001). Besides the Chr 9 QTL, which is most important, the Chr 1 QTL also appears to be important. With a LOD score of 7, the Chr 1 QTL explained about 7% of the F2 phenotypic variance. Therefore, it is a very important QTL to study in wound healing/soft tissue regeneration.

For the Chr 1 congenics, we have advanced the crossing to the N6-7 generations. The congenic fragment from the MRL parent is from 0 to 110 cM on chromosome 1 (**Table 5**). This covers the QTL peak at 49.2 cM. It can be seen that five mice N6#6F, N6#6M, N6#17F, N6#17M and N7#2M are all heterozygous for the chromosomal region, and can be backcrossed to SJL in order to advance the congenics to higher generations.

Specific Objective 5: To continue to evaluate the likely candidate gene by comparing *in vitro* the phenotype produced by the MRL allele compared with the SJL allele.

Cell culture system for in vitro testing.

For in vitro testing, we need to establish a cell culture system, where MRL is more prolific than poor healing strains. In order to determine whether there is a difference in cell proliferation between super healer MRL and poor healing strains, and whether cell culture can be used in the in vitro testing, we have successfully developed methods of establishing cell cultures from ear tissues of individual mice so that proliferation rates can be statistically calculated for different strains (**Figure 6**). In addition, we were also able to determine the proliferation rates using Alamar Blue assay on the passage 3 cultured cells.

Results showed that there was a significant, more than 30% difference between the two mouse strains (**Table 6**). In addition, two lines of evidence suggested that this difference was innate. First, the assay was conducted after cells were cultured for at least two weeks, indicating this difference was not a simple carry-over effect from the tissues. Secondly, cells obtained from the initial punch tissues and cells from the surrounding tissues a week later had the same proliferation rates for each mouse strain. In other words, the proliferation potential was not either stimulated due to the punch injury or lost during in vitro culture. Therefore, the difference of cell proliferation rates between MRL and SJL can explain the healing response of the two strains. In addition, we observed that cells from the male mice tend to proliferate faster than those from the female mice within each strain (**Table 6**), correlating with the in vivo observations that male mice grow faster and are usually bigger than female mice. Therefore, the super healing ability of the MLR mouse is due to the faster proliferation rates of the ear cells of MRL mice. Cell culture can be used as in vitro system to study gene expressions and to test gene functions.

With regard to the time course of the differential proliferations between super healer MRL cells and poor healing SJL cells, we conducted a time course experiment with passage 4 cultures derived from freezing cells. The results showed that MRL and SJL began to show statistically

significant differences as earlier as four hours or even earlier (four hours after the dye was incorporated into the 24 hours acclimated culture) (**Figure 7**). This difference lasted until the cultures became confluent, in other words, there is no room to grow. Therefore, the difference in proliferation rates between MRL and SJL observed at 24 hours is confirmed by that in the earlier hours of the cultures.

In vitro testing of candidate genes.

This work will be initiated shortly.

3. ADDITIONAL PROGRESS

Mechanisms of wound healing and soft tissue regeneration.

In order to identify what mechanisms cause the superior healing ability of the MRL mouse, we carried out two ear punch experiments using MRL mice (15 males and 15 females in each experiment) by punching holes in different regions of the ears. The objective was to determine the effect of ear regions on the healing rates. Normally, we punch one hole at the center of the lower cartilaginous part of the ear for both ears. In the first experiment, we punched a regular hole ("center" punch) on the left ear as the control (**Figure 8**). On the right ear, we punched three holes, all being located differently from the normal position. One hole ("inner" punch) was shifted 2 mm from the regular position towards the ear canal. A second one ("outer" punch), which was shifted to just 2-mm from the farthest edge, was the farthest from the ear canal. The third hole ("edge" punch) was shifted towards the nearest edge of the ear and placed just above the edge of the lower portion of the ear. In the second experiment, we punched two holes on the left ear: a "center" punch and an "inner" punch. One the right ear, we punched two holes: an "inner" punch and an "upper" punch. The "upper" punch is at the same distance from the ear canal but on the upper and thicker part of the ear.

In the first experiment, ANOVA analysis shows that sex of mice and position of the punch affects the healing rate significantly ($P<0.01$). However, there were no significant interactions between these two parameters ($P>0.05$). This means that although sex affected healing of each hole, it did not affect the healing of different holes in different manners. It is known that due to sexual dimorphism, female mice heal faster than male mice. The three punch holes on the right ear all healed significantly differently from each other, and also from the regular punch on the left ear ($P<0.01$) (**Figure 9**). The inner punch healed much faster than the regular punch on the left ear. Most of the mice closed this hole within 25 days as shown in **Figure 9**. It should be noted that based on our past experience there is no difference in healing rates between the normal punch holes of the left and the right ear. While the outer punch healed slower than the regular punch, the slowest healing punch was the edge punch.

For the second experiment, ANOVA analysis indicates that only the position of the punch affects the healing rate ($P<0.01$). On the left ear, just like in the three hole punch experiment, there was a significant difference between the regular punch and the inner punch ($P<0.01$) (**Figure 10**). One the right, there was no significant difference between the inner punch and the upper punch at all ($P>0.05$). Although there is a slight significant difference ($P=0.042$) between the inner

punch one the left and that on the right ear, it may be due to smaller sample sizes. It seems that the inner punch on both ears and the upper punch on the right ear all healed at similar rates.

From the three hole experiment we can see that the farther from the ear canal, the slower the healing rate and inversely, the closer to the ear canal, the faster the healing rate. Therefore, the healing rate is negatively correlated to the distance from the ear canal. The only exception is the healing rate on the edge of the ear, which is slowest. Our conclusion is reinforced by the two hole experiment, where the inner hole and upper hole, at the same distance from the ear canal healed almost at the same rates. These experiments may mean that the agent that caused the faster healing in MRL mice are either carried in or transported by the blood, or at the beginning the neurons extending out from the ear canal.

4. KEY RESEARCH ACCOMPLISHMENTS

- We have developed one sub congenic line for the Chr 9 QTL named 9-2. This congenic line showed similar amount of phenotypic effect on wound healing and soft tissue regeneration as the full congenic line 9-1.

- We have confirmed the Chr 4 QTL using additional F2 mice and fine mapped the QTL region using the Bayesian shrinkage estimation method. These mapping results will help in identification of candidate genes for wound healing and soft tissue regeneration.

- We have advanced the Chr 4 congenics to N10 generation. Among the heterozygous congenic mice, there is one congenic line and one sub congenic line. We have evaluated the phenotypic effect of a few heterozygous mice of the sub congenic line. We are in the process of establishing homozygous congenic lines.

- We have advanced the Chr 1 congenics to N6-7 generation.

- We have successfully developed methods of establishing cell cultures from the tissues of the injured sites of the ears of individual mice so that proliferation rates can be statistically calculated for different strains. In addition, we were also able to determine proliferation rates of the cultured cells using Alamar Blue assay.

- We have determined that the time course of the differential proliferations between super healer MRL cells and poor healing SJL cells was at 4 hours or even earlier.

- We have conducted experiments to determine the mechanisms of wound healing and soft tissue regeneration by examining the healing rates in different regions of the ears. We found the healing rate is negatively correlated with the distance from the ear canal.

5. REPORTABLE OUTCOME

Li X, Quigg R, Zhou J, Xu S, Masinde G, Mohan S, Baylink DJ. A critical Evaluation of the effect of Population Size and Phenotypic Measurement on QTL Detection and Localization using a large F2 Murine Mapping Population. Genetics and Molecular Biology. 29 (1):166-173, 2006.

Yu H, Baylink DJ, Masinde GL, Li R, Nguyen B, Davidson HM, Xu S, Mohan S. (2007) Mouse Chromosome 9 Quantitative Trait Loci for Soft Tissue Regeneration: Congenic Analysis and Fine Mapping. Wound Repair and Regeneration in press.

6. CONCLUSIONS

- Although the 9-2 line only contains part of the Chr 9 QTL, its phenotypic effect on the ear healing rates is the same as that of the longer congenic line. This means that the gene responsible for wound healing and soft tissue regeneration might be located within the 9-2 region of the chromosome.

- Being confirmed in a new MRL X SJL cross, The Chr 4 QTL is one important QTL for wound healing and STR. Phenotypic analysis of one sub congenic line for the Chr 4 QTL using a few heterozygous mice indicated that it significantly improved the ear healing rates compared to the poor healing progenitor mice of SJL. This observation confirms the phenotypic effect of the Chr 4 QTL.

- In vitro cell culture experiments show that there was a significant, more than 30% difference in proliferation rates between super healer MRL and poor healer SJL cells at 24 hours culture. The time course study indicated that the significant difference began at 4 hours culture or even earlier.

- The three hole and two hole punch experiments indicated that the healing rates are inversely correlated with the distance from the ear punch position to the ear canal: the closer to the ear canal, the better the healing rate. Therefore, blood flow seems to promote the healing process.

7. REFERENCES

Blankenhorn EP, Troutman S, Clark LD, Zhang XM, Chen P, Heber-Katz E. (2003) Sexually dimorphic genes regulate healing and regeneration in MRL mice. Mamm Genome. 14, 250-60.

Clark LD, Clark RK, Heber-Katz E. (1998) A new murine model for mammalian wound repair and regeneration. Clin Immunol Immunopathol. 88:35-45.

Heber-Katz E. (1999) The regenerating mouse ear. Semin Cell Dev Biol. 10, 415-9.

Heber-Katz E, Leferovich JM, Bedelbaeva K, Gourevitch D. (2004) Spallanzani's mouse: a model of restoration and regeneration. Curr Top Microbiol Immunol. 280, 165-89.

Li X, Gu W, Masinde G, Hamilton-Ulland M, Xu S, Mohan S, Baylink DJ. (2001) Genetic control of the rate of wound healing in mice. Heredity. 86, 668-74.

Masinde GL, Li X, Gu W, Davidson H, Mohan S, Baylink DJ. (2001) Identification of wound healing/regeneration quantitative trait loci (QTL) at multiple time points that explain seventy percent of variance in (MRL/MpJ and SJL/J) mice F2 population.
Genome Res. 11, 2027-33.

Masinde, GL, Li R, Nguyen B, Yu H, Srivastiva AK, Edderkaoui B, Wergedal JE, Baylink DJ, Mohan S. 2006. New quantitative trait loci (QTL) that regulate wound healing in an intercross progeny from DBA/1J and 129X1/SvJ inbred strains of mice. Functional and Integrated Genomics. 6(2):157-63.

Yu H, Mohan S, Masinde GL, Baylink DJ. 2005. Mapping the dominant wound healing and soft tissue regeneration QTL in MRL X CAST. Mammalian Genome. 16(12): 918-24.

Table 1. Markers used to map soft tissue QTL on chromosome 9.

Marker	WI Map[a] (cM)	MGI Map [b] (cM)	Physical Dis.[c] (Mb)
D9MIT43	2.2	4	10.09
D9MIT90	7.7	9	32.49
D9MIT229	23	28	49.66
D9MIT71	24	29	50.34
D9MIT207	31.7	33	60.78
D9MIT208	33.9	36	62.49
D9MIT336	33.9	35	65.82
D9MIT263	40.4	42	75.97
D9MIT270	41.5	43	76.45
D9MIT343	41.5	43	80.87
D9MIT133	41.5	43	84.52
D9MIT196	42.6	48	86.33
D9MIT111	42.6	48	86.99
D9MIT9	42.6	48	87.62
D9MIT269	41.5	43	88.38
D9MIT157	43.7	49	89.75
D9MIT308	43.7	49	90.59
D9MIT344	42.6	48	94.22
D9MIT76	43.7	49	95.5
D9MIT35	47	52	98.64
D9MIT114	47	52	98.65
D9MIT355	49.2	49.2	98.66
D9MIT182	53.6	55	101.42

[a] Whitehead Mouse Genetic Map

[b] Mouse Genome Database Genetic Map

[c] Physical distance as of September 20, 2004

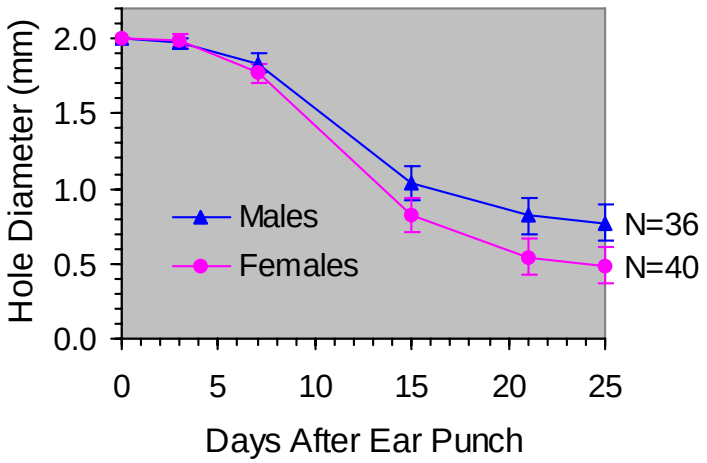

Figure 1. Sexual dimorphism in the ear healing of MRL mice. Values shown are means ± SEM.

Table 2. Genotypes of congenic mice for Chr 9 markers[a]

Map Pos (cM)	2	8	23	24	32	34	40	42	44	47	49	54	56	60	63	70
Map Pos (Mb)	10	32	50	50	61	66	76	76	90	99	99	101	103	111	117	121
Marker (D9Mit-)	43	90	229	71	207	336	263	270	157	35	355	182	347	350	201	151
9-1	S	S	S	S	M	M	M	M	M	M	M	M	M	M	M	M
9-2	S	S	S	S	M	M	M	M	S	S	S	S	S	S	S	S

[a] M: homozygous for MRL; S: homozygous for SJL.

Table 3. Chr 4 markers to be used in genotyping.

Marker	Position (cM)	Position (Mb)
D4Mit264	1.9	9.32
D4Mit227	3.2	9.93
D4Mit18	5.2	13.94
D4Mit268	17.9	20.68
D4Mit196	12.1	39.59
D4Mit214	17.9	45.57
D4Mit17	31.4	62.46
D4Mit178	35.5	66.27
D4Mit9	44.5	94.04
D4Mit31	51.3	106.07
D4Mit308	57.4	123.19
D4Mit203	60.0	128.60
D4Mit204	61.9	132.39
D4Mit170	66.6	137.50
D4Mit234	71.0	
D4Mit42	81.0	150.06
D4Mit190	79.0	152.98
D4Mit256	82.7	153.48

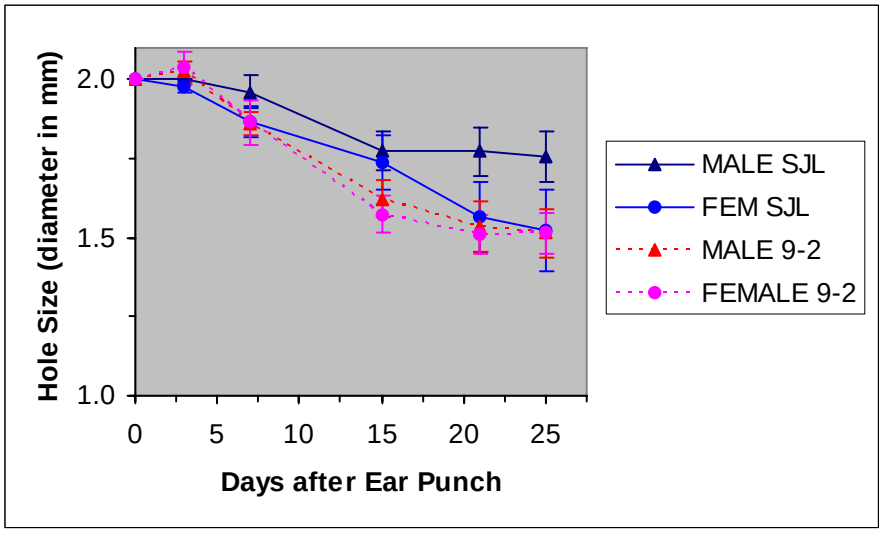

Figure 2. The healing rates of the congenic mice of the 9-2 line compared to the poor healing progenitor mice of SJL. Values shown are mean ± SEM. N = 5 male SJL, 5 female SJL, 16 for male 9-2, 15 for male 9-2 mice.

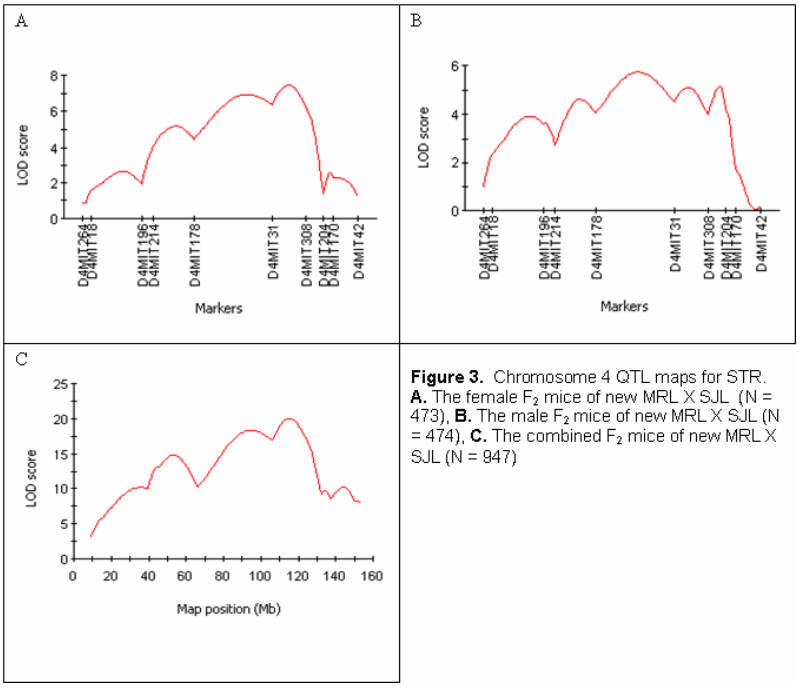

Figure 3. Chromosome 4 QTL maps for STR. **A.** The female F_2 mice of new MRL X SJL (N = 473), **B.** The male F_2 mice of new MRL X SJL (N = 474), **C.** The combined F_2 mice of new MRL X SJL (N = 947)

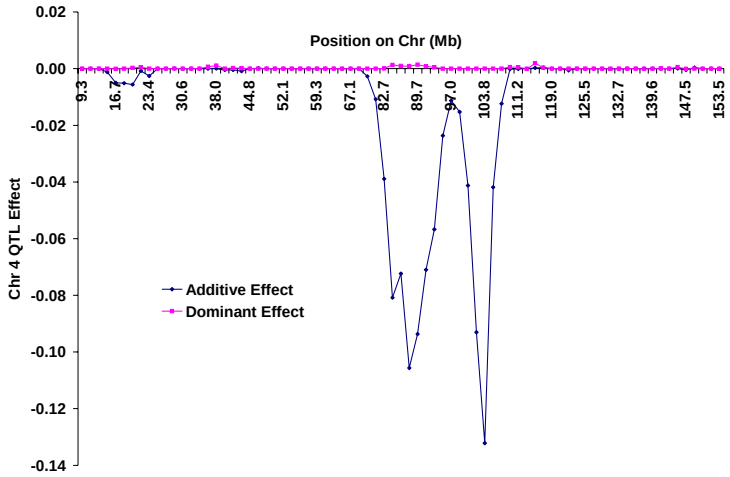

Figure 4. Preliminary Bayesian Shrinkage analysis of the Chr 4 QTL. Negative values indicate the decreasing effect of the QTL on the ear hole sizes.

Table 4. Genotype of congenic mice for Chr 4 markers.

Map Pos (cM)	5.2	12.1	17.9	35.5	51.3	60.0	61.9	69.9	81.0
Marker (D4Mit-)	18	196	214	178	31	203	204	170	42
Congenic #1	H	H	H	H	H	H	H	H	H
Congenic #2	H	H	H	H	H	H	H	S	S

Note: H = heterozgyotes for MRL and SJL; S: homozygouse for SJL.

Table 5. Genotypes of N4 congenic mice for chromosome 1 markers at different chromosomal positions.

Mouse ID	D1MIT64 0 cM	D1MIT316 3.3 cM	D1MIT231 8.7 cM	D1MIT33 36.1 cM	D1MIT19 37.2 cM	D1MIT216 49.2 cM	D1MIT185 59 cM	D1MIT102 75.4 cM	D1MIT291 103.8 cM	D1MIT17 110.4 cM
N6#16F	H	H	H	H	H	H	H	H	H	H
N6#16M	H	H	H	H	H	H	H	H	H	H
N7#2M	H	H	H	H	H	H	H	H	H	H
N6#17M	H	H	H	H	H	H	H	H	H	H
N6#17F	H	H	H	H	H	H	H	H	H	H

H denotes the heterozygous genotype between MRL and SJL.

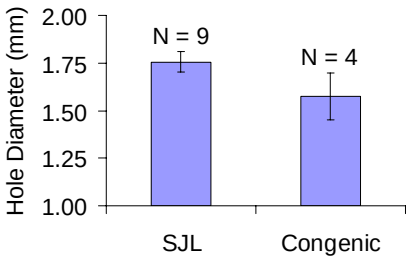

Figure 5. Comparison of wound healing rates between heterozygous congenic #2 mice and homozygous SJL mice 15 days after ear punch. Student's t-Test *P* = 0.037, indicating a significant difference.

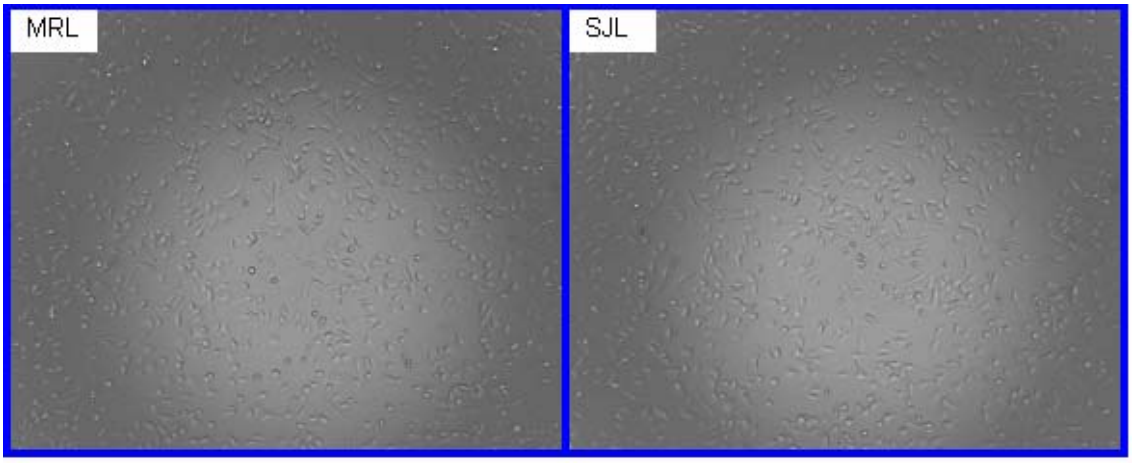

Figure 6. Cultured cells (at 50-60% confluency) derived from the explant tissues of the initial ear punch injury. The images are under 4X magnification.

Table 6. Parameters of growth, healing and *in vitro* cell proliferation for MRL and SJL (mean + SEM) [ab]

	Body Weight at Ear Punch (g)	Body Weight Change in a Week (g)	Ear Hole Size a Week Later (mm)	Cell Density Reading (Signal Unit)
MRL F	20.40 + 0.20	4.72 + 0.35	1.56 + 0.08	439.47 + 8.33
MRL M	19.88 + 0.31	7.49 + 0.58 x	1.59 + 0.06	472.23 + 30.22
SJL F	12.10 + 0.25 xy	3.44 + 0.19 xy	1.76 + 0.05 x	315.43 + 15.89 xy
SJL M	16.03 + 0.86 xyz	2.51 + 0.45 xy	1.93 + 0.05 xy	363.37 + 25.08 xy

[a] x, y, z denote a significant difference ($P < 0.05$) from MRL females, MRL males and SJL females, respectively.

[b] Six holes (3 on each ear) were punched and 48 wells of cells were counted for each mouse. However, statistical analysis presented here was based on the means obtained for each mouse. There were 4 mice in each group.

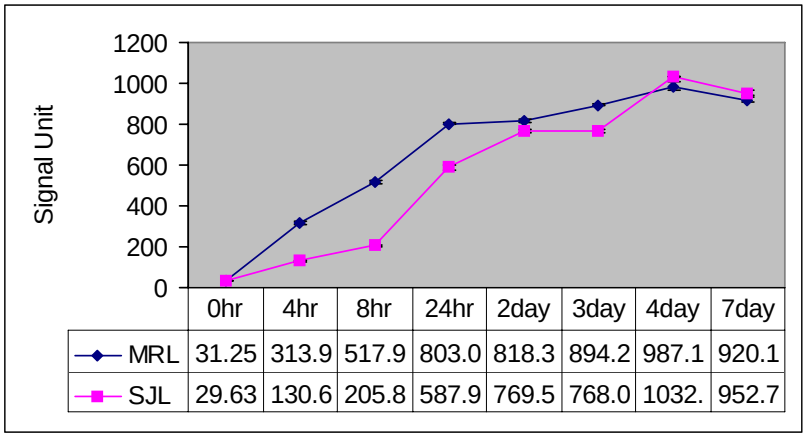

Figure 7. Comparison of differential proliferation rates of passage 4 cells between super healer MRL and poor healing SJL. Each data point is the average of 24 wells in the 96 well plates with half from one of the two male mice used for each strain in the assay. The beginning cell count was 2,000/well. The 0 hour time point refers when the dye was incorporated after 24 hours of acclimation in the culture.

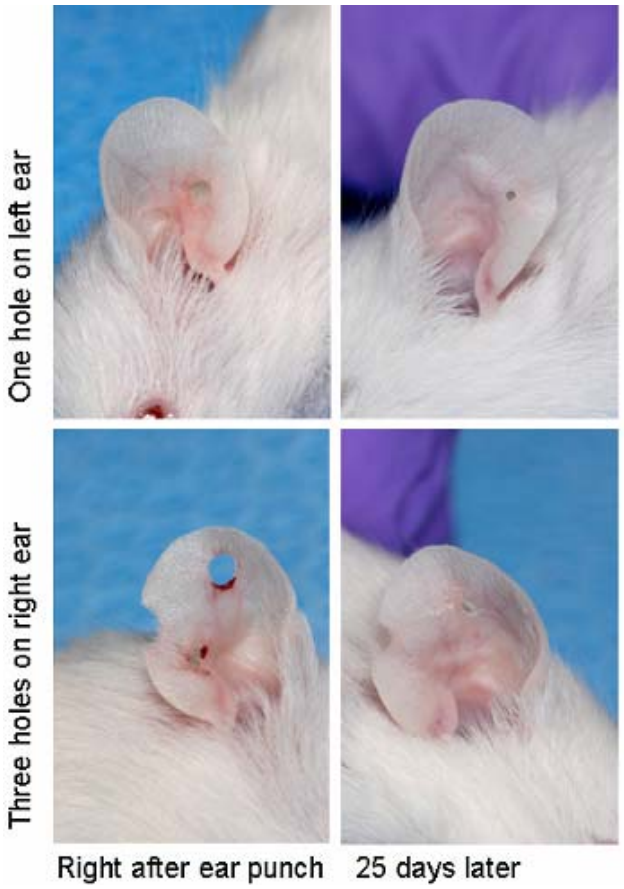

Figure 8. Comparing the healing rates of different regions of the ears in MRL mice.

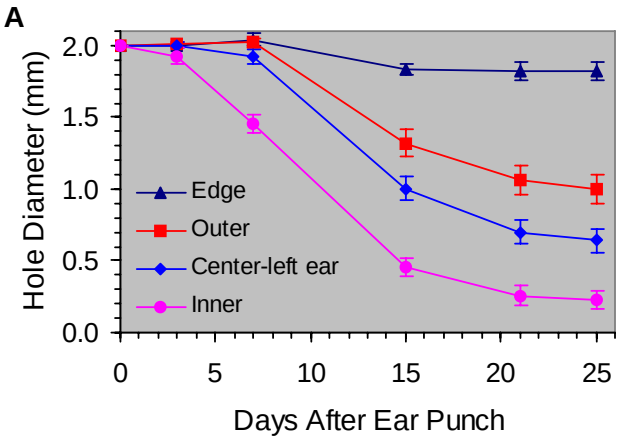

Figure 9. Comparing the healing rates of different regions of the ears in MRL mice. Values are shown as Mean+SEM.

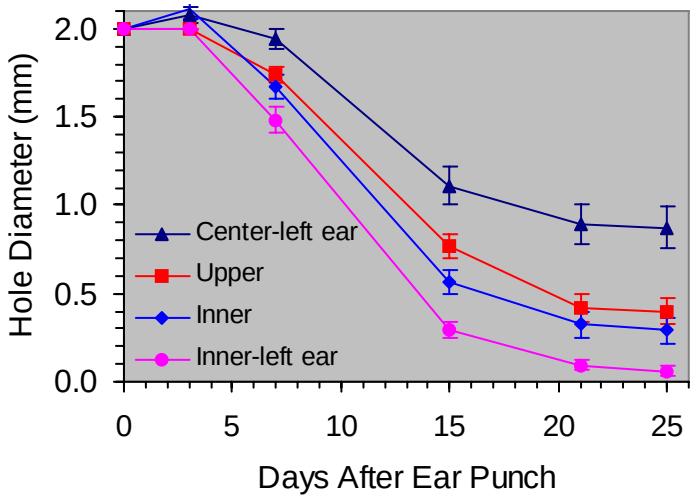

Figure 10. Comparing the healing rates of different regions of the ears in MRL mice. Values are shown as Mean+SEM.

Technical Objective 3: To apply the ENU (Ethyl N-Nitrosourea) mutagenesis to identify new genes that regulates soft- and hard-tissue regeneration in C3H strain of mice.

Introduction

The main goal of Technical Objective-3 is to identify and characterize novel genes or to elucidate the function for known genes that play key role in the soft-tissue regeneration and musculoskeletal phenotypes using the ENU mutagenesis technique in C3H/HeJ (C3H), C57BL/6J (B6), and MRL/MpJ (MRL) mice. Technical Objective 3 was revised for the current grant period; the description of the revised specific objectives is given below.

REVISED NEW SPECIFIC OBJECTIVES

Our specific approaches during the **first 12 months** of this grant period are as follows:

1) To breed selected mutants identified in earlier ENU screens.

a) Breed 5-8 selected lines of previously screened phenodeviants with wild type B6, C3H and MRL mice to confirm inheritability of each mutant line and generate additional affected mice for further characterization of the phenotypes.

b) To perform following screening of the F1-F3 progeny generated from mutant mice: i) body weight; ii) body composition; iii) bone density; iv) biochemical markers; and v) soft-tissue regeneration.

c) Maintain a small breeding colony of all interesting phenodeviants that are confirmed for inheritance testing in specific objective 1.a.

2) To determine the chromosomal location of mutant gene responsible for the selected mutant phenotypes, we will:

a) Select mouse mutant/s for genotyping based on the importance of phenotype and based on the magnitude of change in phenotype induced by ENU mutation

b) Breed selected mutant C3H, B6 or MRL phenodeviant mouse with another inbred strain of mouse (chosen based on the similarity in phenotype with wild type C3H, B6, SJL, or MRL and availability of markers for genotyping) to produce F1 mice

c) Intercross F1 mice to produce approximately 50-100 F2 mice

d) Screen F2 progeny for phenotype and extract genomic DNA from ear punch for genotyping

e) Perform a genome wide scan using appropriate SNPs and/or polymorphic microsatellite informative markers representing all chromosomes with average length of 5-20 cM

f) Perform interval mapping using commercially available software and determine the significance level of interval mapping.

g) Identify unique QTL in ENU mutant mice by comparison of all background QTL's in the progenitor strains. For this purpose, we will breed non-mutagenized MRL mouse with another inbred strain of mouse (same as used for genotyping described above in item #a) to produce F1 mice. Intercross F1 mice to produce approximately 50-100 F2 mice.

Screen F2 progeny for phenotype and extract genomic DNA from ear punch for genotyping. Perform a genome wide scan using appropriate SNPs and/or polymorphic microsatellite informative markers representing all chromosomes with average length of 5-20 cM. Perform interval mapping using commercially available software and determine the significance level of interval mapping.

3) To identify the candidate gene in the chromosomal locus established for the selected mouse mutant in specific objective 2 of year 1:

a) We will extract RNA from appropriate tissue of mutant mice and corresponding control mice
b) We will perform in house microarray to identify genes that are differentially expressed in the mutant versus control mice

Our specific objectives during the final 4 months **of this revision are as follows:**
1) To identify the candidate gene in the chromosomal locus established for the selected mouse mutant:

a) We will analyze the microarray data collected during first 12-months of the grant period to identify differentially expressed genes in mutant mouse as compared to non-mutagenized control mice
b) We will identify if differentially expressed genes represent a pathway that is controlled by an upstream regulatory gene located in the chromosomal region for mutant gene

Our progress on the Revised Specific Objectives 1-3: BODY

I. SPECIFIC OBJECTIVE 1

The main aim of the **Specific Objective-1** was to breed 5-8 selected lines of previously screened phenodeviants with wild type B6, C3H and MRL mice to confirm inheritability and to generate additional affected mice for further characterization of the phenotypes, and to maintain a small breeding colony of all interesting phenodeviants that are confirmed for inheritance testing. Consequently, our progress in Specific Objective 1a-c includes breeding and generation of 11 phenotypic deviant lines identified in previous years. The mice generated and screened included progeny from both dominant and recessive mutations for various phenotypes such as soft tissue regeneration, growth, musculoskeletal phenotypes, blood chemistry, and blood hematology phenotypes.

1. **SPECIFIC OBJECTIVE 1a.** To generate F1 & F3 mice for dominant and recessive screening, respectively, we bred 11 phenodeviants identified in previous reporting periods. Since, we focused on breeding and mapping these interesting mutations we did not generate new mutations. We bred each phenodeviant male or female mice with two 8-12 week old wild type WT B6, C3H or MRL male/female. Females are checked routinely for pregnancy, and the pregnant mice are removed from mating cages and replaced with fresh females. Breeding was continued until at least 20 progeny was screened from each male/female phenodeviant mice. Several phenodeviant mice did not produce the required number of mice and hence could not be confirmed as mutant strain.

The generation and screenings of mice were performed as described in **Figure-1**. For dominant screening, we bred four previously identified phenodeviants (**Table-1**). During this reporting period, we have generated 303 mice from dominant phenodeviants.

For recessive screen, we bred seven previously identified phenodeviants (**Table-2**). Each phenodeviant male or female mice was mated with 2 normal wild type female or male mice at one time. Once the mating was successful, pregnant mice were separated and placed individually to give birth to F2 littermates. If a F2 litter had 3-4 female mice, they were used to generate F3 progeny. Otherwise, a new WT female was bred until 3-4 F2 females were obtained. Each F2 female was reintroduced for mating with an F1 male to produce at least one litter with minimum 4 pups. The aim was to screen a minimum of three litters from each line. During this reporting period, we have generated 277 mice from recessive phenodeviants (**Table-2**). Several of the phenodeviants did not produce sufficient litters to sustain successful F3 breeding. The phenotype screening procedure for recessive screen mice was similar to that described for dominant mutations. A mutation was considered inheritable if the phenotype was recovered in several progeny. The animals were not genotyped at this stage to differentiate mutant from non-mutant genotypes. Thus, phenotype distribution was the only means for separating the mutants from their unaffected littermates. To avoid potential breeding of an un-affected progeny, we relied on breeding only extreme scoring mice for generating affected progeny in subsequent breeding.

2. **SPECIFIC OBJECTIVE 1b.** The dominant and/or recessive screens were performed for: a) growth or body weight; b) total body bone density determined by DEXA instrument PIXImus; c) volumetric bone density of tibia determined by peripheral quantitative computed tomography (pQCT); and d) bone markers. For several phenodeviants we added screens at 3-weeks of age during this reporting period. However, the main phenotype screens on F1 and F3 offspring were carried out at 10-weeks of age. The soft-tissue regeneration screen in progeny from one phenodeviant was performed in 3-week old mice. An abnormality was recognized if a phenotype differs by 2-3 standard deviation (depending on the measurement and population variance) as compared age and sex matched control mice. A mutation was considered inheritable if the phenotype is recovered in several inherited progeny.

3. **SPECIFIC OBJECTIVE 1c.** Detailed phenotypic characterization of selective phenodeviant mice identified in previous dominant & recessive screens are described in this section.

   A. **Dominant Screen (Table-1)**

   i) ***Mutant Line 9.1.7.B.M (Line 917)*** - In our previous ENU screen for dominant musculoskeletal phenotypes using a C57BL/6J (B6) strain of mice, a phenodeviant was discovered which exhibited a highly significant decrease in bone size. Three main parameters that assess bone size, i.e. bone area, bone mineral content (BMC), and periosteal circumference were all significantly lower in affected mice even after adjustment for decreased body weight. Interestingly, the total body bone area phenotype was consistently expressed in males (92% affected), whereas only 6% of females

exhibited partial phenotype. We continued to breed this line to generate additional affected mice for further characterization of mutation. Since only 50% of males are supposed to be affected, we have to produce a significantly higher number of animals to obtain affected male progeny. In the current reporting period, we have generated about 104 additional mice, as shown in **Table-1**. We used some of these male mice to perform bone area measurements at early ages such as 3- and 6-weeks (**Figure-2**). Our new screen data (**Figure-2**) shows that bone area phenotype is not distinguishable between affected and non-affected mice at 3-weeks of age. Thus, indicating that bone size phenotype is not manifested during early postnatal development and that the mutant phenotype is developed during post pubertal growth period and maintained up to 16-weeks or longer time periods. These data also suggest that changes in bone area could be related to changes in sex steroids during puberty. We are currently fine mapping the mutant locus for this mutant line. We will continue to breed this line and maintain a small colony until identification of mutant gene is completed.

ii) ***Mutant 12.18.4.D.F (Line 12184)*** - Line 12184 was generated in a dominant screening of C57BL/6J (B6) strain of mice. The phenodeviant has 10-14% high body weight-adjusted total body bone density and 7-14% high bone mineral content. We bred the phenodeviant with B6 females and generated about 73 progeny in this grant period (**Table-2**). More than 40% of the progeny were classified as affected. Previously, we have shown that 12184 mutation causes higher total bone density and an increase in periosteal bone perimeter measured by pQCT. Our phenotype characterization data suggest that the phenotype could be due to increase periosteal bone formation as well as reduced endocortical bone resorption. Furthermore, we have mapped this mutant line to distal chromosome 4 locus in previous reporting period. In the current reporting period, we evaluated bone density of 3-week old and 6-week old mice. These data are shown in **Figure-3**, and indicate that higher bone density phenotype is mainly expressed after 3-weeks of age and higher bone density is maintained thereafter. We will continue to breed this line and maintain a small colony until identification of mutant gene is completed.

iii) ***Mutant Line 12.13.7.E.M (Line 12137)*** - Line 12.13.7 was generated in a dominant screening of C57BL/6J (B6) strain of mice. We bred the phenodeviant with B6 females and generated about 87 progeny in this grant period. The mutants had 10% high body weight, 10-14% high body weight adjusted total body bone density, and 10-25% high body weight adjusted bone mineral content as compared to wild type control mice. Previous phenotypic characterization data suggest that high BMD phenotype in mutant mice appears to be due to increased endocortical bone formation. More than 40% of IT progeny produced during this reporting period could be classified as affected. Using mice from IT progeny, we performed measurement of total body bone density between 3- and 16-weeks of age. These data, shown in **Figure-4**, indicate that higher bone density phenotype is mainly expressed after 3-weeks of age and higher bone density is maintained up to four months of age. In addition to phenotypic characterization, we analyzed expression levels of genes in skeletal tissues of 12137 mice as compared to WT mice. We will continue to breed this line and maintain a small colony until identification of mutant gene is completed.

iv) ***Line M1.2d*** - Our last dominant line was a phenodeviant that expressed slow or no healing of a 2 mm ear punch hole in MRL strain of mice. We generated 39 mice during this reporting period (**Table-1**). However, due to poor breeding performance and low variability in the soft tissue healing phenotype we have observed that further breeding of this line is currently not feasible.

B. **Recessive Screen (Table-2)**

i) ***Mutant Line Agouti & Low BMD*** – The agouti mutant was generated in recessive screening of the C3H/HeJ (C3H) strain of mice. The mutant mice showed 8-10% lower total body bone density and bone mineral content. To generate additional F3 mice, we bred the affected male and female phenodeviants, which could be easily identified by agouti coat color, which has a greasy appearance. The *in-vivo* DEXA scan of total body bones and tibia shows that bone density was significantly lower in mutant mice as compared to WT control. In the current reporting period we generated 29 additional mice (**Table-2**). We will continue to breed and maintain this line.

ii) ***Phenodeviant with high bone density B2.4***: The phenodeviant (Line 2.4) was identified as a 15-20% high total body bone density and bone mineral content whereas the bone area was largely unaffected. The body weight was about 5-8% higher in the phenodeviant mice, however, the body weight adjusted BMD was 10-12% higher. We generated 76 mice in this grant period for characterization of high bone density phenotype (**Table-2**). We have experienced difficulties in breeding this line in terms of recovery of affected mutant, which was <10%. However, the breeding will be continued because the phenotype is interesting.

iii) ***Phenodeviant with high volumetric bone density Line20***: The phenodeviant (Line 20) was identified as a high bone density measured by PIXI. The total body bone density was 10-17% higher in male or female mice as compared to WT mice (**Table-2**). The high bone density appears to be associated with 9-25% higher bone mineral content as compared to WT control mice, whereas bone area was within only 1-4% different from WT control mice. The body weights of the phenodeviant mice were 6-10% higher, however, the body weight adjusted BMD was also 8-10% higher. This line was not productive and breeding was, therefore, discontinued.

iv) ***Phenodeviant with Low Alkaline Phosphatase Levels & High Bone Density***: We observed one phenodeviant (Line 29.2) with low alkaline phosphatase values (30-40%) in serum and higher bone density. We bred this phenodeviant and produced >40 mice in this line. Preliminary data indicated that alkaline phosphatase levels in some mice were>80% lower as compared to littermates. The bone density in these mice was also higher, which would suggest that mutation affects gene(s) that control bone turnover. This line was not productive and breeding was discontinued.

v) ***Phenodeviant with High Total Body & Volumetric BMD***: Earlier, we identified a phenodeviant (Line 5.4) that expressed high total bone density measured by PIXI that correlated with volumetric bone density and cortical thick ness. The cortical thickness

was > 2SD units different from the wild type control mice. We generated 22 mice this year and recovered a few F3 mice that showed high BMD phenotype. This line showed problems in breeding and recovery of the mutant mice but we are continuing to breed this line.

vi) ***Phenodeviant with Low Body Weight and Low IGF-I***: Earlier, we identified a phenodeviant (Line 15.3) that expressed low body weight (body weight Z-Score=-5.8) and low IGF-I. We bred this line in the current reporting period but mutant mice or F2 heterozygous mice were not productive.

vii) ***Phenodeviant with High Total Body & Volumetric BMD***: Our last recessive line was a phenodeviant (Line 5.3) that also expressed high total bone density measured by PIXI. We generated 36 mice this year. The total body bone density showed significant correlation with volumetric BMD and cortical thickness. The Line 5.3 appears to be similar to Line 5.4 and, in the future, we may only continue further characterization of Line 5.4.

II. **Specific Objective 2.** The aim of this Specific Objective was to determine the chromosomal location of the mutant gene responsible for the phenotypes in selected mutant. We have proposed to achieve this aim by breeding a mutant mice with a different strain of mice to generate F1 mice and then breeding the F1 mice in back-cross or inter-cross breeding scheme to produce 50-100 F2 mice. The F2 mice are phenotyped using pQCT and genotyped using 40-60 micro satellite markers and linkage analysis is employed to identify chromosomal location of mutation. Our progress on the Specific Objective 2 is discussed below.

1. Specific objective 2a-d.

In the current reporting period we selected 917 mutant mice for fine mapping to further narrow the mutant locus. The rationale for selection of this mutant is based on extensive characterization of mutant phenotype, the robust inheritability of the mutation, and the fact that this mutation is already mapped to a putative chromosome 4 locus. In addition, in the previous reporting period we have initiated mapping of three interesting mutant lines, work on which was completed in the current reporting period. Therefore, we have focused our mapping efforts on fine mapping the 917 locus.

Generation of F1 and F2 Mice for Fine Mapping of Line 917

The key factors in high resolution mapping strategies are number of recombination events, the marker density and the effect size of the QTL. Mapping to a resolution of 10 cM usually requires analysis of >300 F2 mice. We believe that our strategy to generate about 100-150 additional F2 males combined with a >10% effect size, and 22 microsatellite markers would lead to a resolution of <1 cM region. By employing a denser map by identifying 10-30 additional markers in the 5cM region, we will be able to narrow the 917M locus to <1 cM. Based on the above rationale, we initiated an intercross of 917 with C3H/HeJ strain of mice to generate approximately 100 additional F2 mice.

In the current reporting period, we bred three affected 917 males with 4 C3H/HeJ females to generate 45 F1 mice. We screened all F1 males and only those showing mutant phenotype (based on low bone size) were bred with F1 females. So far we have generated approximately 143 F2 mice from the intercross. We have screened 66 F2 mice for bone size phenotypes at 10-week and at 16-weeks of age as described in our dominant screen. In addition, we have collected blood from 10-week old mice for biochemical analysis. At 16-weeks of age, mice will be sacrificed and femurs will be collected to measure bone ize phenotype by ex-vivo pQCT. The total body bone size phenotype data of F1 and F2 mice are shown in **Figures 5 & 6**. The total body bone area data (measured by DEXA) of the 917 F2 male mice appears to be normally distributed (based Shapiro-Wilk W statistics) (**Figure-6**). Therefore, interval mapping could be used to identify QTLs affecting bone size.

2. Specific objective 2e-g

In the current reporting period we completed genotype analysis and interval mapping of two mutant lines 12137 and B2.4 for which the genotyping work was initiated in the previous reporting period. The phenotype analysis and genomic DNA extractions for both lines were completed in the previous reporting period. The genotyping and interval mapping was completed in the current reporting period. In addition, we fine mapped the 917 locus (identified earlier) by using additional chromosome 4 markers (**Table-3**) and re-genotyping the genomic DNA from the 69 F2 mice that we have collected in the previous reporting period. We did not produce an F2 intercross of WT MRL mice with another strain of mice because we did not map any MRL mutant line in the current reporting period. Instead, we have fine mapped a B6 mutant line (Line 917) that is intercrossed with C3H mice to generate F2 mice. Since we have already collected (B6xC3H)F2 intercross data in previous reporting periods, therefore, there was no requirement to generate WT (B6xC3H)F2 intercross mice.

Genotyping Procedure

Genotyping was performed by using fluorescent labeled [labeled with FAM (blue), VIC (green), and NED (yellow)] informative markers which were PCR amplified from 62 F2 DNA. Markers were spaced at either end of each chromosome, and in some cases in the middle (for larger chromosomes). We performed approximately >4,000 PCR reactions to achieve genotyping. PCR reactions and running conditions allowed from 4 to 6 microsatellite markers to be multiplexed in a single electrophoretic lane. About 2-6 reactions were run in a single capillary on the ABI 3100 DNA analyzer. Following electrophoresis on the ABI 3100 DNA Analyzer, Genotyper software macros were used to semi-automatically score the allele calls for all the multiplex pools of every single F2 mice. The pooled products were analyzed for fragment size on ABI Model 3100 DNA Analyzer and Genescan software was used to size alleles (Applied Biosystems). After an initial scoring by these macros, allele calls were visually checked and edited if necessary. Allele calls and edits were done using Genotyper software (Applied Biosystems) and exported as tab-delimited tables. A table of the calls was generated and the allele sizes converted into respective allele bins for entering into software program.

Interval Mapping Procedure

The interval mapping was performed by the Pseudomarker (obtained from www.jax.org/research/churchill) MAINSCAN program written for the MATLAB (Mathworks

Inc., Natick, MA, USA) programming environment. Phenotype data and genotype data were imported into the software in excel comma separated text file format; mice with missing phenotypic and genotypic data were coded as phenotype unknown. Threshold for LOD scores (A LOD score is the logarithm of odds score, i.e. the logarithm of the likelihood that two loci are linked/likelihood that loci are unlinked. Thus, a LOD score of 2 indicates that odds are 100:1 that a respective genetic region will show linkage to that trait) for different QTLs were determined by genome wide 1000 permutation test for 5% genome wide error ($p<0.05$). We calculated posterior probability densities for individual chromosome to define the 95% confidence interval (CI) for selected locus. Posterior probability density is a likelihood statistic that gives rise to the 95% confidence intervals. Linkage analyses were also performed using MapQTL 5.0 (DLO Center for Plant Breeding and Reproduction Research, Wageningen, The Netherlands) as described for F2 intercrosses. Both Pseudomarker and MapQTL 5.0 analyses yielded similar results. Percent variance explained by each locus was calculated for peak interval by MapQTL software.

Interval Mapping of Mutant Line 12137

The linkage maps for bone density and bone mineral content phenotypes for mutant line 12137 were generated using 164 F2 mice, which included 103 female and 64 male F2 mice. Since both male and female 12137 mutant mice are equally affected in terms of magnitude of phenotype, the bone density and bone mineral content data from F2 mice was adjusted with the body weight and then combined together for interval mapping. We used 60 genomic markers (**Table-4**) covering the entire mouse genome excluding the sex chromosomes. The results of interval mapping of are shown in **Figures 7 & 8**. One statistically significant QTL was identified on chromosome 4. Strongest linkage was observed on chromosome 4 with LOD 3.4 at 55 cM for total body bone mineral content (**Figure-8**).

Interval Mapping of Mutant Line B2.4

The linkage map for total body bone density phenotype for mutant line B2.4 was constructed using 97 female F2 mice. The results of interval mapping of are shown in **Figure-9**. One statistically significant QTL was identified on chromosome 4. Our results did not disclose significant linkage on any chromosome. Because the mutation was inherited in a recessive mode and we mapped 97 female F2 mice, theoretically, less than 24 F2 mice out of the total 97 F2 females could be mutant. Thus, it could be possible that we have very few mutant mice in the F2 population and our interval mapping strategy has limited power to detect linkage for a recessive mutation. This was in contrast to dominant ENU mutations where we were able to determine QTLs with 69 F2 mice. Additional F2 mice may be needed to increase the power of QTL detection to identify location of mutation. However, we have not pursued mapping this mutant line at high priority at this time because we have already identified chromosomal location of the mutation in several other lines.

Fine Mapping of 917 Locus by Increasing the Marker Density

To fine map the chromosome 4 locus affecting bone density, we used 22 markers on chromosome 4 (**Table-4**). We first established the 95% confidence interval of 917 locus by calculating posterior probability density plot (**Figure-10**) using the Pseudomarker algorithm, which shows peak was located between 2 cM and 20 cM region. Next we identified all microsatellite markers available between C3H/HeJ and C57BL/6J strains of mice for the

chromosome 4 between the 95% confidence interval of 917 locus. We then re-genotyped the F2 male mice (n=69) with these additional polymorphic microsatellite markers. Our results indicate that when additional markers were added, the proximal peak was resolved into three major peaks, each showing significant LOD scores ($p<0.05$) (**Figure-11**). However, the posterior probability density plot shows that probability of middle peak, located at 10-12 cM, harboring the mutant gene is higher (**Figure-11**). We are currently generating additional F2 animal to further refine this locus to <1 cM. Our strategies to identify mutant gene(s) from within the <1 cM region of 917 locus involves first identifying all functional positional candidate genes present in the 917 locus based on function and expression in skeletal tissues. The current understanding suggests that there are 30,000 genes in the mouse genome; thus, we anticipate that total number of predicted genes to be 20-40 in the 917M locus (<1 cM). Based on the rationale that approximately 20% of the 30,000 genes have been well characterized, we believe we have to study 4-8 genes even if all of them are involved in regulating skeletal tissues. We will subsequently sequence coding and/or regulatory region of these selected functional positional candidates.

Fine Mapping of 917 Locus by Genotyping Additional F2 Mice

We believe that our strategy to generate about 100-150 additional F2 males combined with 20-30 microsatellite markers would lead to further resolution of <1 cM region. Based on the above rationale, we have generated approximately 143 additional F2 mice. The tail clips were collected from 66 F2 mice and genomic DNA was extracted for genotyping. Genomic DNA was isolated from tail clips using DNAeasy kits (Qiagen) for mouse tissue. DNA samples were quantified and quality determined by measuring their absorbance at 260 nm and 280 nm. The phenotyping and genotyping of additional F2 mice is currently under progress. Once phenotype analysis of F2 mice is completed and genomic DNA is collected, we will use 20-30 genomic markers to narrow the support interval. The fine mapping will be reported in next report.

III. **Specific Objective 3**. The aim of this objective was to identify the candidate gene in the chromosomal locus established for the selected mouse mutant in Specific Objective 2 of the year 1. To achieve this, we have proposed to use DNA microarray analysis to investigate if the global gene expression pattern was altered in bone from mutant mice compared with wild type control mice. In the current reporting period we selected 12137 mutant because this mutant has been well characterized and mapped to a putative chromosomal location. In addition, we used osteoblasts cells from 917 mutant mice and WT mice to identify candidate genes. The rationale for using the osteoblast from male 917 mice is based on two previous findings: 1) osteoblast cell proliferation was defective; and 2) the 917 mutation affects the bone size in male mice only indicating a role of androgen in mediating the influence of mutant gene.

Furthermore, in the previous year we had performed a microarray experiment using RNA from M1.2 mice. The line M1.2d was identified in MRL/MpJ strain of mice and mutant mice showed slower healing rate which is measured by punching a 2 mm hole in each ear of the mutant progeny when mice were 3-weeks old and recording the size of hole at different time interval. The microarray experiment was performed in previous year but the data analysis was performed in the current reporting period.

Therefore, in the current reporting period we report results from three microarray experiments (data shown in **Tables 5-10**).

1. **SPECIFIC OBJECTIVE 3a.** To collect RNA from mutant mice, we have to rely on phenotype distribution because the genotype is not available currently. Consequently, we screened several female progeny from 12137 for total body bone density at 10-weeks of age and selected those mice that exhibited Z-score of 2.5 or more. We used three replicates from three affected 12137 mice. To collect RNA sample, we sacrificed 12137 mice, tibia and femurs were quickly isolated from any attached tissue. The ends of the tibia and femur were cut to flush out bone marrow, which was collected separately. The bones were then flushed with phosphate buffer saline solution. The bone and marrow were then stored at –70^{o}C in RNALater (Ambion) according to manufacturer's protocol until extracted by pulverizing the bone in liquid nitrogen. Since we proposed to use bones from wild type mice as control, we collected additional tibia and femur from wild type female mice (n=3) exactly as described for mutant mice.

   For extraction of total RNA from bone and marrow tissues, the tissue homogenate were prepared in appropriate amount or lysis solution/beta-mecaptoethanaol mixture (20ul/mg) and cells manually lysed with a mortar and pestle. The cellular debris was removed by centrifuging up to 600ul of homogenate through the mini prefiltration column, for 3 minutes at 13000 rpm, and collecting the filtrate. Equal volume of 70% ethanol added to the filtrate, placed on ice for at least 5 minutes, and further purified using spin columns from RNeasy Total RNA Isolation Kit (Qiagen, Chatsworth, CA, USA) according to the manufacturer's instructions. Using the above protocol, we have obtained very high quality RNA from small amounts of tissue (50 milligrams and less).

   Before microarray analysis, each sample was evaluated for quality of the RNA by spectrophotometric analysis using Agilent 2100 Bioanalyzer. Concentration of the RNA yield was determined by spectrophotometric analysis using the convention that 1 OD at 260 nm equals 40 ug per ml. The absorbance was checked at 260 and 280 nm for determination of sample concentration and purity. Only samples with A260/A280 ratio close to 2.0 were selected for microarray analysis.

2. **SPECIFIC OBJECTIVE 3b.** To perform in-house microarray to identify genes that are differentially expressed in the mutant versus control mice, we analyzed RNA from femur and tibia of 12137 and wild type mice together in three replicates. The pooled RNA was reverse transcribed into cDNA, labeled, and hybridized on our in-house microarray, which was created using Corning UltraGaps II glass slides and includes 25,000 mouse genes, spliced variants, or uncharacterized expressed sequence tag (EST) clone. To make slides the PCR products were spotted using a Genetix Q-Array2 robotic arrayer. The arrays are also spotted with Amersham Lucidea Universal Scorecard controls to insure correct gene expression values were obtained from each array. The Lucidea Universal ScoreCard is a set of 23 unique microarray controls that can be used with samples from most species and with any microarray platform. The controls are artificial genes that generate pre-determined signal intensities that do not change across samples or experiments. Thus, the microarray analysis is not dependent on relative quantification. The controls generate a calibration curve for determining limits of detection, linear range, and data saturation, and they can be used as universal references for validating and normalizing

microarray data. Controls are spotted in duplicate in the first and last PCR plates to insure proper data tracking.

The microarray slides were scanned using a GSI Lumonics ScanArray 4000 scanner. The arrays were scanned at a resolution of 10 microns which corresponds to ~15 pixels in diameter of each of the ~25,000 spots and a spacing of ~5 microns between the spots. The signal intensity of all microarray images was determined using Imagene 5.1 software. This software uses a patented image processing technology to provide quantification of microarray images of high density. Quality control measures include automated flagging of good, marginal and absent spots so that these can be filtered in the expression analysis.

Before the formal analysis, we used the Scatter plot and the Condition tree features of GeneSpring software to evaluate the microarray chips to determine if they are suitable to be included in the analysis. The Scatter plot shows the data skewness between the Cy3 and Cy5 dyes (i.e. the treatment vs. control) for a particular chip if there are too many genes highly expressed in one color, but not in the other, this may indicate that there are problems with the labeling process.

To allow for comparison of gene expression, the gene chips were globally scaled to an average intensity of 500. cDNA from each mice was put on two chips and was compared with the two control chips, generating 8 comparison files in total. Significance of differentially expressed genes was calculated by TTEST analysis, with $p<0.05$ as significantly altered gene expression. An average-fold change for the four comparisons of the selected genes was then calculated. We looked at fold change for all differentially expressed genes with $p<0.05$.

Differentially Expressed Genes for 12137 Mutant Mice

Our preliminary analysis of the microarray data shows that more than 250 genes are significantly up or down regulated in the mutant bones compared to control bones. There were approximately 194 genes unregulated (Table-5) and approximately 68 genes were down regulated (Table-6). All genes that are differentially expressed in the skeletal tissues of mutant 12137 and WT mice ate shown in **Tables 5 & 6**. The list shown in **Table-5** represent genes in 12137 mice that have $p<0.05$ and represent expression levels of >1.2 folds, as compared to WT mice. Similarly, the list shown in **Table-6** represent genes in 12137 mice that have $p<0.05$ and represent expression levels of <0.8 folds, as compared to WT mice. We are currently in the process of identifying the candidate genes that are located in the 12137 support interval on chromosome 4.

Genes Differentially Expressed in Osteoblasts from 917 and WT Mice

To identify candidate gene that are differentially expressed in osteoblasts from 917 mice as compared to osteoblasts from WT mice, we isolated the periosteal osteoblasts from femur and tibiae of 917 mutant and WT mice and propagated them in culture. In brief, the mice were euthanized with CO_2 and decapitated. Soft tissue was removed from femur and tibia without scraping off the bones so that periosteal cells were not lost at this point. Femur and tibia were placed separately in 50 ml falcon tubes containing sterile PBS, and subsequently in culture dish containing 10 ml of DMEM/antibiotics and the left over muscles were removed from the bones. The periosteal cells were extracted from bone by collagenase digestion for 90 minutes at 37^oC. Cells were counted and plated at a density of 10^6 cells per dish and grown with 10%

FBS/DMEM/antibiotics. Periosteal osteoblasts at passage 2-3 were used to study differential display. We performed two experiments: 1) we compared the expression of the genes in the osteoblasts from 917 and WT mice (basal level differences); and 2) we treated osteoblasts from 917 and WT mice with dihydrotestosterone (5α-DHT). Osteoblast cultures were maintained overnight in an Alpha-MEM medium containing 10% steroid stripped fetal calf serum. Then culture medium was replaced with a medium containing 5α-DHT at a concentration of 10^{-8} to 10^{-10} M or vehicle for 48-hours. After 48-hours cells were isolated and RNA extracted as described above.

Results of microarray analysis revealed 164 genes that were differentially expressed in osteoblasts from 917 mice as compared to WT mice (basal level differences in gene expression). Similarly, when osteoblasts were treated with 5α-DHT, approximately 179 genes were significantly different in osteoblasts from 917 as compared to WT mice (details of the gene expression are not shown). To identify what pathways were specifically affected at basal level and what pathways were altered when osteoblasts were treated with 5α-DHT, we performed pathway analysis of differentially expressed genes at both basal and stimulated conditions.

Use of Pathway Specific Array to Identify Candidate Genes for 917 Mutant Line

In addition to genome-wide microarray, we also used a commercially available pathway-focused DNA Microarray (Mouse Androgen Signalling Gene Oligo GEArray, SuperArray Bioscience Corporation, Frederick, MD) to identify candidate genes. The Oligo GEArray is a nylon membrane array matrix permeable support with a high DNA binding capacity. The production process, quality, and reproducibility of these pathway-specific arrays are similar to Microarray. The 60-mer oligonucleotide probes are printed on each microarray. The biotinylated cRNA target and the carefully designed oligonucleotides on the array correspond to the same 3'-biased gene-specific sequences permitting efficient and specific hybridization. The Oligo GEArray is visualized using chemiluminescent detection method, which allows the use of X-ray film for image acquisition.

To perform the androgen specific signaling pathway array, equal amounts of high quality RNA extracted from osteoblasts was reverse transcribed and the PCR amplified product is labeled with a chemiluminescence probe provided by the manufacturer. The labeled probe is then hybridized at 60^{o}C with the membrane. The hybridized membrane is washed, treated with chemiluminescence substrate, and visualized by exposing X-ray film for 10-20 seconds. The androgen specific signaling pathway array contained 112 known genes including house-keeping genes. Our results shown in **Figure-12** shows that 3-4 genes were differentially regulated in response to 5α-DHT treatment of the osteoblasts from 917 mice. We believe that these experiments would provide important clues to prioritize candidate genes for further studies or for identifying mutation.

Differentially Expressed Genes for M1.2D Mutant Mice

Analysis of the microarray data from M1.2 mice and WT MRL mice showed that more than 3000 genes or expressed sequence tags were significantly up or down regulated, including more than 500 known genes. Considering the large number of genes that are differentially expressed in the healing tissue as compared to WT tissue, we investigated pathways that are significantly affected during the healing process. The results of the pathway analysis are described in the next section.

3. **SPECIFIC OBJECTIVE 3c**. Further understanding the role of the differentially expressed genes in the pathways is critical in microarray studies. To more thoroughly characterize sets of functionally related genes differentially expressed between mutant mice (Line 12184) and WT B6 control mice, we used Onto-Express (Khatri P et al, Genomics 2002) to classify genes according to the Gene-Ontology (GO) categories: biological process; cellular role; and molecular function. We used a web-based tool, Pathway-Express (freely available as Onto-Tools suite at http://vortex.cs.wayne.edu/Projects.html), to find the most interesting pathways for their input list of genes. The Onto-Tools database integrates different types of genomic data from 19 sequence, gene, protein, and includes Gene Ontology (GO) annotations. After a list of genes is submitted, the system performs a search and builds a list of all associated pathways. A list of pathways for the input list of genes is calculated from the Onto-Tools database. The Pathway-Express first calculates a perturbation factor *PF(g)* for each input gene. This perturbation factor takes into account the (i) normalized fold change of the gene and (ii) the number and amount of perturbation of genes downstream from it. This gene perturbation factor reflects the relative importance of each differentially regulated gene. The impact factor of the entire pathway includes a probabilistic term that takes into consideration the proportion of differentially regulated genes on the pathway and gene perturbation factors of all genes in the pathway. The impact factors of all pathways are used to rank the pathways. These parameters are shown (Tables 7-10) in pathway analysis performed for various Microarray experiments in the current reporting period.

Pathway Analysis of Gene Expression of M1.2D Mutant Mice

The numbers of genes corresponding to each GO category among the 511 differentially expressed known genes ($p<0.05$) was tallied and compared with the number of genes expected for each GO. Significant differences from the expected were calculated with a two-sided binomial distribution. **Table-7** shows all GO functional classes with a Bonferroni-corrected significance of $p<0.05$, the significance of each class, as well as the number of genes corresponding to each GO functional class identified in our differentially expressed gene list. The functional gene groups demonstrating the most significant representation in our set of differentially expressed genes appear under the biological process ontology and map to the Cell adhesion molecules (CAMs), Axon guidance, and Gap junction. Genes involved in MAPK signaling pathway and Cytokine-cytokine receptor interaction are highly expressed in mutant. Other functional categories significantly represented under the cellular component and molecular function ontologies include genes involved in Tight junction, Leukocyte transendothelial migration, Fc epsilon RI signaling pathway, chemokine signaling, and Focal adhesion.

Pathway Analysis of Gene Expression of 12137 Mutant Mice

Table-8 shows number of genes corresponding to each GO category among the 262 differentially expressed known genes ($p<0.05$) that was tallied and compared with the number of genes expected for each GO. The functional gene groups demonstrating the most significant representation in our set of differentially expressed genes appear under the biological process MAPK signaling pathway, Natural killer cell mediated cytotoxicity, and Regulation of actin cytoskeleton. Other functional categories significantly represented under the cellular component and molecular function ontologies include genes involved in Cytokine-cytokine receptor interaction and Apoptosis.

Pathway Analysis of Gene Expression of 917 Osteoblasts

We performed separate pathway analysis for genes differentially regulated in basal osteoblasts and genes that were differentially regulated when osteoblasts were stimulated with 5α-DHT. Approximately 164 genes were differentially expressed in basal osteoblasts from 917 mice as compared to those from WT mice. Similarly, about 179 genes were differentially expressed when osteoblasts were treated with 5α-DHT.

The numbers genes corresponding to various GO category among the 164 differentially expressed known genes ($p<0.05$) at basal level is shown in **Table-9**. The number of genes corresponding to various GO category among the 179 differentially expressed known genes ($p<0.05$) under stimulated conditions is shown in **Table-10**.

The functional gene groups demonstrating the most significant representation in our set of differentially expressed genes appear under the biological process Phosphatidylinositol signaling system, ECM-receptor interaction, Focal adhesion, TGF-beta signaling pathway (**Table-9**). Other functional categories significantly represented under the cellular component and molecular function ontologies included genes involved in GnRH signaling pathway.

The functional gene groups demonstrating the most significant representation in 5α-DHT treated osteoblasts appeared under similar biological process, as observed in basal osteoblasts such as Phosphatidylinositol signaling system, ECM-receptor interaction, Focal adhesion, TGF-beta signaling pathway. However, genes corresponding to the other functional categories significantly represented under stimulated conditions included genes involved in Cytokine-cytokine receptor interaction and MAPK signaling pathway (**Table-10**). These pathways can provide vital clues for identification of mutant gene and for prioritization of candidate gene to sequence and identify mutation.

Key research accomplishments

- We bred 11 phenotypic deviant mice identified in previous year screens to generate approximately 530 F1 and F3 progeny. We screened approximately 370 mice.
- We have performed phenotypic characterization of selected mutant lines.
- To fine map chromosomal location of a mutation and to identify the mutant gene, we intercrossed a mutant strain with C3H/HeJ (a mapping) strain.
- We have generated 143 F2 mice from intercrosses between mutant and wild type strains.
- We have genotyped >150 F2 mice using >60 genome-wide informative markers.
- We have performed interval mapping and compared QTLs for mutant crosses with that of wild type mice (the wild type crosses were generated previously).
- We have mapped chromosomal location of a mutant with high bone density phenotype (identified earlier in dominant screen) to a distal region of chromosome-4.
- We performed DNA microarray analysis to examine genome wide gene expression pattern in bone from mutant mice and compared that with wild type control mice.
- In our preliminary analysis, we have identified several potential candidate gene or EST clones that are differentially expressed in mutant mice as compared to control mice.
- We have identified several potential pathways that could be altered in the mutant mice. These pathways would help us in the identification of mutant gene.

Reportable outcomes

Manuscript

Srivastava A K**,** Mohan S, Yu H, Masinde GL & Baylink DJ. Identification of quantitative trait loci that regulate obesity and serum lipid levels in MRL/MpJ x SJL/j inbred mice. Journal of Lipid Research, 47, 2006.

Conclusions

We bred 11 phenotypic deviants identified in the previous reporting periods and produced 530 mice in inheritance testing breeding and screened approximately 370 mice. Furthermore, from the mice generated in inheritance-test crosses, we have done additional characterization to identify mutant phenotype at prepubertal stage for several mutant lines. Therefore, we achieved the objectives of 'Specific Objective-1' of breeding and confirming the inheritance of phenotypic deviant mice identified in previous years.

To identify chromosomal location of an ENU mutant strain and to identify mutant gene, we have bred a mutant line with another strain of mice to generate 45 F1 and 143 F2 mice. We have completed genotyping and interval mapping using genomic DNA from >150 F2 mice and >60 genome-wide informative markers to identify QTLs harboring mutant gene (s). We have identified that a distal locus on chromosome 4 could harbor a high bone density mutation. Therefore, we have met the 'Specific Objective-2.' In addition, using higher marker density we have fine mapped a low bone size mutant locus and identified a 2 cM region on proximal chromosome-4 that potentially harbors mutant gene; this was an additional progress from the proposed work.

Finally, to identify the candidate gene in the chromosomal locus established for the bone size mutant mice, we performed DNA microarray analysis of two mutant lines to investigate if the global gene expression pattern was altered in skeletal tissue from mutant mice compared with wild type control mice. In our analysis, we have identified several potential candidate genes that are differentially expressed in mutant mice as compared to control mice. Furthermore, we have evaluated various pathways that were affected by the differentially expressed genes for three mutant lines. Therefore, we have completed all four objectives of 'Specific Objective-3' and exceeded the proposed work.

Table-1. Mutant mice strains that have been identified in earlier dominant screens and bred in current grant period for genotyping and detailed characterization of the phenotypes.

No	ID	Phenotype (Strain)	Number of IT Mice Produced	Number of IT Mice Screened	**Current Status**
1	9.1.7.B.M	15-20% Low Total Body Bone Area and BMC (B6)	104	56	Continued
3	12.18.4.D.F	16% High Total Body BMD & BMC (B6)	73	73	Continued
2	12.13.7.E.M	20% High BW & Total Body BMC (B6)	87	87	Continued
4	M1.2d	STR 1.9 mm, Tibia Midshaft BMD Z-Score=4.2, Trabecular BMD Z-Score=3.7	39	39	Breeding could not be sustained
TOTAL			**303**	**255**	

BMD= Bone Mineral Density, BMC= Bone Mineral Content, Z-Score indicates differences in a particular phenotype in terms of SD units from wild type control mice.
*The phenotype description and Z-scores are also based on data obtained in previous years.

Table-2. Number and current status of recessive screen phenodeviants that have been identified in previous grant periods and continued to be bred this year for further phenotypic characterization or to confirm heritability.

Line ID	Phenotype* at Repeat Screening or 16-Week Confirmation Screen	Number of F1 & F2 Mice Produced	Number of F3 Mice Screened	Current Status
Agouti Line	Agouti & Low BMD	29	14	Continued
B2.4	Total Body BMD Z-Score=3.9, Total Body BMC Z-Score=3.0	76	28	Continued
B20.3	Total Body BMD Z-Score=2.4 to 3.5, Total Body BMC Z-Score=2.4 to 2.5	42	21	Discontinued
B29	30-40% Low Serum Alkaline Phosphatase and Osteocalcin, Total Body BMD Z-Score=1.8	20	16	Discontinued
B5.4	Total Body BMD Z-Score=3.2, Total Body BMC Z-Score=4.2	22	9	Continued
B15.3	Body Weight Z-Score=-5.8 Low IGF-I	52	15	Continued
B5.3	High Cortical Thickness Z-Score=2.0	36	11	Continued
Total		**277**	**114**	

BMD= Bone Mineral Density, BMC= Bone Mineral Content, Z-Score indicates differences in a particular phenotype in terms of SD units from wild type control mice.
*The phenotype description and Z-scores are also based on data obtained in previous years.

Table-3. List of chromosome 4 markers that have been used to fine map the chromosomal location of the mutant gene for bone size mutant 917. Our earlier mapping effort identified a prominent locus in the proximal region of the chromosome 4. Therefore, we have increased the marker density to narrow the mutant interval.

Locus	Chromosome	Genetic Position (cM)
D4Mit149	4	1.0
D4Mit264	4	1.9
D4Mit227	4	3.2
D4Mit50	4	5.4
D4Mit171	4	6.3
D4Mit193	4	7.5
D4Mit172	4	8.6
D4Mit41	4	10.5
D4Mit196	4	12.1
D4Mit237	4	13.3
D4Mit17	4	13.4
D4Mit286	4	14.5
D4Mit91	4	15.6
D4Mit268	4	17.9
D4Mit53	4	19.8
D4Mit80	4	37.7
D4Mit153	4	45.5
D4Mit308	4	57.4
D4Mit203	4	60.0
D4Mit251	4	66.0
D4Mit170	4	66.6
D4Mit209	4	79.4
D4Mit42	4	81.0

Table-4. List of microsatellite markers that have been used to map the chromosomal location of the mutant gene for bone density mutants 12137 and B2.4.

Locus	Chr	Genetic Position (cM)	Locus	Chr	Genetic Position (cM)	Locus	Chr	Genetic Position (cM)
D1Mit64	1	5	D7Mit98	7	53.3	D16Mit131	16	4.3
D1Mit236	1	25.7	D8Mit289	8	11	D16Mit60	16	23.4
D1Mit60	1	58.7	D8Mit178	8	33	D16Mit139	16	43.1
D1Mit406	1	101.2	D8Mit88	8	58	D17Mit245	17	3
D2Mit1	2	1	D9Mit285	9	21	D17Mit51	17	22.9
D2Mit66	2	47.8	D9Mit336	9	35	D17Mit39	17	45.3
D2Mit285	2	86	D9Mit16	9	61	D18Mit64	18	2
D2Mit145	2	98.5	D10Mit213	10	11	D18Mit12	18	17
D3Mit203	3	11.2	D10Mit115	10	38.4	D18Mit48	18	50
D3Mit178	3	13.8	D10Mit233	10	62	D19Mit68	19	6
D3Mit67	3	28	D11Mit2	11	2.4	D19Mit28	19	12
D3Mit311	3	45.2	D11Mit4	11	37	D19Mit103	19	52
D3Mit19	3	87.6	D11Mit214	11	70			
D4Mit227	4	3.2	D12Mit60	12	16			
D4Mit196	4	12.1	D12Mit158	12	38			
D4Mit308	4	57.4	D12Mit133	12	56			
D4Mit42	4	81	D13Mit275	13	16			
D5Mit387	5	15	D13Mit247	13	32			
D5Mit309	5	44	D13Mit151	13	71			
D5Mit95	5	68	D14Mit98	14	3			
D6Mit138	6	0.7	D14Mit5	14	22.5			
D6Mit36	6	46	D14Mit75	14	54			
D6Mit14	6	71.3	D15Mit6	15	13.7			
D7Mit294	7	8	D15Mit70	15	47.7			
D7Mit350	7	41	D15Mit161	15	69.2			

Table-5. List of genes that are significantly up regulated in the bones of mutant 12137 mice as compared to WT control mice.

Gene Name	Gaussian p-value	Description
Slfn4	1.17E-06	Schlafen 4
Ifitm6	2.10E-05	Interferon induced transmembrane protein 6
Vim	0.000166	synonym: MGC102095; Mus musculus vimentin (Vim), mRNA.
Olfr491	0.000305	Olfactory receptor 491
Fcgr3	0.000381	Fc receptor, IgG, low affinity III
Arhgdib	0.000514	Rho, GDP dissociation inhibitor (GDI) beta
Aprt	0.000602	Adenine phosphoribosyl transferase
Cish	0.000668	Cytokine inducible SH2-containing protein
Snx10	0.00068	Sorting nexin 10
Pstpip1	0.000796	Proline-serine-threonine phosphatase-interacting protein 1
Nme7	0.000807	Mus musculus non-metastatic cells 7
Rpl13a	0.000961	Mus musculus ribosomal protein L13a (Rpl13a), mRNA.
Zfp179	0.00103	Zinc finger protein 179
Socs3	0.00106	Suppressor of cytokine signaling 3
Lzp-s	0.00154	P lysozyme structural
Igsf6	0.00158	Immunoglobulin superfamily, member 6
Rgs19	0.00166	Regulator of G-protein signaling 19
Rpl35	0.00171	Ribosomal protein L35
Glipr2	0.00172	GLI pathogenesis-related 2
Glrx1	0.0018	Glutaredoxin 1 (thioltransferase)
Mgst2	0.00211	Microsomal glutathione S-transferase 2
Dstn	0.00236	Mus musculus destrin (Dstn), mRNA.
Rps27l	0.00254	Ribosomal protein S27-like
Ccrn4l	0.00303	CCR4 carbon catabolite repression 4-like (S. cerevisiae)
Hspe1	0.00363	Heat shock protein 1 (chaperonin 10)
Myh1	0.00372	Myosin, heavy polypeptide 1, skeletal muscle, adult
Acp5	0.00382	Acid phosphatase 5, tartrate resistant
Prtn3	0.00391	Proteinase 3
Ccl9	0.00401	Chemokine (C-C motif) ligand 9
Ostf1	0.00403	Osteoclast stimulating factor 1
Rpl15	0.00406	Ribosomal protein L15

Myd88	0.0042	Myeloid differentiation primary response gene 88
Clecsf8	0.0047	C-type lectin domain family 4, member d
Mt2	0.0048	Mus musculus metallothionein 2 (Mt2), mRNA.
Tyrobp	0.00503	TYRO protein tyrosine kinase binding protein
Slpi	0.00505	Secretory leukocyte protease inhibitor
Cox8b	0.0053	Cytochrome c oxidase, subunit VIIIb
Ckmt2	0.00534	Creatine kinase, mitochondrial 2
Fcrl3	0.00565	Fc fragment of IgG, low affinity IIIa, receptor
Vill	0.00592	Villin-like
Mb	0.00594	Myoglobin
Myh2	0.00594	Myosin, heavy polypeptide 2, skeletal muscle, adult
Apobec2	0.00595	Apolipoprotein B editing complex 2
Cyba	0.0061	Cytochrome b-245, alpha polypeptide
Evi2a	0.00619	Ecotropic viral integration site 2a
Pgam2	0.00652	Phosphoglycerate mutase 2
Myo1f	0.00676	Myosin IF
Pygl	0.00692	Liver glycogen phosphorylase
Trem3	0.00697	Triggering receptor expressed on myeloid cells 3
Ly6c	0.00709	Lymphocyte antigen 6 complex, locus C
Ndrg2	0.00716	N-myc downstream regulated gene 2
Gp49a	0.00719	Glycoprotein 49 A
Rpl3l	0.00726	Ribosomal protein L3-like
Ralb	0.00733	V-ral simian leukemia viral oncogene homolog B (ras related)
Eno3	0.0075	Enolase 3, beta muscle
Cox6a2	0.0076	Cytochrome c oxidase, subunit VI a, polypeptide 2
Rps10	0.00789	Ribosomal protein S10
Ncf4	0.00793	Neutrophil cytosolic factor 4
Ryr1	0.00794	Calcium release channel isoform 1; skeletal muscle ryanodine receptor; Mus musculus ryanodine receptor 1, skeletal muscle (Ryr1), mRNA.
Trem2	0.00808	Mus musculus triggering receptor expressed on myeloid cells 2 (Trem2), mRNA.
Mrps26	0.00825	Mitochondrial ribosomal protein S26
Ier3	0.00827	Immediate early response 3
Mrgpra2	0.00859	MAS-related GPR, member A2
Rpl10a	0.00861	Ribosomal protein L10A
Tcap	0.00908	Titin-cap
Myoz1	0.00914	Myozenin 1

Rab32	0.0096	RAB32, member RAS oncogene family
Myom2	0.00973	Myomesin 2
Mybpc2	0.00979	Mus musculus myosin binding protein C, fast-type (Mybpc2), mRNA.
Mrpl33	0.00985	Mitochondrial ribosomal protein L33
Ltb4r1	0.00992	Leukotriene B4 receptor 1
Ms4a3	0.00993	Membrane-spanning 4-domains, subfamily A, member 3
Olfr556	0.0102	Olfactory receptor 556
Actn2	0.0103	Actinin alpha 2
Rps23	0.0105	Ribosomal protein S23
Hmox1	0.0106	Heme oxygenase (decycling) 1
Arhgap9	0.0106	Mus musculus Rho GTPase activating protein 9 (Arhgap9), mRNA.
Vpreb1	0.0108	Pre-B lymphocyte gene 1
Arrb2	0.0108	Arrestin, beta 2
Tnnt3	0.011	Mus musculus troponin T3, skeletal, fast (Tnnt3), mRNA.
Ckm	0.0112	Creatine kinase, muscle
Mylk2	0.0123	Mus musculus myosin, light polypeptide kinase 2, skeletal muscle, transcript variant 1 (Mylk2), mRNA.
Rdh5	0.0126	Retinol dehydrogenase type 5; Mus musculus retinol dehydrogenase 5 (Rdh5), mRNA.
Ndg2	0.0127	Nur77 downstream gene 2
Shfdg1	0.0129	Mus musculus split hand/foot malformation (ectrodactyly) type 1 (Shfm1), mRNA.
Fabp3	0.013	Fatty acid binding protein 3, muscle and heart
Prss16	0.0133	Mus musculus protease, serine, 16 (thymus) (Prss16), mRNA.
Ssr4	0.0134	Mus musculus signal sequence receptor, delta (Ssr4), mRNA.
Serpinb1a	0.0138	Serine (or cysteine) proteinase inhibitor, clade B, member 1a
Hck	0.014	Hemopoietic cell kinase
Pilrb	0.0141	Paired immunoglobin-like type 2 receptor beta
Neurl	0.0144	Neuralized-like homolog (Drosophila)
Ctsk	0.0147	Cathepsin K
Rac2	0.0149	RAS-related C3 botulinum substrate 2
Mybl1	0.0155	Myeloblastosis oncogene-like 1
Rpl18	0.0155	Ribosomal protein L18
Fgr	0.0155	Gardner-Rasheed feline sarcoma viral (Fgr) oncogene homolog
Lyzs	0.0156	Mus musculus lysozyme (Lyzs), mRNA.
Pycr2	0.0157	Pyrroline-5-carboxylate reductase family, member 2
Siva	0.0158	Cd27 binding protein (Hindu God of destruction)
Alox5ap	0.0159	Arachidonate 5-lipoxygenase activating protein

Mepe	0.016	Matrix extracellular phosphoglycoprotein with ASARM motif (bone)
Rpl10	0.0163	Ribosomal protein 10
Gpd1	0.0164	Glycerol-3-phosphate dehydrogenase 1 (soluble)
Pirb	0.0165	Paired-Ig-like receptor A4
Zmynd17	0.0166	Zinc finger, MYND domain containing 17
Ngp	0.0172	Neutrophilic granule protein
Mt1	0.0173	Metallothionein 1
Lmo1	0.0177	LIM domain only 1
Gng2	0.0183	Guanine nucleotide binding protein (G protein), gamma 2 subunit
Ppp1r3a	0.0185	Protein phosphatase 1, regulatory (inhibitor) subunit 3A
Gabarap	0.0189	Gamma-aminobutyric acid receptor associated protein
Lsm8	0.0191	LSM8 homolog, U6 small nuclear RNA associated (S. cerevisiae)
Hk2	0.0192	Hexokinase 2
Tnfsf13	0.0192	Tumor necrosis factor (ligand) superfamily, member 13
Hrc	0.0196	Histidine rich calcium binding protein
Pfdn4	0.0196	Mus musculus prefoldin 4 (Pfdn4), mRNA.
Sh3bgrl3	0.0199	SH3 domain binding glutamic acid-rich protein-like 3
Il1b	0.0202	Interleukin 1 beta
Clca1	0.0202	Chloride channel calcium activated 1
Rnu22	0.0203	
Fstl3	0.0204	Mus musculus follistatin-like 3 (Fstl3), mRNA.
Pyp	0.0205	Pyrophosphatase
Epx	0.0214	Eosinophil peroxidase
Ubd	0.0219	Ubiquitin D
Casq1	0.0222	Calsequestrin 1
Asb2	0.0224	Ankyrin repeat and SOCS box-containing protein 2
Tm6sf1	0.0226	Transmembrane 6 superfamily member 1
Pgam1	0.0226	Phosphoglycerate mutase 1
Hs1bp1	0.0227	HCLS1 associated X-1
Tlr2	0.023	Toll-like receptor 2
Mthfd2	0.0231	Methylenetetrahydrofolate dehydrogenase (NAD+ dependent), methenyltetrahydrofolate cyclohydrolase
Aldoa	0.0241	Aldolase 1, A isoform
Pilra	0.0243	Paired immunoglobin-like type 2 receptor alpha
Ctsg	0.0244	Cathepsin G
Efna1	0.0249	Mus musculus ephrin A1 (Efna1), mRNA.
Csrp2	0.0257	Cysteine and glycine-rich protein 2

Mcpt8	0.0258	Mast cell protease 8
Hint1	0.0258	Histidine triad nucleotide binding protein 1
Sepw1	0.0259	Mus musculus selenoprotein W, muscle 1 (Sepw1), mRNA.
Mlf1	0.0262	Myeloid leukemia factor 1
Olfr65	0.0263	Olfactory receptor 65
Capg	0.0265	Capping protein (actin filament), gelsolin-like
Car3	0.0275	Carbonic anhydrase 3
Sucla2	0.0276	Succinate-Coenzyme A ligase, ADP-forming, beta subunit
Scap2	0.0279	Src family associated phosphoprotein 2
Ankrd23	0.0284	Ankyrin repeat domain 23
Idi1	0.0284	Isopentenyl-diphosphate delta isomerase
Cckbr	0.029	Cholecystokinin B receptor
Tnni2	0.0294	Troponin I, skeletal, fast 2
Oxct2b	0.03	3-oxoacid CoA transferase 2B
Tpm2	0.0304	Tropomyosin 2, beta
Ckap1	0.0307	Cytoskeleton-associated protein 1
Esm1	0.0312	Endothelial cell-specific molecule 1
Acadvl	0.0319	Acyl-Coenzyme A dehydrogenase, very long chain
Slc25a4	0.0319	Solute carrier family 25 (mitochondrial carrier, adenine nucleotide translocator), member 4
Actn3	0.0324	Actinin alpha 3
Cabc1	0.033	Chaperone, ABC1 activity of bc1 complex like (S. pombe)
Irg1	0.0331	Mus musculus immunoresponsive gene 1 (Irg1), mRNA.
Clic1	0.0345	Chloride intracellular channel 1
Olfr1106	0.0354	olfactory receptor MOR172-6; Mus musculus olfactory receptor 1106 (Olfr1106), mRNA.
Mylpf	0.0355	myosin light chain 2; Mus musculus myosin light chain, phosphorylatable, fast skeletal muscle (Mylpf), mRNA.
Hrasls3	0.0356	HRAS like suppressor 3
Ebi3	0.0362	Mus musculus Epstein-Barr virus induced gene 3 (Ebi3), mRNA.
Lcn2	0.0363	Lipocalin 2
Ccl11	0.0365	Small chemokine (C-C motif) ligand 11
Ak1	0.0366	Adenylate kinase 1
Tceal5	0.0372	Transcription elongation factor A (SII)-like 5
Dcn	0.0374	Decorin
Pfkm	0.0376	Phosphofructokinase, muscle
Smpx	0.0377	Small muscle protein, X-linked

Ahrr	0.0383	Mus musculus aryl-hydrocarbon receptor repressor (Ahrr), mRNA.
Gfi1b	0.0389	Growth factor independent 1B
Olfr550	0.0391	Mus musculus olfactory receptor 550 (Olfr550), mRNA.
Bcs1l	0.0397	BCS1-like (yeast)
Rab39b	0.0401	member RAS oncogene family (Rab39b), mRNA.
Cox7a1	0.0405	Cytochrome c oxidase, subunit VIIa 1
Rps16	0.0407	Ribosomal protein S16
Cdh24	0.0411	Cadherin-like 24
Fcna	0.0413	Ficolin A
Car1	0.042	Carbonic anhydrase 1
Ap3s1	0.0439	Adaptor-related protein complex 3, sigma 1 subunit
Il1r2	0.0442	IL-1 receptor beta chain; Mus musculus interleukin 1 receptor, type II (Il1r2), mRNA.
Grik5	0.0447	Glutamate receptor, ionotropic, kainate 5 (gamma 2)
Sephs2	0.0447	Selenophosphate synthetase 2
Bcdo2	0.0461	Beta-carotene 9', 10'-dioxygenase 2
Scd2	0.0466	Stearoyl-Coenzyme A desaturase 2
V1rg6	0.0472	Vomeronasal 1 receptor, G6
Tmsb4x	0.0486	Thymosin, beta 4, X chromosome
Tfrc	0.0491	Transferrin receptor
Olfr1047	0.0496	Olfactory receptor 1047

Table-6. List of genes that are significantly down regulated in the bones of mutant 12137 mice as compared to WT control mice.

Gene Name	Gaussian p-value	Description
Bcdo2	0.0461	Beta-carotene 9', 10'-dioxygenase 2
Grik5	0.0447	Glutamate receptor, ionotropic, kainate 5 (gamma 2)
Car1	0.042	Carbonic anhydrase 1
Fcna	0.0413	Ficolin A
Cox7a1	0.0405	Cytochrome c oxidase, subunit VIIa 1
Gfi1b	0.0389	Growth factor independent 1B
Ahrr	0.0383	Mus musculus aryl-hydrocarbon receptor repressor (Ahrr)
Smpx	0.0377	Small muscle protein, X-linked
Pfkm	0.0376	Phosphofructokinase, muscle
Dcn	0.0374	Decorin
Tceal5	0.0372	Transcription elongation factor A (SII)-like 5
Ak1	0.0366	Adenylate kinase 1
Ccl11	0.0365	Small chemokine (C-C motif) ligand 11
Hrasls3	0.0356	HRAS like suppressor 3
Mylpf	0.0355	phosphorylatable, fast skeletal muscle (Mylpf)
Cabc1	0.033	Chaperone, ABC1 activity of bc1 complex like (S. pombe)
Actn3	0.0324	Actinin alpha 3
Acadvl	0.0319	Acyl-Coenzyme A dehydrogenase, very long chain
Slc25a4	0.0319	Solute carrier family 25, member 4
Cmya5	0.0318	
Esm1	0.0312	Endothelial cell-specific molecule 1
Tpm2	0.0304	Tropomyosin 2, beta
Oxct2b	0.03	3-oxoacid CoA transferase 2B
Tnni2	0.0294	Troponin I, skeletal, fast 2
Cckbr	0.029	Cholecystokinin B receptor
Ankrd23	0.0284	Ankyrin repeat domain 23
Sucla2	0.0276	Succinate-Coenzyme A ligase, ADP-forming, beta subunit
Car3	0.0275	Carbonic anhydrase 3
Mlf1	0.0262	Myeloid leukemia factor 1
Mcpt8	0.0258	Mast cell protease 8
Aldoa	0.0241	Aldolase 1, A isoform
Asb2	0.0224	Ankyrin repeat and SOCS box-containing protein 2
Casq1	0.0222	Calsequestrin 1
Epx	0.0214	Eosinophil peroxidase
Hrc	0.0196	Histidine rich calcium binding protein
Hk2	0.0192	Hexokinase 2
Ppp1r3a	0.0185	Protein phosphatase 1, regulatory (inhibitor) subunit 3A
Zmynd17	0.0166	Zinc finger, MYND domain containing 17
Gpd1	0.0164	Glycerol-3-phosphate dehydrogenase 1 (soluble)
Mepe	0.016	Matrix extracellular phosphoglycoprotein with ASARM motif (bone)
Mybl1	0.0155	Myeloblastosis oncogene-like 1
Neurl	0.0144	Neuralized-like homolog (Drosophila)
Fabp3	0.013	Fatty acid binding protein 3, muscle and heart

Ndg2	0.0127	Nur77 downstream gene 2
Mylk2	0.0123	skeletal muscle, transcript variant 1 (Mylk2)
Ckm	0.0112	Creatine kinase, muscle
Tnnt3	0.011	skeletal muscle fast-twitch TnT
Vpreb1	0.0108	Pre-B lymphocyte gene 1
Hmox1	0.0106	Heme oxygenase (decycling) 1
Actn2	0.0103	Actinin alpha 2
Mybpc2	0.00979	Mus musculus myosin binding protein C, fast-type (Mybpc2)
Myom2	0.00973	Myomesin 2
Myoz1	0.00914	Myozenin 1
Tcap	0.00908	Titin-cap
Ryr1	0.00794	Mus musculus ryanodine receptor 1, skeletal muscle (Ryr1)
Cox6a2	0.0076	Cytochrome c oxidase, subunit VI a, polypeptide 2
Eno3	0.0075	Enolase 3, beta muscle
Rpl3l	0.00726	Ribosomal protein L3-like
Ndrg2	0.00716	N-myc downstream regulated gene 2
Pgam2	0.00652	Phosphoglycerate mutase 2
Apobec2	0.00595	Apolipoprotein B editing complex 2
Mb	0.00594	Myoglobin
Myh2	0.00594	Myosin, heavy polypeptide 2, skeletal muscle, adult
Ckmt2	0.00534	Creatine kinase, mitochondrial 2
Cox8b	0.0053	Cytochrome c oxidase, subunit VIIIb
Myh1	0.00372	Myosin, heavy polypeptide 1, skeletal muscle, adult
Nme7	0.000807	Mus musculus non-metastatic cells 7
Cab	0.000796	Chlorophyll A-B binding protein / LHCI type I (CAB)

Table-7. Pathway analysis of genes that are differentially expressed between soft tissue undergoing healing from mutant Line M1.2 and similar tissue from WT MRL mice as control.

Rank	Pathway Name	Impact Factor	# Genes in Pathway	# Input Genes in Pathway	corrected p-value[A]	corrected gamma p-value[B]	Suma (PF)[C]
1	Cell adhesion molecules (CAMs)	230	147	4	0.127	3.4E-98	227.817
2	Axon guidance	7.0	132	6	0.008	7.4E-03	2.14456
3	Gap junction	6.8	90	3	0.114	8.7E-03	4.6287
4	Tight junction	6.1	117	3	0.198	1.6E-02	4.46608
5	Leukocyte transendothelial migration	6.1	117	4	0.068	1.6E-02	3.39092
6	MAPK signaling pathway	6.0	231	7	0.033	1.7E-02	2.58123
7	Cytokine-cytokine receptor interaction	5.4	241	8	0.014	3.0E-02	1.12264
8	Focal adhesion	5.3	190	4	0.238	3.2E-02	3.84906
9	Fc epsilon RI signaling pathway	5.2	75	4	0.017	3.4E-02	1.13631
10	Colorectal cancer	5.2	77	3	0.080	3.5E-02	2.64735
11	Notch signaling pathway	5.0	46	2	0.121	4.2E-02	2.85794
12	Natural killer cell mediated cytotoxicity	4.9	117	2	0.454	4.5E-02	4.06912
13	Long-term depression	4.8	72	2	0.243	4.7E-02	3.40919
14	GnRH signaling pathway	4.7	93	4	0.034	5.0E-02	1.34769
15	Huntington's disease	4.5	28	2	0.052	5.9E-02	1.57491

[A]Bonferroni-corrected significance of P 0.05

[B]Gamma measure of statistical association

[C]The Pathway-Express first calculates a perturbation factor *PF(g)* for each input gene. This perturbation factor takes into account the (i) normalized fold change of the gene and (ii) the number and amount of perturbation of genes downstream from it. This gene perturbation factor reflects the relative importance of each differentially regulated gene.

Table-8. Pathway analysis of genes that are differentially expressed between skeletal tissues of Line 12137 and WT B6 mice.

Rank	Pathway Name	Impact Factor	#Genes in Pathway	#Input Genes in Pathway	%PathwayGenes in Input	p-value	corrected p-value
1	MAPK signaling pathway	28	231	5	2.165	0.007742	0.007741562
2	Natural killer cell mediated cytotoxicity	18	117	4	3.419	0.001833	0.00183259
3	Regulation of actin cytoskeleton	15	199	4	2.01	0.016658	0.01665797
4	Leukocyte transendothelial migration	11	117	4	3.419	0.001833	0.00183259
5	Toll-like receptor signaling pathway	10	91	3	3.297	0.004755	0.004754854
6	Apoptosis	10	81	4	4.938	3.47E-04	3.47E-04
7	Cytokine-cytokine receptor interaction	10	241	5	2.075	0.009424	0.009424348
8	Adipocytokine signaling pathway	9	69	2	2.899	0.01472	0.014720154
9	Complement and coagulation cascades	8	71	3	4.225	0.001939	0.001938918
10	Neuroactive ligand-receptor interaction	8	311	4	1.286	0.082689	0.082688893
12	Focal adhesion	8	190	3	1.579	0.053483	0.053482761
13	Type II diabetes mellitus	6	45	1	2.222	0.043991	0.043991208
14	Regulation of autophagy	6	31	1	3.226	0.022101	0.022100728
15	Insulin signaling pathway	6	133	2	1.504	0.076686	0.076685837
17	Axon guidance	6	132	2	1.515	0.07535	0.075349633
18	Olfactory transduction	5	30	2	6.667	0.001409	0.001408755
19	Amyotrophic lateral sclerosis (ALS)	5	17	1	5.882	0.006918	0.006917844

Table-9. Pathway analysis of genes that are differentially expressed between osteoblasts isolated from 917 and WT B6 mice. The differential display was determined by microarray technique and pathway analysis was performed by Onto-Tools suite at http://vortex.cs.wayne.edu/Projects.html.

Rank	Pathway Name (Treated)	Impact Factor	#Genes in Pathway	Input Genes in Pathway	p-value	corrected p-value	gamma p-value	corrected gamma p-value	Sum(PF)
1	Phosphatidylinositol signaling system	35.8	73	1	0.3523	0.3523	1.04E-14	1.04E-14	34.8
2	Focal adhesion	25.1	190	13	1.29E-10	1.29E-10	3.34E-10	3.34E-10	2.3
3	ECM-receptor interaction	22.2	85	9	2.06E-09	2.06E-09	5.48E-09	5.48E-09	2.2
4	TGF-beta signaling pathway	15.8	83	5	0.0001	0.0001	2.36E-06	2.36E-06	6.9
5	MAPK signaling pathway	15.7	231	10	1.31E-06	1.31E-06	2.56E-06	2.56E-06	2.1
6	Cytokine-cytokine receptor interaction	14.5	241	10	1.92E-06	1.92E-06	8.14E-06	8.14E-06	1.3
7	Colorectal cancer	11.9	77	5	9.66E-05	9.66E-05	8.88E-05	8.88E-05	2.6
8	Regulation of actin cytoskeleton	9.3	199	6	0.0012	0.0012	0.0009	0.0009	2.6
9	Toll-like receptor signaling pathway	8.2	91	4	0.0021	0.0021	0.0025	0.0025	2.1
10	Complement and coagulation cascades	7.7	71	4	0.0008	0.0008	0.0040	0.0040	0.6
11	Leukocyte transendothelial migration	7.2	117	3	0.0326	0.0326	0.0062	0.0062	3.8
12	Insulin signaling pathway	6.5	133	4	0.0082	0.0082	0.0115	0.0115	1.7
13	B cell receptor signaling pathway	6.4	64	3	0.0065	0.0065	0.0128	0.0128	1.3
14	Apoptosis	6.2	81	3	0.0124	0.0124	0.0152	0.0152	1.8
15	T cell receptor signaling pathway	5.3	94	3	0.0185	0.0185	0.0310	0.0310	1.3
16	Gap junction	5.1	90	2	0.0998	0.0998	0.0369	0.0369	2.8
17	Natural killer cell mediated cytotoxicity	5.1	117	1	0.5018	0.5018	0.0376	0.0376	4.4
18	Jak-STAT signaling pathway	5.1	151	3	0.0610	0.0610	0.0387	0.0387	2.3
19	Long-term depression	5.0	72	1	0.3485	0.3485	0.0404	0.0404	3.9
20	Hedgehog signaling pathway	4.6	53	1	0.2704	0.2704	0.0578	0.0578	3.3
21	Wnt signaling pathway	4.5	143	2	0.2080	0.2080	0.0634	0.0634	2.9
22	mTOR signaling pathway	4.4	49	2	0.0342	0.0342	0.0657	0.0657	1.0
23	GnRH signaling pathway	4.4	93	2	0.1054	0.1054	0.0669	0.0669	2.1

Table-10. Pathway analysis of genes that are differentially expressed between 5α-Dihydro-testosterone treated osteoblasts from 917 and WT B6 mice. The differential display was determined by microarray technique and pathway analysis was performed by Onto-Tools suite at http://vortex.cs.wayne.edu/Projects.html.

Rank	Pathway Name (Basal)	Impact Factor	#Genes in Pathway	#Input Genes in Pathway	p-value	corrected p-value	gamma p-value	corrected gamma p-value	Sum (PF)
1	Phosphatidylinositol signaling system	36.0	73	1	0.32824	0.32824	8.24E-15	8.24E-15	34.9
2	ECM-receptor interaction	28.9	85	11	2.25E-12	2.25E-12	8.15E-12	8.15E-12	2.1
3	Focal adhesion	25.6	190	13	4.31E-11	4.31E-11	2.03E-10	2.03E-10	1.7
4	TGF-beta signaling pathway	20.6	83	7	3.59E-07	3.59E-07	2.50E-08	2.50E-08	5.7
5	GnRH signaling pathway	10.2	93	3	0.01427	0.01427	3.98E-04	3.98E-04	6.0
6	Colorectal cancer	8.9	77	4	8.33E-04	8.33E-04	0.0013	0.0013	1.9
7	Complement and coagulation cascades	8.0	71	4	6.13E-04	6.13E-04	0.00307	0.00307	0.6
8	MAPK signaling pathway	7.3	231	5	0.00872	0.00872	0.0056	0.0056	2.6
9	Cytokine-cytokine receptor interaction	7.0	241	6	0.00209	0.00209	0.00756	0.00756	0.8
10	Jak-STAT signaling pathway	6.4	151	4	0.0094	0.0094	0.01272	0.01272	1.7
11	Toll-like receptor signaling pathway	6.0	91	3	0.01347	0.01347	0.01697	0.01697	1.7
12	Type II diabetes mellitus	5.7	45	2	0.0249	0.0249	0.02165	0.02165	2.0
13	Regulation of actin cytoskeleton	5.6	199	4	0.02349	0.02349	0.02443	0.02443	1.8
14	T cell receptor signaling pathway	5.6	94	3	0.01469	0.01469	0.02533	0.02533	1.3
15	Leukocyte transendothelial migration	5.5	117	3	0.02605	0.02605	0.02636	0.02636	1.9
16	Natural killer cell mediated cytotoxicity	5.2	117	1	0.47172	0.47172	0.03507	0.03507	4.4
17	Adherens junction	4.9	74	2	0.06138	0.06138	0.04504	0.04504	2.1
18	Apoptosis	4.7	81	2	0.07186	0.07186	0.05314	0.05314	2.0
19	Hedgehog signaling pathway	4.6	53	1	0.25081	0.25081	0.05425	0.05425	3.3
20	mTOR signaling pathway	4.6	49	2	0.02916	0.02916	0.05583	0.05583	1.1
21	Wnt signaling pathway	4.5	143	2	0.18231	0.18231	0.05874	0.05874	2.8
23	Insulin signaling pathway	4.3	133	2	0.16301	0.16301	0.0725	0.0725	2.5
24	B cell receptor signaling pathway	4.1	64	2	0.04743	0.04743	0.08311	0.08311	1.1

ENU BREEDING SCHEME

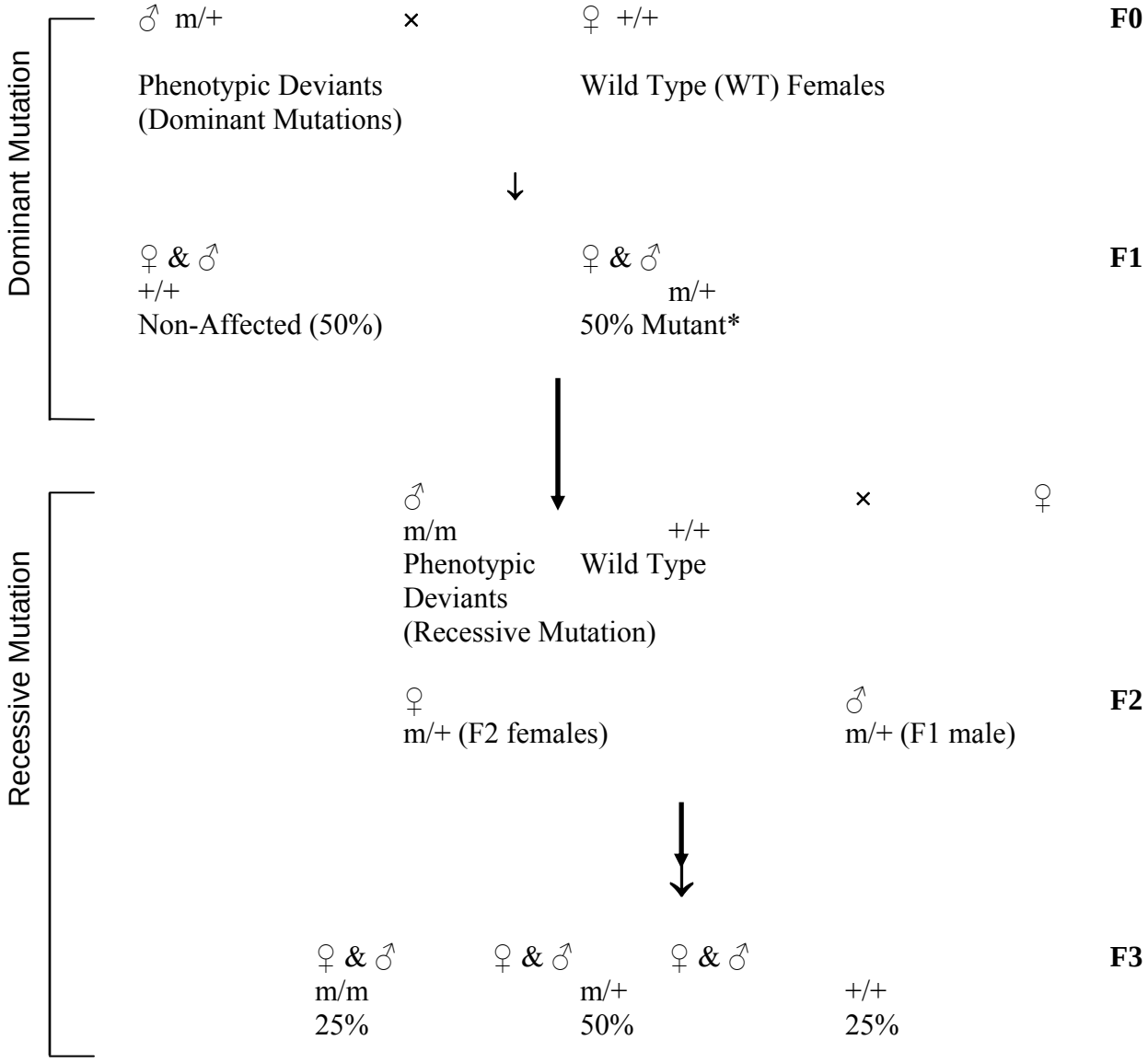

Figure 1. ENU Breeding Scheme. The breeding scheme used for breeding ENU mutants with dominant and recessive mode of inheritance. The percentages reflect theoretical numbers whereas the observed percentages of affected mice show large deviations.

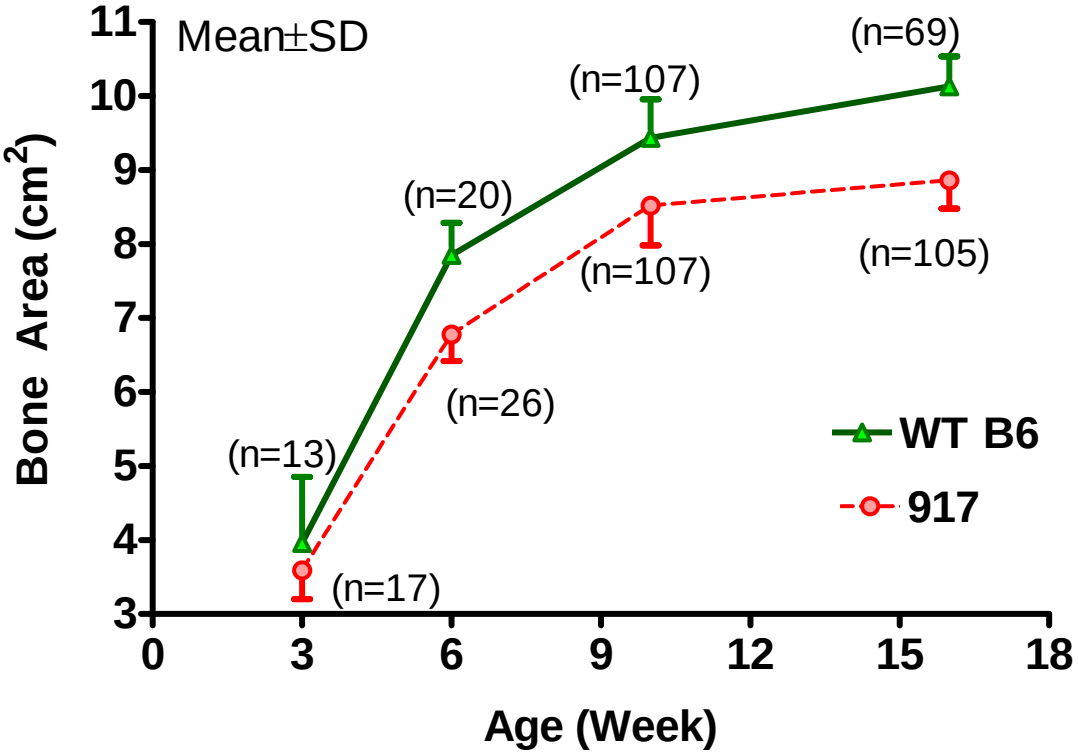

Figure-2. Generation of affected progeny for previously identified phenodeviant with low bone size (Line 917). The y-axis represents total body bone area and x-axis indicates age at which phenotype measurements were performed. The data includes progeny generated during current reporting periods as well as those reported in previous reports (especially 6-16 week data). The 917 data excludes non-affected littermates determined by approximate 2SD cutoff value. The total body bone area were 10-12% lower ($p<0.05$) in mutant mice between 3- and 16-weeks age. Our preliminary data indicates that at 3-week the mutant phenotype is not manifested at 3-weks of age. In this reporting period we generated several new mice for in vivo characterization of the osteoblast proliferation and apoptosis.

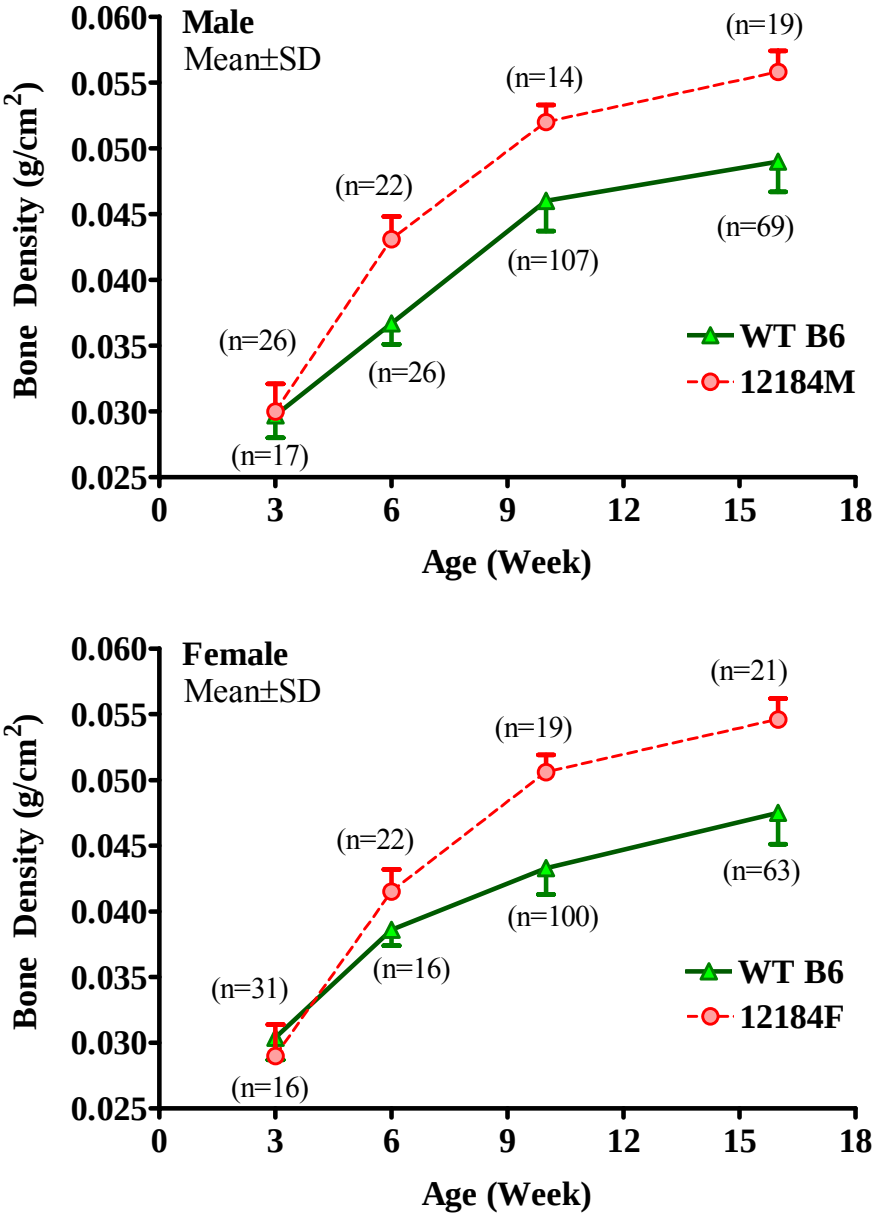

Figure-3. Generation of affected progeny for previously identified phenodeviant with high bone density (Line 12184). The y-axis represents total body bone density and x-axis indicates age at which phenotype measurements were performed. The data represents 12184 progeny generated during current reporting period. The phenotype data excludes non-affected littermates, which was determined by approximate 2SD cutoff value. The total body bone densities were 10-12% higher ($p<0.05$) in mutant mice between 3-weeks and 16-weeks of age. Our preliminary data indicates that at 3-weeks the mutant phenotype is not manifested. In this reporting period we generated several new mice and performed microarray analysis.

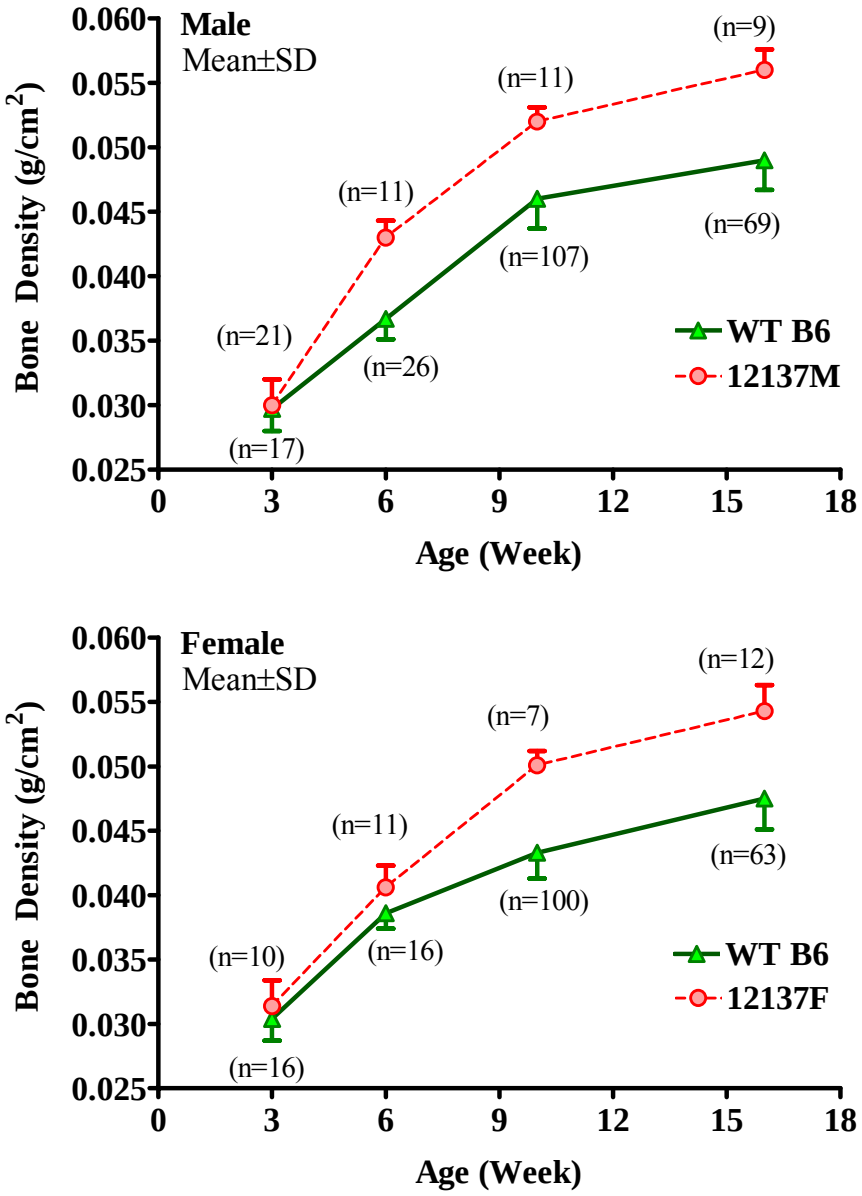

Figure-4. Generation of affected progeny for previously identified phenodeviant with high bone density (Line 12137). The y-axis represents total body bone density and x-axis indicates age at which phenotype measurements were performed. The data represents 12137 progeny generated during current reporting period. The phenotype data excludes non-affected littermates, which was determined by approximate 2SD cutoff value. The total body bone densities were 10-12% higher ($p<0.05$) in mutant mice between 3-weeks and 16-weeks of age. Our preliminary data indicates that at 3-weeks the mutant phenotype is not manifested. In this reporting period we generated several new mice and performed microarray analysis.

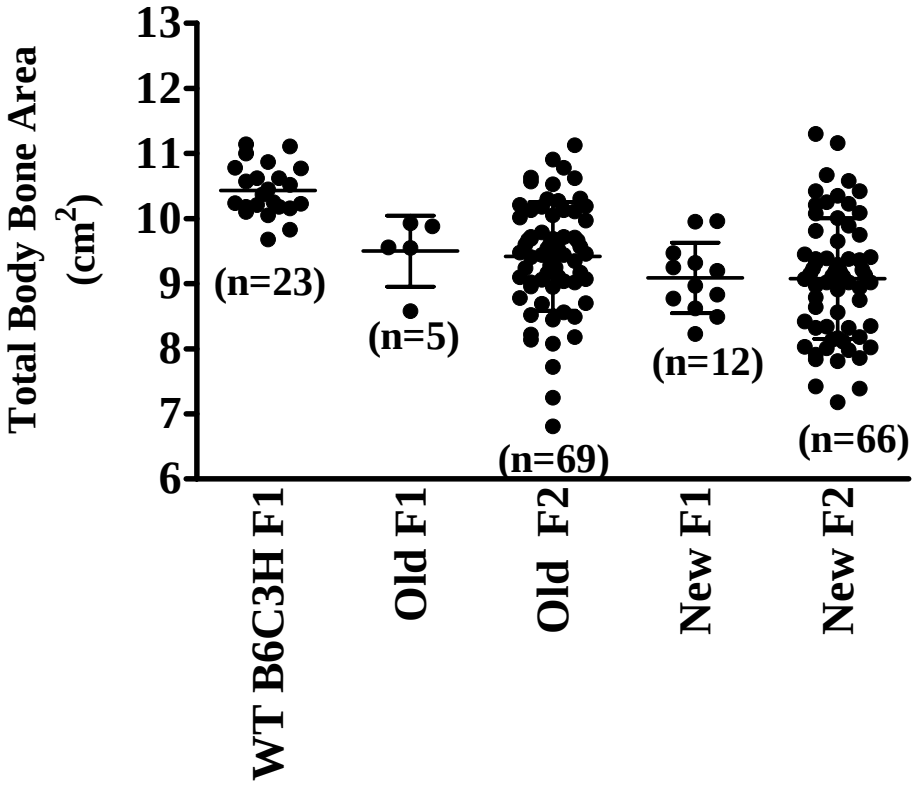

Figure-5. Generation of F1 & F2 progeny for fine mapping of low bone size mutant mice (Line 917). In the current reporting period, we generated several new F1 & F2 mice. This figure shows that the total body bone size phenotype was comparable to those produced previous reporting periods. The bone area data also shows that bone size is robustly expressed in the F1 mice generated from breeding of mutant 917 (B6) with C3H/HeJ mice.

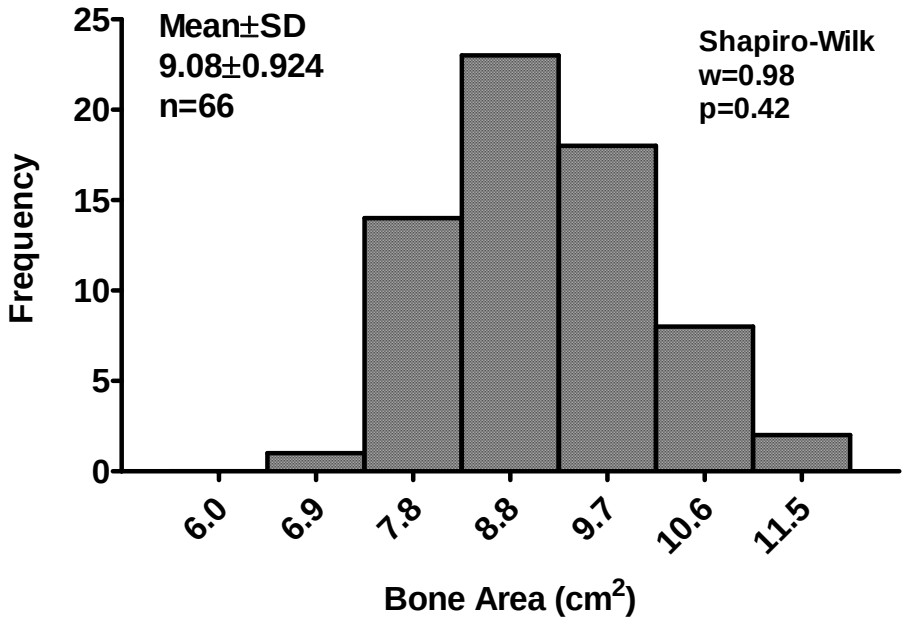

Figure-6. **Frequency distribution of F2 mice (n=66) generated for fine mapping of chromosome 4 locus affecting bone size in 917 mutant mice**. The total body bone area data (measured by DEXA) appears to be normally distributed; therefore, interval mapping could be used to identify QTLs affecting bone size. We are currently producing additional F2 mice to fine map the 917 locus.

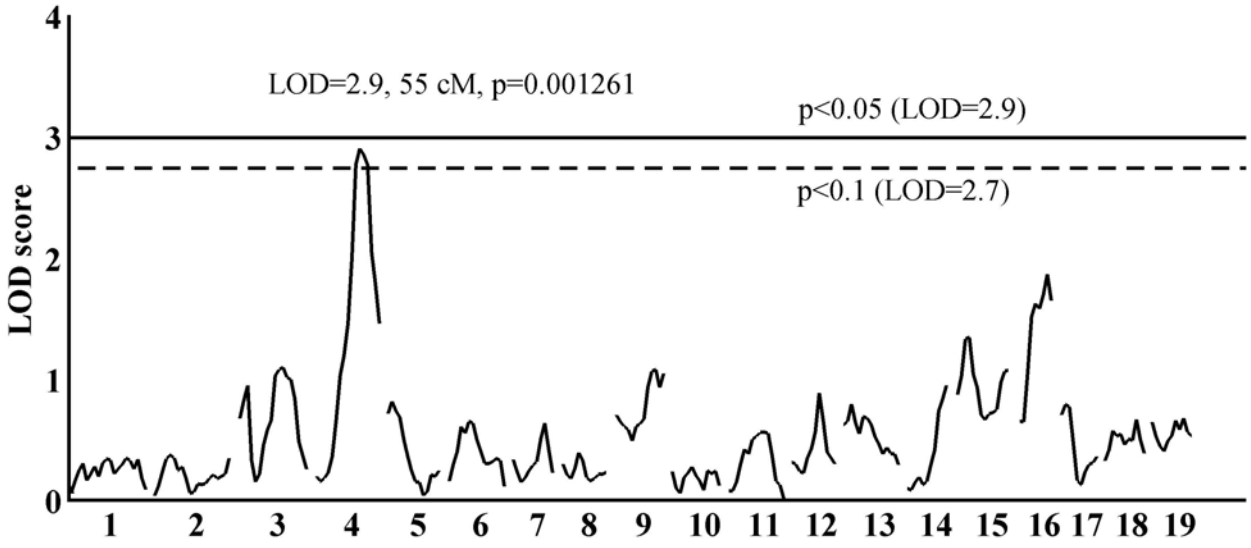

Figure-7. **Mapping chromosomal location of mutation affecting bone mineral density (BMD) in 12137 mutant mice**. Genome wide main QTL(s) associated with total body BMD (measured by DEXA) in 10-week old intercrossed B6C3H F2 male and female mice (n=164 F2 mice and 62 genomic markers) generated from mutant mice 12137. The horizontal lines indicate genome-wide error levels of $p<0.05$ (solid line) and $p<0.1$ (broken line). The interval mapping was performed by Pseudomarker (obtained from www.jax.org/research/churchill) MAINSCAN program written for the MATLAB (Mathworks Inc., Natick, MA, USA) programming environment. Chromosome 4 locus showed suggestive linkage with bone density and bone mineral content in F2 progeny. All F1 & F2 mice used for mapping the 12137 mutation were generated in the previous reporting periods. Total body BMD from male and female F2 mice were statistically different, however, body weight adjusted BMD were similar in male and female F2 mice. Hence, data from male and female F2 could be combined for QTL mapping.

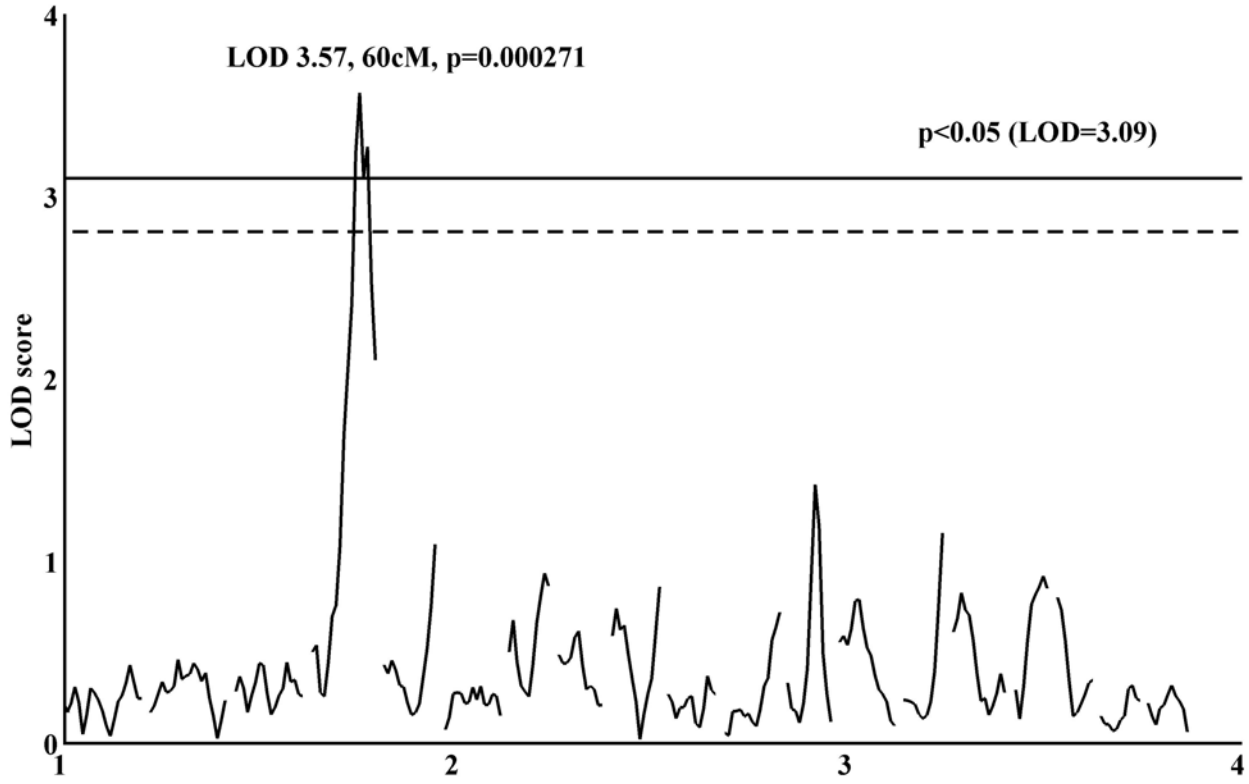

Figure-8. **Mapping chromosomal location of mutation affecting BMC in 12137 mutant mice**. Genome wide main QTL(s) associated with total body bone mineral content (BMC) (measured by DEXA) in 10-week old intercrossed B6C3H F2 male and female mice (n=164) generated from mutant mice 12137. The horizontal lines indicate genome-wide error levels of $p<0.05$ (solid line) and $p<0.1$ (broken line). The interval mapping was performed by Pseudomarker (obtained from www.jax.org/research/churchill) MAINSCAN program written for the MATLAB (Mathworks Inc., Natick, MA, USA) programming environment. Chromosome 4 locus showed a highly significant linkage with bone mineral content in F2 progeny. The total body BMC from male and female F2 mice were statistically different, however, body weight adjusted BMC were similar in male and female F2 mice. Hence, data from male and female F2 could be combined for QTL mapping.

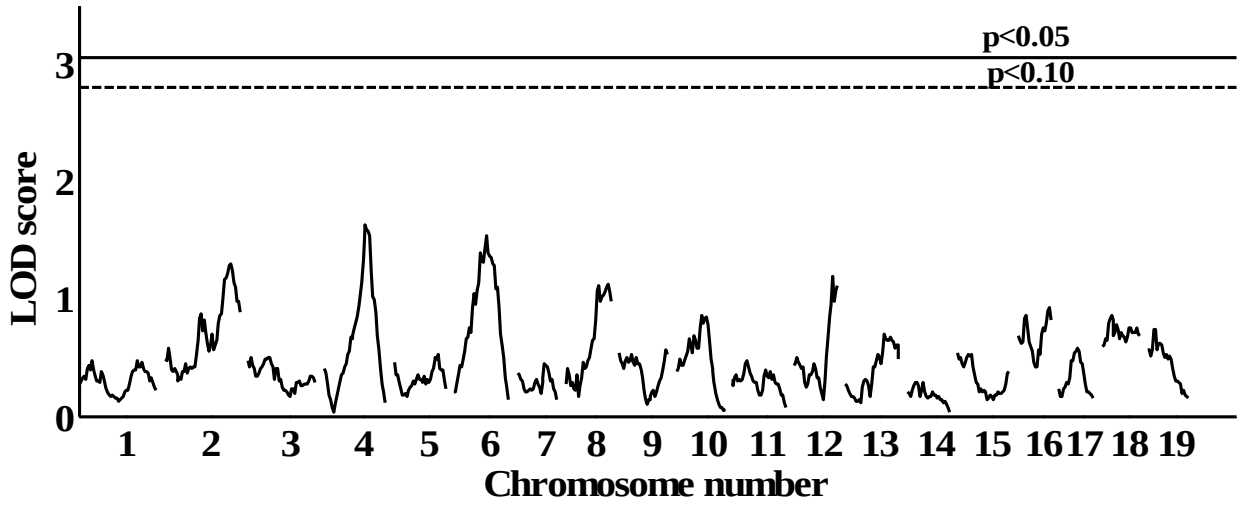

Figure-9. **Interval mapping results of a recessive mutant line B2.4 with high BMD**. Genome wide main QTL(s) associated with total body bone mineral density (BMD) (measured by DEXA) in 10-week old intercrossed B6C3H F2 female mice (n=97) generated from mutant mice B2.4. The horizontal lines indicate genome-wide error levels of $p<0.05$ (solid line) and $p<0.1$ (broken line). The interval mapping was performed by Pseudomarker (obtained from www.jax.org/research/churchill) MAINSCAN program written for the MATLAB (Mathworks Inc., Natick, MA, USA) programming environment. Our results did not disclose significant linkage with any locus. Because the mutation was inherited in a recessive mode and we only mapped a limited number of F2 mice, it could be possible that we have very few mutant mice in the F2 population. Thus, our interval mapping strategy has limited power to detect linkage to a recessive mutation. This was in contrast to dominant ENU mutations where we were able to determine QTLs with only 69 F2 mice. In future studies, we may be able to generate additional F2 mice to increase the power of QTL detection to identify location of mutation.

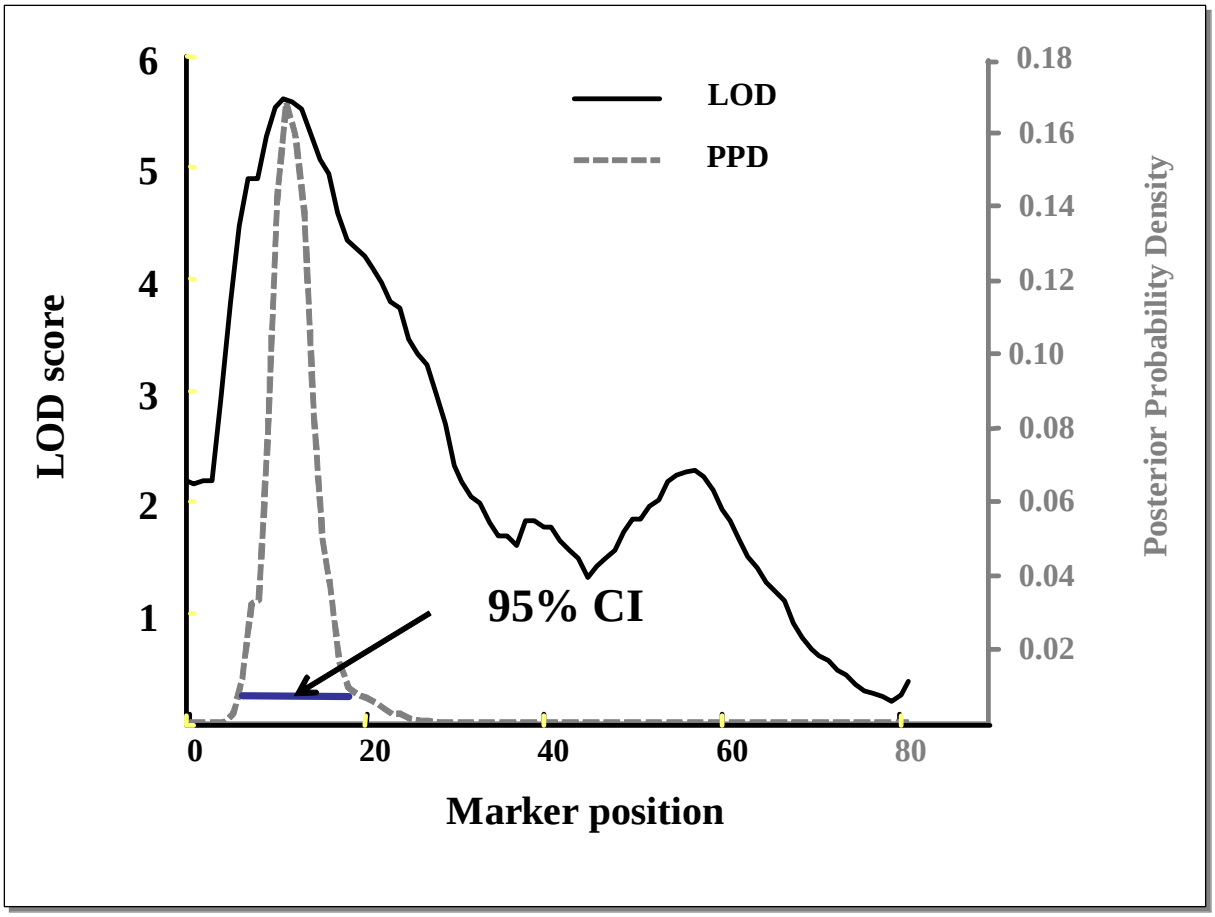

Figure-10. LOD score and posterior probability density plot (calculated by Pseudomarker) for a major quantitative trait locus (QTL) influencing bone size for the mutant line 917 (the data used for generating this plot was reported in previous reporting period). Posterior probability density is a likelihood statistic that gives rise to the 95% confidence intervals and it is shown as thick black horizontal bar. The 95% confidence interval of 917 mutant locus indicated a large region encompassing 4-18 cM. In the current reporting period we added additional markers in this region and re-genotyped the DNA from 917 F2 mice (n=69). The posterior probability density plot for analysis is shown in next figure.

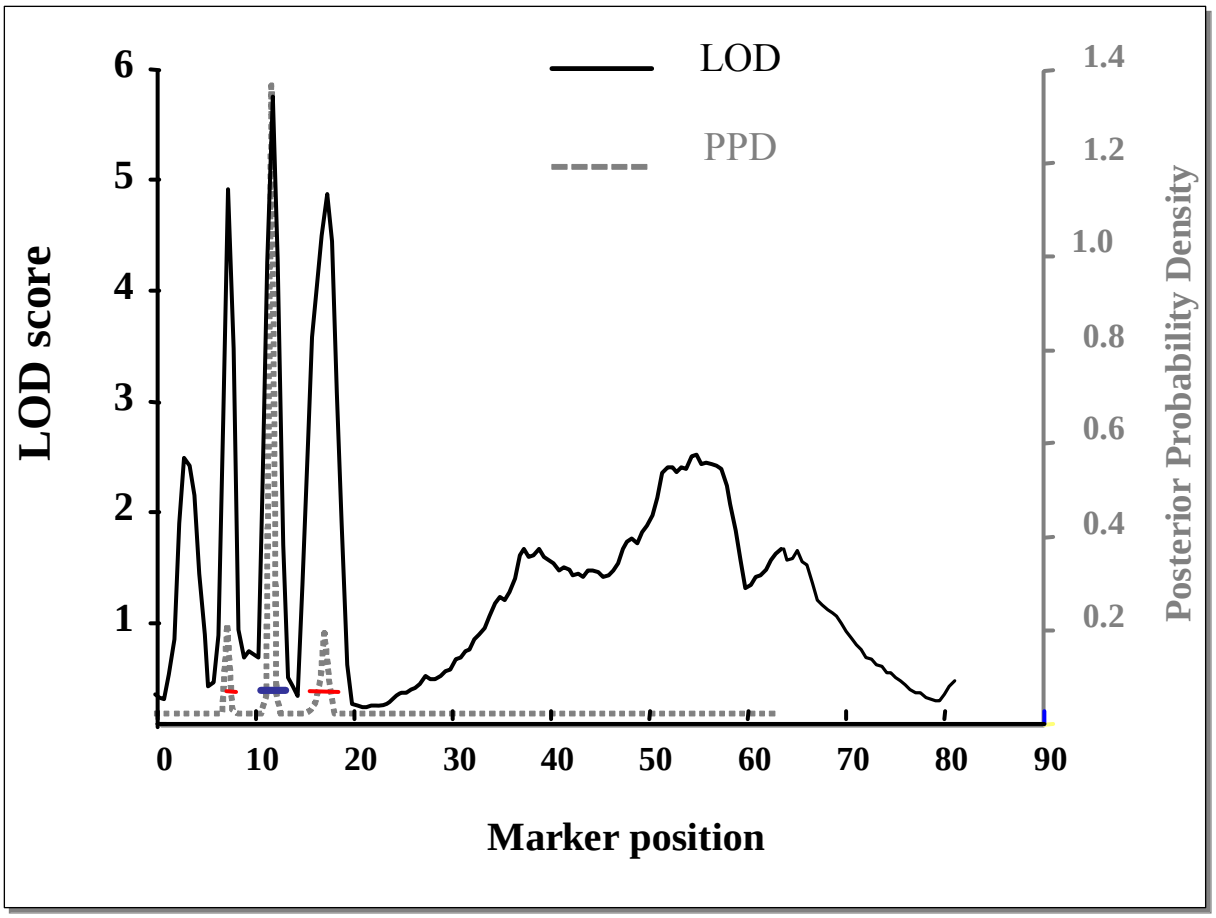

Figure-11. The posterior probability density plot for a fine mapped region of 917 locus using additional marker. LOD score and posterior probability density plot for a major quantitative trait locus (QTL) influencing bone size for the mutant line 917. Posterior probability density is a likelihood statistic that gives rise to the 95% confidence intervals indicated by black horizontal bar. In the current reporting period we added additional markers described in the Table-4 in this region and re-genotyped the DNA from 917 F2 mice (n=69). The figure shows that when additional markers were added the proximal peak was resolved into three major peaks, each showing significant LOD scores ($p<0.05$). However, the posterior probability density plot shows that probability of middle peak, located at 10-12 cM, harboring the mutant gene is higher. We are currently generating additional F2 animal to further refine this locus so that we can focus on small region to identify mutant gene.

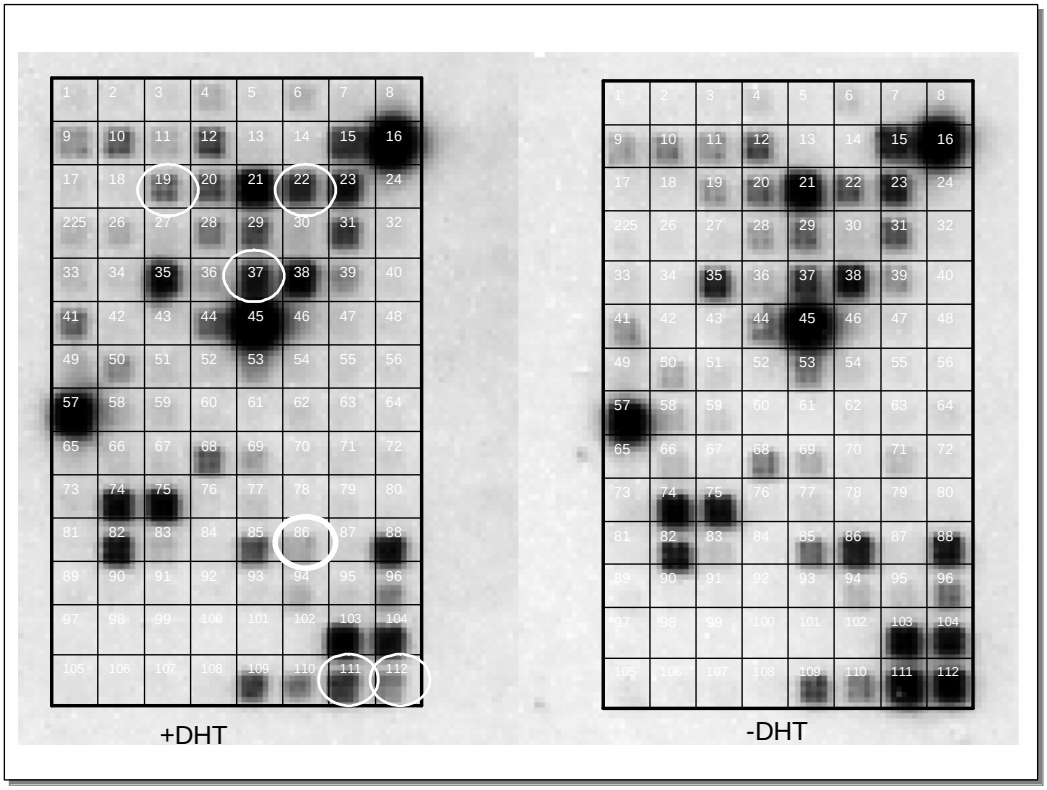

Figure-12. To identify candidate genes for 917 mutation, we used a commercially available pathway-focused DNA array (Mouse Androgen Signalling Gene Oligo GEArray, SuperArray Bioscience Corporation, Frederick, MD). Periosteal osteoblasts were isolated from 10-week old mutant 917 mice and grown in cultures. Osteoblast cultures were maintained overnight in an Alpha-MEM medium containing 10% steroid stripped fetal calf serum. Then culture medium was replaced with a medium containing dihydrotestosterone (5α-DHT) at a concentration of 10^{-8} M (+DHT) or vehicle (-DHT) for 48-hours. After 48-hours cells were isolated and RNA extracted, reverse transcribed, labeled, and hybridized with the membrane. The array, which contained 112 genes, showed several genes (circled) were differentially regulated in response to 5α-DHT treatment of the osteoblasts from 917 mice. We believe that these experiments would provide important clues to prioritize candidate genes for further studies to identify the mutant gene.

APPENDICIES

Edderkaoui B, Baylink DJ, Beamer WG, Wergedal Je, Porte R, Chaudhuri A, and Mohan S. Identification of Duffy antigen receptor for Chemokines (DARC) as a BMD gene. Genome Research, In press, 2007

Li X, Quigg R, Zhou J, Xu S, Masinde G, Mohan S, Baylink DJ. A Critical Evaluation of the Effect of Population Size and Phenotypic Measurement on QTL Detection and Localization using a Large F2 Murine Mapping Population. Genetics and Molecular Biology. 29 (1):166-173, 2006

Yu H, Mohan S, Edderkaoui B, MasindeG, Davidson H, Wergedal JE, Beamer, Baylink DJ. Detecting Novel Bone Density and Bone Size QTL Using a Cross of MRL/MpJ and CAST/EiJ Inbred Mice. Calcif Tissue Int. 80:103-110, 2007.

Srivastava AK, Mohan S, Masinde GL, Yu H, Baylink DJ. Identification of quantitative trait loci that regulate obesity and serum lipid levels in MRL/MpJ x SJL/J inbred mice. J Lipid Res. Jan; 47(1):123-33, 2006

Identification of mouse Duffy Antigen Receptor for Chemokines (Darc) as a BMD QTL gene

Bouchra Edderkaoui, David J. Baylink, Wesley G. Beamer, Jon E. Wergedal, Ryan Porte, Asok Chaudhuri and Subburaman Mohan

Genome Res. published online Apr 6, 2007;
Access the most recent version at doi:10.1101/gr.6009507

Article

Identification of mouse Duffy Antigen Receptor for Chemokines (*Darc*) as a BMD QTL gene

Bouchra Edderkaoui,[1] David J. Baylink,[2] Wesley G. Beamer,[3] Jon E. Wergedal,[1,2] Ryan Porte,[1] Asok Chaudhuri,[4] and Subburaman Mohan,[1,2,5]

[1]*Musculoskeletal Disease Center, Jerry L. Pettis Memorial VA Medical Center, Loma Linda, California 92357, USA;* [2]*Department of Medicine and Biochemistry, Loma Linda University, Loma Linda, California 92354, USA;* [3]*The Jackson Laboratory, Bar Harbor, Maine 04609, USA;* [4]*Laboratory of Cell Biology, New York Blood Center, New York, New York 10021, USA*

It is now well known that bone mineral density (BMD) variance is determined by both genetic and environmental factors. Accordingly, studies in human and animal models have revealed evidence for the presence of several quantitative trait loci (QTL) that contribute to BMD variations. However, the identification of BMD QTL genes remains a big challenge. In the current study, we focused our efforts to identify the BMD candidate gene in chromosome 1 (Chr 1) QTL that was detected from a cross involving high BMD CAST/Ei] (CAST) and low BMD C57BL/6] (B6) mice. To this end, we have combined several approaches including: (1) fine mapping the BMD QTL in Chr 1 of the B6.CAST F_2 female mice using a large number of polymorphic markers; (2) the generation of congenic sublines of mice by repeated backcrossing of CAST with B6 mice and phenotype characterization; (3) expression profiling genes in the QTL region; and (4) SNP analyses to identify the mouse Duffy Antigen Receptor for Chemokines (*Darc*) as a candidate gene for Chr 1 BMD *QTL2*. We verified the involvement of the Darc protein in BMD variation by evaluating the skeletal phenotype of *Darc*-knockout mice and congenic sublines of mice carrying small chromosomal segments from CAST BMD QTL. Based on the findings that Darc-antibody blocked formation of multinucleated osteoclasts in vitro and that Darc from CAST binds chemokines, known to regulate osteoclast formation, with reduced affinity compared with Darc from B6 mice, we conclude that *Darc* regulates BMD negatively by increasing osteoclast formation, and that the genetic association between *Darc* gene polymorphism and BMD variations in humans merits investigation.

[Supplemental material is available online at www.genome.org.]

Osteoporosis is a condition associated with decreased bone strength and an increased fracture risk. Its prevalence is increasing as more individuals with low bone mineral density (BMD), the strongest predictor of fracture risk, are detected. Thus, molecular dissection of the BMD regulatory system may reveal novel therapeutic targets for the treatment of osteoporosis. Several studies preformed on both humans and mice have shown that BMD has a strong heritable component, with estimates that genes account for 60%–80% of BMD variance (Morrison et al. 1994; Beamer et al. 1996; Devoto et al. 1998; Klein et al. 1998; Eisman 1999; Niu et al. 1999; Baldock and Eisman 2004). Accordingly, linkage studies in humans and experimental animal models have identified several BMD QTLs. However, the big challenge has been identifying the "QTL gene." To our knowledge, only a single QTL gene, *Alox15*, has been identified thus far as a BMD QTL gene (Klein et al. 2004).

To screen for BMD candidate genes, we have chosen to dissect the BMD QTL in chromosome 1, because this QTL has been identified in four different intercrosses: C57BL/6J (B6) × Cast/EiJ (CAST) (Beamer et al. 1999), B6 × C3H/HeJ (Beamer et al. 2001), B6 × DBA/2 (Klein et al. 1998), and MRL/MpJ × SJL/J (Masinde et al. 2002). Furthermore, a syntenic region in human chromosome 1q21-q43 carries a previously identified BMD QTL, which has been reported in independent studies using human populations (Koller et al. 2000; Ralston 2002). In this report, we present data on the identification of Duffy Antigen Receptor for Chemokines (*Darc*) as a BMD QTL gene by utilizing a variety of molecular genetic approaches.

[5]Corresponding author.
E-mail Subburaman.Mohan@va.gov; fax (909) 796-1680.
Article published online before print. Article and publication date are at http://www.genome.org/cgi/doi/10.1101/gr.6009507.

Results

Fine mapping and congenic sublines of mice

In a recently published study (Edderkaoui et al. 2006), we reported the identification of three BMD loci at Chr 1 by superimposing the CAST chromosomal regions carried by each congenic subline. The *Bmd1a* locus was located between *D1mit133* and *D1mit453* (133.2–165.2 Mb), the *Bmd1b* locus was located between *D1mit113* and *D1mit150* (171.86–174.76 Mb), and a *Bmd1c*, which regulates BMD negatively, was located between *D1mit221* and *D1mit511* (184.86–192.06 Mb). In this study, we further fine mapped the Chr 1 QTL region by genotyping 565 B6.CAST F_2 female mice with a large number of polymorphic markers from this region. Interval mapping using MapQTL 4.0 to identify the linkage between polymorphic markers and femur total volumetric BMD (vBMD) within the F_2 female mice showed three peaks/QTL: peak 1 at marker *D1mit453* (*Bmd1a*, at 165.2 Mb), peak 2 at marker *D1mit354* (*Bmd1b*, at 172.98 Mb), and peak 3 at marker *D1mit359* (designated as *BMD1-4* at 177.4 Mb) (Fig. 1), which were significantly associated with femoral vBMD. MapMaker software also identified three significant linkages at the same positions (Supplemental Table 1), which explained 9.3%, 10.7%, and 9% of the BMD variation within the B6.CAST

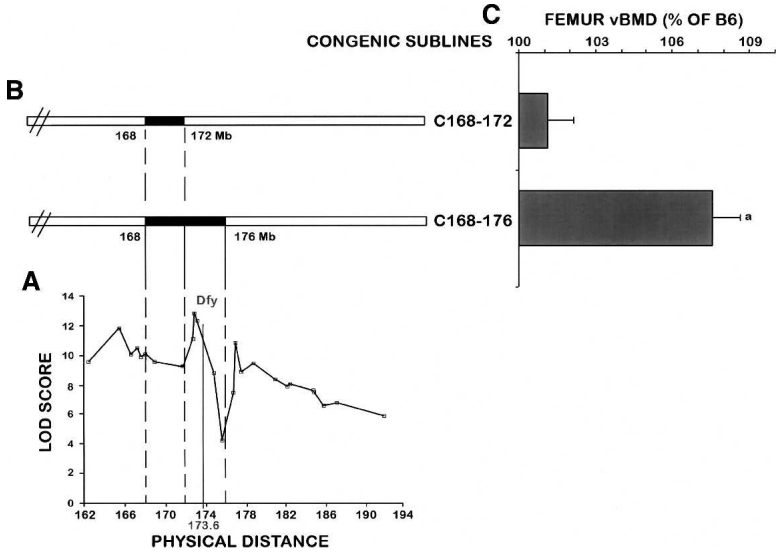

Figure 1. Genetic localization of the *Darc* gene and BMD phenotype of the two congenic sublines C168–172 and C168–176. (*A*) Fine mapping of BMD QTL in chromosome 1 using 33 polymorphic markers. Linkage analyses showed three peaks suggesting at least three BMD QTLs within Chr 1. The *X*-axis represents the physical distance beginning with the centromeric side and extending toward the telomeric side of Chr 1, starting from marker *D1mit106* at 162.33 Mb according to the National Center for Biotechnology Information database (http://www.ncbi.nlm.nih.gov/). The *Y*-axis represents the likelihood values for the presence of a segregating QTL at each marker (LOD score). Genetic localization of the *Darc* gene within the second BMD QTL (*Bmd1b*) is indicated. (*B*) Solid bars represent the CAST chromosomal regions carried by each congenic sublines. (*C*) Femoral vBMD at the mid-diaphysis of the two sublines C168–172 and C168–176 compared with B6 control mice. Each congenic subline is presented (C, referring to the *cast* allele), followed by the position (in megabases) of the two markers flanking the donated CAST segment. We designated the congenic subline B6.CAST-1$^{D1mit370\text{-}D1mit403}$ as C168–176, which indicates the approximate proximal and distal megabase limits known for the CAST chromosomal region, and the congenic subline B6.CAST-1$^{D1mit370\text{-}D1mit113}$ was designated as C168–172. Data are expressed as a percentage of B6 and are mean ± SEM. (a) $P < 0.01$ as measured by Student's *t*-test in congenic subline vs. B6 mice. $n = 10$–14.

F_2 population, respectively. Thus, Chr 1 contains at least four BMD loci, three of which regulate BMD positively and one negatively.

Since the *Bmd1b* QTL showed the highest LOD score, we chose to screen BMD candidate genes within this locus. Therefore, to narrow down the size of the *Bmd1b* QTL region to permit our candidate gene search, we generated additional congenic sublines from the C168–185 subline, as described in Edderkaoui et al. (2006). In the present study, we compared the skeletal phenotype of the congenic subline that carries the CAST chromosomal segment from *D1mit370* to *D1mit403* (168–176 Mb) and the congenic subline that carried the CAST chromosomal region *D1mit370-D1mit113* (168–172 Mb) located between the first and the second peaks/QTL with the B6 control mice (Fig. 1). The congenic subline C168–176 exhibited a significantly greater vBMD compared with the B6 mice (7.5%, $P = 0.01$), while C168–172 did not show any differences compared with the B6 controls. Using this data, we could safely eliminate the genes located at the 168–172 Mb chromosomal region from further analyses (Fig. 1), which narrowed down the size of the *Bmd1b* locus to 172–176 Mb from the centromere in Chr 1. Furthermore, the C168–176 subline exhibited a significantly smaller femur trabecular volume and reduced midshaft endosteal circumference, but no difference in the periosteal circumference (Fig. 2). These changes contributed to an increase in the cortical thickness and correspondingly higher vBMD in the femurs of C168–176 subline compared with the B6 control mice. There was no difference in body weight between C168–C176 and B6 control mice (Fig. 2), suggesting that the variation in BMD phenotype between congenic and B6 mice cannot be explained on the basis of size difference.

Gene expression profiling

In order to screen for potential BMD candidate genes in the 172–176 Mb region, we compared the expression levels of all known genes and ESTs located in this region between the bones of the B6 control mice and the two congenic sublines described above. We chose gene expression change to identify candidate genes, since it is known that SNPs at both the regulatory regions (promoter, 3′-UTR) and coding regions (via feedback loop) could affect the expression of the gene (Schadt et al. 2003; Chesler et al. 2005). In addition, this strategy has been successfully used in a recent study by Klein et al. (2004) to identify a QTL gene that negatively regulates peak bone density. Since C168–172 does not show a BMD phenotype it was used as a negative control, so only genes that showed a difference in the expression between C168–176 and B6, but not between C168–172 and B6, were further analyzed. Among all genes analyzed, only the *Darc* gene, located at 173.6 Mb, showed a sixfold increase of the expression in the C168–176 congenic subline when compared with the control progenitors (Supplemental Table 2), while no difference was found in expression between the C168–172 and B6 control mice. Since none of the other genes exhibited more than twofold difference that is significant, we focused on *Darc* as a candidate gene.

Skeletal phenotype of *Darc*-KO mice

If the increase of *Darc* gene expression in B6.CAST-1 congenic mice is responsible for the greater femur BMD exhibited by the C168–176 mice, we would expect *Darc* knockout (KO) mice to show a lower femur BMD compared with control mice. To test this hypothesis, we compared the phenotype of *Darc*-KO mice generated in a B6 background with that of age-gender-matched wild-type B6 progenitors. Body weight as well as femur length were similar for the two strains (Fig. 2), while total femur vBMD was increased in the *Darc*-KO mice compared with the wild-type control mice. The trabecular volume was 13% smaller in the *Darc*-KO mice compared with the wild-type mice ($P < 0.01$), the endosteal circumference was decreased by 3.8%, and there was no change in periosteal circumference, which resembles the phenotype of the C168–176 subline and confirms the involvement of the *Darc* gene in BMD variation. Based on these data we considered an alternate possibility that the high expression of *Darc* might be secondary to a loss of the protein function.

SNP analyses

We next sequenced the *Darc* gene to determine the SNPs that might be the cause of the difference in the expression between

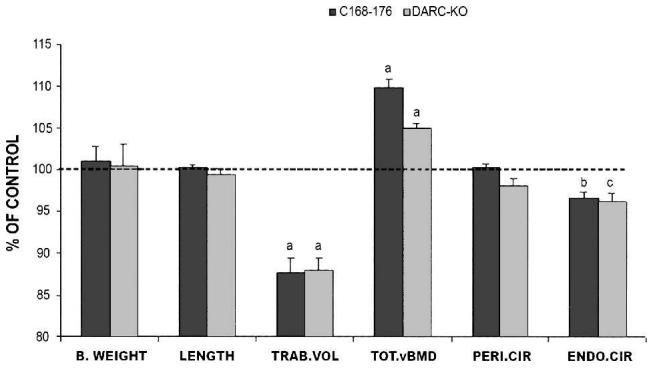

Figure 2. Femoral and body weight data from the C168–176 congenic subline of mice and *Darc*-KO mice. Data are expressed as a percentage of B6 and are mean ± SEM. (a) $P < 0.01$, (b) $P = 0.01$, (c) $P = 0.05$ as measured by Student's *t*-test, with $n = 10–14$. (B.WEIGHT) Body weight, (LENGTH) femur length, (TRAB.VOL) total femur trabecular volume, (TOT.vBMD) total volumetric bone mineral density, (PERI.CIR) periosteal circumference, (ENDO.CIR) endosteal circumference.

the B6 mice and the high BMD congenic subline of mice. Using the NCBI database and in-house sequencing, we have identified 28 polymorphisms that distinguish the *Darc* gene in B6 from the CAST strain (Table 1), with three SNPs located at the promoter region, 15 polymorphism sequences located at the intervening sequence, and 10 polymorphisms at the coding region. Among the polymorphisms in the coding region, only six led to amino acid changes (Table 1). None of the polymorphisms discovered in the promoter region covered the consensus sequences that potentially regulate the transcription process, so it is likely that the difference in the expression of the *Darc* gene is due to the SNPs in the coding region. In order to determine if the SNPs in the *Darc* gene could be responsible for BMD variation, we compared the *Darc* gene sequence of B6 and CAST with another high BMD strain, namely C3H/HeJ (C3H). We found that the six informative SNPs in the coding region were conserved in both CAST and C3H, suggesting that one or more of these SNPs could contribute to the high BMD phenotype exhibited by CAST and C3H mice (Table 1).

Table 1. Summary of sequence variants detected in *Darc* gene

Nucleotide change CAST/C3H/B6	Polymorphism position (bp)	Intron/exon	Amino acid change CAST/C3H/B6	Amino acid position
A/A/C	−456	Promoter		
A/A/C	−325	Promoter		
G/A/G	−234	Promoter		
T/T/G	−169	Promoter		
A/–/T[a]	129	Intron		
GT/GT/Del.	131	Intron		
C/C/T	147	Intron		
C/C/T	163	Intron		
G/A/A	184	Intron		
T/T/C	201	Intron		
C/C/T	285	Intron		
T/T/C	308	Intron		
A/A/T	310	Intron		
A/A/G	372	Intron		
G/G/T	382	Intron		
A/A/T	405	Intron		
G/G/A	408	Intron		
T/T/C	454	Intron		
C/C/T	467	Intron		
C/C/A	493	Exon 2	T/T/N	10
A/A/G	631	Exon 2	D/D/G	56
G/G/T	644	Exon 2	L/L/L	60
G/A/G	690	Exon 2	G/S/G	76
T/C/C	830	Exon 2	H/H/H	122
T/T/C	920	Exon 2	N/N/N	152
T/C/T	997	Exon 2	L/S/L	178
A/A/G	1044	Exon 2	T/T/A	194
CT/CT/TG	1084	Exon 2	T/T/M	207
T/T/C	1126	Exon 2	L/L/P	221
C/C/T	1267	Exon 2	T/T/I	286
T/T/C	1286	Exon 2	C/C/C	292

The positions of the SNPs in the promoter regions were taken according to the sequence reported by Luo et al. (2000), while the polymorphism sequences located within the gene from the start codon to the stop codon were taken according to CAST sequence AB039077. The gene was sequenced from −580 bp to the stop codon.
[a](–) Data unavailable.

Binding assay

The *Darc* gene is an acidic glycoprotein that spans the plasma membrane with seven transmembranous helices, like all members of the G-protein-coupled chemokine receptors (Fig. 3). As the name implies, the Darc protein is known to bind to several chemokines such as CC chemokines, monocyte chemotactic protein-1 (Ccl2), Ccl5 (regulated on activation, normal T cell expressed and secreted), and interleukin-8 (Il8). These cytokines have been shown to regulate formation and activity of osteoclasts via tumor necrosis factor ligand (Tnfsf11)-dependent and -independent mechanisms (Wise et al. 2002; Bendre et al. 2003, 2005; Kim et al. 2005).

Tournamille et al. (1997) have reported that the chemokine binding pocket of the Darc protein is located in the first and fourth extracellular domains, which are brought into close vicinity by a disulfide bridge (Fig. 3). Among the six SNPs found in the coding region, the aspartic acid at position 56 seems to be significant due to its location close to the cysteine at position 49, which is required to form the disulfide bridge between transmembrane helices 1 and 7 in the chemokine binding pocket. The change of a small and neutral amino acid glycine with a negatively charged aspartic acid could change the conformation of the protein as well as the chemical environment of the binding sites, which consequently may affect the binding of the Darc protein to the chemokines and/or the stability of Darc protein. Accordingly, we predict that the Darc protein in CAST binds to chemokines much less efficiently compared with the Darc protein from B6 mice. The decreased protein function could contribute to increased expression as a consequence of loss of the feedback control. To test this hypothesis, we analyzed the binding of chemokines to nonadherent bone marrow cells (NABMC) derived from *Darc* knockout and congenic mice. We chose Ccl2, Ccl5, and Il8 as ligands for the binding studies based on previous findings that these chemokines bound to the Darc protein and all the three chemokines have been shown to regulate osteoclast formation. By using ^{125}I-labeled Ccl2, Il8, and Ccl5 for the

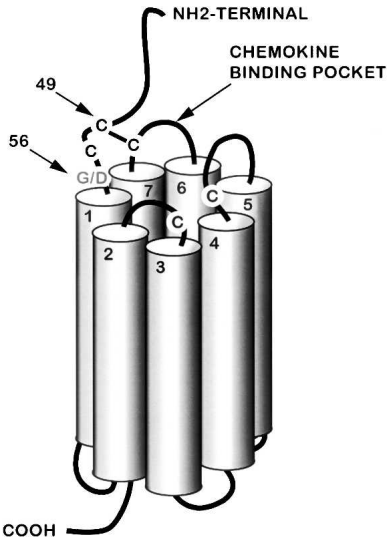

Figure 3. Schematic presentation of the predicted model of Darc protein based on analogy with the Il8 type A receptor (modified from Tournamille et al. 1997). The three cysteine residues that form the chemokine binding site are brought into close proximity by a disulfide bridge between the first and the fourth extracellular domains of the Darc protein. The cysteine residue at the N terminus that forms the bridge is at position 49 in the mouse *Darc* sequence. The position of the SNP G56D is indicated.

binding studies, we found that the specific binding of the three chemokines was significantly reduced in the NABMC derived from both the C168–176 subline and *Darc*-KO mice compared with B6 mice (Fig. 4A).

In vitro osteoclast formation assay

Since Darc protein binds to a number of chemokines that regulate osteoclastogenesis, we next determined if reduced binding of chemokines to Darc in congenic mice is associated with corresponding changes in osteoclast formation.

We treated nonadherent bone marrow cells (NABMC) with Tnfsf11 and macrophage colony stimulating factor (Csf1), the two major cytokines reported to be involved in osteoclast formation (Quinn et al. 1998; Takahashi et al. 1999). The *Darc*-KO mice showed a 50% decrease in the number of TRAP-positive MNC compared with the wild-type mice. Furthermore, despite the increase of *Darc* gene expression in C168–176, this subline showed a 70% decreased formation of TRAP-positive MNC compared with B6 control mice (Fig. 4B). In addition, treatment of NABMC with Darc-antibody (Darc-Ab) in the presence of Tnfsf11 and Csf1 resulted in a significant reduction in the number of TRAP-positive multinucleated cells (Fig. 4C,D). These data together offer strong evidence that Darc protein is involved in osteoclast formation and/or activity, and that the reduced osteoclast formation in the NABMC of CAST mice could be explained on the basis of reduced activity of Darc protein in CAST mice compared with B6 mice.

In vivo histomorphometry study

Consistent with the in vitro data, we found that the TRAP-positive bone resorbing surface was significantly reduced both at the endosteum (47%, $P = 0.002$) and the periosteum (8%, $P = 0.02$) of femurs isolated from *Darc*-KO mice compared with control mice as determined by histomorphometric analyses (Fig. 5). In contrast, bone formation rate was not significantly different in the femurs of *Darc*-KO mice compared with control mice (Fig. 5). We are in the process of breeding a congenic subline of mice carrying the *Bmd1b* locus for the purpose of performing histomorphometry studies in order to confirm that the increased BMD in congenic mice is also due to reduced bone resorption.

Discussion

Osteoporosis is a common disease characterized by reduced bone mass and increased risk of fragility fractures. Because of the well recognized importance of a genetic component in the pathogenesis of osteoporosis, there is now considerable interest among researchers in the bone field to identify genes that contribute to variation in peak bone mass. To identify osteoporosis genes, several approaches have been employed that include association studies and linkage analysis in humans and in experimental model organisms. While the association studies have identified a number of potential candidate genes that contribute to osteoporosis susceptibility, relatively few candidate gene polymorphisms have been validated by large-scale studies. Linkage studies in humans and various animal models, on the other hand, have revealed evidence in almost every chromosome for the presence of genetic loci that regulate bone mass (Beamer et al. 1999, 2001; Koller et al. 2000; Kammerer et al. 2003; Karasik et al. 2004; Volkman et al. 2004; Peacock et al. 2005; Ralston et al. 2005). Together, the association and linkage studies point to the fact that osteoporosis susceptibility is determined by a large number of genes with a modest or small effect size and not by few genes of major effect as originally thought. Accordingly, our data with a large number of congenic strains carrying overlapping CAST chromosomal segments from Chr 1 BMD QTL have revealed that there are at least four BMD loci in Chr 1, each contributing to 4%–12% of the variation in peak bone mass (this work and Edderkaoui et al. 2006).

The successful cloning of the QTL gene depends on the ability to resolve genetic effects into sufficiently small intervals to make gene identification feasible. In this regard, we were able to utilize strategies involving high-resolution mapping with a large number of markers and congenic sublines of B6 mice containing overlapping segments of CAST Chr 1 in the QTL region to successfully narrow down the size of the *Bmd1b* locus to 4 Mb. Since the 4-Mb regions did not contain any obvious functional candidate gene for peak bone mass, we utilized the alternate approach of identifying candidate genes based on gene expression changes and SNP analyses. This approach led to the identification of the *Darc* gene, which was subsequently confirmed as a BMD QTL gene by functional studies. Our findings along with those of Klein et al. (2004) provide feasibility that the small effect of BMD QTL genes can be identified by an integrated approach involving fine mapping, use of congenic sublines containing the QTL gene, gene expression profiling, SNP analyses, and functional studies.

In the current study, *Darc* was identified as a BMD *QTL1-2* candidate gene based on differential expression and SNP analyses between congenic sublines and B6 mice. The basis for the increased expression of *Darc* in congenic mice can only be speculated at this time. In this regard, it is possible that the loss of protein function caused by changes in key amino acids in the chemokine binding pocket could lead to increased expression due to the loss of negative feedback. Accordingly, we found re-

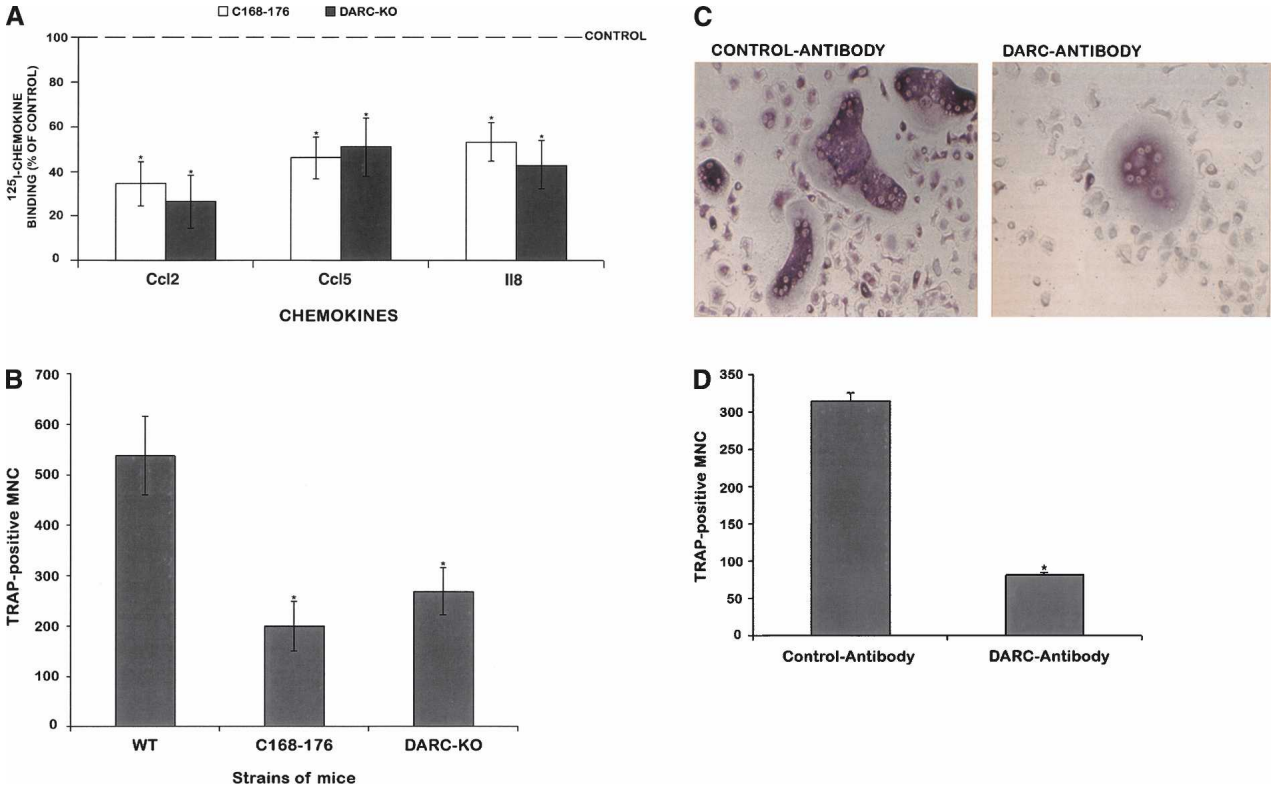

Figure 4. In vitro analysis of nonadherent bone marrow cells (NABMC) from B6, C168–176 congenic subline, $Darc^{+/+}$, and $Darc^{-/-}$ mice. (*A*) Binding of three chemokines to NABMC. NABMC were incubated at 37°C/RT in the presence of either ^{125}I-chemokine only or both labeled and unlabeled chemokine. The specific binding was expressed as the CPM value in the absence of cold chemokine subtracted from the CPM value in the presence of cold chemokine. Data are expressed as a percentage of ^{125}I-chemokine binding to NABMCs derived from B6 control mice, $n = 8–10$. (*B*) Osteoclast generation in response to Tnfsf11 (100 ng/mL) and Csf1 (100 ng/mL). After 10 d in culture, cells were stained for TRAP activity, and only cells with more than two nuclei (MNC: multinucleated cells) were counted. Data are expressed as a mean ± SEM. Six to eight mice were used for each strain of mice. (WT) Wild-type mice. Groups were compared with wild-type mice with Student's *t*-test. (*) $P < 0.05$ vs. B6 control mice. (*C*) Effect of Darc-antibody on TRAP-positive cells derived from NABMC of wild-type B6 mice. After 6 d of treatment with goat polyclonal Darc-Ab in the presence of Tnfsf11 and Csf1 (*right* panel), the number of TRAP-positive multinucleated cells decreased considerably compared with cells treated with control IgG in presence of Tnfsf11 and Csf1 (*left* panel). (*D*) Number of TRAP-positive MNC derived from NABMC of wild-type B6 treated with Tnfsf11 and Csf1 in the presence of either Darc-antibody or control antibody. The data are expressed as mean ± SEM. The experiment was repeated twice with cells derived from four mice each time. (*) $P < 0.05$ vs. control antibody (normal goat IgG).

duced binding of a number of chemokines to Darc from congenic mice compared with B6 mice. Alternatively, the increased expression may be caused by SNPs in the regulatory regions that are involved in transcriptional regulation and/or mRNA stability. In any case, the proof that the *Darc* gene is the BMD *QTL1-2* gene came from in vitro and in vivo functional studies. We have found that *Darc*-knockout mice exhibited a similar skeletal phenotype as that of the congenic subline of mice carrying the *Bmd1b* locus. The higher BMD in the congenic subline of mice carrying the *Bmd1b* locus and *Darc*-knockout mice is contributed by cortical thickness that is caused by reduced endosteal circumference. The reduced bone marrow cavity in the absence of functional *Darc* could be due to reduced resorption and/or increased bone formation at the endosteum. In this regard, our in vitro osteoclast formation assay using NABMC revealed a significant reduction in osteoclast formation in NABMC derived from congenic as well as *Darc*-knockout mice compared with B6 mice. Consistent with these data, bone resorption but not bone formation was significantly reduced in the *Darc*-knockout mice compared with B6 mice. Based on these data, we conclude that *Darc* is a negative regulator of osteoclasts and that bone resorption is reduced in the absence of *Darc*, resulting in increased BMD.

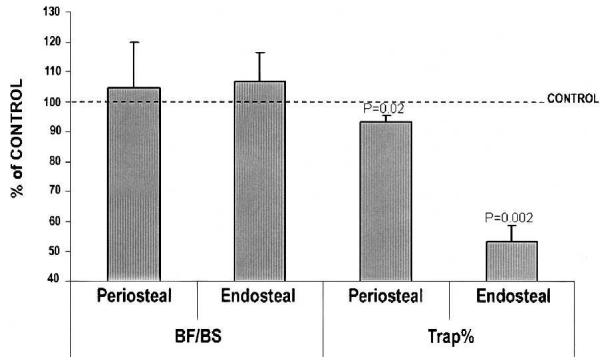

Figure 5. Bone formation and bone resorption rates in femur from *Darc*-KO mice. Bone formation is calculated as bone formation surface (BF) divided by total bone surface (BS). Bone resorption (Trap%) is calculated as (the resorbing surface/bone surface) × 100. The data are expressed as the percentage of wild-type values, $n = 8–13$, (*) $P < 0.05$ vs. wild-type control mice.

As to how Darc regulates osteoclast formation, it is known that Darc binds to chemokines that are involved in osteoclast formation. Although Darc was first identified as Duffy blood

antigen (Pogo and Chaudhuri 2000), there is now considerable evidence that Darc regulates cell trafficking and modulates the bioavailability of several chemokines such as Ccl2 and Ccl5 (Chaudhuri et al. 2003; Kashiwazaki et al. 2003), which are chemotactic signals for monocytes and are responsible for the migration of osteoclast precursors to fuse into differentiated osteoclasts (Kim et al. 2005). Therefore, based on our data and the previously published data about *Darc* and the chemokines function, we postulate a model of *Darc* involvement in osteoclast formation. As reported by Kim et al. (2005), the activation of osteoclast precursors by Tnfsf11 and Csf1 leads to an increase in the expression of Ccl2 and Ccl5, which are known to bind to *Darc*. Since Darc is involved in cell trafficking, and based on our finding that Darc-antibody inhibits osteoclast formation, we postulate that Darc–chemokine signaling is involved in osteoclast precursors trafficking for subsequent fusion into differentiated osteoclasts. Accordingly, the disruption of Duffy as in *Darc*-KO mice or C168–176 mice would lead to an alteration of osteoclast formation (Fig. 6). Our current studies are focused on testing the possibility that Darc is involved in the trafficking of osteoclast precursors for subsequent fusion.

In humans, the Duffy blood group system consists of four alleles, five phenotypes, and five antigens (Pogo and Chaudhuri 2000). Duffy-negative individuals are predominantly Africans and American blacks; they lack the Duffy protein on erythrocytes and are resistant to *Plasmodium vivax* and *Plasmodium knowlesi* infections (Miller et al. 1975, 1976). In addition, it has been well established that African-Americans exhibit significantly higher BMD compared with Caucasians (Yanovski et al. 2000; Cauley et al. 2005). Our finding that total femur vBMD is increased in *Darc*-KO mice compared with B6 mice raises the interesting possibility that BMD variation between African-Americans and Caucasians could be due in part to a difference in the function of Darc between the two groups.

Since *Darc*-KO mice were generated in a mixed genetic background involving 129 and B6 strains, it is important to rule out the possibility that another gene contributed by the 129 strain was responsible for the increased BMD in the *Darc*-KO mice. In this regard, *Darc*-KO mice used in this study have been backcrossed with B6 mice for at least eight generations to minimize the genetic contribution of the 129 strain. After eight backcrosses, the genetic contribution of the donor strain is estimated to be <1% (Silver 1995). Accordingly, much of Chr 1 is derived from B6 mice except a small region surrounding the *Darc* gene that was found to be homozygous for 129 (171–177 Mb), which was not surprising since homologous recombination to disrupt the *Darc* gene was carried out using stem cells derived from 129 mice, and since mice carrying the *Darc*-KO gene from 129 were selected for subsequent backcrosses with B6 mice. Our findings that NABMC derived from both congenic and *Darc*-KO mice exhibit reduced potential to form TRAP-positive multinucleated osteoclasts in vitro and that blockage of *Darc* action using neutralizing antibody to *Darc* reduced osteoclast formation in NABMC derived from B6 mice provided further experimental data for the *Darc* being the Chr 1 BMD *QTL2* gene. However, the ultimate proof for *Darc* as a BMD QTL gene will require knock-in of a CAST copy of the *Darc* gene in the B6 background or vice versa and demonstration of the corresponding BMD phenotype in the knock-in mice.

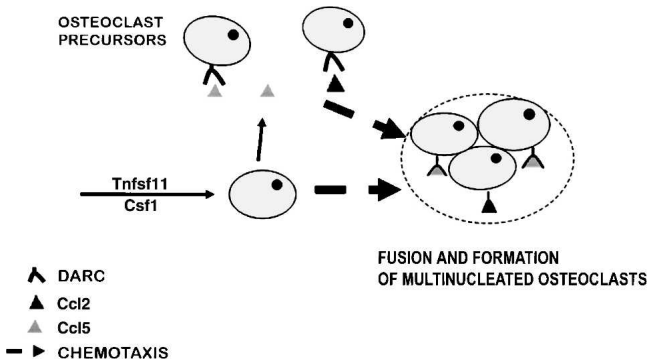

Figure 6. Model of *Darc* involvement in osteoclast generation. Activation of osteoclast precursors leads to increased expression of Ccl2 and Ccl5, which bind to Darc protein. Darc–chemokine signaling is involved in osteoclast precursor trafficking for subsequent fusion into differentiated osteoclasts.

In conclusion, this was the first study, to our knowledge, to provide strong evidence that the *Darc* gene plays an important role in regulating femur BMD via controlling osteoclastogenesis. Investigations into the molecular mechanism by which the Duffy protein regulates osteoclastogenesis could lead to the development of novel drug targets for the diagnosis and/or treatment of osteoporosis.

Methods

Mice

The study used two inbred strains of mice, C57BL/6J (B6) and CAST/EiJ (CAST), which have been previously shown to differ widely in total femur vBMD at 16 wk of age (Beamer et al. 1999). The rationale for selecting these two inbred mouse strains was based on the fact that these strains are highly polymorphic for genetic differences at >95% of their genomes (Dietrich et al. 1996). The B6.CAST F_2 mice were produced and maintained at the animal research facility of The Jackson Laboratory (TJL; Bar Harbor, ME), as previously described (Beamer et al. 1999), while the congenic sublines of mice were generated and maintained at the Jerry L. Pettis VA Medical Center (LL; Loma Linda, CA) under the standard conditions previously described by Edderkaoui et al. (2006). The animal work performed in this study was approved by the institutional animal care and use committees at both TJL and LL. *Darc*-knockout (*Darc*-KO) mice as well as the control mice were generated as previously described by Luo et al. (2000), and were bred and maintained in LL under the same conditions previously described by Edderkaoui et al. (2006).

Fine mapping the B6.CAST F_2 population

Spleens from 565 B6.CAST F_2 female mice were received from Wes Beamer (TJL) to be used for genotyping. Extractions of genomic DNA from the spleens were performed following the Gentra PurGene protocol (PUREGENE Tissue kit, part no. D-7000A). In order to fine map the BMD QTL in Chr 1, we used 33 polymorphic markers located within the BMD QTL region that covers 24.6 cM in mouse Chr 1, between *D1mit106* and *D1mit511* as described by Edderkaoui et al. (2006), instead of the seven markers that were previously used to identify the major BMD QTL in this region (Beamer et al. 1999). The number of markers was increased in order to detect and evaluate the effect of more potential recombinations within the major QTL region.

Genotyping data from the F_2 population were analyzed using MapQTL (4.0) software (CPRO-DLO), and Mapmaker software was used to test the reproducibility of MapQTL data. MapQTL interval mapping was used for quantitative trait loci

mapping, and the LOD score significant thresholds were calculated using MapQTL permutation tests at a confidence level of 99%.

Generation of congenic sublines and genotyping

The B6.CAST-1$^{D1mit370\text{-}D1mit152}$ congenic (C168–185) subline, previously described by Edderkaoui et al. (2006), was used to generate more congenic sublines and break down the cast region first transferred to the B6 background. Additional crosses between the C168–185 congenic subline and the B6 progenitor produced new recombinations carrying smaller overlapping segments that were fixed by crossing the heterozygous mice of same recombination between one another. Each subline was genotyped using the polymorphic markers that encompass the region 168–185 Mb from the centromere (Edderkaoui et al. 2006).

Darc-KO mice were generated as previously described (Papaioannou and Johnson 1993; Luo et al. 2000) and backcrossed with C57BL mice. DNA extraction and genotyping were performed as described by Edderkaoui et al. (2006).

Phenotypic analyses

Based on data from previous studies, which showed that rapid acquisition of vBMD peaked at ~16 wk, resulting in significant higher density values in the CAST females compared with the B6 females (Beamer et al. 1999), only females were used in this study and all measurements were performed at 16 wk of age.

All the measurements for the B6.CAST F_2 mice were performed at TJL as described by Beamer et al. (1999). For the B6 control mice and B6.CAST-1 congenic sublines of mice, bones were stored and processed as described by Edderkaoui et al. (2006).

The measured parameters for the congenic sublines of mice as well as knockout mice were expressed as the percentage of B6 control mice and were mean ± SEM. Characteristics of the congenic sublines as well as knockout mice were compared with the B6 control progeny using a Student's *t*-test, and differences were judged statistically significant when $P < 0.05$. Data from the congenic sublines mice were compared with B6 progenitors provided by TJL and bred in LL, while the *Darc*-KO mice data were compared with the B6 control mice provided by Dr. Chaudhuri (New York Blood Center, New York) and bred in LL.

RNA isolation and real-time PCR analyses

We isolated total RNA from femurs without bone marrow following the protocol supplied by Life Technologies Company using Trizol reagent. Since the BMD phenotype was analyzed in 16-wk-old female mice, only female mice 14 wk of age were used for gene expression studies to screen for candidate genes responsible for this phenotype. We synthesized cDNA by priming 500 ng of total RNA with oligodT in the presence of M-MLV-reverse transcriptase following the manufacturer's protocol (http://www.promega.com/tbs/9pim170/9pim170.pdf).

The quantification of mRNAs was performed in the ABI Prism 7900HT Sequence Detection System (Applied Biosystems) using SYBR Green as a detector dye. The reaction mixture contained 12.5 µL of Brilliant SYBR Green (Stratagene), 2 pmol of each primer, 1 µL of template cDNA, and RNase-free water to a final volume of 25 µL. The oligonucleotide primers were designated in order to amplify the most specific sequence in the coding region of each gene or EST. The relative differences in expression between the groups were determined using cycle time (Ct) values as follows: The Ct values of the genes of interest were first normalized with 18S of the same sample; then the relative differences between the B6 mice and congenic sublines of mice were calculated and expressed as relative increases or decreases, setting the control as 100%. Assuming the Ct value reflects the initial starting copy and there is 100% efficiency, a difference of one cycle is equivalent to a twofold difference in starting copy.

If a significant difference in the expression between the congenic sublines and B6 mice was found for a certain gene, another pair of primers was used to confirm the results, so only the genes that showed a difference with at least two pairs of primers are reported herein. For the *Darc* gene, we have used four pairs of primers. The first two pairs of primers showed a 12-fold increase of the RNA expression in C168–176 compared with B6 mice. However, after sequence analysis, we found that the two primers used for real-time PCR (RT-PCR) covered the polymorphism sequences between B6 and CAST, so we decided to design new primers to determine whether the difference showed by RT-PCR was due to the mismatch or due to any difference in mRNA levels. The new primers that do not cover any SNP showed a sixfold increase of *Darc* expression in the C168–176 compared with B6 control mice.

The primers used to determine *Darc* gene expression level are:

Darc-F1. TCGGGTGGAAACCCTTTCA
Darc-R1. AGCTGGTGTCAGGCTGTAGTCA
Darc-F2. CCTGAATCCCAGACTGAATATTGG
Darc-R2. GAAAGGTGCAGAAGCCATTGTAA
Darc-F3. CCCATTCTGGCAGAGTTAGCA
Darc-R3. TCAACAGAGCTTGGGGAAAAA
Darc-F4. TTCTTCCACTGGCAGATTTGC
Darc-R4. ACCATACCCAGTAGCCCAGGTT

SNPs analyses

We identified SNPs by direct DNA sequence analysis of PCR products. To sequence the promoter region, we have designated primers using the DNA sequence reported by Luo et al. (2000). More primers were designated to amplify overlapping regions from the start codon to the stop codon of the *Darc* gene using a B6 sequence from NCBI, accession no. AC084073.

Chemokine binding to nonadherent bone marrow cells

Bone marrow cells were obtained from femurs isolated from 6-wk-old female B6, C168–176 subline, and *Darc*-KO mice. Femurs were dissected, the ends of the bones were cut, and the marrow was flushed out using a 2-mL syringe and transferred into 15-mL Falcon tubes. Bone marrow cells were dispersed by repeated aspiration of the cell preparation containing Dulbecco's modified Eagle's medium (DMEM) supplemented with 10% heat-inactivated fetal bovine serum (FBS, HyClone). Cells were seeded in 10-cm petri dishes and incubated at 37°C in a humidifier incubator with 5% CO_2. After 24 h, all NABMC were transferred to new 50-mL Falcon tubes and were then counted with a hemocytometer. Cells were then spun down, the supernatant was removed, and the pellet was resuspended in binding medium (DMEM supplemented with 10 mM HEPES, 0.1% BSA at pH 7.4). Each reaction contained 2–4 $\times$ 10^6 cells in a total volume of 250 µL of binding buffer. Cells were incubated for 1 h at 37°C with 200,000 CPM ^{125}I-MCP1 (Ccl2)/Il8 and with or without unlabeled murine Ccl2/Human recombinant Il8 (PeproTech). We have found that Ccl5 binds better at room temperature (RT), so the cells were incubated with ^{125}I-RANTES (Ccl5) for 3 h at RT with and without unlabeled murine RANTES (Ccl5). The reactions were terminated by centrifugation for 10 min at 3000 rpm. The supernatant was removed and the precipitates were washed three times with the binding buffer. Then the radioactivity was

quantified using a gamma counter. Each reaction was carried out using 8–10 replicates.

Cell culture

NABMC were isolated as described above. The pellet was resuspended in DMEM supplemented with 10% FBS at a density of 8×10^5 cells/mL. Cells were then seeded into 24-well plates at a density of 2×10^5 cells/well and treated with murine soluble Tnfsf11 (100 ng/mL, Peprotech) and murine colony-stimulating factor (Csf1, 100 ng/mL, Peprotech). The cultures were maintained for up to 10 d and re-fed twice a week. After 10 d of treatment, the adherent osteoclasts were rinsed with phosphate-buffered saline (PBS), fixed with citrate (4%)–acetone (60%), and then stained using a Leukocyte acid phosphatase kit (Sigma-Aldrich). A Darc-specific polyclonal antibody (Darc-Ab) generated in a goat model against the N-terminal domain of the Darc mouse protein (Santa Cruz Biotechnology) was used to neutralize the Darc protein of B6 wild-type mice. NABMC were treated for 6 d with Tnfsf11 and Csf1 (as described above) in presence of Darc-Ab or control IgG (Sigma-Aldrich). Then the TRAP-positive (pink/purple) multinucleated (MNC) osteoclasts were visualized and counted under light microscopy, and only cells with more than two nuclei were considered.

Histomorphometry study

Femurs from 8-wk-old *Darc*-KO mice and wild-type B6 mice were defleshed and embedded in methylmethacrylate. Thick cross sections (0.5-mm thickness) were cut from the midpoint of the shaft with a diamond wire Histo-saw (Delaware Diamond Knives). The cross sections were ground lightly, mounted in aqueous Fluoromount-G (Fisher Scientific), and examined under an Olympus BH-2 fluorescent/brightfield microscope to measure bone areas and calcein labels. All bone histomorphometric parameters were measured as previously described (Kasukawa et al. 2003).

Acknowledgments

This work was supported by Assistance Award DAMD17-99-1-9571. The US Army Medical Research Acquisition Activity, 820 Chandler Street, Fort Detrick, MD 21702-5014, USA is the awarding and administering acquisition office. All work was performed in facilities provided by the Department of Veterans Affairs and the Jackson Laboratory (AR43618). The information contained in this publication does not necessarily reflect the position or the policy of the Government, and no official endorsement should be inferred. We thank Nancy R. Dunn, Nancy Lowen, and Joe Rung-Aroon for technical assistance.

References

Baldock, P.A. and Eisman, J.A. 2004. Genetic determinants of bone mass. *Curr. Opin. Rheumatol.* **16:** 450–456.

Beamer, W.G., Donahue, L.R., Rosen, C.J., and Baylink, D.J. 1996. Genetic variability in adult bone density among inbred strains of mice. *Bone* **18:** 397–403.

Beamer, W.G., Shultz, K.L., Churchill, G.A., Frankel, W.N., and Baylink, D.J. 1999. Quantitative trait loci for bone density in C57BL/6J and CAST/EiJ inbred mice. *Mamm. Genome* **10:** 1043–1049.

Beamer, W.G., Shultz, K.L., Donahue, L.R., Churchill, G.A., Sen, S., Wergedal, J.E., Baylink, D.J., and Rosen, C.J. 2001. Quantitative trait loci for femoral and lumbar vertebral bone mineral density in C57BL/6J and C3H/HeJ inbred strains of mice. *J. Bone Miner. Res.* **16:** 1195–1206.

Bendre, M.S., Montague, D.C., Peery, T., Akel, N.S., Gaddy, D., and Suva, L.J. 2003. Interleukin-8 stimulation of osteoclastogenesis and bone resorption is a mechanism for the increased osteolysis of metastatic bone disease. *Bone* **33:** 28–37.

Bendre, M.S., Margulies, A.G., Walser, B., Akel, N.S., Bhattacharrya, S., Skinner, R.A., Swain, F., Ramani, V., Mohammad, K.S., Wessner, L.L., et al. 2005. Tumor derived interleukin-8 stimulates osteolysis independent of the receptor activator of nuclear factor-κB ligand pathway. *Cancer Res.* **65:** 11001–11009.

Cauley, J.A., Lui, L.Y., Ensrud, K.E., Zmuda, J.M., Stone, K.L., Hochberg, M.C., and Cummings, S.R. 2005. Bone mineral density and the risk of incident nonspinal fractures in black and white women. *JAMA* **293:** 2102–2108.

Chaudhuri, A., Rodriguez, M., Zbrzezna, V., Luo, H., Pogo, A.O., and Banerjee, D. 2003. Induction of Duffy gene (FY) in human endothelial cells and in mouse. *Cytokine* **21:** 137–148.

Chesler, E.J., Lu, L., Shou, S., Qu, Y., Gu, J., Wang, J., Hsu, H.C., Mountz, J.D., Baldwin, N.E., Langston, M.A., et al. 2005. Complex trait analysis of gene expression uncovers polygenic and pleiotropic networks that modulate nervous system function. *Nat. Genet.* **37:** 233–242.

Devoto, M., Shimoya, K., Caminis, J., Ott, J., Tenenhouse, A., Whyte, M.P., Sereda, L., Hall, S., Considine, E., and Williams, C.J. 1998. First-stage autosomal 27 genome screen in extended pedigrees suggests genes predisposing to low bone mineral density on chromosomes 1p, 2p and 4q. *Eur. J. Hum. Genet.* **6:** 151–157.

Dietrich, W.F., Miller, J., Steen, R., Merchant, M.A., Damron-Boles, D., Husain, Z., Dredge, R., Daly, M.J., Ingalls, K.A., and O'Connor, T.J. 1996. A comprehensive genetic map of the mouse genome. *Nature* **380:** 149–152.

Edderkaoui, B., Baylink, D.J., Beamer, W.G., Wergedal, J.E., Dunn, N.R., Shultz, K.L., and Mohan, S. 2006. Multiple genetic loci from CAST/EiJ chromosome 1 affect vBMD either positively or negatively in a C57BL/6J background. *J. Bone Miner. Res.* **21:** 97–104.

Eisman, J.A. 1999. Genetics of osteoporosis. *Endocr. Rev.* **20:** 788–804.

Kammerer, C.M., Schneider, J.L., Cole, S.A., Hixson, J.E., Samollow, P.B., O'Connell, J.R., Perez, R., Dyer, T.D., Almasy, L., Blangero, J., et al. 2003. Quantitative trait loci on chromosomes 2p, 4p, and 13q influence bone mineral density of the forearm and hip in Mexican Americans. *J. Bone Miner. Res.* **18:** 2245–2252.

Karasik, D., Cupples, L.A., Hannan, M.T., and Kiel, D.P. 2004. Genome screen for a combined bone phenotype using principal component analysis: The Framingham study. *Bone* **34:** 547–556.

Kashiwazaki, M., Tanaka, T., Kanda, H., Ebisuno, Y., Izawa, D., Fukuma, N., Akimitsu, N., Sekimizu, K., Monden, M., and Miyasaka, M. 2003. A high endothelial venule-expressing promiscuous chemokine receptor Darc can bind inflammatory, but not lymphoid, chemokines and is dispensable for lymphocyte homing under physiological conditions. *Int. Immunol.* **15:** 1219–1227.

Kasukawa, Y., Baylink, D.J., Wergedal, J.E., Amaar, Y., Srivastava, A.K., Guo, R., and Mohan, S. 2003. Lack of insulin-like growth factor I exaggerates the effect of calcium deficiency on bone accretion in mice. *Endocrinology* **144:** 4682–4689.

Kim, M.S., Day, C.J., and Morrison, N.A. 2005. MCP-1 is induced by receptor activator of nuclear factor-κB ligand, promotes human osteoclast fusion, and rescues granulocyte macrophage colony-stimulating factor suppression of osteoclast formation. *J. Biol. Chem.* **280:** 16163–16169.

Klein, R.F., Mitchell, S.R., Phillips, T.J., Belknap, J.K., and Orwoll, E.S. 1998. Quantitative trait loci affecting peak bone mineral density in mice. *J. Bone Miner. Res.* **13:** 1648–1656.

Klein, R.F., Allard, J., Avnur, Z., Nikolcheva, T., Rotstein, D., Carlos, A.S., Shea, M., Waters, R.V., Belknap, J.K., Peltz, G., et al. 2004. Regulation of bone mass in mice by the lipoxygenase gene *Alox15*. *Science* **30:** 229–232.

Koller, D.L., Econs, M.J., Morin, P.A., Christian, J.C., Hui, S.L., Parry, P., Curran, M.E., Rodriguez, L.A., Conneally, P.M., Joslyn, G., et al. 2000. Genome screen for QTLs contributing to normal variation in bone mineral density and osteoporosis. *J. Clin. Endocrinol. Metab.* **85:** 3116–3120.

Luo, H., Chaudhuri, A., Zbrzezna, V., He, Y., and Pogo, A.O. 2000. Deletion of the murine Duffy gene (*Dfy*) reveals that the Duffy receptor is functionally redundant. *Mol. Cell. Biol.* **20:** 3097–3101.

Masinde, G.L., Li, X., Gu, W., Wergedal, J.E., Mohan, S., and Baylink, D.J. 2002. Quantitative trait loci for bone density in mice: The genes determining total skeletal density and femur density show little overlap in F2 mice. *Calcif. Tissue Int.* **71:** 421–428.

Miller, L.H., Mason, S.J., Dvorak, J.A., McGinniss, M.H., and Rothman, I.K. 1975. Erythrocyte receptors for (*Plasmodium knowlesi*) malaria: Duffy blood group determinants. *Science* **189:** 561–563.

Miller, L.H., Mason, S.J., Clyde, D.F., and McGinniss, M.H. 1976. The resistance factor to *Plasmodium vivax* in blacks. The Duffy-blood-group genotype, FyFy. *N. Engl. J. Med.* **295:** 302–304.

Morrison, N.A., Qi, J.C., Tokita, A., Kelly, P.J., Crofts, L., Nguyen, T.V., Sambrook, P.N., and Eisman, J.A. 1994. Prediction of bone density

from vitamin D receptor alleles. *Nature* **367:** 284–287.
Niu, T., Chen, C., Cordell, H., Yang, J., Wang, B., Wang, Z., Fang, Z., Schork, N.J., Rosen, C.J., and Xu, X. 1999. A genome-wide scan for loci linked to forearm bone mineral density. *Hum. Genet.* **104:** 226–233.
Papaioannou, V. and Johnson, R. 1993. Production of chimeras and genetically defined offspring from targeted ES cells. In *Gene targeting, a practical approach* (ed. A.L. Joyner), pp. 107–146. Oxford University Press, Oxford.
Peacock, M., Koller, D.L., Fishburn, T., Krishnan, S., Lai, D., Hui, S., Johnston, C.C., Foroud, T., and Econs, M.J. 2005. Sex-specific and non-sex-specific quantitative trait loci contribute to normal variation in bone mineral density in men. *J. Clin. Endocrinol. Metab.* **90:** 3060–3066.
Pogo, A.O. and Chaudhuri, A. 2000. The Duffy protein: A malarial and chemokine receptor. *Semin. Hematol.* **37:** 122–129.
Quinn, J.M., Elliott, J., Gillespie, M.T., and Martin, T.J. 1998. A combination of osteoclast differentiation factor and macrophage-colony stimulating factor is sufficient for both human and mouse osteoclast formation in vitro. *Endocrinology* **139:** 4424–4427.
Ralston, S.H. 2002. Genetic control of susceptibility to osteoporosis. *J. Clin. Endocrinol. Metab.* **87:** 2460–2466.
Ralston, S.H., Galwey, N., MacKay, I., Albagha, O.M., Cardon, L., Compston, J.E., Cooper, C., Duncan, E., Keen, R., Langdahl, B., et al. 2005. Loci for regulation of bone mineral density in men and women identified by genome wide linkage scan: The FAMOS study. *Hum. Mol. Genet.* **14:** 943–951.
Schadt, E.E., Monks, S.A., Drake, T.A., Lusis, A.J., Che, N., Colinayo, V., Ruff, T.G., Milligan, S.B., Lamb, J.R., Cavet, G., et al. 2003. Genetics of gene expression surveyed in maize, mouse, and man. *Nature* **422:** 297–302.
Silver, L.M. 1995. Mouse genetic concepts and applications. Oxford University Press. Adapted for the web (http://www.informatics.jax.org/silver/) by Mouse Genome Informatics. The Jackson Laboratory, Bar Harbor, ME, November 2001. Revised February 2005.
Takahashi, N., Udagawa, N., and Suda, T. 1999. A new member of tumor necrosis factor ligand family, ODF/OPGL/TRANCE/RANKL, regulates osteoclast differentiation and function. *Biochem. Biophys. Res. Commun.* **256:** 449–455.
Tournamille, C., Le Van Kim, C., Gane, P., Blanchard, D., Proudfoot, A.E., Cartron, J.P., and Colin, Y. 1997. Close association of the first and fourth extracellular domains of the Duffy antigen/receptor for chemokines by a disulfide bond is required for ligand binding. *J. Biol. Chem.* **272:** 16274–16280.
Volkman, S.K., Galecki, A.T., Burke, D.T., Miller, R.A., and Goldstein, S.A. 2004. Quantitative trait loci that modulate femoral mechanical properties in a genetically heterogeneous mouse population. *J. Bone Miner. Res.* **19:** 1497–1505.
Wise, G.E., Yao, S., Zhang, Q., and Ren, Y. 2002. Inhibition of osteoclastogenesis by the secretion of osteoprotegerin in vitro by rat dental follicle cells and its implications for tooth eruption. *Arch. Oral Biol.* **47:** 247–254.
Yanovski, J.A., Sovik, K.N., Nguyen, T.T., and Sebring, N.G. 2000. Insulin-like growth factors and bone mineral density in African American and White girls. *J. Pediatr.* **137:** 826–832.

Received October 3, 2006; accepted in revised form February 5, 2007.

Genetics and Molecular Biology, 29, 1, 166-173 (2006)

www.sbg.org.br

Research Article

A critical evaluation of the effect of population size and phenotypic measurement on QTL detection and localization using a large F2 murine mapping population

Xinmin Li[1,3], Richard J Quigg[1,4], Jian Zhou[1], Shizhong Xu[2], Godfred Masinde[3], Subburaman Mohan[3] and David J. Baylink[3]

[1]*University of Chicago, Division of Biological Sciences, Functional Genomics Facility, Chicago, IL, USA.*
[2]*University of California, Department of Botany and Plant Sciences, Riverside, CA, USA.*
[3]*JL Pettis VA Medical Center and Loma Linda University, Musculoskeletal Disease Center, Molecular Genetics Division, Loma Linda, CA, USA.*
[4]*University of Chicago, Department of Medicine, Section of Nephrology, Chicago, IL, USA.*

Abstract

Population size and phenotypic measurement are two key factors determining the detection power of quantitative trait loci (QTL) mapping. We evaluated how these two controllable factors quantitatively affect the detection of QTL and their localization using a large F2 murine mapping population and found that three main points emerged from this study. One finding was that the sensitivity of QTL detection significantly decreased as the population size decreased. The decrease in the percentage logarithm of the odd score (LOD score, which is a statistical measure of the likelihood of two loci being lied near each other on a chromosome) can be estimated using the formula 1 - n/N, where n is the smaller and N the larger population size. This empirical formula has several practical implications in QTL mapping. We also found that a population size of 300 seems to be a threshold for the detection of QTL and their localization, which challenges the small population sizes commonly-used in published studies, in excess of 60% of which cite population sizes <300. In addition, it seems that the precision of phenotypic measurement has a limited capacity to affect detection power, which means that quantitative traits that cannot be measured precisely can also be used in QTL mapping for the detection of major QTL.

Key words: QTL mapping, mice, detection power, population size, phenotypic measurement.

Received: November 23, 2004; Accepted: May 31, 2005.

Introduction

Quantitative trait loci (QTL) mapping has become increasingly informative in genomic data integration (Fischer *et al*., 2003; Vitt *et al*., 2004; Flint *et al*., 2005), but the number of QTL which can be detected and the precision with which they can be located on the chromosome remain two key issues facing this type of mapping (Churchill and Doerge, 1994; Dupuis and Siegmund, 1999; Lander and Kruglyak, 1995; Liu, 1997). Many factors affect both the number of QTL which can be detected and the precision with which they can be located. Some of these factors are often unknown at the start of a study and beyond experimental control, while other factors are known and controllable. Among the controllable factors, population size, phenotypic measurement and marker density contribute to QTL detection and localization.

Send correspondence to Xinmin Li. University of Chicago, 5841 S Maryland Ave., 60637 Chicago, IL, USA. E-mail: xli@medicine.bsd.uchicago.edu.

One of the most frequently asked questions when designing a mapping experiment is 'What population size should be used?', *i.e.*, what is the statistical power needed to detect linkage given a certain population size and are N individuals enough to estimate the recombination fraction with a given precision. Theoretically, population size can be estimated based on the statistical power (γ), hypothetical recombination fraction (θ) and significance level being used (α). Several simulation experiments have been carried out to address the question of population size (Darvasi *et al*., 1993; Darvasi and Soller, 1997; Belknap, 1998) and formulae have been developed to calculate the population size required for the detection of QTL when assuming that the dominance and standardized allele effects are known (Soller *et al*., 1976; Lander and Botstein, 1989) but, in practice, population sizes are still difficult to estimate without any assumption. Consequently, time and cost is generally used to determine the population size needed for QTL analysis. We surveyed 71 F2-based murine mapping experi-

ments published during the past five years, of which 21 (30%) had a population size between 100 and 200 mice, 43 (61%) less than 300, 18 (25%) between 300 and 600, and only 10 (14%) more than 600 mice (Figure 1). This severely biased distribution toward small F2 populations strengthens the need to practically evaluate the effect of population size on the detection and localization of QTL.

Another important factor for QTL mapping is the precision of phenotypic measurement, because high measurement error will reduce the estimated heritability and decrease the detection power. Unfortunately, measurement error is normally mixed with other environmental residuals and cannot be separated from them using current statistical models, because of which we know very little about its effect on the detection of QTL and it is difficult to evaluate the applicability of imprecisely measured quantitative traits to QTL mapping.

The role of marker density in QTL mapping has been widely investigated and several studies have shown that marker density is a function of detection power within a certain density range and has little effect beyond 10 centimorgans (cM) (Darvasi *et al*., 1993; Piepho, 2000; Frisch *et al*., 1999).

The objective of the study described in this paper was to use an empirical approach to evaluate the effect of population size and phenotypic measurement on the detection of QTL. We hypothesized that the effect of population size and the precision of phenotypic measurement on QTL detection and localization can be empirically studied by using a large and properly selected mapping population. We tested this hypothesis using an F2 mapping population which we had previously used for genetic dissection of wound healing in mice (Masinde *et al*., 2001). Our findings challenge the size of populations commonly used in published studies and provide an empirical guideline for the design of future F2 mapping experiments.

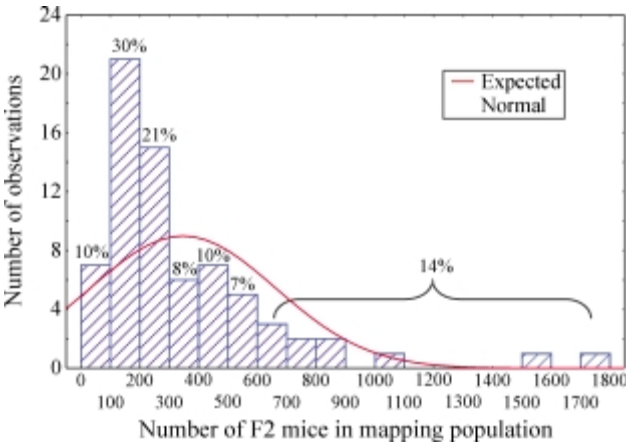

Figure 1 - Distribution of F2 progeny size in the mouse mapping experiments. Data were derived from publications in the last five years (n = 71). The number on the top of each bar represents the percentage of the number of experiments in that population size group in respect to the total experiments surveyed.

Materials and methods

Experimental data

All the genotype data, phenotypic measurements and wound healing QTL data used in this study were derived from Masinde *et al*. (2001) who described a murine wound-healing trait mapping experiment using a mapping population of 633 (MRL/MpJ X SJL/J) F2 female mice genotyped with 119 polymorphic markers. The wound-healing phenotype was defined by punching a 2 mm diameter hole in the soft external tissue of one ear and measuring the diameter of the hole after 21 days, the average value being 0.69 ± 0.05 mm.

Four previously identified soft tissue heal (Sth) QTL were selected for this study: Sth1 (LOD sore = 6.8) responsible for 5.6% of the phenotypic variation and Sth5 (LOD sore = 4.5) responsible for 4% of the phenotypic variation, representing medium-sized QTL; Sth9 (LOD sore = 15.6) responsible for 13% of the phenotypic variation, representing a large QTL; and Sth10 (LOD sore = 3) responsible for 2.6% of the phenotypic variation, representing a small presumptive QTL.

Data sampling

From the original data set of 633 female mice (genotype file and corresponding phenotype file), five data sub-sets of 500, 400, 300, 200 and 100 mice were randomly generated using a computer-assisted selection procedure. Each data sub-set included thirty replicates. For example, to generate a data sub-set of 500 animals, we randomly selected 500 mice from the original 633 mice and created new genotype and phenotype files corresponding to the 500 randomly selected mice, this random selection procedure being repeated 30 times to generate 30 genotype/phenotype files with each set of files corresponding to a different group of 500 mice. This procedure was repeated for data sub-sets of 400, 300, 200 and 100 mice randomly selected from the original 633 mice, 30 genotype/phenotype files being generated for each data sub-set as described in the previous sentence. Each set of data (a unique genotype file, unique phenotype file and the original linkage map file) was then applied to interval mapping using the MAPQTL (4.0) software (Wageningen, the Netherlands). The total of 150 QTL analyses were performed for the 5 sub-data sets (30 replicates X 5 sub-data sets).

Corruption of phenotypic measurement data

The original ear-hole measurement data were corrupted by adding to, or subtracting from, the phenotypic measurement 1, 2, 3, 4, 5, 6, 7 or 8 standard deviations (SD), previously determined to be 0.05 mm (Li *et al*., 2001). To decide the direction of data corruption we randomly allocated either a 1 or a 0 to each of the 633 ear measurement data points from the F2 mice. If the randomly allocated number corresponding to data point X was a 1

then the original measurement X would become X plus one standard deviation, or X plus two standard deviations etc., continuing up to X plus eight standard deviations, but if the randomly allocated number was 0 then the original measurement X would become X minus one standard deviation, or X minus two standard deviations, etc., continuing up to X minus eight standard deviations. In other words, eight artificial data sets were generated, the first by corrupting the original data set by one standard deviation, the second by corrupting the original data set by two standard deviations and so on up to eight standard deviations. The entire process from the random allocation of 1's or 0's to the production of the eight artificial data sets was repeated 30 times, generating a total of 240 artificial data sets consisting of 30 replicates for each of eight data sets. Each data set had a unique phenotype file with corrupted data and an original genotype and linkage map which were then applied to QTL mapping. We performed 240 QTL analyses using the corrupted data sets.

QTL mapping

Interval mapping was performed to detect any significant association between ear wound healing and marker loci in the F2 sub-data sets (different population size) and artificial data sets (corrupted phenotypic data) using the MapQTL software version 4 (Wageningen, the Netherlands). The critical threshold values for significance of association were determined by the permutation test (Churchill and Doerge 1994; Van Ooijen 1999) to be a LOD score of ≥ 3.5 for significant linkage and ≥ 2.7 for suggestive linkage.

Data analysis

Computations were performed using the Statistca 5.1 (StatSoft Inc., Tulsa, OK) statistical package. The estimation of genetic variance used the difference between variances of different populations method in which the F_1, P_1 and P_2 populations are non-segregating populations whose variances (V_{F_1}, V_{P_1} and V_{P_2}) are purely due to environmental factors, while the F2 population is a segregating population whose variance (V_{F_2}) is determined by the sum of the genotypic and environmental effects. Therefore, $V_{F_2} - (½V_{F_1} + ¼V_{P_1} + ¼V_{P_2})$ is an estimate of the genotypic variance. The broad-sense heritability is then estimated from:

$$\hat{H}^2 = \frac{V_{F_2} - (½V_{F_1} + ¼V_{P_1} + ¼V_{P_2})}{V_{F_2}}$$

The average variance from 30 randomly generated data sets (as described above) was used to estimate heritability. The coefficient of variation (CV = SD/Mean) was used to evaluate variation of peak LOD score and map position over 30 replicates.

Results

Effect of population size on QTL detection and localization

We found that the LOD scores decreased dramatically as the population size decreased (Figure 2). When the population size was reduced to 100 none of the four QTL were significant and when the population size was 300 only the large Sth9 QTL was significant (Table 1). The percentage decrease in the LOD score is a function of the population size and can be approximately expressed as 1 - n/N, where N is the larger and n is the smaller population size. A comparison of the average percentages of decrease in the LOD score with the decrease of the LOD score predicted from the formula (1 - n/N) showed no significant difference between the two data sets (t = -0.13, p = 0.899). This empirically derived formula can be proved theoretically since the expected LOD score can be approximated by $LOD_n = 0.217n\sigma_x^2 a^2/\sigma_e^2$ and $LOD_N = 0.217N\sigma_x^2 a^2/\sigma_e^2$ for population sizes n and N, respectively, where σ_x^2 is the variance of the genotypic indicator variable, a is the additive genetic effect and σ_e^2 is the residual variance. The percentage of LOD score reduction is defined as

$$\frac{LOD_N - LOD_n}{LOD_N} = \frac{1 - LOD_n}{LOD_N} = 1 - \frac{n}{N}$$

Thus, this 'empirical formula' is applicable to F2-design mapping experiments in general. Using this formula the QTL LOD scores for the same phenotype but derived from different population sizes can be converted into an expected LOD score for a fixed population size. In addition, a minimum population size required for a LOD score of 3.5 (the significance threshold) for a particular QTL can be predicted based on the known population size and the LOD score for that QTL (Table 2).

The variation in the peak LOD score over 30 replicates increased with decreasing population size (Figure 3A), the effect being much more pronounced for a population size of less than 300 than it was for a population size of from 500 to 300. Smaller QTL generally have a greater variation in peak LOD score. Variation in peak position over 30 replicates shared a similar trend with that of the peak LOD score, though smaller in magnitude (Figure 3B).

Effect of phenotypic measurement on QTL detection and localization

The average LOD score plots for all 240 corrupted data sets are shown in Figure 4. Random deviation of one standard deviation (1 deviation unit) from the original data had little effect on QTL detection and localization compared to the original data set (Table 3). Variation among the 30 replicates was also negligible (data not shown). A deviation of three standard deviations from the original data reduced the heritability from the 89% estimated by Li *et al.* (2001) to 74% but all four QTL could still be detected. As

the number of standard deviations from the original phenotypic data increased small QTL became insignificant while the medium-sized QTL (Sth1) remained significant up to six standard deviations (h^2 = 42%) and the largest QTL (Sth9) remained significant up to eight standard deviations (h^2 = 29%).

The decrease in peak LOD score was linearly related to the deviation of the phenotypic measurement, which can

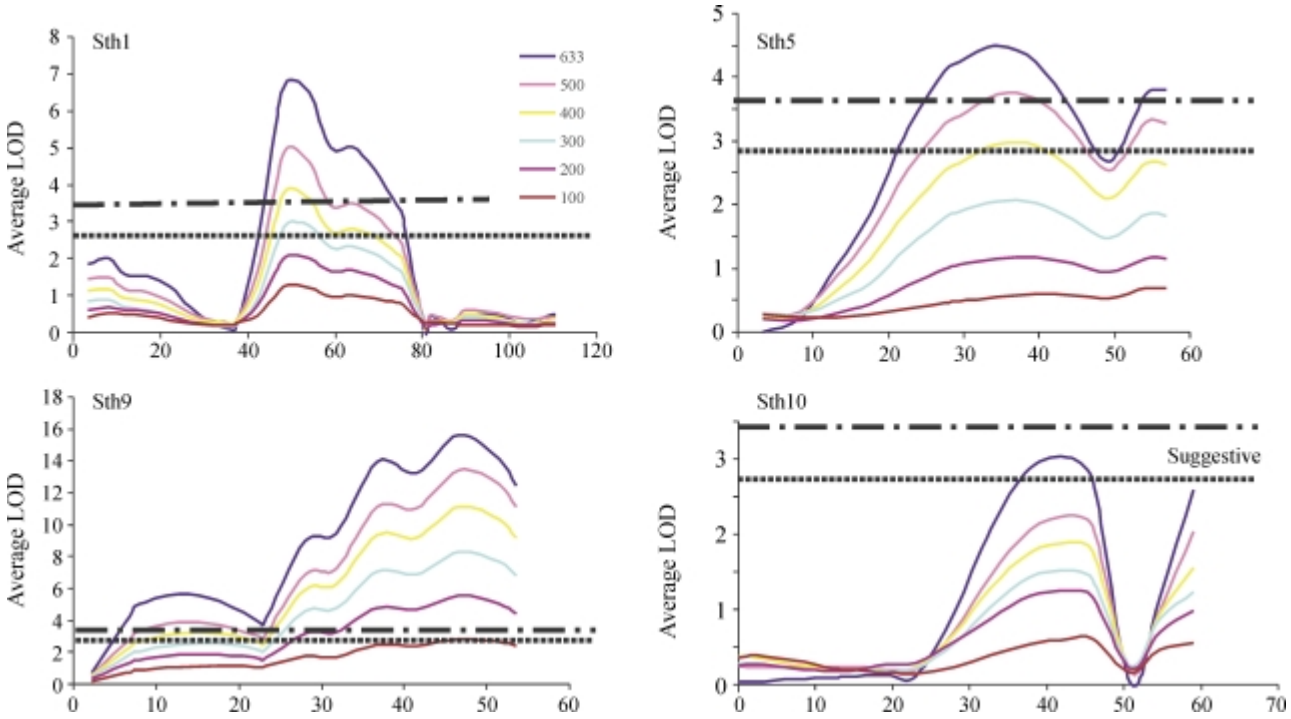

Figure 2 - Logarithm of the odd (LOD) score plots for four quantitative traits with different population sizes. Each individual quantitative trait loci (QTL) picture was the average LOD score plots of 30 replicates for each of the five different population sizes. For comparison the plot for each of the QTL from the original data set (blue line) is also included. Horizontal dashed lines indicate significant LOD thresholds and dotted lines presumptive LOD thresholds.

Table 1 - How the average peak logarithm of the odd (LOD) score decreases with decreasing population size[a]

Quantitative trait locus (QTL)	Number of mice					
	633	500	400	300	200	100
Sth1	6.83	5.04 ± 1.65	3.88 ± 1.38	2.98 ± 1.46	2.09 ± 1.24	1.30 ± 0.90
Sth5	4.50	3.73 ± 1.59	2.95 ± 1.34	2.06 ± 1.03	1.16 ± 0.83	0.55 ± 0.52
Sth9	15.62	13.43 ± 2.81	11.07 ± 3.06	8.31 ± 2.55	5.55 ± 2.20	2.83 ± 1.36
Sth10	3.01	2.24 ± 1.08	1.89 ± 1.06	1.51 ± 0.87	1.24 ± 0.85	0.61 ± 0.49

[a]Data are expressed as means ± standard deviation (SD, n = 30). The threshold LOD score for significance was ≥ 3.5.

Table 2 - Comparison of the logarithm of the odd (LOD) scores for a population size of 500 with the LOD score converted to 500 from different sample sizes using the empirical formula 1 - n/N, where n is the smaller and N the larger population size.

Quantitative trait locus (QTL)	LOD Score for 500 mice	Converted LOD score for this number of mice					Number of mice[b] required for a LOD score of 3.5
		100	200	300	400	633	
Sth1	5.0	6.5	5.2	5.0	4.9	5.4	350
Sth5	3.7	2.8	2.9	3.4	3.7	3.6	473
Sth9	13.4	14.1	13.9	13.9	13.8	12.3	130
Sth10	2.2	3.1	3.1	2.5	2.4	2.4	795
Average[a]	6.1	6.6	6.3	6.2	6.2	5.9	437

[a]No significant difference between any two of the average LOD scores by t-test.
[b]Predicted from the LOD score for a population size of 500.

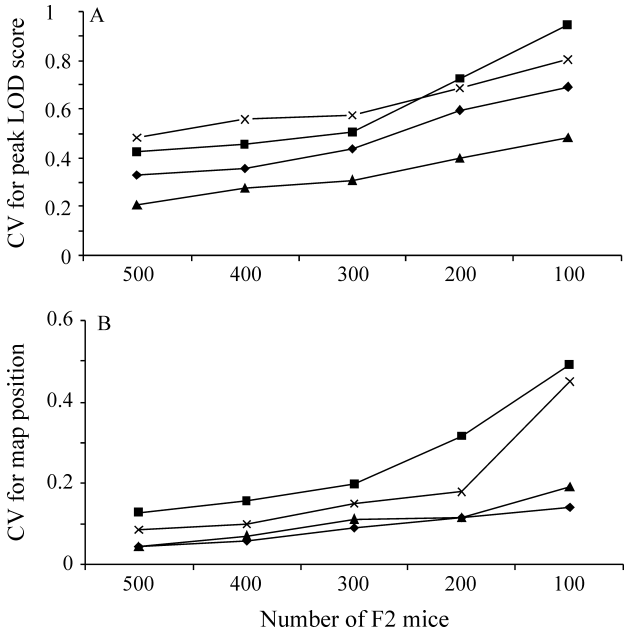

Figure 3 - Increase of variation in peak logarithm of the odd (LOD) score and quantitative trait loci (QTL) map position between replicates with a decrease in population size. (A) peak LOD score; (B) QTL map position. QTL map position refers to the map position corresponding to the peak LOD score. Variation is expressed as coefficient of variation (CV).

be expressed as $y = 0.0857*x - 0.0608$, $R^2 = 0.9962$, where x is standard deviation and y is the percentage decrease in LOD score compared to the original data (Figure 5). This formula gave a decrease in LOD score of about 8.6% for each increase of one standard deviation (slope = 0.086). Concomitant with the decrease in LOD score, variation of the peak LOD score (CV) linearly increased as the error in phenotypic measurement was increased (Figure 6A). A nonlinear and small increase was also observed for the variation in chromosomal location (Figure 6B).

Comparison of the effect of population size with that of phenotypic measurement on QTL detection and localization

Our analysis shows that decreased population size had a much greater effect on the peak LOD score than increasing the number of standard deviations by which the data was corrupted (Figure 7). Corrupting the original phenotypic value by three standard deviations was equivalent to reducing the population size from 633 to 500, while six-and-a-half standard deviations was equivalent to reducing the population to 300. On average, decreasing the population by 50 mice had a similar effect on the LOD score as corrupting the phenotypic measurement by one standard deviation. In addition, the effect of phenotypic deviation on the variation of peak LOD score and QTL position over replicates was significantly smaller than that of reducing the population size (Figures 3 and 6).

Discussion

The purpose of this study was to provide a practical appraisal of the effect of population size and phenotypic measurement on QTL detection and localization and to provide an empirical guideline for future experimental design and data interpretation. Several interesting points emerged from this study that are worthy of discussion.

The mapping population used for such a study is a critical issue. We chose the (MRL/MpJ X SJL/J) F2 mapping population for several reasons: 1) the large population size of 633 F2 mice which is within the top 14% population size surveyed in the literature; 2) high marker density (119) which is almost saturated in this experiment. Further increase has little effect on the power of QTL detection (Piepho, 2000); 3) precise phenotypic measurement which has a coefficient of variation of 2.4% when the average hole size is 1.4 mm in diameter and 4.6% when the average size is 0.96 mm in diameter (Li *et al*., 2001); and 4) wound healing is a typical quantitative trait controlled by multiple genes with complex gene-gene interactions (Masinde *et al*., 2001). These features have made it a feasible population to evaluate the effect of sample size and phenotypic measurement on QTL detection and localization.

Table 3 - How the average peak logarithm of the odd (LOD) score decreases as the number of standard deviations (SD) used to corrupt the data increases. The original 21-day ear-hole measurement data were corrupted by adding to, or subtracting from, the phenotypic measurement 1, 2, 3, 4, 5, 6, 7 or 8 standard deviations (SD), previously determined to be 0.05 mm for a mean of 0.69 mm. (Li *et al*., 2001).

	Uncorrupted data for 633 mice	Number of standard deviations (SD) used to corrupt the data							
		±1SD (7.2%)[a]	±2SD (14.5%)[a]	±3SD (22%)[a]	±4SD (29%)[a]	±5SD (36%)[a]	±6SD (43%)[a]	±7SD (51%)[a]	±8SD (58%)[a]
Quantitative trait locus (QTL)	LOD score	LOD score[b]							
Sth1	6.83	6.60 ± 0.30	6.12 ± 0.54	5.48 ± 0.72	4.80 ± 0.84	4.14 ± 0.90	3.55 ± 0.92	3.05 ± 0.92	2.62 ± 0.89
Sth5	4.50	4.40 ± 0.26	4.12 ± 0.48	3.74 ± 0.63	3.31 ± 0.72	2.90 ± 0.77	2.52 ± 0.77	2.19 ± 0.76	1.91 ± 0.73
Sth9	15.62	15.1 ± 0.55	13.9 ± 1.02	12.4 ± 1.35	10.8 ± 1.56	9.30 ± 1.66	7.93 ± 1.69	6.77 ± 1.68	5.79 ± 1.63
Sth10	3.01	3.02 ± 0.24	2.89 ± 0.45	2.68 ± 0.61	2.43 ± 0.72	2.17 ± 0.78	1.93 ± 0.81	1.71 ± 0.81	1.53 ± 0.80

[a]Percentage deviation from the uncorrupted data for 633 mice.
[b]Data are expressed as means ± SD. n = 30. The threshold LOD score for significance was determined to be ≥ 3.5.

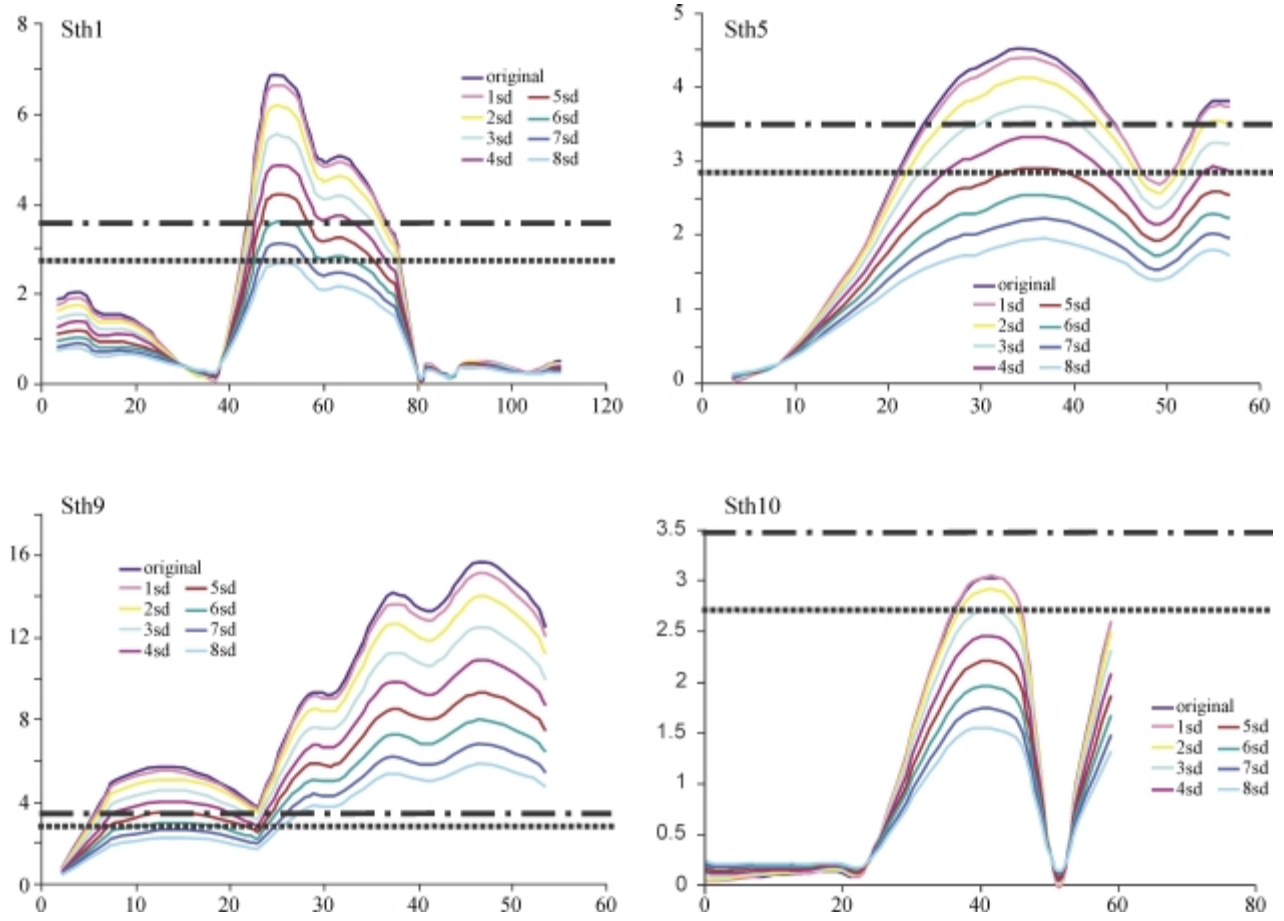

Figure 4 - Logarithm of the odd (LOD) score plots as error was systematically introduced into phenotypic measurement. Each individual quantitative trait loci (QTL) picture was the average LOD score plots of 30 replicates for each of the 8 data sets. For comparison the plot for each of the QTL from the original data set (blue line) is also included. Horizontal dashed lines indicate significant LOD thresholds and dotted lines presumptive LOD thresholds.

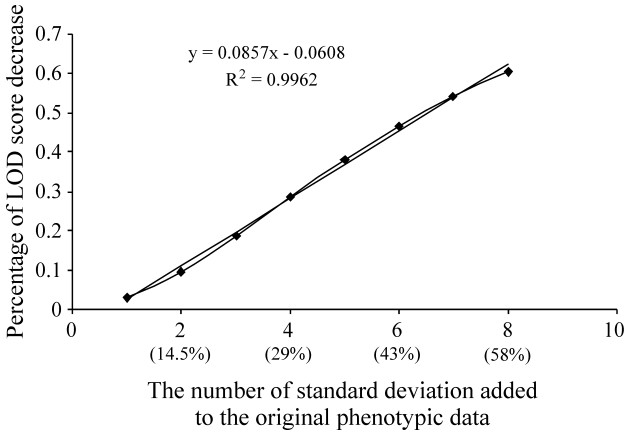

Figure 5 - The plot of the percentage logarithm of the odd (LOD) score decreases as error is systematically introduced into phenotypic measurement from the original data set. The number in the bracket on the x-axis represents the percentage deviation from the original phenotypic data.

Population size has a profound effect on the sensitivity of QTL detection and precision of QTL localization. Reduction in size is linearly associated with decreased LOD score. The percentage decrease can be empirically calculated from the expression: 1 - n/N. This empirical formula was derived from the reduction of population size from 633 → 500 → 400 → 300 → 200 → 100. This range of size covers 77% of the mouse mapping experiments surveyed in this study. Because the LOD score is a function of population size, the traditional LOD score significance threshold (3.5) may be too high for small population. In such populations, medium-sized QTL could not reach the defined threshold of 3.5, resulting in an increased Type II error (not detecting a QTL when there is one). This has clearly been demonstrated in this study: none of the three highly significant QTL could be declared as significant at the LOD score of 3.5 when the population size was reduced from 633 to 100. A population size of 300 appears to be a turning point for sensitive and reliable detection of QTL (F2 design). Beyond this point, the medium effect QTL (Sth1) could not be detected and variation in QTL peak and map position was drastically increased. This empirical 'threshold' is much higher than theoretically calculated (Liu, 1997). This finding suggests that current mapping population sizes, which are driven by time and cost (over 60% of F2 mapping experiments used less than 300 mice in literature), seem to be

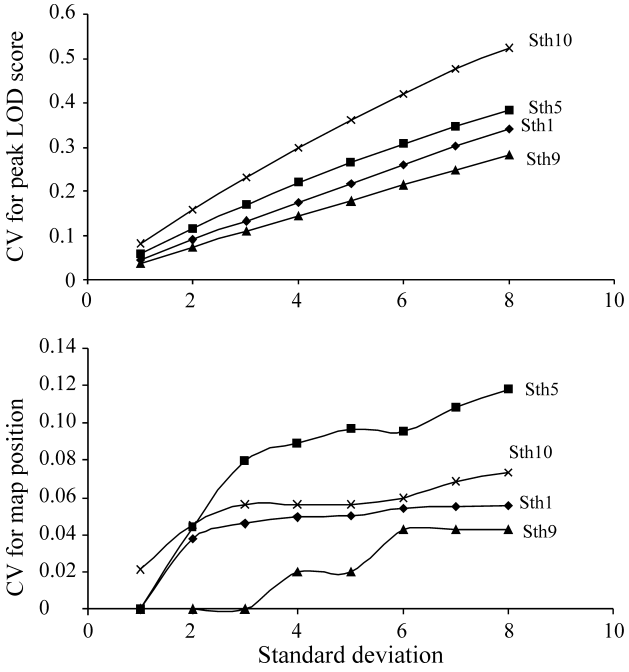

Figure 6 - Effect of variation in phenotype on peak logarithm of the odd (LOD) score and quantitative trait loci (QTL) map position. (A) peak LOD score; (B) QTL map position. Standard deviation (x-axis) shows the amount of error introduced into the measurement.

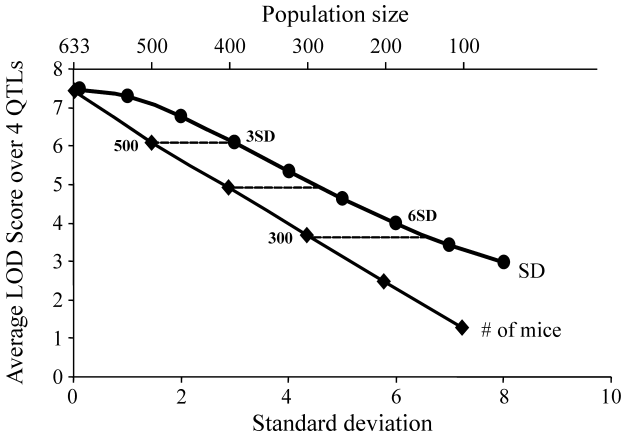

Figure 7 - Comparison of the effect of a decrease in population size on the average peak logarithm of the odd (LOD) score with that of increase of phenotype deviation (SD). The scales above the x-axis represent population size while below the x-axis they represent the number of standard deviations from the original measurement.

too small to be able to reliably detect even a medium-sized QTL.

Based on the quantitative relationship between LOD score and population size we established an empirical formula (1 - n/N, where N is the larger and n the smaller sample size) which predicts the percentage sample-size dependent LOD score decrease. Because this empirical formula can be derived theoretically it should be generally applicable to other F2-design mapping studies. This formula can be used to estimate the expected LOD score for a specific population size (*e.g.* 500), which means that it can make the LOD scores of the QTL for the same phenotype comparable between different mouse mapping experiments and can also estimate the LOD score using a reasonable population size if there is a practical limitation in setting up a large mapping population, this attribute being particularly useful for mapping studies that are used for initial screening or for confirmation of previous studies.

Previously, it was not known how phenotypic measurement affects detection power and to address this question we conducted the study described in this paper in which we generated 8 artificial data sets by adding a constant level of noise to the original phenotypic data set (note that we did not simulate natural noise, a random event). We were rather surprised to find that the detection of QTL is highly tolerant of variation (or errors) in the phenotypic measurement. Increased phenotypic measurement error will lead to a decrease in heritability thereby affecting the power to detect QTL. For the data set analyzed in this study the average ear hole size (a phenotypic measurement) of 633 F2 mice at day 21 was 0.69 ± 0.05 mm, three standard deviations (± 0.15 mm) being equivalent to a 22% (0.15/0.69 = 0.22) deviation from the original measurements. This artificial noise reduced the heritability from 89% to 74% but did not significantly affect the four QTL measured. This observation suggests that there is a limited loss of detection power when measurement error increases within a certain heritability range which, in this study, was between 70% and 90%. Identification of the medium sized QTL (Sth1) when the data was corrupted by six standard deviations (a 43% deviation from the original data, heritability reduced to 42%) and the large QTL (Sth9) when the data was corrupted by eight standard deviations (a 58% deviation from the original data, heritability reduced to 29%) further suggests that virtually all quantitative traits can be applied to genetic mapping for identification of major quantitative trait loci, including those that are difficult to measure precisely and have low heritability.

We estimated that, in terms of QTL detection, the effect of reducing the population size by 50 mice is equivalent to a variation in phenotypic measurement of one standard deviation (*i.e.* 7.2% deviation from the original phenotypic value). If this empirical relationship can be extrapolated to other mapping populations, it can provide a convenient guide to select a cost- and time-effective compromise between increasing the F2 population size and improving the precision of quantitative trait measurement.

It should be noted that the empirical relationships reported here were established through one specific experiment (Masinde *et al.* 2001), which involves a particular genetic architecture governing the phenotypy of interest. Robustness of these relationships across different genetic architecture deserves further evaluation. Thus, extrapolation of these empirical relationships to other mapping populations should be made with caution. Nevertheless, this

report represents the first attempt to use a real mapping experiment to quantitatively evaluate the effect of sample size and phenotypic measurement on major quantitative trait loci mapping efficiency. Our results could serve as a guide to design QTL mapping experiments and aid in the interpretation of results.

Acknowledgments

This work was supported by Assistance Award n. DAMD17-99-1-9571. The U.S. Army Medical Research Acquisition Activity, 820 Chandler Street, Fort Detrick MD 21702-5014, is the awarding and administering acquisition office. The information contained in this publication does not necessarily reflect the position or the policy of the Government of the United States and no official endorsement should be inferred. The authors would like to thank Heather Davidson for her excellent technical support.

References

Belknap JK (1998) Effect of within-strain sample size on QTL detection and mapping using recombinant inbred mouse strains. Behav Genet 28:29-38.

Churchill GA and Doerge RW (1994) Empirical threshold values for quantitative trait mapping. Genetics 138:963-971.

Darvasi A and Soller M (1997) A simple method to calculate resolving power and confidence interval of QTL map location. Behav Genet 27:125-132.

Darvasi A, Weinreb A, Minke V, Weller JL and Soller M (1993) Detecting marker-QTL linkage and estimating QTL gene effect and map location using a saturated genetic map. Genetics 134:943-951.

Dupuis J and Siegmund D (1999) Statistical methods for mapping quantitative loci from a dense set of markers. Genetics 151:373-386.

Frisch M, Bohn M and Melchinger AE (1999) Minimum sample size and optimal positioning of flanking markers in marker-assisted backcrossing for transfer of a target gene. Crop Science 39:967-975.

Fischer G, Ibrahim SM, Brockmann GA, Pahnke J, Bartocci E, Thiesen HJ, Serrano-Fernandez P and Moller S (2003) Expressionview: Visualization of quantitative trait loci and gene-expression data in Ensembl. Genome Biol 4:R77.

Flint J, Valdar W, Shifman S and Mott R (2005) Strategies for mapping and cloning quantitative trait genes in rodents. Nat Rev Genet 6:271-86.

Lander E and Kruglyak L (1995) Genetics dissection of complex traits: Guidelines for interpreting and reporting linkage results. Nat Genet 11:241-247.

Lander ES and Botstein D (1989) Mapping mendelian factors underlying quantitative traits using RFLP linkage maps. Genetics 121:185-199.

Li X, Gu W, Masinde G, Hamilton-Ulland M, Xu S, Mohan S and Baylink D (2001) Genetic control of the rate of wound healing in mice. Heredity 86:668-674.

Liu BH (1997) Statistical Genomics: Linkage, Mapping and QTL Analysis. CRC Press, Florida, pp 375.

Masinde G, Li X, Gu W, Heather D, Mohan S and Baylink DJ (2001) Identification of wound healing/regeneration QTLs at multiple time points that explain seventy percent of variance in (MRL/MpJ X SJL/J) F_2 population. Genome Research 11:2027-2033.

Piepho HP (2000) Optimal marker density for interval mapping in a backcross population. Heredity 84:437-440.

Soller M, Genizi A and Brody T (1976) On the power of experimental designs for the detection of linkage between marker loci and quantitative loci in crosses between inbred lines. Theor Appl Genet 47:35-39.

Van Ooijen JW (1999) LOD significance thresholds for QTL analysis in experimental populations of diploid species. Heredity 83:613-624.

Vitt U, Gietzen D, Stevens K, Wingrove J, Becha S, Bulloch S, Burrill J, Chawla N, Chien J, Crawford M, Ison C, Kearney L, Kwong M, Park J, Policky J, Weiler M, White R, Xu Y, Daniels S, Jacob H, Jensen-Seaman MI, Lazar J, Stuve L and Schmidt J (2004) Identification of candidate disease genes by EST alignments, synteny, and expression and verification of Ensembl genes on rat chromosome 1q43-54. Genome Res14:640-50.

Editor: Fábio de Melo Sene

Calcif Tissue Int (2007) 80:103–110
DOI: 10.1007/s00223-006-0187-z

Calcified Tissue International

Laboratory Investigations

Detecting Novel Bone Density and Bone Size Quantitative Trait Loci Using a Cross of MRL/MpJ and CAST/EiJ Inbred Mice

H. Yu,[1] S. Mohan,[1,2,3] B. Edderkaoui,[1] G. L. Masinde,[1] H. M. Davidson,[1] J. E. Wergedal,[1,2,3] W. G. Beamer,[4] D. J. Baylink[3]

[1]Musculoskeletal Disease Center, Jerry L. Pettis Memorial VA Medical Center, 11201 Benton Street, Loma Linda, CA 92357, USA
[2]Department of Biochemistry, Loma Linda University, 11234 Anderson Street, Loma Linda, CA 92354, USA
[3]Department of Medicine, Loma Linda University, 11234 Anderson Street, Loma Linda, CA 92354, USA
[4]The Jackson Laboratory, 600 Main Street, Bar Harbor, ME 04609, USA

Received: 3 July 2006 / Accepted: 7 November 2006 / Online publication: 2 February 2007

Abstract. Most previous studies to identify loci involved in bone mineral density (BMD) regulation have used inbred strains with high and low BMD in generating F_2 mice. However, differences in BMD may not be a requirement in selecting parental strains for BMD quantitative trait loci (QTL) studies. In this study, we intended to identify novel QTL using a cross of two strains, MRL/MpJ (MRL) and CAST/EiJ (CAST), both of which exhibit relatively high BMD when compared to previously used strains. In addition, CAST was genetically distinct. We generated 328 MRL × CAST F_2 mice of both sexes and measured femur BMD and periosteal circumference (PC) using peripheral quantitative computed tomography. Whole-genome genotyping was performed with 86 microsatellite markers. A new BMD QTL on chromosome 10 and another suggestive one on chromosome 15 were identified. A significant femur PC QTL identified on chromosome 9 and a suggestive one on chromosome 2 were similar to those detected in MRL × SJL. QTL were also identified for other femur and forearm bone density and bone size phenotypes, some of which were colocalized within the same chromosomal positions as those for femur BMD and femur PC. This study demonstrates the utility of crosses involving inbred strains of mice which exhibit a similar phenotype in QTL identification.

Key words: Mouse — Bone density — Bone size — Quantitative trait locus

Osteoporosis is a disease of bone loss that leads to weak and fragile bones. The consequence of osteoporosis is a higher rate of bone fracture. Heritability for osteoporotic fracture, however, is quite low [1], which has made it difficult to understand its genetic basis. Bone susceptibility (or resistance) to fracture is determined by bone strength, which itself is influenced by three factors: bone density, bone size, and bone quality. The most easily measured manifestation of osteoporosis is the reduction in bone density. While bone quality is ill defined, bone density and bone size can be measured by parameters obtained from the femurs such as bone mineral density (BMD) and periosteal circumference (PC). Bone density and bone size account for >40% of bone strength variation [2]. Heritability of BMD is relatively high, ranging 0.5–0.9 in humans [1, 3–6] and around 0.6–0.7 in mice [7, 8]. Studies have shown that lower BMD is directly associated with higher risk of osteoporotic fracture [9, 10].

A number of mouse quantitative trait loci (QTL) studies have been conducted to identify genes for bone density and bone size. QTL that significantly affect BMD have been identified on nearly all chromosomes [11, 12]. Most of these studies have employed inbred strains of mice with high and low BMD to produce genetically segregating F_2 progeny for correlation of phenotypes with chromosomal regions. Such crosses include low-BMD C57BL/6J (B6) × high-BMD C3H/HeJ (C3H) [13], low-BMD B6 × high-BMD CAST/EiJ (CAST) [7, 14–16], high-BMD MRL/MpJ (MRL) × low-BMD SJL/J (SJL) [17–19], and high-BMD SAMP2 × low-BMD SAMP6 [20–22]. In addition to these studies where BMD was determined on the femur by peripheral quantitative computed tomography (pQCT), other studies where BMD was measured on the whole body by dual-energy X-ray absorptiometry (DXA) utilized the cross of B6 × DBA/2 (DBA) with similar low BMD [23–25]. These studies showed that higher-BMD alleles of the identified QTL were contributed not only by the high-BMD parental strain but also by the low-BMD strain. To generalize this observation, it seems that due to genetic diversity in inbred strains even those

Correspondence to: S. Mohan; E-mail: Subburaman.Mohan@med.va.gov

Table 1. Bone and body parameters of the 7-week-old animals of MRL and CAST[a]

Strain	Sex	Mice (*n*)	Body weight (g)	Femur BMD (mg/cm^3)	Femur length (mm)	Femur PC (mm)	Femur EC (mm)
MRL	Male	5	33.80 ± 0.50	782.02 ± 16.35	15.61 ±0.20	5.28 ± 0.08	2.71 ± 0.03
	Female	7	31.31 ± 1.04	721.07 ± 12.46	15.31 ± 0.14	5.17 ± 0.05	2.83 ± 0.05
	All	12	32.35 ± 0.72	748.77 ± 11.84	15.45 ± 0.12	5.22 ± 0.05	2.78 ± 0.03
CAST	Male	5	11.46 ± 0.31	655.98 ± 12.48	12.78 ± 0.09	4.24 ± 0.04	2.23 ± 0.02
	Female	5	10.86 ± 0.11	619.08 ± 6.91	12.26 ± 0.14	3.92 ± 0.02	2.09 ± 0.02
	All	10	11.16 ± 0.19	637.53 ± 9.11	12.52 ± 0.12	4.08 ± 0.06	2.16 ± 0.03

[a] Values are mean ± SE

strains with similar BMD may harbor different alleles at BMD loci. Thus, differences in BMD may not be a requirement in selecting parental strains for BMD QTL studies.

In this study, we intended to identify novel QTL for bone density and bone size with a cross of two inbred strains, MRL and CAST, both of which exhibit relatively high BMD when compared to previously used strains, such as B6. Although MRL and CAST both have high BMD, their alleles at virtually all loci are different, stemming from their different evolutionary origins. While nearly all inbred strains used in experimental crosses were predominantly derived from the *domesticus* subspecies of *Mus musculus*, CAST was derived from the *castaneus* subspecies [26]. In addition, more polymorphisms between MRL and CAST due to the genetic distinctness of CAST would facilitate the QTL analysis.

Materials and Methods

Mice

The inbred mouse strains MRL/MpJ (MRL) and CAST/EiJ (CAST) were obtained from the Jackson Laboratory (Bar Harbor, ME). The animals were housed at the Animal Research Facility, Jerry L. Pettis Memorial VA Medical Center. Housing and breeding conditions were described previously [17, 18]. The experimental protocols were in compliance with the established animal welfare regulations and approved by the animal research committee of Jerry L. Pettis Memorial VA Medical Center. The MRL and CAST mice were intercrossed, and the resultant F_1 progeny were mated with each other to generate 328 F_2 progeny, which included 171 females and 157 males.

Phenotyping

The F_2 mice were killed at 7 weeks of age. Body weight was recorded for each animal. Liver was isolated for DNA extraction. Femurs were isolated from both legs and stored in phosphate-buffered saline buffer supplemented with 0.05% sodium azide. Femur BMD and PC were determined from the midshaft portion of the right femur (left only when right was not available) using pQCT (Stratec XCT 960 M; Norland Medical System, Ft. Atkinson, WI). The outer and inner thresholds were set at 300 mg/cm^3. The femurs were only scanned once at the midpoint. Similarly, we also measured the same parameters for the radii of the forearms *in vivo* on the live mice. Mice were first anesthetized using an i.p. dose of 50/10 mg/kg ketamine/xylazine solution. For the forearms, the outer threshold was set at 40 mg/cm^3 and the inner threshold at 710 mg/cm^3. In all, we measured total volumetric BMD (total BMD), cortical volumetric BMD (cortical BMD), PC, and endosteal circumference (EC) for both the legs and the forearms.

Genotyping

A total of 86 markers were genotyped for the MRL × CAST F_2 mice. The method of genotyping was previously described [17, 18]. The average distance between markers was 17 cM. Thirty-three percent of intermarker distances were > 20 cM.

Data Analysis

Standard statistical analyses on the phenotypes, such as correlation analysis, were conducted using the STATISTICA program (release 7; StatSoft, Tulsa, OK). Genotype data for the genomewide scans were analyzed mainly in MapQTL (5.0) [27]. MapQTL's interval mapping option was employed. Genomewide threshold logarithm of odds (LOD) scores adjusted for multiple testing were obtained by MapQTL's permutation test and considered significant when $P < 0.05$ and suggestive when $P < 0.33$.

We also employed Pseudomarker, a program on the platform of MATLAB (MathWorks, Natick, MA) [28]. To assess the effect of body size on QTL mapping, genomewide scans for BMD and PC with or without body weight as an additive covariate were carried out using Pseudomarker's MAINSCAN function. QTL interactions between different chromosomal regions were determined using the PAIRSCAN function. The amount of variance for main QTL and QTL interactions explained in the F_2 population was calculated using the FITQTL function.

When multiple bone density and bone size parameters were considered simultaneously in the QTL analyses, more stringent threshold significances were generated to mitigate the increased likelihood of false-positives as the results of assessments of multiple correlated traits. This was done using the Zmapqtl and JZmapqtl options of QTL Cartographer [29].

Results

At 7 weeks of age, the mid-diaphyseal femur BMD of CAST mice was 637.5 mg/cm^3 and lower than that of MRL mice, which was 748.8 mg/cm^3 (Table 1). Because of their small body size as measured by body weight, CAST mice also had smaller bone size than MRL mice as measured by femur length and femur PC and EC (Table 1). The distribution of femur BMD values in the

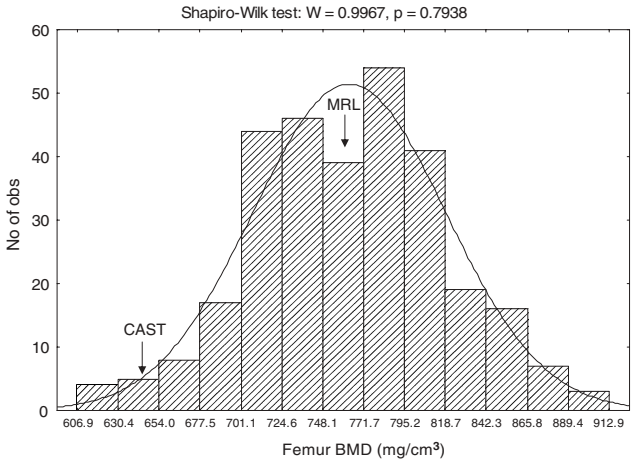

Fig. 1. Histogram showing the distribution of femur BMD obtained from 7-week-old MRL × CAST F_2 mice. The *x* axis shows the mean femur BMD (mg/cm^3) for each group. The *y* axis shows the number of mice in each group. The distribution is fitted with a bell-shaped line as expected from a normal distribution.

F_2 mice of the MRL × CAST cross did not deviate significantly from normal, as expected for a polygenic trait (Fig. 1). Probably due to the genetic distinctness of CAST, these values were much higher in MRL × CAST than in MRL × SJL. They varied between 606.9 and 912.9 mg/cm^3 in the combined F_2 of both sexes of MRL × CAST (Fig. 1). Much lower values were reported in the F_2 females of MRL × SJL: 510−790 mg/cm^3 [18]. The fact that only female mice were used in the latter cross cannot explain all of the differences. Comparison between the F_2 males and females of MRL × CAST indicated that males had only slightly higher femur BMD (average 769.6 mg/cm^3) than females (average 756.6 mg/cm^3).

Interval mapping using MapQTL identified two QTL for femur BMD with LOD scores of 3.4 and 2.7 on chromosomes 10 and 15 at 24 and 22.7 cM positions, respectively (Table 2). The *P* value of the chromosome 10 QTL nearly achieved significance ($P = 0.06$). It was significant ($P < 0.05$) in a Pseudomarker analysis (Fig. 2A, B). The chromosome 15 QTL achieved a suggestive LOD score. The high-density allele was contributed by the CAST strain in the chromosome 10 QTL and by the MRL strain in the chromosome 15 QTL. A number of significant QTL interactions were identified by Pseudomarker's PAIRSCAN function between main QTL as well as between main QTL and chromosomal positions with no significant QTL (Table 2). The largest interaction with a LOD score of 4 occurred between chromosomes 15 and 19. It is noteworthy that out of five QTL interactions, four involved chromosome 10, where a main QTL was identified. QTL interactions together accounted for 12.7% of the variance. Overall, main QTL and interactions between QTL accounted for about 26.8% of the phenotypic variance.

For femur PC, there were two QTL, with LOD scores of 3.0 and 3.5 on chromosomes 2 and 9 at positions 59.4 and 31 cM, respectively (Table 3). The chromosome 9 QTL was significant, while the chromosome 2 QTL was suggestive. The alleles for larger PC were attributed to the MRL strain in both QTL. Four significant interactions were identified involving both main QTL regions and chromosomal regions that contained no significant QTL (Table 3). The largest interaction with a LOD score of 3.9 explained 4% of the phenotypic variance. This interaction occurred between 80 cM on chromosome 4 and 30 cM on chromosome 10, where neither position had a significant bone size QTL. Overall, main QTL and QTL interactions explained 31.3% of the phenotypic variance.

There was a difference in body size between MRL and CAST: CAST mice were smaller than MRL mice. The average body weight of the 7-week-old animals was 11.2 g and 32.4 g for CAST and MRL, respectively (Table 1). In addition, the bone density and bone size parameters were correlated with body size (e.g., $r = 0.16$ and 0.57 for femur BMD and femur PC, respectively, with body weight, $P < 0.05$). Therefore, body size was taken into consideration in the QTL mapping. We analyzed the genomewide data for femur BMD and femur PC in Pseudomarker using body weight as an additive covariate. For femur BMD, the peak height of two QTL on chromosomes 10 and 15 was not much affected (Fig. 2A, B). However, a new QTL on chromosome 4 with a suggestive LOD score was present when the analysis was adjusted for body weight (Fig. 2B). Similarly for femur PC, the main QTL on chromosome 9 was not much affected by the adjustment (Fig. 2C, D). When the analysis was adjusted by body weight, the height of chromosome 2 QTL peak was reduced to nonsignificance (Fig. 2D). Thus, the chromosome 2 QTL for femur PC was partially explained by body size.

In order to identify sex-specific QTL, separate analyses based on sex were also carried out for femur BMD and femur PC. In the males, no QTL were detected for femur BMD and only one suggestive QTL existed for femur PC. In the females, no significant QTL were detected for both phenotypes. The QTL identified in the combined population were also present with suggestive LOD scores in the females. Based on the calculations by Darvasi [30], a study to detect an additive QTL with 50% of power, allele effect of 0.25, and a LOD threshold of 4.3 would require at lease of 524 F_2 individuals. Therefore, with fewer than half of the required number of mice of each sex, the result that only suggestive QTL were detected in the sex-stratified analyses was expected.

To support the analyses on femur BMD and PC, we also determined other bone density and bone size parameters using pQCT. These included cortical BMD

Table 2. Significant and suggestively significant QTL and QTL interactions for mid-shaft femur BMD in MRL × CAST F_2

Effect[a]	Chromosome	Position (cM)	Marker	LOD score	P[b]	Variance explained (%)	Allele source
Main QTL	10	24	D10Mit31	3.4	0.060	8.9	CAST
Main QTL	15	22.7	D15Mit115	2.7	0.240	5.2	MRL
Interaction	5 × 10	45 × 30	–	2.8	0.013	1.1	–
Interaction	8 × 10	15 × 35	–	3.3	0.004	2.0	–
Interaction	10 × 14	35 × 10	–	3.0	0.008	2.5	–
Interaction	10 × 19	30 × 0	–	3.3	0.004	2.2	–
Interaction	15 × 19	25 × 25	–	4.0	0.001	5.0	–
Total						26.8	

[a] Main QTL were obtained from MapQTL (Interval Mapping option); QTL interactions from Pseudomarker (PAIRSCAN function)
[b] P values for the main QTL were obtained from the permutation test in MapQTL

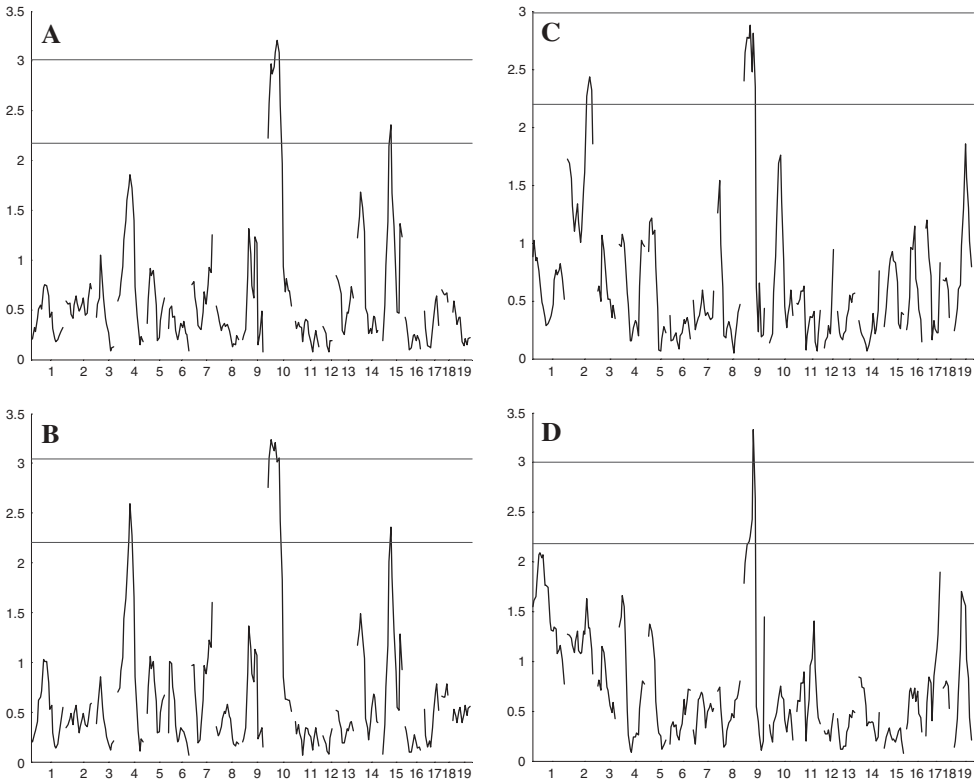

Fig. 2. LOD score graphs of the genomewide scans for femur BMD and femur PC obtained from MRL × CAST F_2 using Pseudomarker (MAINSCAN function). The x axis of the graphs shows the map position in chromosome numbers. The y axis shows the LOD score. The *upper and lower horizontal lines* indicate the LOD thresholds for significant and suggestive significance at $P < 0.05$ and 0.33, respectively. (**A**) Femur BMD analyzed without covariates. (**B**) Femur BMD analyzed with body weight as an additive covariate. (**C**) Femur PC analyzed without covariates. (D) Femur PC analyzed with body weight as an additive covariate.

Table 3. Significant and suggestively significant QTL and QTL interactions for mid-shaft femur PC in MRL × CAST F_2

Effect[a]	Chromosome	Position (cM)	Marker	LOD score	P[b]	Variance explained (%)	Allele source
Main QTL	2	59.4	D2Mit411	3.0	0.130	11.0	MRL
Main QTL	9	31	D9Mit336	3.5	0.040	7.5	MRL
Interaction	2 × 9	75 × 20	–	2.2	0.041	3.6	–
Interaction	3 × 9	20 × 10	–	2.5	0.024	3.0	–
Interaction	4 × 10	80 × 30	–	3.9	0.001	4.0	–
Interaction	9 × 10	10 × 35	–	2.9	0.010	2.2	–
Total						31.3	

[a] Main QTL were obtained from MapQTL (Interval Mapping option); QTL interactions from Pseudomarker (PAIRSCAN function)
[b] P values for the main QTL were obtained from the permutation test in MapQTL

Table 4. LOD scores and locations (shown as cM in parentheses) of significant and suggestive bone density and bone size QTL obtained from MRL × CAST F_2 using MapQTL (Interval Mappinq option)[a]

	Femur				Forearm			
Chr	Total BMD	Cortical BMD	PC	EC	Total BMD	Cortical BMD	PC	EC
2			3.0 (59.4) *,NS					
3		2.7 (24.8) *,NS						
8					4.8 (60.0) ***,*		3.2 (6.0) **,*	3.2 (6.0) **,*
9			3.5(31.0)**,**	5.1 (28.0) ***,**	4.0 (35.0) **,**		4.2 (35.0) **,***	4.2 (35.0) **,***
10	3.4 (24.0) **,*							
15	2.7 (22.7) *,NS	2.5 (28.0) *,NS						
16						2.9 (55.2) *,NS		

[a] Significance levels are indicated by two sets of asterisks, separated by a comma; the first set of significances was obtained from MapQTL, and the second set from QTLCartographer (Zmapqtl and JZmapqtl options). NS = not significant. One asterisk indicates suggestive LOD scores at $P < 0.33$; two and three asterisks indicate significant LOD scores at $P < 0.05$ and 0.01, respectively

and EC for the femur and total BMD, cortical BMD, EC, and PC for the radii of the forearms. Table 4 lists QTL with significant and suggestive LOD scores for all phenotypes obtained from MapQTL. Chromosomes 2, 3, 10, and 16 carried QTL for only one measured phenotype. Chromosomes 8, 9, and 15 carried QTL for at least two phenotypes. Among these, chromosome 9 carried QTL for five phenotypes, which were femur EC, femur PC, forearm BMD, forearm EC, and forearm PC. These QTL were all colocalized within the same region (28−35 cM). To reduce the increased likelihood of false-positives due to the assessment of multiple correlated traits, more stringent significance thresholds were also generated from QTL Cartographer. It can be seen that these chromosome 9 QTL for different bone phenotypes were still significant after adjusting for the correlations among phenotypes (Table 4).

Discussion

We have identified two QTL for femur BMD: one significant on chromosome 10 and one suggestive on chromosome 15. The chromosome 10 QTL is novel and has not been detected in the previously published cross B6 × CAST or other published crosses including MRL × SJL (Table 5) [11, 12]. Beamer et al. [7] identified a QTL on chromosome 15 associated with marker D15Mit29 at 42.8 cM. Whether the suggestive QTL we identified on chromosome 15 associated with D15Mit115 at 22.7 cM (Table 5) is the same or not remains to be determined. Therefore, we identified one novel QTL on chromosome 10 and possibly a second one on chromosome 15 in this study. The chromosome 10 QTL alleles contributed by CAST appear to exert an important role in bone. It is noteworthy that the chromosomal region where this QTL is located also interacted with other chromosomes to contribute to high BMD; four of the five significant interactions involved this QTL region. Therefore, there must be important bone loci within this QTL region.

One of the most important femur BMD QTL is on chromosome 1. LOD scores of 10.4 at 86.3 cM in B6 × CAST [7] and 3.9 at 82 cM in MRL × SJL were found [17, 18]. A similar, if not the same, QTL associated with D1Mit291 at 101.50 cM was also identified on the whole-body BMD by DXA [24, 25]. However, this distal QTL was totally absent in MRL × CAST in this study. In addition, chromosome 1 had no significant interactions with other chromosomal regions. This could suggest that similar and high-BMD alleles are present in the both high-BMD parental strains, and these alleles cannot be phenotypically discriminated in MRL × CAST. The possibility that effects of the distal chromosome 1 QTL are expressed later in this cross as skeletal maturity is being achieved is unlikely since this QTL was already detected in the 7-week-old F_2 mice of MRL × SJL [18].

Table 5. Femur BMD QTL identified in the F_2 mice of complementary crosses using pQCT[a]

Cross[b]	Chromosome	Marker	Position (cM)	LOD score	References
MRL × CAST	10	D10Mit31	24	3.4	This study
	15	D15M15	22.7	2.7	This study
B6 × CAST	**1**	**D1Mit15**	**86.3**	**10.4**	**Beamer et al. [7]**
	5	D5M12	42	5	Beamer et al. [7]
	13	D13M6	10	42.8	Beamer et al. [7]
	15	D15Mit29	4.8	3	Beamer et al. [7]
MRL × SJL	**1**	**D1Mit33**	**82**	**3.9**	**Li et al. [17], Masinde et al. [18]**
	1	D1Mit291	103.8	>2.7	Li et al. [17]
	1	D1Mit362	110.4	5.9	Masinde et al. [18]
	3	D3Mit217	43.7	2.7	Masinde et al. [18]
	4	D4Mit204	61.2	2.9	Li et al. [17], Masinde et al. [18]
	9	D9Mit270	41.5	3.1	Li et al. [17], Masinde et al. [18]
	12	D12M56	28.4	>2.7	Li et al. [17]
	12	D12Mit201	29	3	Masinde et al. [18]
	14	D14M32	0	>2.7	Li et al. [17]
	17	D17M75	6.6	5.8	Li et al. [17], Masinde et al. [18]
	17	D17M76	12	4.4	Masinde et al. [18]
	18	D18M52	25.1	3.1	Masinde et al. [18]
	18	D18M85	27.3	>2.7	Li et al. [17]
	19	D19Mit53	32.8	>2.7	Li et al. [17]

[a] Bold font indicates common QTL present in more than one study
[b] Mice in MRL × CAST amd MRL × SJL were 7 weeks of age, while those in B6 × CAST were 16 weeks of age

Table 6. Femur PC QTL identified in the F_2 mice of complementary crosses using pQCT[a]

Cross	Chromosome	Marker	Position (cM)	LOD	Reference
MRL × CAST	**2**	**D2Mit411**	**59.4**	**3.0**	**This study**
	9	**D9Mit336**	**31**	**3.5**	**This study**
MRL × SJL	1	D1Mit44	50.3	6.8	Masinde et al. [19]
	1	D1Mit33	82	4.8	Masinde et al. [19]
	2	**D2Mit62**	**54.6**	**6.8**	**Masinde et al. [19]**
	3	D2Mit263	78.7	5.4	Masinde et al. [19]
	6	D6Mit123	17.5	4.9	Masinde et al. [19]
	6	D6Mit291	54.2	5.8	Masinde et al. [19]
	9	D9Mit90	7.7	3.8	Masinde et al. [19]
	9	**D9Mit263**	**42**	**2.8**	**Masinde et al. [19]**
	11	D11Mit36	43.7	3.6	Masinde et al. [19]
	14	D14Mit19	52.5	4.1	Masinde et al. [19]
	15	D15Mit62	33.4	6.7	Masinde et al. [19]
	17	D17Mit176	17	4.6	Masinde et al. [19]

[a] Bold font indicates common QTL present in more than one study
[b] Mice in all crosses were 7 weeks of age

We identified two QTL related to bone size. The chromosome 2 QTL was suggestive, and the chromosome 9 QTL was significant. These bone size QTL appeared to be the same as those found in MRL × SJL by Masinde et al. [19] (Table 6). The suggestive QTL associated with D2Mit411 (59.4 cM) on chromosome 2 in this study corresponded to the bone size QTL associated with D2Mit63 (54.6 cM) by Masinde et al. [19]. Similarly, the QTL associated with D9Mit336 (31 cM) on chromosome 9 in this study matched the bone size QTL associated with D9Mit263 (42 cM) by Masinde et al. [19].

Table 4 shows that chromosome 9 not only carried a QTL for femur PC but also carried QTL for femur EC, forearm PC and EC, and forearm BMD. The presence of QTL for multiple bone density and bone size parameters confirms the presence of femur PC QTL on chromosome 9. It also demonstrates QTL's widespread pleiotropic effect. Another example of pleiotropy is QTL on chromosome 8 for BMD, PC, and EC of the forearm.

Another rationale of using the MRL × CAST cross was to exploit the information that might be obtained as complementary to B6 × CAST and MRL × SJL, two crosses which were already published [7, 17, 18]. Since a

common parent was used in more than one cross, QTL in one cross might confirm those in the others. In addition, haplotype could be constructed for the progenitors used in these crosses in order to pinpoint the polymorphisms, especially single-nucleotide polymorphisms, which may be potentially responsible for the QTL. In other words, using complementary crosses could facilitate the QTL mapping process. This has been demonstrated by Ishimori et al. [31].

We chose 7 weeks as the age of euthanasia because of the requirement of another study on soft tissue regeneration [32]. Mice at this age have not attained peak bone density, and QTL identified at this stage may not be the same as would have been identified at peak bone density. However, we believe that the 7-week-old mice would have accreted approximately 70% of bone mass based on the acquisition curves in previous studies [7, 13]. Therefore, an equal proportion of bone QTL would be already expressed at this age. Another limitation of the study was the difference in body size between the parental strains, with MRL being much larger than CAST. Although we used body weight as a covariate in QTL mapping, variability in body weight due to rapid growth in the 7-week-old animals could not fully correct the confounding effect of skeletal growth rate on bone density and bone size. Therefore, some bone QTL could likely be attributed to skeletal growth rate genes.

In conclusion, we identified two femur BMD QTL (one significant on chromosome 10, one suggestive on chromosome 15), two femur PC QTL (one significant on chromosome 9, one suggestive on chromosome 2), and multiple bone density and bone size QTL of the femur and the forearm by crossing the inbred lines of MRL and CAST, both of which exhibit relatively high BMD.

Acknowledgements. This work was supported by Assistance Award DAMD17-99-1-9571. The U.S. Army Medical Research Acquisition Activity is the awarding and administering acquisition office. The information contained in this publication does not necessarily reflect the position or policy of the government, and no official endorsement should be inferred. The authors thank Courtney Kruse for technical assistance and the staff of the Jerry L. Pettis Memorial VA Medical Center, where this work was performed, for their support.

References

1. Deng HW, Chen WM, Conway T, Zhou Y, Davies KM, Stegman MR, Deng H, Recker RR (2000) Determination of bone mineral density of the hip and spine in human pedigrees by genetic and life-style factors. Genet Epidemiol 19:160–177
2. Wergedal JE, Sheng MH, Ackert-Bicknell CL, Beamer WG, Baylink DJ (2005) Genetic variation in femur extrinsic strength in 29 different inbred strains of mice is dependent on variations in femur cross-sectional geometry and bone density. Bone 36:111–122
3. Deng HW, Stegman MR, Davies KM, Conway T, Recker RR (1999) Genetic determination of variation and covariation of peak bone mass at the hip and spine. J Clin Densitom 2:251–263
4. Dequeker J, Nijs J, Verstraeten A, Geusens P, Gevers G (1987) Genetic determinants of bone mineral content at the spine and radius: a twin study. Bone 8:207–209
5. Gueguen R, Jouanny P, Guillemin F, Kuntz C, Pourel J, Siest G (1995) Segregation analysis and variance components analysis of bone mineral density in healthy families. J Bone Miner Res 10:2017–2022
6. Slemenda CW, Christian JC, Williams CJ, Norton JA, Johnston CC Jr (1991) Genetic determinants of bone mass in adult women: a reevaluation of the twin model and the potential importance of gene interaction on heritability estimates. J Bone Miner Res 6:561–567
7. Beamer WG, Shultz KL, Churchill GA, Frankel WN, Baylink DJ, Rosen CJ, Donahue LR (1999) Quantitative trait loci for bone density in C57BL/6J and CAST/EiJ inbred mice. Mamm Genome 10:1043–1049
8. Li X, Mohan S, Gu W, Wergedal J, Baylink DJ (2001) Quantitative assessment of forearm muscle size, forelimb grip strength, forearm bone mineral density, and forearm bone size in determining humerus breaking strength in 10 inbred strains of mice. Calcif Tissue Int 68:365–369
9. Cummings SR, Kelsey JL, Nevitt MC, O'Dowd KJ (1985) Epidemiology of osteoporosis and osteoporotic fractures. Epidemiol Rev 7:178–208
10. Melton LJ 3rd, Kan SH, Frye MA, Wahner HW, O'Fallon WM, Riggs BL (1989) Epidemiology of vertebral fractures in women. Am J Epidemiol 129:1000–1011
11. Huang QY, Recker RR, Deng HW (2003) Searching for osteoporosis genes in the post-genome era: progress and challenges. Osteoporos Int 14:701–715
12. Recker RR, Deng HW (2002) Role of genetics in osteoporosis. Endocrine 17:55–66
13. Beamer WG, Shultz KL, Donahue LR, Churchill GA, Sen S, Wergedal JR, Baylink DJ, Rosen CJ (2001) Quantitative trait loci for femoral and lumbar vertebral bone mineral density in C57BL/6J and C3H/HeJ inbred strains of mice. J Bone Miner Res 16:1195–1206
14. Edderkaoui B, Baylink DJ, Beamer WG, Wergedal JE, Dunn NR, Shultz KL, Mohan S (2006) Multiple genetic loci from CAST/EiJ chromosome 1 affect vBMD either positively or negatively in a C57BL/6J background. J Bone Miner Res 21:97–104
15. Gu W, Li X, Lau KH, Edderkaoui B, Donahae LR, Rosen CJ, Beamer WG, Shultz KL, Srivastava A, Mohan S, Baylink DJ (2002) Gene expression between a congenic strain that contains a quantitative trait locus of high bone density from CAST/EiJ and its wild-type strain C57BL/6J. Funct Integr Genomics 1:375–386
16. Gu WK, Li XM, Edderkaoui B, Strong DD, Lau KH, Beamer WG, Donahue LR, Mohan S, Baylink DJ (2002) Construction of a BAC contig for a 3 cM biologically significant region of mouse chromosome 1. Genetica 114:1–9
17. Li X, Masinde G, Gu W, Wergedal J, Mohan S, Baylink DJ (2002) Genetic dissection of femur breaking strength in a large population (MRL/MpJ × SJL/J) of F2 Mice: single QTL effects, epistasis, and pleiotropy. Genomics 79:734–740
18. Masinde GL, Li X, Gu W, Wergedal J, Mohan S, Baylink DJ (2002) Quantitative trait loci for bone density in mice: the genes determining total skeletal density and femur density show little overlap in F_2 mice. Calcif Tissue Int 71:421–428
19. Masinde GL, Wergedal J, Davidson H, Mohan S, Li R, Li X, Baylink DJ (2003) Quantitative trait loci for periosteal circumference (PC): identification of single loci and epistatic effects in F_2 MRL/SJL mice. Bone 32:554–560
20. Benes H, Weinstein RS, Zheng W, Thaden JJ, Jilka RL, Manolagas SC, Shmookler Reis RJ (2000) Chromosomal mapping of osteopenia-associated quantitative trait loci

using closely related mouse strains. J Bone Miner Res 15:626–633
21. Shimizu M, Higuchi K, Bennett B, Xia C, Tsuboyama T, Kasai S, Chiba T, Fujisawa H, Kogishi K, Kitado H, Kimoto M, Takeda N, Matsushita M, Okumura H, Serikawa T, Nakamura T, Johnson TE, Hosokawa M (1999) Identification of peak bone mass QTL in a spontaneously osteoporotic mouse strain. Mamm Genome 10:81–87
22. Shimizu M, Higuchi K, Kasai S, Tsuboyama T, Matsushita M, Mori M, Shimizu Y, Nakamura T, Hosokawa M (2001) Chromosome 13 locus, Pbd2, regulates bone density in mice. J Bone Miner Res 16: 1972–1982
23. Klein RF, Allard J, Avnur Z, Nikolcheva T, Rotstein D, Carlos AS, Shea M, Waters RV, Belknap JK, Peltz G, Orwoll ES (2004) Regulation of bone mass in mice by the lipoxygenase gene *Alox15*. Science 303:229–232
24. Klein RF, Carlos AS, Vartanian KA, Chambers VK, Turner EJ, Phillips TJ, Belknap JK, Orwoll ES (2001) Confirmation and fine mapping of chromosomal regions influencing peak bone mass in mice. J Bone Miner Res 16:1953–1961
25. Orwoll ES, Belknap JK, Klein RF (2001) Gender specificity in the genetic determinants of peak bone mass. J Bone Miner Res 16:1962–1971
26. Wade CM, Kulbokas EJ 3rd, Kirby AW, Zody MC, Mullikin JC, Lander ES, Lindblad-Toh K, Daly MJ (2002) The mosaic structure of variation in the laboratory mouse genome. Nature 420:574–578
27. Van Ooijen JW (2004) MapQTL® 5, software for the mapping of quantitative trait loci in experimental populations. Kyazma BB, Wageningen, The Netherlands
28. Sen S, Churchill GA (2001) A statistical framework for quantitative trait mapping. Genetics 159:371–387
29. Basten CJ, Weir BS, Zeng Z-B (2003) QTL Cartographer. A reference manual and tutorial for QTL mapping. Department of Statistics, North Carolina State University, Raleigh
30. Darvasi A (1998) Experimental strategies for the genetic dissection of complex traits in animal models. Nat Genet 18:19–24
31. Ishimori N, Li R, Walsh KA, Korstanje R, Rollins JA, Petkov P, Pletcher MT, Wiltshire T, Donahue LR, Rosen CJ, Beamer WG, Churchill GA, Paigen B (2006) Quantitative trait loci that determine BMD in C57BL/6J and 129S1/SvImJ inbred mice. J Bone Miner Res 21: 105–112
32. Yu H, Mohan S, Masinde GL, Baylink DJ (2005) Mapping the dominant wound healing and soft tissue regeneration QTL in MRL X CAST. Mamm Genome 16:918–924

Identification of quantitative trait loci that regulate obesity and serum lipid levels in MRL/MpJ × SJL/J inbred mice

Apurva K. Srivastava,[1,*,†] Subburaman Mohan,[*,†] Godfred L. Masinde,[2] Hongrun Yu,[*] and David J. Baylink[*,†]

Musculoskeletal Disease Center,* Loma Linda VA Health Care Systems, Loma Linda, CA 92357; and Department of Medicine,† Loma Linda University, Loma Linda, CA 92354

Abstract **The total body fat mass and serum concentration of total cholesterol, HDL cholesterol, and triglyceride (TG) differ between standard diet-fed female inbred mouse strains MRL/MpJ (MRL) and SJL/J (SJL) by 38–120% ($P < 0.01$). To investigate genetic regulation of obesity and serum lipid levels, we performed a genome-wide linkage analysis in 621 MRL× SJL F_2 female mice. Fat mass was affected by two significant loci, *D11Mit36* [43.7 cM, logarithm of the odds ratio (LOD) 11.2] and *D16Mit51* (50.3 cM, LOD 3.9), and one suggestive locus at *D7Mit44* (50 cM, LOD 2.4). TG levels were affected by two novel loci at *D1Mit43* (76 cM, LOD 3.8) and *D12Mit201* (26 cM, LOD 4.1), and two suggestive loci on chromosomes 5 and 17. HDL and cholesterol concentrations were influenced by significant loci on chromosomes 1, 3, 5, 7, and 17 that were in the regions identified earlier for other strains of mice, except for a suggestive locus on chromosome 14 that was specific to the MRL × SJL cross. In summary, linkage analysis in MRL × SJL F_2 mice disclosed novel loci affecting TG, HDL, and fat mass, a measure of obesity. Knowledge of the genes in these quantitative trait loci will enhance our understanding of obesity and lipid metabolism.**—Srivastava, A. K., S. Mohan, G. L. Masinde, H. Yu, and D. J. Baylink. **Identification of quantitative trait loci that regulate obesity and serum lipid levels in MRL/MpJ × SJL/J inbred mice.** ***J. Lipid Res.*** **2006.** 47: **123–133.**

Supplementary key words body fat mass • HDL cholesterol • cholesterol • triglyceride

Cardiovascular disease (CVD) is currently the leading cause of morbidity and mortality world wide, and its incidence is likely to increase. Elevated cholesterol, especially LDL cholesterol and triglyceride (TG) levels, low HDL cholesterol levels, hypertension, type 2 diabetes, and obesity modulate risk for CVD (1, 2). Such risk factors are present in 80–90% of CVD patients. Current understanding supports a complex etiology involving both environmental and genetic determinants. Environmental risk factors for CVDs identified in humans include diet, physical activity, cigarette smoking, high blood pressure, uncontrolled diabetes, obesity and overweight, stress, and adverse lipid profile (2). However, little is known about the genetic regulation of blood lipid levels, with only some of the genes that regulate production or blood levels of lipids having so far been identified (3–9). Because of inherent difficulties in carrying out linkage analyses for complex traits in humans, inbred strains of mice have been used as a powerful tool for identifying quantitative trait loci (QTLs) that contribute to variations in circulating levels of lipids (10–29). QTL studies in mice have not only revealed a large number of loci that regulate lipid levels in blood but also have shown that there is a high degree of concordance between human QTLs that regulate lipid levels and their corresponding mouse loci (30, 31). More than 60 QTLs on chromosomes 1, 2, 3, 5, 7, 8, 9, 14, 16, 17, 18, and 19 that affect plasma lipid levels, as well as body fat mass QTLs, have been identified in several strains of mice (10–29). The rationale for using different crosses is based on the fact that each parental mouse strain represents unique mapping panels for the identification of QTLs for a complex trait. The phenotypic differences between parental strains, the extent of allelic variation, and the strain background are critical factors that determine whether a given QTL can be detected in a particular cross. This implies that a best estimate of all genes that account for a total variation of lipid levels in humans and mice can only be achieved by comparing the results of multiple crosses.

Mouse strains MRL/MpJ (MRL) and SJL/J (SJL) display extreme rates of soft-tissue healing and regeneration, and our laboratory has used these two strains in the past to reveal linkage to several loci that control soft-tissue healing (32) and musculoskeletal phenotypes (33–37). We have observed that when MRL and SJL mice are fed a standard

Manuscript received 11 July 2005 and in revised form 21 September 2005 and in re-revised form 26 October 2005.

Published, JLR Papers in Press, October 27, 2005.
DOI 10.1194/jlr.M500295-JLR200

Abbreviations: apoA-II, apolipoprotein A-II; CVD, cardiovascular disease; LOD, logarithm of the odds ratio; QTL, quantitative trait locus; SNP, single-nucleotide polymorphism; TG, triglyceride.

[1] To whom correspondence should be addressed.
e-mail: apurva.srivastava@med.va.gov

[2] Present address of Godfred L. Masinde: Long Beach Genetics-Esoterix, Rancho Dominguez, CA 90220.

diet, they also display large differences in serum levels of cholesterol, HDL, TG, and body fat mass. To examine the genetic basis of these differences, we measured serum levels of cholesterol, HDL, TG, and body fat mass in the F_2 progeny. The aim of this study was to identify loci that regulate body fat mass, cholesterol, HDL, and TG in the F_2 mice of MRL × SJL crosses. Because multiple phenotypes were measured in this study, an additional aim was to identify common loci that regulate obesity and lipid levels.

MATERIALS AND METHODS

Mice

Acquisition of MRL/MpJ (MRL) and SJL/J (SJL) mice, generation of F_1 and F_2 progeny, collection of DNA samples, and collection and processing of blood were performed as described previously (32). In brief, MRL females were mated with SJL males to produce F_1 mice. Brother-sister mating was established to produce F_2 mice. Only female F_2 mice were weaned onto standard diet (TD 99479; Harlan Teklad, Madison, WI) at 21 days and housed three to six animals per cage. Mice were fed standard diet up to 7 weeks of age, when they were euthanized and bled without fasting. Age-matched parent mice were purchased from the Jackson Laboratory for plasma lipid analyses. All mice were allowed free access to standard food and water throughout the course of the study.

All blood samples were collected in the afternoon at the same time of day (±2 h) under nonfasting conditions. Blood was collected directly into 1.5 ml plastic tubes (Eppendorf), and serum was separated from cells by centrifugation within 1 h of blood collection. Serum was stored at −70°C until analyzed. The experimental protocols were in compliance with animal welfare regulations and approved by the Institutional Animal Care and Use Committee, Jerry L. Pettis VA Medical Center.

Serum cholesterol, HDL, and TG measurements

Total cholesterol, HDL cholesterol, and TG were measured by direct enzymatic colorimetric assays using a fully automated Hitachi 912 Clinical Chemistry Analyzer (Roche Diagnostics; Indianapolis, IN). Measurements of cholesterol, HDL, and TG were validated in our laboratory for reproducibility and analytical recovery in mice serum. The inter-assay (n = 12) and intra-assay (n = 5) coefficients of variation for all three assays were <7%. The mean analytical recovery of the diluted mouse serum samples (n = 3; up to 4-fold) was 100.3%. The sensitivity of the cholesterol and HDL assay was 3 mg/dl, and that of the TG assay was 4 mg/dl. The measuring range for cholesterol and TG was 3–800 mg/dl. The measuring range for HDL was 3–200 mg/dl in mouse serum.

Analysis of fat mass

The percent fat mass was measured using peripheral dual-energy X-ray absorptiometry (PIXIMUS densitometer; Lunar Corp., Madison, WI), a method that has been validated for mice (14). The precision of PIXIMUS for measurement of total body fat mass is coefficient of variance <2%. The body mass index (BMI) was calculated as described previously (14).

Construction of linkage map

Extraction of genomic DNA and PCR-based genotyping with 137 microsatellite markers have been described previously (32–36). Alleles derived from the MRL/MpJ parent were designated A, SJL/J-derived alleles were designated B, and MRL/SJL heterozygotes were designated H in data analyses. Marker orders were estimated from the publicly available Mouse Genome Database. A total of 132 markers distributed across the 19 autosomes were used for statistical analyses (excluding the X-chromosome). A list of markers and the resulting linkage map are available from the authors.

Statistical analyses

Data were analyzed using GraphPad Prism (Windows version 4.02; GraphPad Software, San Diego, CA). The Shapiro-Wilk test was used to test the normality of the F_2 population (32–37). One-way ANOVAs with Newman-Keuls test were used to compare pairs of data in order to determine statistically significant differences in plasma lipid levels, BMI, and percent fat between mouse groups.

Genotype data were analyzed using the Pseudomarker MAINSCAN algorithm (38) written for the MATLAB (Mathworks, Inc.; Natick, MA) programming environment (available from www.jax.org/research/churchill). Thresholds for logarithm of the odds ratio (LOD) scores for different QTLs were determined by genome-wide 1,000-permutation test for 1% genome-wide error ($P < 0.01$) and 5% genome-wide error ($P < 0.05$). Linkage analyses were also performed using MapQTL 5.0 (DLO Center for Plant Breeding and Reproduction Research; Wageningen, the Netherlands) as described for F_2 intercrosses. Pseudomarker and MapQTL 5.0 analyses yielded comparable results. Percent variance explained by each locus was calculated for peak interval by MapQTL software.

To study genome-wide interactions between QTLs, we used the Pseudomarker PAIRSCAN algorithm. This program analyzes the phenotypic effect of each marker or marker interval taken singly (MAINSCAN) and also the phenotypic effects of pairs of markers or intervals taken jointly (PAIRSCAN) for their effects on the trait. The PAIRSCAN allows a genome-wide search for epistasis. For PAIRSCAN, we tested the combined (or full model) effects on trait of a marker pair, which reflects the main effects of both markers plus their interaction (38). The threshold for genome-wide significance was set at 5%, which was estimated by a 200-permutation test carried out on F_2 data.

RESULTS

Serum lipoprotein cholesterol profiles of MRL, SJL, F_1, and F_2 intercross mice

The fat mass calculated as percent body weight was 38% ($P < 0.001$) higher in MRL mice as compared with SJL mice (**Table 1**). The MRL mice had 60% ($P < 0.001$) higher body weight as compared with SJL mice (details not shown). However, there was a moderate but highly significant correlation between percent fat mass and body weight (Pearson r value = 0.25; $P < 0.001$), indicating that about 6.2% of the body weight was explained by variance in percent fat mass. Serum concentrations of cholesterol and HDL were higher in MRL mice by 82% ($P < 0.001$), and 120% ($P < 0.001$), respectively, as compared with SJL mice (Table 1). The TG levels were 58% ($P < 0.001$) higher in SJL mice compared with MRL mice. The percent fat mass, cholesterol, and HDL levels were intermediate (Table 1) and significantly different in F_1 mice ($P < 0.01$ by ANOVA) compared with those of the parental strains.

TABLE 1. Percent body fat mass and lipid levels in standard diet-fed female MRL/MpJ and SJL/J mice

Mice	Body Weight	Fat Mass	Cholesterol	HDL	Triglyceride
	g	%		*mg/dl*	
MRL/MpJ (n = 20)	29.8 ± 1.7	16.9 ± 2.7	155.2 ± 18.7	152.2 ± 18.7	140.9 ± 32.8
SJL/J (n = 10–20)	18.1 ± 0.8[b]	12.3 ± 1.8	89.1 ± 7.5[b]	69.1 ± 5.1[b]	235.8 ± 61.8[b]
F_1 (n = 34)	26.8 ± 1.9[a]	14.4 ± 2.1[a]	131.8 ± 18.9[a]	115.5 ± 14.9[a]	202.7 ± 53.1[c]

[a] $P < 0.01$ vs MRL and SJL.
[b] $P < 0.01$ vs MRL.
[c] $P < 0.01$ from MRL but not significantly different from SJL.

These data suggest that high cholesterol, HDL, and fat mass were inherited in an additive manner. The TG levels in F_1 mice were significantly higher than in MRL mice but comparable to those of SJL mice ($P > 0.05$ by ANOVA), suggesting that TG levels were inherited in a dominant fashion (Table 1).

The distributions of fat mass, cholesterol, HDL, and TG among standard diet-fed female F_2 mice are shown in **Fig. 1A, C, E, G**. The distributions of fat mass did not pass the normality test (Shapiro Wilk $W = 0.9$; $P < 0.05$; n = 621; mean ± SD, 12.9 ± 3.1). As expected for mice fed a standard diet, there was a highly significant correlation between cholesterol and HDL levels in the F_2 mice (n = 518; Pearson correlation coefficient, $r = 0.96$; $P < 0.0001$). The distributions of cholesterol (mean ± SD, 133 ± 27 mg/dl), HDL (mean ± SD, 112 ± 25 mg/dl), and TG (mean ± SD, 207 ± 75 mg/dl) were continuous (Fig. 1C, E, G) but did not pass the normality test (Shapiro Wilk $W = 0.95$–0.98; $P < 0.01$). However, the range of F_2 values exceeded mean ± 2 SD parental intervals for each trait. The correlation between fat mass and lipid levels was very weak (Pearson r values 0.006, 0.021, 0.05 for HDL, cholesterol, and TG) and nonsignificant ($P > 0.05$). Cholesterol levels showed a highly significant correlation with TG (Pearson

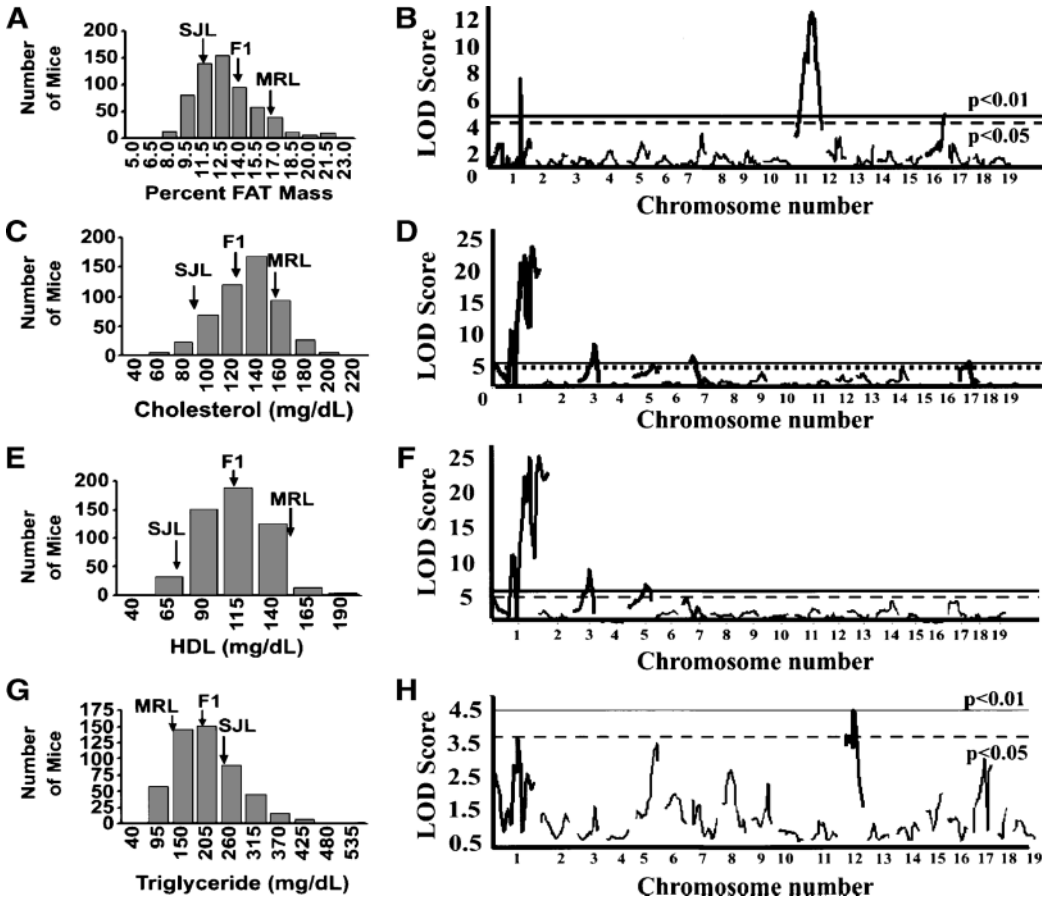

Fig. 1. Genome-wide linkage map of percent fat mass in MRL × SJL F_2 female mice. A, C, E, and G: Distribution of percent fat mass, cholesterol, HDL cholesterol, and triglyceride (TG) in MRL × SJL female F_2 mice (n = 518–621). B, D, F, H: Linkage maps of percent fat mass, cholesterol, HDL cholesterol, and TG in MRL × SJL female F_2 mice. Solid horizontal lines in B, D, F, and H indicate the threshold for genome-wide significance for $P < 0.01$. Broken horizontal lines in B, D, F, and H indicate the threshold for genome-wide significance for $P < 0.05$.

$r = 0.34$; $P < 0.0001$). Taken together, these data also suggest a complex inheritance of serum lipid levels and fat mass in this cross.

Identification of genetic loci affecting obesity or body fat mass

The linkage map for body fat mass was constructed using a panel of 621 MRL × SJL F_2 mice. Two significant QTLs were identified on chromosomes 11 and 16 (Fig. 1B), with strongest linkage (LOD score 11) on chromosome 11 (**Table 2**). Because single-marker D16Mit51 indicated the linkage on chromosome 16, mapping of D16Mit51 should be considered provisional; the locus is located at the end of a chromosome and confirmatory polymorphic markers flanking the linked marker (D16Mit51) could not be identified. A suggestive QTL was identified on chromosome 7 at 50 cM with an LOD score of 2.4 (genome-wide significance; $P < 0.68$). In addition, we observed a QTL on chromosome 1 at 82 cM linked to the marker D1Mit33 with an LOD score of 6.6 ($P < 0.0001$); however, this QTL was not supported by flanking markers, and hence was excluded from any further analysis. **Figure 2** shows posterior probability plots, likelihood statistics that give rise to the 95% confidence interval for a locus. Taken together, the three QTLs (excluding chromosome 1 QTL) explained approximately 18% of the phenotypic variance in F_2 female mice. We also calculated LOD scores for the BMI trait, which failed to pass the threshold of significance for suggestive linkage ($P < 0.63$) for any loci (data not shown), indicating that linkage of fat mass was largely independent of BMI in this cross.

Localization of cholesterol, HDL, and TG QTLs

The linkage maps for lipids were generated using a panel of 518 (MRL × SJL) F_2 mice for which blood was available. The results of interval mapping of these traits are shown in Table 2 and Fig. 1. Five statistically significant cholesterol QTLs were identified on chromosomes 1, 3, 5, 7, and 17 (the three strongest linkages are shown in **Fig. 3**). The highest LOD score was observed for the chromosome 1 locus, with peak LOD score of 22 at *D1Mit453* (Fig. 3). As expected for mice fed a standard diet, the HDL loci were coincident with loci underlying cholesterol levels, but only three QTLs on chromosomes 1, 3, and 5 reached the threshold of genome-wide significance (shown in **Figs. 3**, **4** along with the alleles contributing to closest peak marker). The QTL on chromosome 1 exerted the strongest effect on cholesterol and HDL, explain ing 28% and 30%, respectively, of the variance (Table 2) in F_2 mice. Significant linkage for TG was observed on two loci on chromosomes 1 and 12 (**Fig. 5**). Two suggestive linkages were observed for TG on chromosomes 5 and 17 (Table 2).

The LOD scores for cholesterol were comparable to analogous scores for HDL levels at chromosomes 1, 3, and 5 QTLs, whereas LOD scores for cholesterol and HDL for chromosomes 7 and 17 appear to be differentially regulated, suggesting additional QTL(s) that may regulate non-HDL cholesterol levels. To investigate this further, we performed linkage analysis using non-HDL cholesterol levels (calculated by subtracting HDL from total cholesterol) in female F_2 mice (Table 2). Linkage to non-HDL cholesterol was detected in F_2 mice on chro-

TABLE 2. Major QTLs that influence body fat mass and lipid levels in standard diet-fed female MRL/MpJ and SJL/J mice

Phenotype	Chromosome	Peak Marker (cM)	LOD Score	*P*	Variance Explained by Peak Interval
Fat mass	7	50	2.42[b]	0.003780	1.9
	11[a]	43.0	11.51[c]	<0.000001	12.0
	16	50.0	3.99[c]	0.000102	3.6
Cholesterol	1	95	22.00[c]	<0.000001	27.7
	3	40	6.61[c]	<0.000001	11.2
	5	50	3.32[c]	0.000479	3.3
	7	10	4.74[c]	0.000018	4.9
	14	40	2.62[b]	0.002415	2.9
	17	25	3.73[c]	0.000180	5.1
HDL	1	95	23.29[c]	<0.000001	30.0
	3	40	7.02[c]	<0.000001	11.7
	5	45	4.86[c]	0.000014	4.8
	7	10	2.95[b]	0.001116	2.2
	14	45	2.43[b]	0.003747	2.6
	17	25	2.5[b]	0.003170	3.5
Triglyceride	**1**	76.2	3.80[c]	0.000152	3.4
	5	55.0	3.05[b]	0.000900	3.7
	12	26.0	4.10[c]	0.000079	4.6
	17	30.0	2.59[b]	0.002547	3.6
Non-HDL cholesterol	7	15	3.69[c]	0.000206	4.0
	12	5	5.09[c]	0.000008	6.2
	9	40	2.73[b]	0.001847	3.0

LOD, logarithm of the odds ratio; QTL, quantitative trait locus.

[a] QTL identified earlier in same cross (Reference #33) also corresponds to body length (43.7 cM, LOD 4.8) and muscle mass (43.7 cM, LOD 2.7). QTLs in bold letters indicate novel QTL finding.

[b] Suggestive QTLs genome-wide significance calculated for cutoff <0.68.

[c] Kruskal-Wallis test results of significant markers $P < 0.001$.

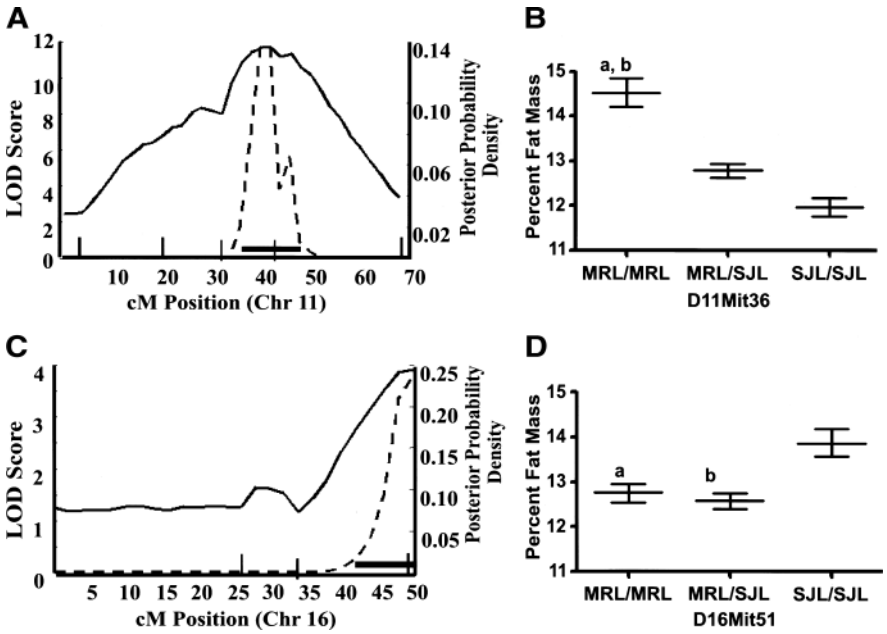

Fig. 2. A, B: Logarithm of the odds ratio (LOD) score and posterior probability density plots for the major quantitative trait loci (QTLs) influencing percent fat mass. C, D: Allelic contribution of closest marker located on major QTL peak. MRL/MRL represents homozygosity for MRL/MpJ alleles; SJL/SJL represents homozygosity for SJL/J alleles; and heterozygosity at a locus is represented by MRL/SJL. Chromosome 11 was analyzed using five markers, and chromosome 16 was analyzed using three markers. Locations of these markers are shown as vertical lines on the x axis. Posterior probability density is a likelihood statistic that gives rise to the 95% confidence intervals indicated by black horizontal bars. Error bars represent SEM. a = P 0.05 vs SJL/SJL; b = $P < 0.05$ vs MRL/SJL (by ANOVA). Chr, chromosome; cM, centimorgan.

mosome 7 (D7Mit76), accounting for 4.0% variance. Additional linkages were observed for chromosome 12 (D12Mit182), accounting for 6.2% variance, and chromosome 9 (D9Mit208), accounting for 3.0% variance (inherited in an additive manner; data not shown). The peaks on chromosome 7 and chromosome 17 were coincident with the peaks for cholesterol and HDL levels (Table 2). Although the above data provide genetic evidence for differential regulation of non-HDL cholesterol, however, the results on non-HDL cholesterol should be interpreted cautiously because the blood levels of non-HDL cholesterol are very low.

Nonparametric mapping with the Kruskal-Wallis Test to assess fat mass and lipid QTLs

The interval-mapping approach for QTL analysis is based on the assumption that the residual environmental variation follows a normal distribution. However, the fat mass and lipid data showed slight deviation from normal distribution. Therefore, the Kruskal-Wallis rank sum test, which makes no assumptions about the probability distributions of the phenotypic data, was also employed to determine trait-marker association. The Kruskal-Wallis analysis, performed with fat mass and serum lipid level phenotype data in the MapQTL program, confirmed all loci identified by interval mapping. The Kruskal-Wallis K values ranged between 15 and 90 for different loci; most importantly, the significance level for all significant loci identified by interval mapping was $P < 0.001$ (Table 2).

Allelic variation for QTLs affecting lipid levels and body fat mass

At the peaks of linkage for cholesterol, HDL, TG, and fat mass, the genotypic means in F_2s, represented by the closest markers, were calculated for F_2 females and are shown in Figs. 2–5. For fat mass locus on chromosome 11, the homozygotes for the MRL allele had 21.3% ($P < 0.0001$) higher fat mass, as compared with the homozygotes for the SJL allele. At the chromosome 7 locus, the mean fat mass for the homozygous MRL and SJL alleles were 5–8% lower than that of heterozygotes (data not shown). For the loci on chromosome 16, homozygotes for the SJL allele had 8.7% ($P < 0.05$) higher fat mass than the homozygotes for the MRL allele. At the chromosome 11 locus, the phenotypic effect of the MRL allele best fit an additive model, whereas for the chromosome 16 locus, the phenotypic effect of the SJL allele best fit a recessive mode of inheritance.

For cholesterol and HDL, the phenotypic effects of the MRL allele at loci on chromosomes 1, 3, 5, 7, and 17 are inherited in an additive manner. For cholesterol, HDL, and TG, the loci on chromosome 1 of the MRL allele were 27, 31, and 19%, respectively (all $P < 0.001$), higher than the those of the homozygotes for the SJL allele. For the locus on chromosome 14, the homozygous SJL alleles have 9% higher cholesterol and HDL levels as compared with MRL homozygotes (details not shown). At the locus on chromosome 12 for TG, homozygotes for the SJL allele had 19.2% ($P < 0.001$) higher TG levels than the

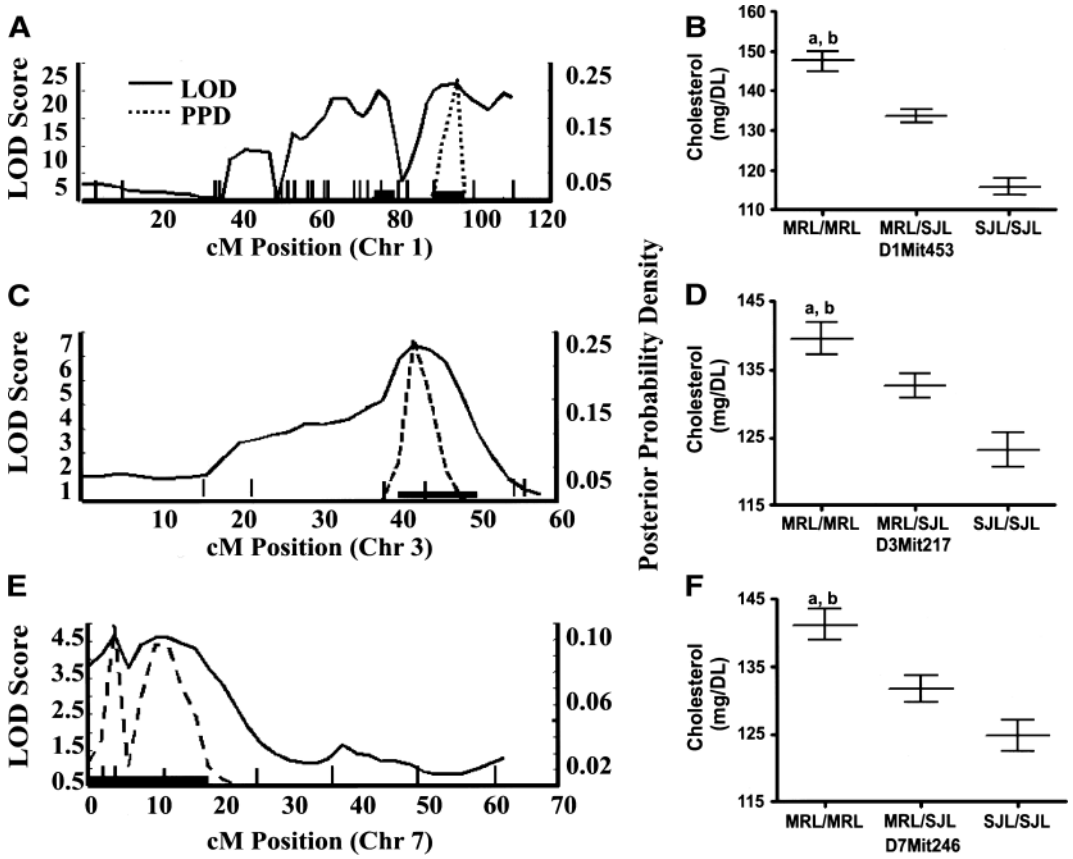

Fig. 3. A, C, E: LOD score and posterior probability density plots for the major QTLs influencing cholesterol. B, D, F: Allelic contribution of closest marker located on major QTL peak. MRL/MRL represents homozygosity for MRL/MpJ alleles; SJL/SJL represents homozygosity for SJL/J alleles; and heterozygosity at a locus is represented by MRL/SJL. Chromosome 1 was analyzed using 22 markers, chromosome 3 was analyzed using 5 markers, and chromosome 7 was analyzed using 7 markers. Locations of these markers are shown as vertical lines on the x axis. Posterior probability density is a likelihood statistic that gives rise to the 95% confidence intervals indicated by the black horizontal bars. Error bars represent SEM. a = $P < 0.05$ vs SJL/SJL; b = $P < 0.05$ vs MRL/SJL (by ANOVA). Chr, chromosome; cM, centimorgan; PPD, posterior probability density.

homozygotes for the MRL allele, and the SJL allele are inherited in an additive manner.

Although the fat mass, cholesterol, and HDL levels were higher in the MRL strain, it is noteworthy that recessive SJL alleles at chromosome 16 increased fat mass (Fig. 2), and a dominant chromosome 14 SJL allele increased HDL and cholesterol levels (data not shown). Similarly, parental SJL strains have higher TG levels than do parental MRL strains, yet QTL analysis in the F_2s revealed that dominant MRL alleles at chromosome 1 increase TG levels (Fig. 5). This type of finding has been observed in other QTL analyses (39), and presumably means that the MRL or SJL alleles at these loci are phenotypically silent (39) in the context of the MRL and SJL genomes, respectively, but the increase fat mass or lipid levels in the presence of one or more SJL alleles.

QTL-QTL interactions

Two loci showed interactions when the genotype at one locus affected the effect of the other locus. However, the LOD scores for all locus interactions, determined using the Pseudomarker PAIRSCAN software program, were suggestive in nature (data not shown).

Pleiotropic effects on fat mass and lipid levels

Our results show that the two loci on chromosome 1 and chromosome 11 have pleiotropic effects on multiple phenotypes. The chromosome 1 locus at 82 cM has a pleiotropic effect on cholesterol, HDL, and TG levels. In addition to phenotypes described in this study, we have also obtained QTLs for body weight, body length, and several musculoskeletal phenotypes (33–36). Interestingly, loci on chromosome 1 and chromosome 11 showed concordance with QTLs that regulate some skeletal phenotypes. The chromosome 1 locus (D1Mit33) was concordant with the total body bone density and volumetric bone density at tibia midshaft described previously in the same F_2 female mice (35). The chromosome 11 locus (D11Mit36) was concordant with QTLs identified for fat mass, body weight, muscle mass, and body length (QTLs for these phenotypes have been described previously) (33). In addition, the chromosome 11 locus showed concordance with the QTL that affects radial bone size (periosteal circumference at midshaft tibia).

To investigate how lipid QTLs affect fat mass, we compared the genotype influence of loci (*D11Mit36* and *D16Mit51*) that regulate fat mass in a subset of female F_2

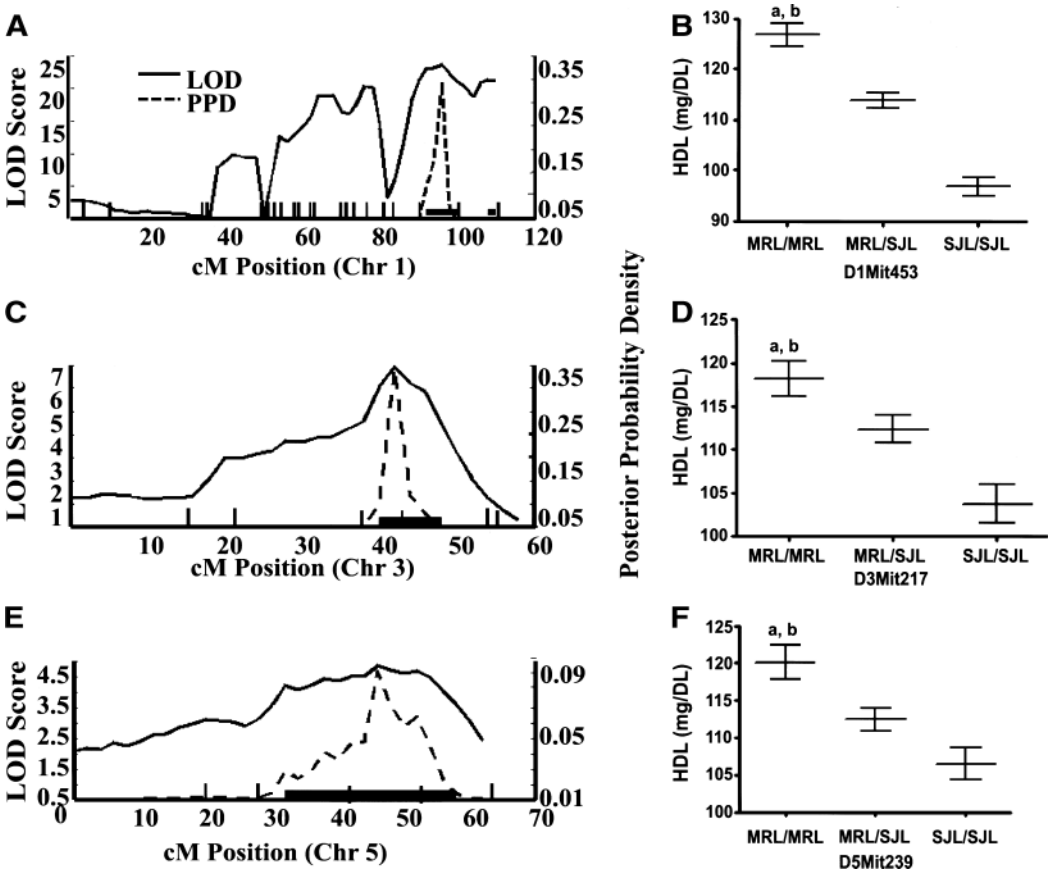

Fig. 4. A, C, E: LOD score and posterior probability density plots for the major QTLs influencing HDL. B, D, F: Allelic contribution of closest marker located on major QTL peak. MRL/MRL represents homozygosity for MRL/MpJ alleles; SJL/SJL represents homozygosity for SJL/J alleles; and heterozygosity at a locus is represented by MRL/SJL. Chromosome 1 was analyzed using 22 markers; chromosomes 3 and 5 were analyzed using 5 markers each. Locations of these markers are shown as vertical lines on the x axis. Error bars represent SEM. Posterior probability density is a likelihood statistic that gives rise to the 95% confidence intervals indicated by the black horizontal bars. a = $P < 0.05$ vs SJL/SJL; b = $P < 0.05$ vs MRL/SJL (by ANOVA). Chr, chromosome; cM, centimorgan.

mice grouped by genotype of loci that regulate cholesterol and HDL (*D1Mit453*, *D3Mit217*, *D7Mit246*, *D5Mit136*, and *D12Mit201*). Genotype groups that showed significant differences (by ANOVA) between homozygous MRL and SJL alleles are shown in **Fig. 6**. For genotype *D1Mit453*, F_2 mice homozygous for the MRL-derived allele for *D11Mit36* (Fig. 6A) exhibited 7% higher fat mass ($P < 0.05$ by ANOVA), as compared with those derived from homozygous SJL alleles. For genotype *D1Mit453*, F_2 mice homozygous for the SJL-derived allele for *D16Mit51* (Fig. 6B) exhibited 10% higher fat mass ($P < 0.05$ by ANOVA) as compared with those derived from homozygous MRL alleles. For female F_2 mice grouped by genotype for *D1Mit453*, F_2 mice homozygous for the SJL-derived allele for genotype *D12Mit201* exhibited 20–28% higher levels of TG ($P < 0.05$) as compared to those derived from homozygous MRL alleles (Fig. 6C). The relative effects of *D1Mit453* alleles on fat mass among the F_2 mice indicate that locus *D1Mit453*, in addition to regulating cholesterol and HDL levels, represents an important determinant of the fat mass variation between the MRL and SJL strains. Taken together, these data suggest that the genes underlying loci of chromosomes 1, 11, 12, and 16 could play critical roles in determining both fat mass and lipid levels.

DISCUSSION

The genome-wide scans of MRL × SJL F_2 mice for associations between marker genotypes and the quantitative phenotypes of total body fat mass and serum lipid levels resulted in the localization of several novel QTLs, particularly for percent fat mass and TG levels. Fat mass has a significant heritability (40) and previous studies have identified >20 loci (**Table 3**) that regulate total body fat mass (12, 14, 17, 26, 40–44). However, only two major loci, located on chromosome 2 (17) and chromosome 8 (14) have been concordant in more than one cross. A body fat QTL identified on chromosome 2 in NZB/BINJ × SM/J mice (17) was concordant with a QTL in a C57BL/6J × CAST/Ei (29) cross. The region of chromosome 2 QTL in these two crosses is syntenic with a large region of human chromosome 20, which shows linkage to body fat mass. Recently Ishimori et al. (14) have shown a locus on chromosome 8 in the C57Bl/6J ×

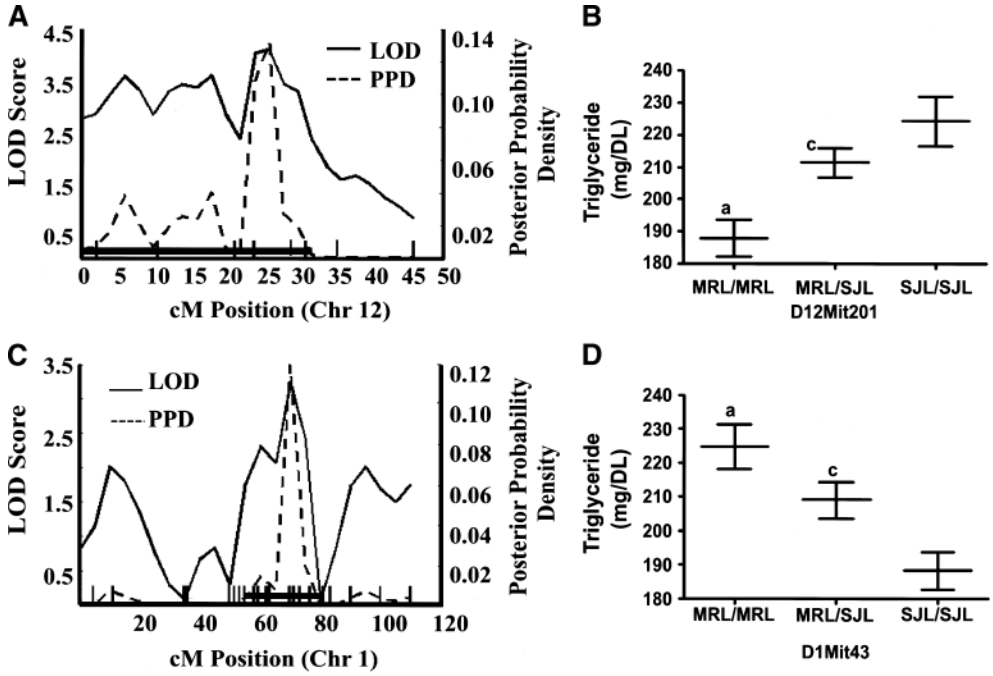

Fig. 5. A, C: LOD score and posterior probability density plots for the major QTLs influencing TG. B, D: Allelic contribution of closest marker located on major QTL peak. MRL/MRL represents homozygosity for MRL/MpJ alleles; SJL/SJL represents homozygosity for SJL/J alleles; and heterozygosity at a locus is represented by MRL/SJL. Chromosome 1 was analyzed using 22 markers, and chromosome 12 was analyzed using 8 markers. Locations of these markers are shown as vertical lines on the x axis. Error bars represent SEM. Posterior probability density is a likelihood statistic that gives rise to the 95% confidence intervals indicated by the black horizontal bars. a = $P < 0.05$ vs SJL/SJL; c = $P < 0.05$ vs MRL/MRL and SJL/SJL (by ANOVA). Chr, chromosome; cM, centimorgan.

129S1/SvlmJ cross that regulates fat mass similar to that identified previously in the C57Bl/6J × CAST/Ei cross (29). These findings suggest that the full repertoire of QTLs affecting fat mass has not yet been determined and that identification of candidate genes that regulate obesity is still in its early phase. QTLs observed in this study account for approximately 18% of the total variance in percent fat mass in F_2 mice. The lower estimates

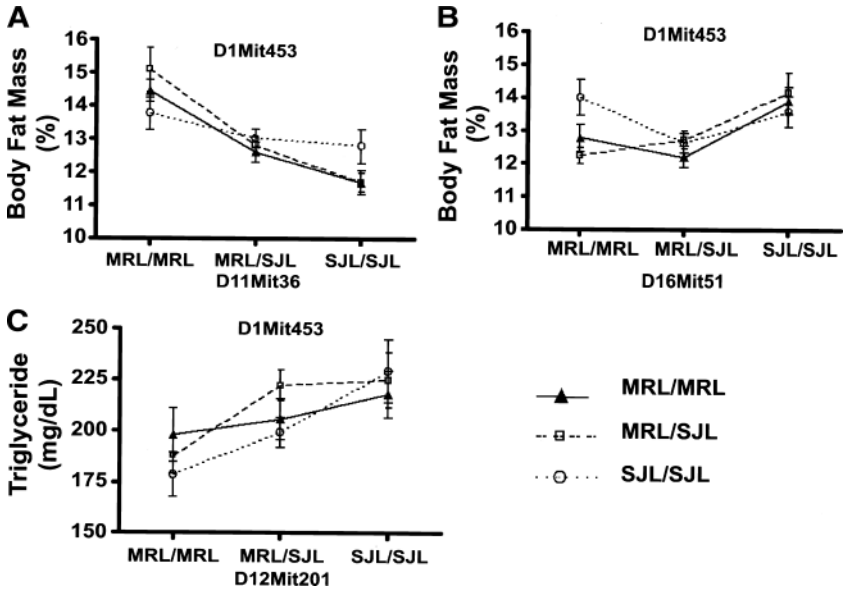

Fig. 6. A, B: Genotypic influence of three loci (D11Mit36 and D16Mit51) regulating fat mass in a subset of female F_2 mice grouped by genotype of locus (D1Mit453) regulating blood cholesterol and HDL levels. C: Genotypic influence of locus (D12Mit201) regulating TG in a subset of female F_2 mice grouped by genotype at locus (D1Mit453) regulating cholesterol. Data points and error bars represent mean ± SEM.

TABLE 3. Body fat mass or obesity QTLs detected in female mice in various genetic crosses

Cross	Chromosome	Peak cM or (Range in cM)	LOD Score	Reference
C57BL/6J × 129S1/J (F_2)	**8**[a]	48 (42–53)	10.0	14
	1[a]	74 (48–108)	2.3	
	12[a]	2 (0–16)	2.9	
	6[a]	0 (0–10)	2.6	
NZB/B1NJ × SM/J (F_2)	**2**[a]	15–30	4.3	17
C57BL/6J × SPRET (F_2)	6[b]	2.8	4.8	44
	7[a]	60	4.2	
	12[a]	52	4.8	
	15[b]	6.7	3.4	
129/Sv × Le/Suz (F_2)	1[b]	2–16	2.9	41
	7[b]	3–25	3.5	
C57BL/6J × AKR/J (F_2)	**2**[b]	50	5.1	12
	17[b]	5	4.6	
C57BL/6J × CAST/Ei (F_2)	**2**[a]	95.5	5.8	43
	8[b]	53.3	3.2	
	9[b]	42	4.7	
C57BL/6J × KK (F_2)	9[b]	15–23	6.3	42

Numbers in bold represent loci colocalized in more than one cross.

[a] Body fat mass.

[b] Fat pad weight or other measure of fat mass.

of total F_2 variance explained by the loci identified in this study could be due to the presence of QTLs that have a small effect on F_2 variance and hence are difficult to identify. In addition, the best estimate of total variance explained is obtained by identifying plieotropic interactions, which is a challenging task because of lower power to detect such interactions. We did not observe any significant interaction, which may partly explain the lower variance explained by the loci identified in this study. Taken together, our results and published findings indicate that results from several F_2 crosses may be necessary for identifying the majority of QTLs that affect fat mass. Out of three loci (chromosomes 7, 11, and 16) that regulate body fat mass, two QTLs on chromosomes 11 and 16 were specific to the MRL × SJL cross. Previous data published by our laboratory on the MRL × SJL F_2 mice (33) indicated that the chromosome 7 (LOD 2.4) locus was colocalized with a locus that regulates lean body mass (5.5 cM, LOD 2.9). In addition, the locus on chromosome 11 colocalizes with QTLs that regulate body weight, muscle mass, body length, and radial bone size. It could be speculated that the effect of the chromosome 11 locus on radial bone size is indirectly related to bone adaptive response to mechanical loading resulting from higher body weight. In mice, the major effect of mechanical loading is reflected in an increase in the periosteal perimeter of long bones. It is noteworthy that there was a significant correlation between body weight and percent fat mass ($r = 0.25$; $P < 0.0001$), indicating that the same gene(s) may regulate these phenotypes. Together, these findings suggest that the chromosome 7 and chromosome 11 loci that regulate fat mass have pleiotropic effects on body weight. It remains to be verified whether the same gene or independent genes under these loci regulate the multiple phenotypes.

Several candidate genes have been identified for all fat mass loci. The prominent candidates for the chromosome 11 locus include*Nos2* (nitric oxide synthase 2), *Hcrt* (hypocretin), *Alox12*, *Alox3*, *Alox15*, *Alox12b*, and *Alox12e* (all belong to a family of lipoxygenases that are a class of iron-containing dioxygenases that catalyze the hydroperoxidation of lipids), and Lpd1, a mouse insertional mutation lpd (lipid defect) whose phenotype includes elevated plasma TG (45) and is a potential candidate gene for the chromosome 16 QTL. Although the above-mentioned genes are obvious candidates, on the basis of their known functions, ultimately, identification of the gene(s) underlying a particular QTL will be necessary for determining which subset of genes contributes to the genetic variation of a trait across species.

Previous linkage studies have identified >20 loci regulating TG on chromosomes 4, 8, 9, 11, 12, 14, 18, and 19 (as shown in **Table 4**). However, only two loci on chromosome 2 and chromosome 8 have been colocalized in multiple crosses. In this study, four loci on chromosomes 1, 5, 12, and 17 were in linkage with serum levels of TGs. The chromosome 12 QTL (at 25 cM) identified in this study does not appear to be concordant with any previously known QTL on chromosome 12, which showed a peak at 39 cM. Therefore, the majority of TG QTLs identified in the MRL × SJL cross appear to be novel. The QTL on chromosome 12, however, incorporates QTLs identified earlier for fat mass (at 29 cM) (46) and HDL (at 17.2 cM) (31) in mice. For non-HDL cholesterol, the locus identified in this study on chromosome 7 was concordant with the cholesterol and HDL locus, suggesting that the candidate gene in this region may regulate both HDL and non-HDL cholesterol. The chromosome 12 locus was proximal to the TG QTL located on chromosome 12 and

TABLE 4. QTLs affecting triglyceride levels in various genetic crosses

Cross	Chromosome	Peak (cM)	LOD Score	Reference
C57BL/6J × 129S1/J (F_2)	**9**	**66**	**2.2**	14
	14	14	2.0	
	18	42	2.9	
RR × KK (F_2)	8	—	4.7	27
SM/J × A/J (F_2)	**4**	**35.4**	**2.4**	10
	8	8	3.4	
	9	**71**	**2.3**	
	11	57	2.8	
	12	39	2.5	
	19	50	2.2	
SMXA (RI)	4	4.3	2.5	11
	11	64	2.6	
C57BL/6J × RR (F_2)	1	94.8	4.4	28
MRL/lpr × Balb/C (F_2)	**4**	**66**	**2.9**	21
	15	70	2.1	
	15	45	2.7	
	19	3	4.0	

Numbers in bold represent loci colocalized in more than one cross.

could independently regulate non-HDL cholesterol. The locus on chromosome 9 appears to be novel for non-HDL cholesterol. The TG QTLs identified in this study have a limitation in that the blood samples were collected under nonfasting conditions and some of the QTLs could be influenced by nongenetic factors.

QTLs on chromosomes 1, 3, 5, 7, and 17 (14, 30, 31) that regulate HDL and cholesterol levels are concordant with linkages previously identified in standard diet-fed F_2 mice. Location and peaks of all the loci identified in this study, with the exception of the chromosome 14 locus, coincide with published HDL cholesterol peaks. These findings confirm the belief that, in general, we may have reached saturation as far as identification of HDL and cholesterol QTLs are concerned. Results of this study show that almost 70% (Table 2) of the total variance in cholesterol levels in F_2 mice was explained by the QTLs identified in this study. The strongest linkage for cholesterol was identified on chromosome 1 in MRL $\times$ SJL F_2 mice. This chromosome 1 locus contains the apolipoprotein A-II (apoA-II) gene, which has polymorphism that has been implicated as an HDL QTL gene in seven different crosses (47). The MRL strain carries the APOA2b haplotype allele (47) known to impart higher HDL levels, whereas the SJL strain carries the apoA-IIc allele, which is responsible for lower HDL levels. However, a high LOD score of 21–24 for two distinct peaks may indicate the possible involvement of other unknown gene(s) present in this region. The chromosome 14 locus observed in this study, although suggestive in nature, was located in the distal region of any known chromosome 14 QTL (30, 31) and therefore could represent a distinct linkage finding. Several candidate genes for cholesterol and HDL have been located within the QTL regions identified in this study. A comprehensive list of these genes is available in a recently published review (31).

Identifying the gene underlying a QTL is a complex task; therefore, the process of identifying genes for QTLs discovered to date has been slow. Recently it was shown that single-nucleotide polymorphisms (SNPs) can be used to narrow a QTL, because gene(s) underlying a QTL should be in the region where the parental strains have a haplotype divergence (47–49). Consequently, haplotype analysis of the chromosome 1 QTL (confirmed in multiple crosses) led to identification of a polymorphism in the *Apoa2* gene that affected HDL levels (47). In this regard, our findings on HDL and cholesterol QTLs could be important for future research directed toward the search for genes that regulate lipid levels. Results from each analysis were compared on the assumption that more common variants would be detected more frequently across the strains and that the QTL genes that are detected in these multiple crosses could be discovered quickly by analyzing their SNPs and haplotypes in multiple strains. The inferred haplotype data may also facilitate the refinement of QTL regions, such that candidate genes can be more easily identified and characterized.

In summary, we have identified several distinct linkages for TG and body fat mass and have confirmed the loci that regulate HDL and cholesterol that were identified in previous genetic crosses. The presence of similar QTLs in previous crosses suggests that for some genes, there are higher degrees of polymorphism. On the other hand, identification of novel loci may indicate the presence of additional genes or modifier genes that regulate a given trait. Thus, our data contribute to the growing knowledge of the genetic complexity of lipid metabolism and obesity and also underscore the importance of strain background in the evaluation of the linkage for a complex trait. It is hoped that the discovery of genes at these loci may help in explaining the variability in lipid levels in humans.

This work was supported by Army Assistance Award DAMD17-99-1-9571. The U.S. Army Medical Research Acquisition Activity (Fort Detrick, MD) 21702-5014 is the awarding and administering acquisition office for the DAMD award. The information contained in this article does not necessarily reflect the position or the policy of the U.S. government, and no official endorsement should be inferred. All work was performed in facilities provided by the Department of Veterans Affairs.

REFERENCES

1. Kannel, W., W. Castelli, T. Gordon, and P. McNamara. 1971. Serum cholesterol, lipoproteins, and the risk of coronary heart disease: the Framingham Study. *Ann. Intern. Med.* **74:** 1–12.
2. North, K. E., B. V. Howard, T. K. Welty, L. G. Best, E. T. Lee, J. L. Yeh, R. R. Fabsitz, M. J. Roman, and J. W. MacCluer. 2003. Genetic and environmental contributions to cardiovascular disease risk in American Indians: the strong heart family study. *Am. J. Epidemiol.* **157:** 303–314.
3. Breslow, J. I. 1996. Battling heart disease. *Science.* **273:** 15.
4. Brousseau, T., A. M. Dupuy-Gorce, A. Evans, D. Arveiler, J. B. Ruidavets, B. Haas, J. P. Cambou, G. Luc, P. Ducimetiere, P. Amouyel, and N. Helbecque. 2002. Significant impact of the highly informative (CA)n repeat polymorphism of the APOA-II gene on the plasma APOA-II concentrations and HDL subfractions: the ECTIM study. *Am. J. Med. Genet.* **110:** 19–24.
5. Brown, M. S., and J. L. Goldstein. 1997. The SREBP pathway: regulation of cholesterol metabolism by proteolysis of a membrane-bound transcription factor. *Cell.* **89:** 331–340.
6. Bu, X., C. H. Warden, Y. R. Xia, C. De Meester, D. L. Puppione, S. Teruya, B. Lokensgard, S. Daneshmand, J. Brown, R. J. Gray, et al. 1994. Linkage analysis of the genetic determinants of high density lipoprotein concentrations and composition: evidence for involvement of the apolipoprotein A-II and cholesteryl ester transfer protein loci. *Hum. Genet.* **93:** 639–648.
7. Cases, S., S. J. Smith, Y. W. Zheng, H. M. Myers, S. R. Lear, E. Sande, S. Novak, C. Collins, C. B. Welch, A. J. Lusis, et al. 1998. Identification of a gene encoding an acyl CoA:diacylglycerol acyltransferase, a key enzyme in triacylglycerol synthesis. *Proc. Natl. Acad. Sci. USA.* **95:** 13018–13023.
8. Wang, X., M. Ria, P. M. Kelmenson, P. Eriksson, D. C. Higgins, A. Samnegard, C. Petros, J. Rollins, A. M. Bennet, B. Wiman, et al. 2005. Positional identification of TNFSF4, encoding OX40 ligand, as a gene that influences atherosclerosis susceptibility. *Nat. Genet.* **37:** 365–372.
9. Castellani, L. W., A. Weinreb, J. Bodnar, A. M. Goto, M. Doolittle, M. Mehrabian, P. Demant, and A. J. Lusis. 1998. Mapping a gene for combined hyperlipidaemia in a mutant mouse strain. *Nat. Genet.* **18:** 374–377.
10. Anunciado, R. V., M. Nishimura, M. Mori, A. Ishikawa, S. Tanaka, F. Horio, T. Ohno, and T. Namikawa. 2003. Quantitative trait locus analysis of serum insulin, triglyceride, total cholesterol and phospholipid levels in the (SM/J x A/J)F2 mice. *Exp. Anim.* **52:** 37–42.
11. Anunciado, R. V., T. Ohno, M. Mori, A. Ishikawa, S. Tanaka, F.

Horio, M. Nishimura, and T. Namikawa. 2000. Distribution of body weight, blood insulin and lipid levels in the SMXA recombinant inbred strains and the QTL analysis. *Exp. Anim.* **49:** 217–224.
12. Taylor, B. A., and S. J. Phillips. 1997. Obesity QTLs on mouse chromosomes 2 and 17. *Genomics.* **43:** 249–257.
13. Gu, L., A. Weinreb, X. P. Wang, D. J. Zack, J. H. Qiao, R. Weisbart, and A. J. Lusis. 1998. Genetic determinants of autoimmune disease and coronary vasculitis in the MRL-lpr/lpr mouse model of systemic lupus erythematosus. *J. Immunol.* **161:** 6999–7006.
14. Ishimori, N., R. Li, P. M. Kelmenson, R. Korstanje, K. A. Walsh, G. A. Churchill, K. Forsman-Semb, and B. Paigen. 2004. Quantitative trait loci that determine plasma lipids and obesity in C57BL/6J and 129S1/SvImJ inbred mice. *J. Lipid Res.* **45:** 1624–1632.
15. Korstanje, R., J. J. Albers, G. Wolfbauer, R. Li, A. Y. Tu, G. A. Churchill, and B. J. Paigen. 2004. Quantitative trait locus mapping of genes that regulate phospholipid transfer activity in SM/J and NZB/BlNJ inbred mice. *Arterioscler. Thromb. Vasc. Biol.* **24:** 155–160.
16. Korstanje, R., R. Li, T. Howard, P. Kelmenson, J. Marshall, B. Paigen, and G. Churchill. 2004. Influence of sex and diet on quantitative trait loci for HDL cholesterol levels in an SM/J by NZB/BlNJ intercross population. *J. Lipid Res.* **45:** 881–888.
17. Lembertas, A. V., L. Perusse, Y. C. Chagnon, J. S. Fisler, C. H. Warden, D. A. Purcell-Huynh, F. T. Dionne, J. Gagnon, A. Nadeau, A. J. Lusis, et al. 1997. Identification of an obesity quantitative trait locus on mouse chromosome 2 and evidence of linkage to body fat and insulin on the human homologous region 20q. *J. Clin. Invest.* **100:** 1240–1247.
18. Lyons, M. A., R. Korstanje, R. Li, K. A. Walsh, G. A. Churchill, M. C. Carey, and B. Paigen. 2004. Genetic contributors to lipoprotein cholesterol levels in an intercross of 129S1/SvImJ and RIIIS/J inbred mice. *Physiol. Genomics.* **17:** 114–121.
19. Lyons, M. A., H. Wittenburg, R. Li, K. A. Walsh, G. A. Churchill, M. C. Carey, and B. Paigen. 2003. Quantitative trait loci that determine lipoprotein cholesterol levels in DBA/2J and CAST/Ei inbred mice. *J. Lipid Res.* **44:** 953–967.
20. Lyons, M. A., H. Wittenburg, R. Li, K. A. Walsh, R. Korstanje, G. A. Churchill, M. C. Carey, and B. Paigen. 2004. Quantitative trait loci that determine lipoprotein cholesterol levels in an intercross of 129S1/SvImJ and CAST/Ei inbred mice. *Physiol. Genomics.* **17:** 60–68.
21. Gu, L., M. W. Johnson, and A. J. Lusis. 1999. Quantitative trait locus analysis of plasma lipoprotein levels in an autoimmune mouse model: interactions between lipoprotein metabolism, autoimmune disease, and atherogenesis. *Arterioscler. Thromb. Vasc. Biol.* **19:** 442–453.
22. Diament, A. L., P. Farahani, S. Chiu, J. Fisler, and C. H. Warden. 2004. A novel mouse chromosomeomosome 2 congenic strain with obesity phenotypes. *Mamm. Genome.* **15:** 452–459.
23. Mu, J. L., J. K. Naggert, K. L. Svenson, G. B. Collin, J. H. Kim, C. McFarland, P. M. Nishina, D. M. Levine, K. J. Williams, and B. Paigen. 1999. Quantitative trait loci analysis for the differences in susceptibility to atherosclerosis and diabetes between inbred mouse strains C57BL/6J and C57BLKS/J. *J. Lipid Res.* **40:** 1328–1335.
24. Paigen, B., N. J. Schork, K. L. Svenson, Y. C. Cheah, J. L. Mu, F. Lammert, D. Q. Wang, G. Bouchard, and M. C. Carey. 2000. Quantitative trait loci mapping for cholesterol gallstones in AKR/J and C57L/J strains of mice. *Physiol. Genomics.* **4:** 59–65.
25. Pitman, W. A., R. Korstanje, G. A. Churchill, E. Nicodeme, J. J. Albers, M. C. Cheung, M. A. Staton, S. S. Sampson, S. Harris, and B. Paigen. 2002. Quantitative trait locus mapping of genes that regulate HDL cholesterol in SM/J and NZB/B1NJ inbred mice. *Physiol. Genomics.* **9:** 93–102.
26. Singer, J. B., A. E. Hill, L. C. Burrage, K. R. Olszens, J. Song, M. Justice, W. E. O'Brien, D. V. Conti, J. S. Witte, E. S. Lander, et al. 2004. Genetic dissection of complex traits with chromosome substitution strains of mice. *Science.* **304:** 445–448.
27. Suto, J., and K. Sekikawa. 2003. Quantitative trait locus analysis of plasma cholesterol and triglyceride levels in KK x RR F2 mice. *Biochem. Genet.* **41:** 325–341.
28. Suto, J., Y. Takahashi, and K. Sekikawa. 2004. Quantitative trait locus analysis of plasma cholesterol and triglyceride levels in C57BL/6J x RR F2 mice. *Biochem. Genet.* **42:** 347–363.
29. York, B., K. Lei, and D. B. West. 1996. Sensitivity to dietary obesity linked to a locus on chromosome 15 in a CAST/Ei x C57BL/6J F2 intercross. *Mamm. Genome.* **7:** 677–681.
30. Wang, X., and B. Paigen. 2005. Genetics of variation in HDL cholesterol in humans and mice. *Circ. Res.* **96:** 27–42.
31. Wang, X., and B. Paigen. 2002. Quantitative trait loci and candidate genes regulating HDL cholesterol: a murine chromosome map. *Arterioscler. Thromb. Vasc. Biol.* **22:** 1390–1401.
32. Masinde, G. L., X. Li, W. Gu, H. Davidson, S. Mohan, and D. J. Baylink. 2001. Identification of wound healing/regeneration quantitative trait loci (QTL) at multiple time points that explain seventy percent of variance in (MRL/MpJ and SJL/J) mice F2 population. *Genome Res.* **11:** 2027–2033.
33. Masinde, G. L., X. Li, W. Gu, H. Davidson, M. Hamilton-Ulland, J. Wergedal, S. Mohan, and D. J. Baylink. 2002. Quantitative trait loci (QTL) for lean body mass and body length in MRL/MPJ and SJL/J F(2) mice. *Funct. Integr. Genomics.* **2:** 98–104.
34. Masinde, G. L., X. Li, W. Gu, J. Wergedal, S. Mohan, and D. J. Baylink. 2002. Quantitative trait loci for bone density in mice: the genes determining total skeletal density and femur density show little overlap in F2 mice. *Calcif. Tissue Int.* **71:** 421–428.
35. Masinde, G. L., X. Li, W. Gu, M. Hamilton-Ulland, S. Mohan, and D. J. Baylink. 2002. Quantitative trait loci that harbor genes regulating muscle size in (MRL/MPJ x SJL/J) F(2) mice. *Funct. Integr. Genomics.* **2:** 120–125.
36. Masinde, G. L., J. Wergedal, H. Davidson, S. Mohan, R. Li, X. Li, and D. J. Baylink. 2003. Quantitative trait loci for periosteal circumference (PC): identification of single loci and epistatic effects in F2 MRL/SJL mice. *Bone.* **32:** 554–560.
37. Srivastava, A. K., G. Masinde, H. Yu, D. J. Baylink, and S. Mohan. 2004. Mapping quantitative trait loci that influence blood levels of alkaline phosphatase in MRL/MpJ and SJL/J mice. *Bone.* **35:** 1086–1094.
38. Sugiyama, F., G. A. Churchill, D. C. Higgins, C. Johns, K. P. Makaritsis, H. Gavras, and B. Paigen. 2001. Concordance of murine quantitative trait loci for salt-induced hypertension with rat and human loci. *Genomics.* **71:** 70–77.
39. Dansky, H. M., P. Shu, M. Donavan, J. Montagno, D. L. Nagle, J. S. Smutko, N. Roy, S. Whiteing, J. Barrios, T. J. McBride, et al. 2002. A phenotype-sensitizing Apoe-deficient genetic background reveals novel atherosclerosis predisposition loci in the mouse. *Genetics.* **160:** 1599–1608.
40. Barsh, G. S., I. S. Farooqi, and S. O'Rahilly. 2000. Genetics of bodyweight regulation. *Nature.* **404:** 644–651.
41. Taylor, B. A., and S. J. Phillips. 1996. Detection of obesity QTLs on mouse chromosomes 1 and 7 by selective DNA pooling. *Genomics.* **34:** 389–398.
42. Taylor, B. A., L. M. Tarantino, and S. J. Phillips. 1999. Gender-influenced obesity QTLs identified in a cross involving the KK type II diabetes-prone mouse strain. *Mamm. Genome.* **10:** 963–968.
43. Mehrabian, M., P. Z. Wen, J. Fisler, R. C. Davis, and A. J. Lusis. 1998. Genetic loci controlling body fat, lipoprotein metabolism, and insulin levels in a multifactorial mouse model. *J. Clin. Invest.* **101:** 2485–2496.
44. Warden, C. H., J. S. Fisler, S. M. Shoemaker, P. Z. Wen, K. L. Svenson, M. J. Pace, and A. J. Lusis. 1995. Identification of four chromosomal loci determining obesity in a multifactorial mouse model. *J. Clin. Invest.* **95:** 1545–1552.
45. Wen, X. Y., R. A. Hegele, J. Wang, D. Y. Wang, J. Cheung, M. Wilson, M. Yahyapour, Y. Bai, L. Zhuang, J. Skaug, et al. 2003. Identification of a novel lipase gene mutated in lpd mice with hypertriglyceridemia and associated with dyslipidemia in humans. *Hum. Mol. Genet.* **12:** 1131–1143.
46. Brockmann, G. A., J. Kratzsch, C. S. Haley, U. Renne, M. Schwerin, and S. Karle. 2000. Single QTL effects, epistasis, and pleiotropy account for two-thirds of the phenotypic F(2) variance of growth and obesity in DU6i x DBA/2 mice. *Genome Res.* **10:** 1941–1957.
47. Wang, X., R. Korstanje, D. Higgins, and B. Paigen. 2004. Haplotype analysis in multiple crosses to identify a QTL gene. *Genome Res.* **14:** 1767–1772.
48. Park, Y. G., R. Clifford, K. H. Buetow, and K. W. Hunter. 2003. Multiple cross and inbred strain haplotype mapping of complex-trait candidate genes. *Genome Res.* **13:** 118–121.
49. Manenti, G., F. Galbiati, R. Gianni-Barrera, A. Pettinicchio, A. Acevedo, and T. A. Dragani. 2004. Haplotype sharing suggests that a genomic segment containing six genes accounts for the pulmonary adenoma susceptibility 1 (Pas1) locus activity in mice. *Oncogene.* **23:** 4495–4504.